DFT Studies on the Nature, Strength and Cooperativity of Intermolecular Interactions in Dipolar Organic Molecules, Polyynes and Carbon Rings

Thesis submitted to the
UNIVERSITY OF KERALA
for the award of Degree of

DOCTOR OF PHILOSOPHY

in Chemistry under the Faculty of Science

By

REMYA K.

Chemical Sciences and Technology Division
CSIR-National Institute for Interdisciplinary Science and Technology
Thiruvananthapuram – 695 019
Kerala, India

2016

DECLARATION

I hereby declare that the Ph.D. thesis entitled "**DFT Studies on the Nature, Strength and Cooperativity of Intermolecular Interactions in Dipolar Organic Molecules, Polyynes and Carbon Rings**" is an independent work carried out by me at the Chemical Sciences and Technology Division, CSIR-National Institute for Interdisciplinary Science and Technology (CSIR-NIIST), Trivandrum, under the supervision of Dr. C. H. Suresh and it has not been submitted elsewhere for any other degree, diploma or title.

Remya K

20.06.2016

CERTIFICATE

This is to certify that the work embodied in the thesis entitled "**DFT Studies on the Nature, Strength and Cooperativity of Intermolecular Interactions in Dipolar Organic Molecules, Polyynes and Carbon Rings**" has been carried out by Ms. Remya K. under my supervision and guidance at the Chemical Sciences and Technology Division, CSIR-National Institute for Interdisciplinary Science and Technology (CSIR-NIIST), Trivandrum and the same has not been submitted elsewhere for a degree.

Dr. C. H. Suresh

(Thesis Supervisor)

ACKNOWLEDGEMENT

First and foremost I would like to express my heartfelt gratitude and deep regards to my research supervisor Dr. C. H. Suresh, Principal Scientist, Chemical Sciences and Technology Division, CSIR-NIIST, Trivandrum for his invaluable guidance, timely advices and strong motivation. Without his immense scientific knowledge, constant motivation and support, it would have been impossible for me to finish this thesis.

I express my profound thanks to Dr. A. Ajayaghosh, Director, CSIR-NIIST and former director, Dr. Suresh Das, for giving me an opportunity to carry out my doctoral work in this prestigious institution.

My sincere thanks are due to Dr. S. Savithri, Dr. Elizabeth Jacob, Dr. K. G. K. Warrier, Dr. S. Shukl and Roschen Sasikumar for their invaluable advices encouragement. I also express my heartfelt gratitude to Dr. K. P. Vijayalakshmi, VSSC for her generous advices and moral support.

I extend my sincere thanks to all my friends at NIIST for making my stay at NIIST, memorable. The help and support provided by my senior colleagues Dr. Sandhya, Dr. Sajith, Dr. Neetha, Dr. Fareed Basha, Dr. Ajitha, Dr. Jomon and Dr. Prabha are gratefully acknowledged. Special thanks are due to my lab mates Rakhi, Remya P. R., Della, Remya G. S, Anjali, Bijina, Divya and Raji for a pleasant and healthy working atmosphere. The invaluable friendship of Harsha, Lekshmi, Gayathri, Linsha, Mahesh, Manu and Namitha are greatly appreciated. I would also like to express my thanks to the administrative and technical staff of CSIR-NIIST for their cooperation and help in their respective roles.

I gratefully acknowledge the Council of Scientific and Industrial Research (CSIR), Govt. of India, for the research fellowship. The high performance computational facilities at CSIR-CMMACS, Bangalore and CSIR-NCL, Pune are also sincerely acknowledged.

I am deeply grateful to my family members, especially my beloved husband, Mr. Jyothish, who has been my strength throughout my Ph. D life. He has always been there to

share the worries, sorrows and the short term delights of my research life. He always understood the hurdles of my research life and never insisted me to come home frequently. Without his love, care and support I would never have been able to finish my thesis in a satisfactory way. I also gratefully acknowledge the love and care provided by my parents and in-laws. It is my pleasure to acknowledge the love and care of my sister, Dr. Soumya and her family and also my brother Hari. My special thanks to all my beloved teachers for enlightening me with knowledge at different stages of life.

Remya K.

CONTENTS

List of Tables

List of Figures

List of Schemes

List of Abbreviations

ACM : Adiabatic Connection Method

AO : Atomic Orbital

BSSE : Basis Set Superposition Error

BCP : Bond Critical Point

CCP : Cage Critical Point

CSD : Cambridge Structural Database

CI : Configuration Interaction

CC : Coupled Cluster

CCSD : Coupled Cluster Single and Double

DFT : Density Functional Theory

EDA : Energy Decomposition Analysis

GTO : Gaussian-Type Orbitals

GGA : Generalized Gradient Approximation

HF : Hartree-Fock

HK : Hohenberg-Kohn

IUPAC : International Union of Pure and Applied Chemistry

KS : Kohn Sham

LCAO : Linear Combination of Atomic Orbitals

LSDA : Local Spin Density Approximation

LDA : Local-Density Approximation

LC : Long-range Correction

MAD : Mean Absolute Deviation

MD : Molecular Dynamics

MESP : Molecular Electrostatic Potential

MM : Molecular Mechanics

MO : Molecular Orbital

MP : Møller-Plesset Perturbation Theory

MCSCF : Multi-Configurational Self Consistent Field

NBO : Natural Bond Orbital

NNA : Non-Nuclear Attractor

NCP : Nuclear Critical Point

NICS : Nucleus-Independent Chemical Shift

QSAR : Quantitative Structure-Activity Relationship

QM : Quantum Mechanics

QTAIM : Quantum Theory of Atoms in Molecules

RCP : Ring Critical Point

RMSD : Root-Mean-Square-Deviation

SCF : Self Consistent Field

STO : Slater-Type Orbitals

XC : Exchange Correlation

Preface

The importance of non-covalent interactions lies in widespread areas such as the study of biomolecules, supramolecular self assemblies, nanomaterials, catalysis, drug discovery, crystallography and even some chemical reactions. With the development of novel theoretical methods, the study of non-covalent interactions has emerged as a warm area of research among the theoretical chemists. Accurate assessment of the nature and strength of non-covalent interactions is of prime importance in several research fields and is a challenge for the computational chemists. Density functional theory (DFT) methods, giving a good balance between accuracy and computational coast, are the best candidates for solving this problem. However, since there is no universal density functional available that can be applied for any computational problem, it is necessary to do a benchmark study before applying one to a problem. The present thesis describes the nature, strength and cooperativity of non-covalent interactions in dipolar organic molecules, polyynes and carbon rings using highly accurate DFT methods located via an extensive benchmark study.

The thesis is divided into four chapters. The first chapter gives a detailed introduction on non-covalent interactions and their cooperativity, giving emphasis to different types of interactions involving the main group elements such as halogen bonds, chalcogen bonds, pnicogen bonds and tetrel bonds that have been described recently using novel theoretical as well as experimental methods. The second part of this chapter briefly describes the computational chemistry methods, with emphasis being given to those used in this thesis.

The second chapter describes a thorough benchmark study for locating suitable density functional for the study of non-covalently interacting systems. A total of 382 density functionals were tested for their applicability in studying the geometry and interaction energy of 3 different classes of non-covalently interacting dimers. The DFT results are compared against high accuracy geometries and interaction energies. A list of best performing density functionals has been made, in which, the *meta*-GGA functional M06L outperforms all the other functionals. The effect of Long-range correction (LC) by Hirao and co-workers to exchange-correlation functionals is also discussed in this chapter. Using the methods thus selected, problems in non-covalently interacting systems such as

their clustering and cooperativity have been addressed, which is described in the subsequent chapters.

In the first part of the third chapter, a detailed study of different cluster growth patterns of acetonitrile has been described. The relative stability and cooperativity of cyclic, ladder type, cross-stacked, stacked and mixed clusters of acetonitrile clusters are compared up to hexamers and the study of the most stable clusters is extended up to 27 monomers. Relative stability of the clusters is explained based on the number of intermolecular interactions and pair-wise interaction energies. A remarkable (300%) increase in the value of interaction energy per monomer (E_m) from dimer to **27mer** is observed, which arises due to strong cooperativity of intermolecular interactions. Based on this study, we predict the possibility of a more stable and more ordered crystal structure for acetonitrile than its α and β forms. The study of acetonitrile clusters revealed the presence of intermolecular C···C bonding interaction between the nitrile carbon atoms of two antiparallelly oriented acetonitrile molecules and these interactions are studied in detail in the second part of this chapter. These interactions, unlike the typical donor-acceptor type non-covalent interactions (where donor and acceptor atoms belong to different chemical environments) are between two carbon atoms in similar chemical environments and are studied for the first time. Clear evidence for the aforementioned kind of interaction in homogeneous dimers of several organic molecules is obtained using quantum theory of atoms-in-molecules (QTAIM) and molecular orbital (MO) analyses. These interactions are explained based on the molecular electrostatic potential (MESP) features and the nature charge transfer in these interactions has been analyzed using natural bond orbital (NBO) methods. The evidence for similar type of N···N and O···O interactions between atoms in similar chemical environments is also obtained.

The intermolecular C···C interactions between carbon atoms in similar chemical environments in polyynes and carbon rings are described in the fourth chapter. In the first part of this chapter, polyynes, the smaller analogues of the one dimensional *sp* hybridized carbon allotrope, carbyne, are analysed for the nature and cooperativity of the intermolecular interactions in their molecular complexes. Evidence for intermolecular C···C interactions is obtained with the help of QTAIM analysis and these interactions are explained based on their MESP features. The effect of end group substitutions and chain

length of polyynes on the nature and strength of C···C interactions are also analyzed. The number of C···C interactions and interaction energy increased with increase in chain lengths and the effect of end group substitutions were found to exist up to 100 carbon atoms. Thus, tuning of their intermolecular interaction strengths can be made possible, which can lead to materials with desirable mechanical properties. These results are of prime importance since the trends in the physical and chemical properties of polyynes are viewed by chemists as pointers towards those of the *sp* hybridized allotrope, carbyne. In the second part, the intermolecular interactions in planar monocyclic carbon rings containing 4N and 4N+2 carbon atoms are studied. The dimers of aromatic C_{4N+2} systems with cumulenic structure and delocalized π systems showed least tendency towards dimerization with very few number of C···C interactions and low interaction energies. On the other hand, the C_{4N} rings with acetylenic structures with clear bond length alternation showed large number of C···C interactions and high magnitudes for interaction energies. The aromatic and antiaromatic features of the C_n rings are also discussed in terms of MESP and magnetic features.

CHAPTER 1

Introduction

Part A – Non-Covalent Interactions and Cooperativity

&

Part B - Computational Chemistry

Part A: Non-Covalent Interactions and Cooperativity

1.1 Introduction to Non-Covalent Interactions

Various kinds of inter-molecular interactions whose formation do not include the breaking or making of a chemical bond and hence are not energetically as demanding as covalent bonds are collectively known as non-covalent interactions. Different types of non-covalent interactions include the van der Waals interactions, hydrogen bonds, π-π stacking, cation-π interactions, anion-π interactions, dipole-dipole interactions, dispersion interactions etc. With the development of novel theoretical as well as experimental methods, several new types of interactions involving the main group elements such as halogen bonds, chalcogen bonds, pnicogen bonds, tetrel bonds etc. have been discovered relatively recently. Non-covalent inter-molecular interactions were first observed by van der Waals in 1870, who has shown that significant attractive interactions exist between real gas molecules [Hobza *et al*. 2006]. Among the different types of non-covalent interactions, hydrogen bonds have been the most widely studied. The importance of non-covalent interactions lies in widespread areas such as studies of biomolecules, supramolecular self assemblies, nanomaterials, catalyst interaction with surfaces, drug discovery, crystallography and even some chemical reactions. The study of non-covalent interactions has emerged as a warm area of research in recent years among the theoretical chemists. Enormous theoretical and experimental studies have been conducted on the nature, cause, strength and effects of non-covalent interactions and studies focusing on interactions involving the main group elements will be discussed herein.

1.1.1 Non-Covalent Interactions Involving the Main Group Elements

1.1.1.1 Hydrogen bond

An intermolecular hydrogen bond represented using the notation X–H···Y describes the interaction between the electron rich Y atom in one molecule with an electron deficient H atom in another molecule and connected to a more electronegative X than H [Hobza *et al.* 2006]. The atoms X and Y are called the hydrogen bond donor and acceptor atoms, respectively. The most electronegative atoms N, O and F are the most frequently encountered X and Y atoms in X–H···Y interactions [Pauling 1960]. Over the

years, a vast variety of hydrogen bonds, which do not lie under this definition of hydrogen bonds have been recognized. For instance, it has been identified that X and Y can be any atom more electronegative than hydrogen and that π electrons can also act as hydrogen bond acceptors [Desiraju and Steiner 1999; Kollman and Allen. 1972; Kumler 1935; Wulf *et al.* 1936]. In 2011, IUPAC introduced [Arunan *et al.* 2011] a definition for the term hydrogen bond applying the theoretical and experimental knowledge acquired over several years. According to this definition, 'the hydrogen bond is an attractive interaction between a hydrogen atom from a molecule or a molecular fragment X–H in which X is more electronegative than H, and an atom or a group of atoms in the same or a different molecule, in which there is evidence of bond formation.' This definition emphasizes the need for clear evidence for hydrogen bond formation such as a shift in stretching frequency or NMR chemical shift on the formation of an X–H···Y hydrogen bond.

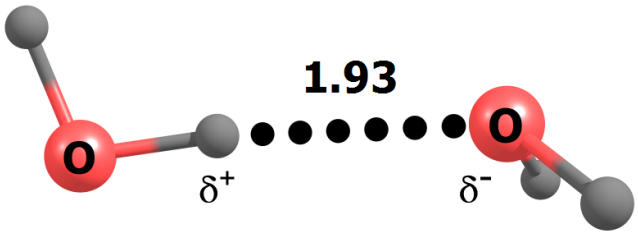

Figure 1.1 Representation of a hydrogen bond in water dimer with typical interaction distance in Å.

The hydrogen bonds vary in strength from about 1 to 40 kcal/mol, which can be classified as weak (< 4 kcal/mol), moderate (4 - 15 kcal/mol, classical hydrogen bonds) and strong (15 – 40 kcal/mol) depending on their strength [Parthasarathi *et al.* 2006]. These vital interactions are responsible for several phenomena observed in physics, chemistry and biology such as properties of water, structure of DNA and the structure and function of several other biologically relevant molecules such as proteins and enzymes. The hydrogen bond in a water dimer is shown in Figure 1.1 and the strength of this bond is ~ -5 kcal/mol.

1.1.1.2 Halogen Bond

An interaction of the type R–X···Y–Z, where X is a halogen atom covalently bonded to R and Y is an electron rich atom bonded to Z. The molecular unit R is the halogen bond donor moiety while Z is the halogen bond acceptor moiety. The halogen

bond interactions are highly directional and are observed along the extension of the R–X bond axis. The strength of a halogen bond shows a direct dependence on the polarizability of the X-atom and also on the electronegativity of the species R directly connected to X. The halogen bonding in $H_3N\cdots BrF$ complex is given in Figure 1.2 which gives ~ -19 kcal/mol energetic stabilization to the complex.

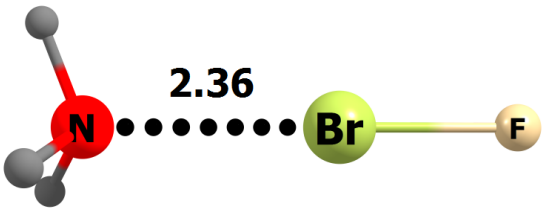

Figure 1.2 Representation of a halogen bond in $H_3N\cdots BrF$ complex with typical distance parameter in Å.

The halogen bonding is explained by Politzer and co-workers [Clark *et al.* 2007] by introducing the concept of 'σ-hole'. A σ-hole is a region of positive electrostatic potential on the outermost portion of the halogen's surface, centred on the R–X axis. The σ-hole on CF_3–X molecule (X = Cl, Br and I) is illustrated by Politzer's group [Clark *et al.* 2007] with the help of molecular electrostatic potential (MESP) maps (Figure 1.3). The three lone pairs on the X atom form a belt of negative MESP value around its central part, leaving a positive region, (σ-hole) along the z-axis (along the R–X axis). This will happen only if the reminder part of the molecule is electron withdrawing, and hence a σ-hole will be observed in CF_3–X and not in CH_3–X. Also, a σ-hole can be seen in CF_3–Cl, CF_3–Br and CF_3–I, but not in CF_3–F (Figure 1.3). This is because, in CF_3–F, the σ-hole will be neutralized by high electronegativity as well as significant *sp* hybridization of fluorine atom. The fact that the σ-hole is present on the extension of the C–X bond gives the characteristic near-linearity to a halogen bond [Politzer and Murray 2013]. In an attempt to simplify the concepts, Politzer and Murray have very well explained the halogen bonding and σ-hole in terms of physically observables such as geometries, interaction energies electrostatic potentials etc [Politzer and Murray 2013]. They have also shed light on the importance of halogen bonding in bio molecules, crystal engineering and drug design.

The importance of halogen···halogen interactions in the crystal structures of halogenated organic molecules were discussed earlier by Desiraju and Parthasarathy in 1989 [Desiraju and Parthasarathy 1989]. Crystals of organic halides were examined for the

number of these interactions and the numbers were compared with other inter atomic contacts. They concluded that the halogen···halogen interactions, except the F···F interactions are stabilizing in nature. In 1994, Desiraju and co-workers [Pedireddi *et al.* 1994] analyzed 794 crystal structures using Cambridge Structural Database (CSD) and 1051 X···X (I···I, Br···Br Cl···Cl, I···Br, I···CI, Br···CI, I···F, Br···F and CI···F) type interactions were found in them. Lommerse *et al* [Lommerse *et al.* 1996] observed an attractive interaction between carbon-bonded halogens (except F), C–X and electronegative atoms (oxygen and nitrogen) using CSD. These highly directional interactions (observed in the direction of the extended C–X bond axis) were found to have important role in holding the crystal structures of several molecules. The directionality of this interaction was explained as due to anisotropic distribution of electron density around the halogen nucleus. These interactions were stated to have an important role in the study of self assembly processes as revealed by Metrangolo and Resnati [Metrangolo and Resnati 2001].

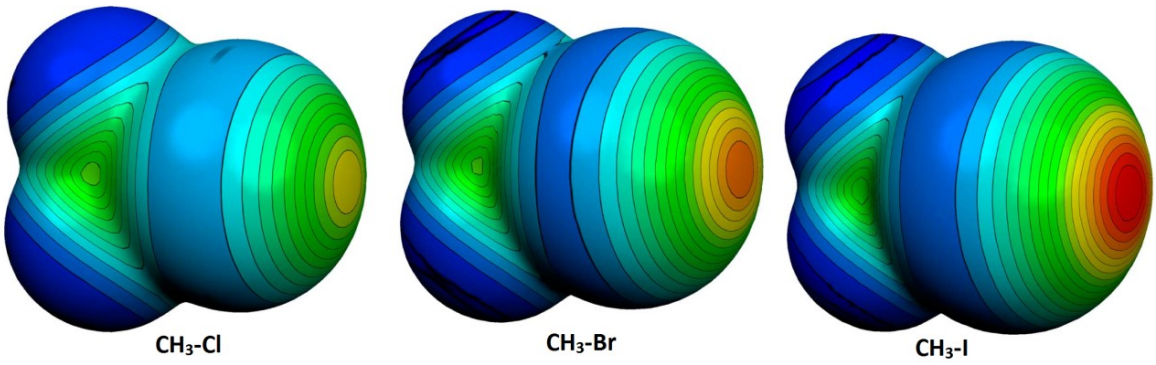

Figure 1.3 Maps of molecular electrostatic potential (in Hartrees, at the 0.001 electrons Bohr^{-3} isodensity surface) showing the σ-hole regions on CH_3–Cl, CH_3–Br and CH_3–I [Politzer and Murray 2013].

The importance of the use of halogen bonding as a substitute or compliment to hydrogen bonding in molecular recognition process and drug discovery has been illustrated by Metrangolo and Resnati [Metrangolo and Resnati 2008] in 2008. A. C. Legon, in 2010 compared the nature of hydrogen bond and halogen bond by comparing several hydrogen bonded complexes with their halogen bonded analogues [Legon 2010]. The author found that both type of interactions are analogous when formed in gas phase except that hydrogen bond tends to be non-linear. Hydrogen bonds and halogen bonds in the crystal structures as well as in the gaseous forms of dichloro acetic acid were analyzed by

Esrafili [Esrafili 2012]. An *et al* [An *et al.* 2013] compared halogen and hydrogen bonds in complexes formed by formamidine and hypohalous acids. Shaik and co-workers [Wang *et al.* 2014] studied 55 halogen bonded complexes and showed that the halogen bonds are mainly held by charge transfer interactions. They have also emphasized on the previous finding that halogen bonds are more directional compared to hydrogen bonds.

1.1.1.3 Chalcogen Bond

Wang *et al*. in 2009 [Wang *et al.* 2009b] introduced the term 'chalcogen bond' and described it as a 'sister non covalent interaction' to the halogen bond. In chalcogen bonds, chalcogens act as acceptors of electron density and is formed due to a misshaped electron clouds (formation of σ-hole) on a chalcogen atom, similar to halogen bond. Physical properties such as shifts in bond lengths, interaction energies and electron density features are similar in halogen and chalcogen bonds. The chalcogen bond in $H_2O\cdots SeCF_3CH_3$ complex is shown in Figure 1.4 and the interaction energy is ~ 4 kcal/mol.

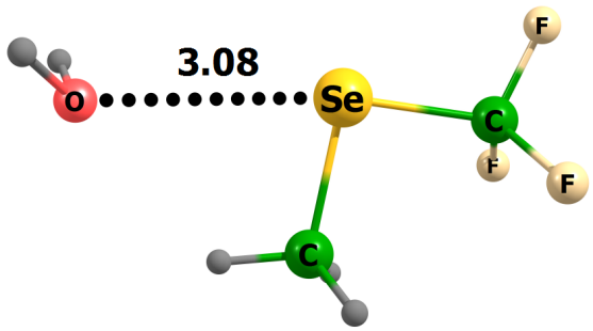

Figure 1.4 Representation of a chalcogen bond in $H_2O\cdots SeCF_3CH_3$ complex with typical interaction distance in Å.

Politzer and co-workers [Murray *et al.* 2007a] introduced the concept of σ-hole in divalently bonded chalcogens defined as regions of positive electrostatic potential on the outer surfaces of such atoms located along the extensions of their existing covalent bonds. A σ-hole is the strongest in an atom with the lowest electronegativity and highest polarizability. Electron withdrawing groups on a chalcogen atom can strengthen the σ-hole on it. These positive regions can interact with electron rich donor sites.

Extensive theoretical as well as experimental studies on interactions involving the oxygen group elements have been reported in the history of non-covalent interactions. Many of them include donor-acceptor type interactions in which divalent chalcogen atoms

act as donor and acceptor. Studies on directionality and strength of these interactions were reported even before the introduction of the σ-hole concept. In 1997, Rosenfield *et al* [Rosenfield *et al.* 1977] analyzed non bonded interactions with divalent sulphur in several crystal structures and found that nucleophiles tend to approach the sulphur atom along the extension of one of the covalent bonds while electrophiles approach through about 20^0 from the perpendicular to the X–S–Y plane. They predicted this observation to be an indication of the electron distribution and the orientation of highest occupied and lowest unoccupied molecular orbitals. Later, these studies were extended to include the nature of S···S interactions [Row and Parthasarathy 1981]. In most of the cases, the direction of approach of one of the two interacting sulphur atoms was similar to that of a nucleophile while that of the second sulphur was similar to that of an electrophile. A third type of S···S interaction was also observed, where, the direction of approach of both the sulphur atoms were similar, which was attributed to a crystallographic centre of symmetry. Biologically relevant intermolecular sulphur···oxygen and selenium···oxygen non-bonded interactions in thiazole and selenazole nucleosides were studied by Burling and Goldstein [Burling and Goldstein 1992]. These interactions resulted from electrostatic interaction between positively charged sulphur or selenium hetero atoms with negatively charged oxygen. Nagao *et al* [Nagao *et al.* 1998] have also detected such intramolecular S···O interaction in the crystal structures of (Acylimino) thiadiazoline derivatives using theoretical as well as experimental methods. Iwaoka *et al* [Iwaoka *et al.* 2002] analyzed the directionality of S···O interaction between divalent sulphur and carbonyl oxygen within and between molecules using Cambridge Structural Database and MP2 calculations. According to their findings, oxygen atoms tend to approach sulphur along the extension of the C–S or S–S bonds (σ_s^* direction) while sulphur atoms tend to approach oxygen either along the carbonyl plane (n_o direction) or from the vertical direction (π_o direction). Gleiter *et al* [Gleiter et al. 2003; Werz et al. 2002] reported the formation of tubular structures (that can function as host structures for guest molecules such as toluene) by self assembly of molecules, of which, directional chalcogen···chalcogen (S···S, Se···Se and Te···Te) interactions are the main driving force. The building blocks for these columnar structures were either large cyclic compounds or rigid open chain compounds. With the help of *ab initio* calculations on complexes with chalcogen···chalcogen interactions (from O···O to Te···Te), Gleiter's group [Bleiholder *et al.* 2006] showed that these interactions are the weakest for oxygen and the strongest for Te. For oxygen containing complexes, hydrogen

bonds were the dominant inter molecular forces. With increasing polarizability of the chalcogen atom, chalcogen··· chalcogen interactions became more and more significant. They have also shown that induction and dispersion contribute to the bonding interaction in all the cases but electrostatic effects are important only in the case of oxygen···oxygen interactions.

The functional organic molecule 7,9-di(thiophen-2-yl)-8Hcyclopenta[a]acenaphthylen-8-one (DTCPA) was recently found to have a very high conductance in its crystalline state, which was explained as due to the presence of non-covalent interactions such as S···S chalcogen bonding, π–π stacking and C–H···O hydrogen bonding interactions [Bai *et al.* 2014]. Recently, Azofra and Scheiner [Azofra and Scheiner 2014] studied complexes of SO_2 with several carbonyl containing molecules and found that in the global minima of all the complexes, monomers were primarily held together by S···O chalcogen bonds. The chalcogen bond here differs from the usual ones in that here, the charge transfer occurs from the lone pair on oxygen atom to the π^* antibonding SO orbital.

1.1.1.4 Pnicogen Bond

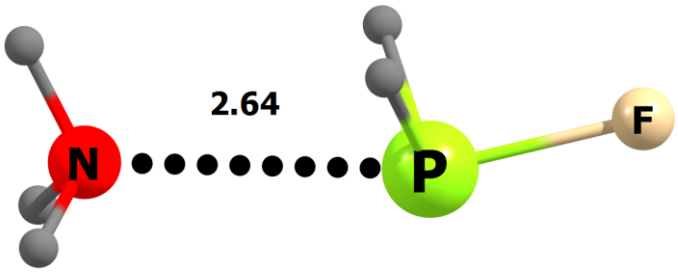

Figure 1.5 Representation of a pnicogen bond in $H_3N\cdots PFH_2$ complex with typical interaction distance in Å.

The term 'pnicogen bond' is brought in by Zahn *et al* [Zahn *et al.* 2011], observing the evidence for a P···P non-bonding interaction in the $^{13}C\{^1H\}$-NMR spectrum of an ortho-carbaborane derivative. This resulted from the interaction of the lone pair on one phosphorous atom with the positive region on the other, which can be enhanced by a better leaving group along the P···P axis (by improving the charge transfer from lone pair to σ^* orbital) or by a an electron-donating group perpendicular to the P···P bond axis. The formation of a region of positive electrostatic potential in an R_3X (X is a group V atom) molecule along the extension of R–X bonds and its possible interaction with nucleophiles

was predicted by Politzer and co-workers in 2007 [Murray *et al.* 2007b]. Several studies have been conducted on such interactions involving nitrogen group elements (pnicogens/pnictogens) in recent years. N···P pnicogen bond in $H_3N\cdots PFH_2$ is shown in Figure 1.5 and the strength of this bond is ~ 8 kcal/mol.

An interaction between nitrogen and phosphorous atoms in complexes of HSN with phosphines has been reported by Scheiner's group [Solimannejad *et al.* 2011]. Dispersion, charge transfer (from lone pair on nitrogen to the σ^* orbital of P–H bond) and electrostatic effects were regard as responsible for this interaction. In another study [Scheiner 2011b], Scheiner has shown that the global minimum of a $PH_3\cdots NH_3$ complex is the one with a P···N interaction. This directional interaction (nearly 180^0 between H–P and N) is a result of charge transfer from nitrogen lone pair to σ^* antibonding P–H orbital. A charge transfer from phosphorous lone pair to N–H σ^* orbital was also observed, but with a lesser magnitude. According to the author, there is no need of a positive σ-hole on the phosphorous atom and even two atoms of similar electrostatic potentials take part in such interaction. For instance, P···P interactions are observed in PH_3 homo dimer. Also, these interactions are not as sensitive towards the directionality as are the halogen bonds, which rely on σ-hole. Scheiner has also shown that of substituting the hydrogen atoms on phosphorous with an electron withdrawing halogen atom enhances the P···N interaction strength, but not beyond mono substitution [Scheiner 2011a]. Del Bene *et al* [Del Bene *et al.* 2011] studied the effect of mono substitution on P and N in complexes with P···N interactions. The complex $H_2FP{:}NFH_2$ showed the shortest P···N distance and highest interaction energy. The binding energies correlated with P···N distances and other bonding parameters obtained from quantum theory of atoms in molecules (QTAIM), natural bond orbital (NBO) and symmetry-adapted perturbation theory (SAPT) analyses. Both the nitrogen and phosphorous containing molecules acted as electron pair donors as well as acceptors, with phosphorous being a better donor and nitrogen being a better acceptor, which was also observed by Scheiner in his study on $PH_3\cdots NH_3$ complexes [Scheiner 2011b]. Pnicogen bonds between nitrogen on nitrile derivatives and Lewis bases are studied by Sanchez-Sanz *et al* [Sanchez-Sanz *et al.* 2013]. Molecular electrostatic potential maps showed positive regions on nitrile nitrogen atoms that are responsible for the interaction. According to Eskandari and Mahmoodabadi [Eskandari and Mahmoodabadi 2013], the P···N, P···P and N···N pnicogens bonds can be described as lump-hole interactions, where a lump is a 'region of

charge concentration and excess potential energy in the valence shell charge concentration (VSCC)' and a hole is a 'region of charge depletion and excess kinetics energy in the VSCC' on a chalcogen atom in a molecule. In their study based on Laplacian of electron density, they have also shown that NH_3 cannot act as an electron acceptor species due to the lack of a hole while NH_2F can. Guan and Mo [Guan and Mo 2014] studied the nature of charge transfer in pnicogen bonded complexes of X_nPH_{3-n} with NH_3. They have shown using block-localized wave function (BLW) based energy decomposition analysis that electron transfer and polarization energies are the major cause of pnicogen bonds. They found that charge transfer occurs from the HOMO of NH_3 (the lone pair) to LUMO of in $X_nPH_{3-n,}$ which is the σ^* P–X orbital in most cases, except in cases where X = NO_2 and CN, where the $d\pi^*$ (results from interaction between the π orbital of CN/NO_2 and d orbital of P) is the LUMO.

Scheiner analyzed the formation of hydrogen bonded and X···N (X = P, S, Cl and As) bonded complexes of NH_3 with PH_3, H_2S, HCl AsH_3 and NH_3 [Scheiner 2011c]. Except NH_3, all others formed X···N complexes. Whereas the properties of hydrogen bonded complexes showed a strong dependence on the nature of X, those of X···N bonded complexes were invariant to it. The linear nature of X···N interaction is found to maximizes charge transfer. This study considered complexes containing halogen, chalcogen and pnicogen bonds. In a review Scheiner compared pnicogen bonds with halogen and chalcogen bonds in detail [Scheiner 2013]. Halogen, chalcogen and pnicogens bonds are caused by electrostatic, induction and dispersion forces. A σ-hole on the extension of B–A (A is the acceptor atom and B is the atom directly bonded to it) bond serves as a positive charge attracting the donor atom. In pnicogens bonds, even in the absence of a well defined σ-hole, electrostatic forces play a key role. A charge transfer from the donor species to the antibonding σ^* B–A orbital is the second important factor responsible for these interactions. A liner D···A–B (D is the donor atom) arrangement facilitates the charge transfer and the presence of additional electrons in the anti bonding orbital elongates the B–A covalent bond. All these types of interactions are almost similar in energies, enhanced by an electronegative substituent on B atom and increased polarizability of the A atom and are directional in nature.

1.1.1.5 Carbon Bond and Tetrel Bond

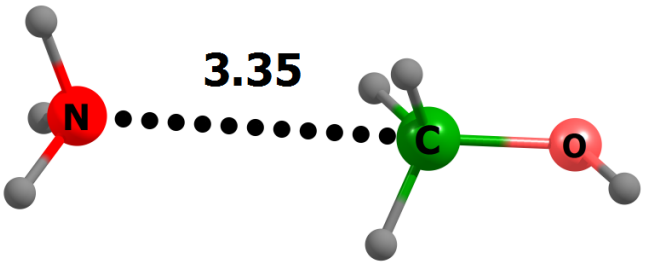

Figure 1.6 Representation of carbon bond in $H_3N\cdots CH_3OH$ complex with typical interaction distance in Å.

The term 'carbon bond' is introduced by Mani and Arunan [Mani and Arunan 2013] to represents the interaction between the positive region on carbon atom of CH_3X along the extension of X–C (X = F/O) covalent bond with electron rich centres such as O, S, F, Cl, Br, N or P. According to the authors, these interactions are important in S_N2 reactions and in hydrophobic interactions. The presence of a positive σ-hole on a covalently bonded group IV element was previously predicted and their interactions with some nucleophiles was shown by Politzer and co-workers [Murray *et al.* 2009] in 2009. The N···C carbon bond in $H_3N\cdots CH_3OH$ complex is represented in Figure 1.6. This type of a bond gives ~1 kcal/mol stabilization to the complex.

The name 'tetrel bonding' is given to the interaction of heavier group IV elements (tetrels) with electron rich centres by Bauzá *et al* [Bauzá *et al.* 2013]. The same group studied the formation of σ-hole between two CX_2 carbon atoms in cycloalkane molecules with a CX_2–CX_2 moiety (X = F, CN) [Bauzá *et al.* 2014]. These σ-holes are most exposed in the smallest ring (cyclopropane) and their interactions with electron donor species such as CN^-, OH^- and H_2CO are highly directional in nature. Evidences for the interaction between electron rich species with $(CN)_2C$–$C(CN)_2$ were found using Cambridge structural database and cyclopropane/butane with this moiety are predicted to be new supramolecular synthons.

In 2013, Politzer and co-workers [Bundhun *et al.* 2013] compared the relative σ-hole strengths on M (C, Si and Ge) and X (F, Cl, Br and I) atoms on F_3MX and H_3MX molecules and their interaction with lone pair on HCN. The positive value of the σ-hole was found to increase with the polarizability of M and X atoms and with the electronegativity of the remaining (F and H) atoms. The formation of a tetrel bond is

shown to be the preliminary stage of an S_N2 reaction by Grabowski [Grabowski 2014]. The formation of such an interaction results in a redistribution of electronic charge in favour of S_N2 reaction. Varadwaj *et al* [Varadwaj *et al.* 2014] termed non-covalent C···C the interaction between the σ-hole on a methylated carbon (CH_3–X) and CO molecule as 'dicarbon bond', which is analogous to the concept of a dihydrogen bond. Recently, Thomas *et al* [Thomas *et al.* 2014] have given experimental evidence for carbon bond using X-ray charge density analysis. McDowell reported an unusual anionic complex $[FX\cdots CH_3\cdots YF]^-$ (X, Y = Cl, Br), where the negative charge localized on the central carbon atom interact with the σ-holes formed on the X/Y atoms along the F/Y–X bond and the three hydrogen atoms lie perpendicular to the linear X···C···Y axis [McDowell 2014]. Ionic complexes of the type $X\cdots AH_3$–Y (X = F^-, Cl^-, Br^-, Li^+, Be^{2+}; A = C, Si, Ge; Y = F, Cl, Br) were also studied by McDowell and Joseph [McDowell and Joseph 2014], where the species were held together by ion-σ-hole, ion-dipole and polarization forces and the binding energies of the complexes were found to depend on the polarizability of the C–Y bond.

The electrostatics of halogen, chalcogen, pnicogen and tetrel bonds is studied in detail by Politzer *et al* [Politzer *et al.* 2013]. All these types of interactions are classified as σ-hole bonding. Representative examples given by Politzer *et al* [Politzer *et al.* 2013] for σ-hole regions on group IV-VII elements are given in Figure 1.7.

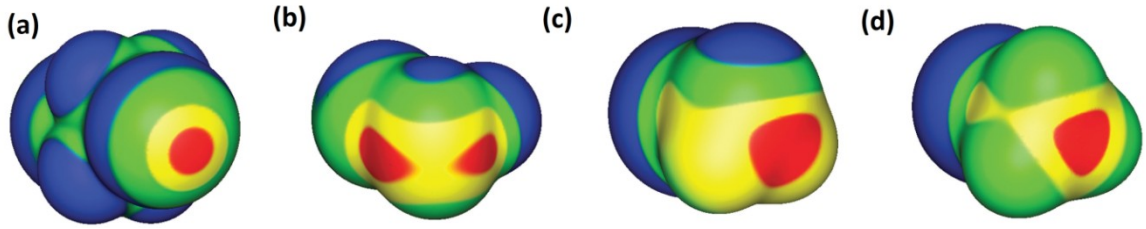

Figure 1.7 Regions of positive electrostatic potential (σ-holes) on (a) I of ICF_2CF_2I (b) Se of SeFCl (c) P of PH_2Cl and (d) Ge of GeH_3Br [Politzer *et al.* 2013].

1.1.2 The Phenomenon of Cooperativity

The phenomenon of cooperativity arises when there is interplay between two or more types of interactions and the resulting system behaves differently from expectations based on the properties of the individual interactions [Hunter and Anderson 2009]. Cooperativity can be positive or negative depending on whether one interaction favours or

disfavours the other. Binding of oxygen to haemoglobin is a typical example of cooperativity, where binding at each of the four binding sites increases the oxygen affinity of the remaining sites [Perutz 1989] (Figure 1.8(a)). Folding of biopolymers such as DNA and proteins with sharp melting transitions is another example for this phenomenon [Berg *et al.* 2007] (Figure 1.8(b)). Supramolecular self assemblies also show cooperative behaviour in their physical properties (Figure 1.8(c)). In the case of binding of oxygen to haemoglobin, once an oxygen molecule is bound at one of the binding sites, the oxygen affinity of the remaining sites increases and the forward reaction takes place spontaneously. Thus, if sufficient oxygen concentration is available, all the haemoglobin molecules will be in a fully bound. In such a case, the concentration of intermediates will be very low.

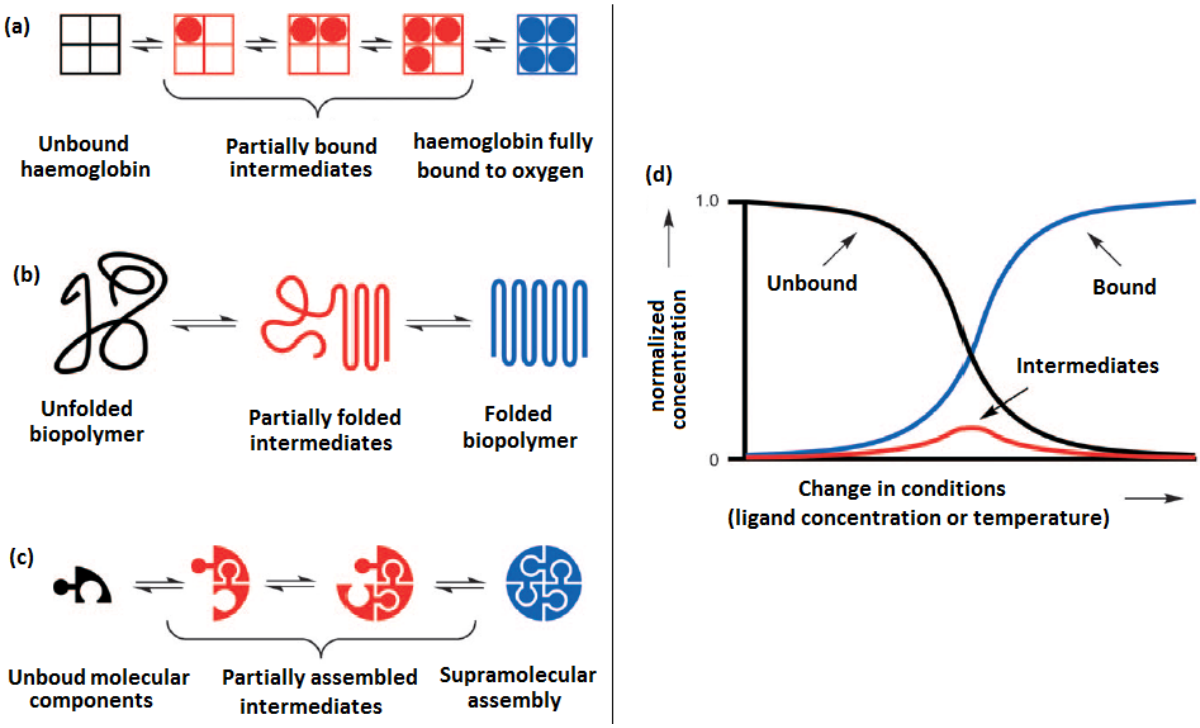

Figure 1.8 Illustration of cooperativity in (a) binding of oxygen to haemoglobin (b) protein folding (c) supramolecular self assembly and (d) speciation profile [Hunter and Anderson 2009].

Thus, the equilibria shown in Figure 1.8 shift with respect to conditions such as oxygen concentration (in the case of haemoglobin binding), temperature or the concentration of denaturant (in the case of folding of DNA or proteins) and concentration or temperature (supramolecular self assembly). If the system exhibits positive cooperativity, then, either all the components will be in a bound state or in a free state. There will be minimum

concentration of intermediates in a system showing positive cooperativity. This behaviour is called 'all or nothing' behaviour. This is illustrated in Figure 1.8(d), in which a switching between unbound and unbound states with respect to change in conditions and a very small concentration of intermediates can be clearly seen. This behaviour is the key consequence of positive cooperativity.

1.1.2.1 Cooperativity in Molecular Clusters

The phenomenon of cooperativity obliges the individual molecules to form molecular clusters. Cooperativity is a non-additive phenomenon, which means that, the binding energy of a cluster will be higher in a large molecular cluster than the sum of individual interactions in small clusters such as a dimer or trimer. Molecular properties such as vibrational frequencies, NMR chemical shifts and absorption spectra of molecular clusters are influenced by cooperativity. At the macroscopic level, this phenomenon influences properties such as tertiary and quaternary structure of proteins and solvation behaviour of liquids.

Numerous theoretical studies have been conducted for understanding the phenomenon of cooperativity in molecular clusters. In 1969, Del Bene and Pople published *ab initio* minimal basis calculations on water polymers [delBene and Pople 1969]. They showed that the hydrogen bonds in clusters of water molecules deviate considerably from additivity and hence are cooperative in nature. Later, in 1980, Clementi *et al* [Clementi *et al.* 1980] showed that the non additivity in the interaction energy of water trimers is not as high as that showed by Pople *et al*. they have also shown that the non-additivity is mainly caused by long range induction interactions. The influence of cluster formation on the infrared spectrum of acetonitrile have been shown by Mathieu *et al* [Mathieu *et al.* 1993] using *ab initio* methods. Using HF and MP2 levels of theory, Suhai [Suhai 1994] has shown that hydrogen bonding interactions in the molecular crystals of hydrogen cyanide and formamide are highly cooperative in nature. Using HF and including electron correlation of up to MP4 level, the same author studied the cooperativity in oligomers and infinite one-dimensional chains of water molecules and has shown that the hydrogen bonding in ice is highly cooperative in nature in various forms of ice [Suhai 1994]. Suhai [Suhai 1996] has also investigated infinite periodic networks of formamide crystals and found reduced bond lengths and increased binding energies in these networks compared to dimers, which is attributed to cooperativity. A study on the

hydrogen bond cooperativity in water clusters was reported by Liu *et al* [Liu *et al.* 1996], which helped in an increased understanding of solid and liquid water behaviour. Hydrogen bond cooperativity in water has been quantified by Cruzan *et al* [Cruzan *et al.* 1996]. S. S. Xantheas [Xantheas 2000] conducted studies on the cooperativity of hydrogen bond network in water clusters and explained the highest stability of cyclic homodromic (exhibiting donor - acceptor arrangements between all water molecules) clusters among the trimers, tetramers and pentamers of water molecules as due to cooperativity. In this work, water clusters were shown to behave non-additively and three-body terms were found to be the most important. Cooperative enhancement of hydrogen bond strength with size in clathrate-like water clusters including Buckminsterfullerene of water molecules has been shown by Ludwig and Appelhagen [Ludwig and Appelhagen 2005]. Studies on cooperativity of the clusters of water, N-methyl formamide and N-methyl acetamide and temperature dependence of their equilibrium properties were published by Ludwig *et al* [Ludwig 2000; Ludwig *et al.* 1995; Ludwig *et al.* 1997a; Ludwig *et al.* 1997b]. Most of these clusters showed non-additive behaviour. Using quantum cluster equilibrium (QCE) theory, they have also modelled the binding energies, cooperativity and geometries of supramolecular clusters in hydrogen bonded liquids including ammonia and alcohols [Huelsekopf and Ludwig 2000 ; Ludwig *et al.* 1998]. Cabaleiro-Lago and Ríos reported significant cooperativity in hydrogen bonded clusters of hydrazine containing up to four monomers [Cabaleiro-Lago and Ríos 1999]. Hydrogen bond cooperativity in hydrogen fluoride clusters containing up to eight monomers has been described by Rincón *et al* [Rincón *et al.* 2001] using MP2 and B3LYP methods. The cooperativity in hydrogen bonded cyclic clusters of methanol, ethanol, 1-propanol and methanethiol has been studied by Sum and Sandler [Sum and Sandler 2000]. The authors have attributed the strong cooperativity observed in these clusters to forces among the molecules such as interactions between molecules that are not directly hydrogen bonded due to the longer distances of interactions. The hydrogen bond cooperativity in $I^-.(CH_3OH)_n$ was detected by means of red shift in OH stretching frequency by Robertson *et al* in 2002 [Robertson *et al.* 2002]. Xia *et al* [Xia *et al.* 2003] found strong hydrogen bond cooperativity in trimers and tetramers of hydrazoic acid using B3LYP method. Kar and Scheiner compared the cooperativity of CH···O (in $(H_2CO)_n$ and $(HFCO)_n$) and OH···O (in $(H_2O)_n$) hydrogen bonds and found the former to be less cooperative than the latter. They found a direct dependence of the degree of cooperativity on the strength of the hydrogen bond. The role

of charge transfer in hydrogen bond cooperativity in *cis* - N-methylformamide oligomers has been studied by Tan *et al* [Tan *et al.* 2005]. The stability of multiple hydrogen bonded complexes has been studied by Xu *et al* [Xu *et al.* 2006] and they found cooperativity to be an important factor in determining the stability of clusters. Cooperativity between halogen bond and hydrogen bond in complexes of the type $H_3N\cdots XY\cdots HF$ (where X, Y = F, Cl, Br), each containing both the types of bonds have been examined by Li *et al* [Li *et al.* 2008]. Their studies showed significant cooperativity between these two types of interactions, which is greater than that between hydrogen bonds. Cooperative interplay between hydrogen and pnicogen bonds in $nFH:(H_2FP:NFH_2)$ complexes [Del Bene *et al.* 2012] and between hydrogen bonds and beryllium bonds in $(H_2O)nBeX_2$ complexes [Albrecht *et al.* 2012] (n = 1–3, X = H, F) has been analyzed. Manna and Mugesh [Manna and Mugesh 2012] have described how cooperative interplay between halogen and chalcogen bonds accelerates the regioselective deiodination of T4 and T3 hormones by *peri*-substituted naphthalenes. The cooperative effects of lithium and hydrogen bond in (LiCN)n and (HCN)n clusters respectively have been compared and the latter is found to be more significant in cyclic clusters [Esrafili *et al.* 2013]. Using molecular tailoring approach, Deshmukh *et al* [Deshmukh *et al.* 2008] quantified individual intramolecular hydrogen bonds and their cooperativity in carbohydrates. In the ternary complex $Y\cdots HCN\cdots HCN$, the $Y\cdots HCN$, bond dissociation energy was shown to be decreased compared to bare $Y\cdots HCN$ due to cooperativity [McDowell and Buckingham 2010]. The cooperativity in trimers containing HCN and water molecules has also been studied [Li *et al.* 2011]. Cooperative effects in metal ion-ammonia and metal ion-ammonia-water clusters have been studied by Orabi and Lamoureux [Orabi and Lamoureux 2013], where the metal ions used are Li^+, Na^+, K^+, Rb^+ and Cs^+.

De Meyts *et al* [De Meyts *et al.* 1973] presented experimental evidence for negative cooperativity by studying the binding of the polypeptide hormone, insulin, to its membrane, where they have shown that in the presence of unlabeled hormone, the dissociation rate of the tracer was increased.

King and Weinhold, using RHF and MP2 methods, have studied the cooperativity in linear HCN clusters [King and Weinhold 1995]. They have studied clusters containing up to nine monomers and have shown using their geometries, bond energies and other physical properties that strong cooperativity exists in them. The hydrogen bond energies, average dipole moments and the frequency and intensity of C–H stretching vibration

showed a drastic increase with chain length. They have also shown an increase in the strength of the hydrogen bond with the increase of chain length and also as we go towards the interior of a chain. Dannenberg *et al* have studied the cooperative phenomena in nitroaniline crystal [Turi and Dannenberg 1996], urea and thiourea crystals [Masunov and Dannenberg 2000], hydrogen bonded formamide chains [Kobko *et al.* 2001], and peptide chains [Wieczorek and Dannenberg 2003a; Wieczorek and Dannenberg 2003b]. The difference in crystal patterns in urea (chains, Figure 1.9 (a)) and thiourea (ribbons, Figure 1.9 (b)) despite their similar molecular structures was explained by Masunov and Dannenberg based on the phenomenon of cooperativity [Masunov and Dannenberg 2000]. The authors studied aggregates of thiourea and urea corresponding to both chain and ribbon patterns and found that though, in small cases, ribbon form was favoured for both the molecules, the cooperative interaction enable urea chains to overcome the energy of ribbon in the case of larger rings. However, in thiourea, the cooperativity is insufficient to overcome the interaction energy of the ribbon form.

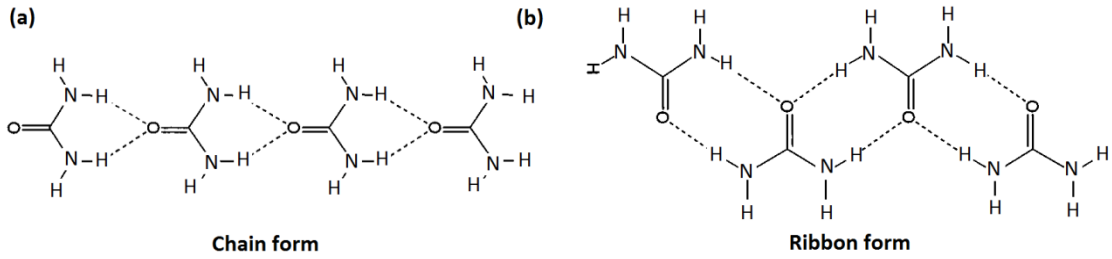

Figure 1.9 (a) Chain and (b) ribbon patterns of urea [Masunov and Dannenberg 2000].

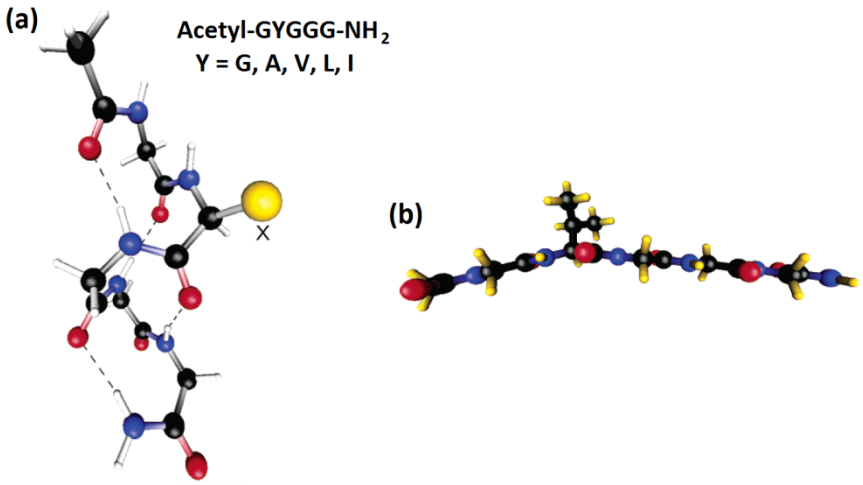

Figure 1.10 (a) Helical peptides and (b) β-strand (for $GVGGGNH_2$) [Wieczorek and Dannenberg 2003b].

Importance of hydrogen bond cooperative in peptide structures has been studied by several groups. Dannenberg *and* co-workers [Kobko *et al.* 2001] presented a data showing very strong cooperativity in linear hydrogen bonding chains of formamide molecules containing 2 - 10 monomers. The energy of each of the hydrogen bonds in a chain was found to depend on its position in the chain and the length of the chain. The strength of the central hydrogen bond in the decamer is found to be about 2.5 times stronger than that in the dimer, indicating a strong cooperativity.

Wu and Zhao studied poly glycines containing up to fourteen amino acids in β-strand, 2_7-ribbon, 3_{10}-helix, and α-helix forms using simple repeating unit approach and found that whereas β-strand, 2_7-ribbon show little evidence for cooperativity, the phenomenon is significant in 3_{10}-helices, and α-helices [Wu and Zhao 2001]. The same authors have also studied the cooperativity of parallel and antiparallel complexes (dimers, trimers etc.) of polypeptides having β-sheet confirmation [Zhao and Wu 2002]. Wieczorek and Dannenberg [Wieczorek and Dannenberg 2003b] compared the energies of five penta peptides in their 3_{10}-helical and β-strand forms. Whereas there are four hydrogen bonds in the helical structure, no hydrogen bond is present in the β-strand structure (Figure 1.10). The penta peptides showed a small preference towards 3_{10}-helix formation compared to β-strands due to the strain caused by the formation of hydrogen bonds in the former. According to the authors, the preference for 3_{10}-helix will increase with the number of monomers, as cooperativity would make the hydrogen bonds relatively stronger. This prediction was proved right by the same authors in another work [Wieczorek and Dannenberg 2003a] published in same year, in which they have studied the effect of hydrogen bond cooperativity and amino acid sequence on the relative energies of α-helices and β-strands. In the larger peptides (17-aminoacid peptides) they have studied, the hydrogen bond strength was sufficiently large to overcome the strain in the helical backbone due to cooperativity and hence α-helical forms were preferred over β-strands. Average hydrogen bond strengths in these larger peptides are about 3 times as high as in that in their previous study [Wieczorek and Dannenberg 2003b] containing smaller peptides. Thus, hydrogen bond cooperativity significantly affects helical stability. Ireta *et al* [Ireta *et al.* 2003] showed that due to cooperativity effects, the hydrogen bond in an infinite network of polyalanine in the α-helical structure is twice as strong as an isolated one. σ and π cooperativity in microsolvation of formamide clusters has been studied by

Blanco *et al* [Blanco *et al.* 2006]. Cooperativity is shown to be significant in linear chains of acetamide [Esrafili *et al.* 2008], methyl acetamide [Jiang and Wang 2009] and urea [Esrafili *et al.* 2011].

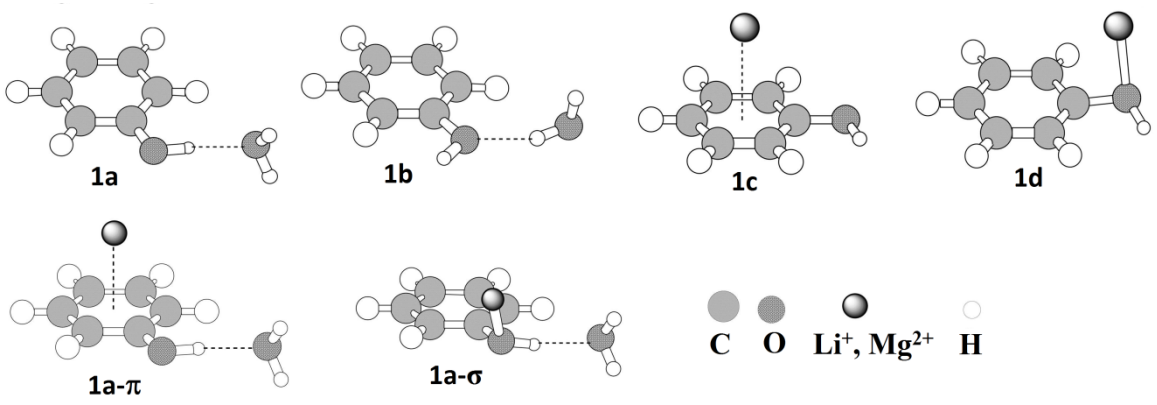

Figure 1.11 The phenol-acceptor, phenol-metal and metal-phenol-acceptor ternary complexes with positive cooperativity [Vijay *et al.* 2008].

Sastri *et al* have conducted several studies on the cooperativity on molecular complexes [Mahadevi and Sastry 2016]. These include studies on ternary complexes in which cation-π and hydrogen bonding interactions coexist [Vijay *et al.* 2008], water and their ionized counterparts [Neela *et al.* 2010], acetamide clusters where hydrogen bonding plays the major role [Mahadevi *et al.* 2011] etc. An extensive study showed cooperativity to be unimportant in benzene clusters where CH···π and π···π interactions coexist. They have very well described the cooperativity between cation…π and hydrogen bonding interactions using metal-phenol-acceptor systems where Li^+ and Mg^{2+} were the metal cations and H_2O, HCOOH and HCN were used as acceptors [Vijay *et al.* 2008]. The most stable type of phenol-acceptor complex is the one in which phenol acts as a hydrogen bond donor, named as 1a in Figure 1.11. The metal cation forms both π and σ complexes (named as 1a-π and 1a- σ respectively in Figure 1.11) with 1a. In these complexes, both hydrogen bond and cation…π interactions coexist. The authors quantified the extent to which the two interactions act in concert (E_{coop}) by comparing the overall interaction energy (ΔE_{APM}) and the three individual interaction energies ($\Delta E_{AP,}$ $\Delta E_{MP,\ and}$ ΔE_{MA}) as,

$$E_{coop} = \Delta E_{APM} - \Delta E_{AP} - \Delta E_{MP} - \Delta E_{M\text{-}A} \qquad \text{(Eq. 1.1)}$$

The degree of cooperativity was alternatively quantified by calculating the hydrogen bond strengths in the presence and the absence of the metal cations. The result of

these analyses was that the presence of the metal strengthened the phenol-acceptor hydrogen bond and hence, there exists a positive cooperativity.

Parra *et al* presented a few studies on three-centre hydrogen bonding interactions [Parra *et al.* 2005; Parra *et al.* 2001; Parra and Ohlssen 2008; Parra and Streu 2011]. Two types of three centre hydrogen bonds are possible *viz*. a two-donor type (H_1AH_2 type) and a two-acceptor type [Parra *et al.* 2001] (A_1HA_2 type). A study on the cooperativity of H_1AH_2 type hydrogen bonds in cyclic clusters of *cis-cis* isomer of carbonic acid) containing 3 – 9 monomers was published in 2005, in which, cooperative effects based on binding energies were studied [Parra *et al.* 2005]. They have shown using MP2 method and different basis sets that the interaction energy per bifurcated hydrogen bond shows a clear increase with the number of monomers. Cooperativity was also manifested using dissociation energies (which showed 77% enhancement with increase in size), vibrational frequencies and cooperativity factor in the bifurcated hydrogen bonding using the equation,

$$\text{Cooperativity factor} = \frac{(D_n - nD_2)}{(n-1)} \qquad \text{(Eq. 1.2)}$$

where D_n and D_2 are the dissociation energies of 'nmer' and dimer respectively

Parra and Ohlssen also studied the cooperativity of intra molecular bifurcated hydrogen bonds using substituted anthraquinone, dihydrophenazine and acridone as model systems [Parra and Ohlssen 2008]. Di and tetra substituted forms of these molecules serve as examples for bifurcated hydrogen bond donors, bifurcated hydrogen bond acceptors and both in the same molecule, respectively. The cooperative co existence of the two types of three-centre hydrogen bonds in the same molecule are shown based on their geometries, shifts in vibrational frequencies, changes in electron density in QTAIM analysis, and stabilization energies in NBO analysis. With the formation of the second hydrogen bonds, the change in geometries was such that the two three centre hydrogen bonds reinforced each other. Parra *et al* [Parra *et al.* 2001] have also demonstrated the phenomenon of negative cooperativity in complexes formed by *tans-trans* isomer of diacetamide with HCN and methanol. HCN and methanol formed both two centre and three centre hydrogen bonds with the diacetamide molecule in which, the latter acts as a double acceptor. The individual hydrogen bonds were stronger in the two centre hydrogen bond compared to in three centre bond, indicating negative cooperativity in the three centre hydrogen bonded complexes.

1.1.3 Computational Methods for Studying Non-Covalent Interactions

Accurate assessment of the nature and strength of non-covalent interactions is important in several research fields and is a challenge for computational chemists. Methods keeping a good balance between accuracy and computational demand are suitable candidates for studying non-covalent interactions. For locating suitable theoretical methods for the study of non-covalent interactions, several groups have conducted comparative studies using highly reliable theoretical or experimental results as benchmark values.

Johnson and DiLabio [Johnson and DiLabio 2006] conducted a study on the performance of several DFT methods and the MP2 method in calculating the binding energies of van der Waals dimers (dispersion dominated, dipole-dipole, hydrogen bonded etc.) using CCSD(T) results as benchmark. According to their results, the performance of DFT methods improved with the strength of non-covalent interactions. That is, most of the methods gave accurate results for the complexes with the strongest (hydrogen bonded) interactions. MP2 method did not perform well in the case of complexes with dispersion interactions. For complexes other than of dispersion type, MP2 and B971 showed good performance. Of all the methods studied, B971 DFT with 6-311++G(3df,3pd) basis set gave the best results. Mackie and DiLabio [Mackie and DiLabio 2011] calculated accurate binding energies of ten non-covalent dimers using different correlation corrected methods such as MP2, CCSD, CCSD(T) and correlation consistent basis sets such as aug-cc-PVDZ, aug-cc-PVTZ and aug-cc-PVQZ. According to their results, prediction of accurate binding energies are possible using a composite method, which combines CCSD(T)/aug-cc-pVDZ with energy corrections obtained using basis set extrapolated MP2 which uses aug-cc-pVQZ and aug-cc-pVTZ basis sets, provided all of the energies are calculated by averaging the counterpoise and non-counterpoise energies. Accurate benchmark values for binding energies, potential energy curves and inter molecular distances of complexes formed by benzene and a series of first- and second-row hydrides and rare gas atoms are set by Crittenden [Crittenden 2009] using CCSD(T) method and aug-cc-pvQZ basis set. This data is useful for the development and testing of accurate methods for the study of the aforementioned systems.

Reliable high accuracy databases on the properties of non-covalent complexes are necessary for testing the performance of existing methods as well as the development of

new methods to be applied in this area. Availability of accurate data on the nature and strength of intermolecular interactions in bio molecules such as DNA, RNA and proteins is of primary importance since such interactions play a key role in determining the structure and biological activity these molecules. Hobza and group conducted several studies using high accuracy methods such as CCSD(T) with a complete basis set (CBS) extrapolation on the intermolecular interactions in important bio molecules such as DNA bases [Dąbkowska *et al.* 2005; Hobza and Šponer 2002; Jurečka and Hobza 2003; Jurečka *et al.* 2004; Pérez *et al.* 2005; Šponer *et al.* 2004] and amino acids [Vondrášek *et al.* 2005]. These include high accuracy calculations of the stacking energy of homo-dimers of DNA bases [Hobza and Šponer 2002], binding energies of hydrogen bonded and stacked Guanine···Cytosine, Adenine···Thymine pairs and their derivatives [Jurečka and Hobza 2003], geometry and interaction energy of hydrogen bonded nucleic acid base pairs [Dąbkowska *et al.* 2005; Pérez *et al.* 2005; Šponer *et al.* 2004] and potential energy surface scan of cytosine dimer [Jurečka *et al.* 2004]. Due to increased demand from different groups for these high accuracy data, in 2006, they have published a benchmark database named after the initials of author names as JSCH-2005 [Jurečka *et al.* 2006]. This data set contains accurate MP2 and CCSD(T)/CBS geometries and interaction energies of more than 100 DNA base pairs, amino acid pairs and small model complexes and is meant to be used for testing the accuracy of less trustworthy computational methods such as DFT and semiempirical methods. Since working with this whole set of 100 complexes may not be always possible, a smaller test set containing high accuracy energy data for 22 model complexes (named as S22) is also included in the database. Later, the S22 database is modified by Sherrill and co-workers [Takatani *et al.* 2010] in which they extrapolated all the CCSD(T)/CBS calculations using larger basis sets, giving it an increased level of accuracy. They named the new data set as S22A and tested the performance of several methods using it. Among the methods they tested, B2PLYP-D showed the best performance. In 2011, Hobza's group [Řezáč et al. 2011] developed S66, the high accuracy CCSD(T)/CBS data set for 66 non-covalent complexes which contained 594 points including 66 equilibrium geometries and 528 dissociation curves. S66 database also contains 1056 interaction energies calculated at CCSD(T)/CBS level for nonequilibrium geometries. Several QM methods were tested against this database and SCS-MI-CCSD method was found to be a promising one. The database named X40 which includes high accuracy CCSD(T)/CBS interaction energies of different types of complexes formed by halogenated molecules is also created by Hobza

and co-workers [Řezáč et al. 2012]. They used this database for the analysis of the performance of several post-HF methods.

GMTKN30 database is developed by Goerigk and Grimme [Goerigk and Grimme 2010; Goerigk and Grimme 2011a] for application to main group thermo chemistry, kinetics, and non-covalent interactions. They have also carried out a benchmark study using this database [Goerigk and Grimme 2011b], which tested the performance of 47 different density functionals including LDA, GGA, meta-GGA, hybrid and double hybrid functionals. They recommended B97-D3 and revPBE-D3 at GGA level oTPSS-D3 at the meta-GGA level and PW6B95 along with DFT-D3 among the hybrid functionals. They found w-B97X-D method to be promising and discouraged the use of the popular B3LYP method. The GMTKN30 database was used by Hujo and Grimme [Hujo and Grimme 2011] for calculating the performance the van der Waals density functional VV10 by Vydrov and Voorhis [Vydrov and Van Voorhis 2010] and its GGA variants. The VV10 type functionals performed well for the complexes in the database with the accuracy being comparable to that of DFT-D3 functionals. In 2005, Zhao and Truhlar presented a benchmark database for non-covalently bound complexes [Zhao and Truhlar 2005a]. This database contained binding energy data of complexes having four types of non-covalent interactions *viz*. hydrogen bonding, charge transfer, dipole interactions, and weak interactions. 44 DFT methods were tested against this database and suitable method for each type of interactions were recommended. Among all the tested methods, MPWB1K showed the best performance.

The functionals PW6B95 and PWB6K were developed by Zhao and Truhler [Zhao and Truhlar 2005b] and their applicability was benchmarked against several datasets. Both these methods were found to be good for the study of non-covalent interactions. They have also done an extensive benchmark study [Zhao *et al.* 2006] using different benchmark databases on the applicability of M05 and M05-2X functionals developed by them as well as several other density functionals for the study of several properties including non-covalent Interactions. Based on this study, M05-2X, M05, PW6B95, PWB6K, and MPWB1K functionals were found to give good results for non-covalently interacting systems, among which, M05-2X showed the best performance for hydrogen bonding, $\pi\cdots\pi$ stacking and interaction of nucleobases. Using the JSCH-2005 dataset as benchmark, the performance of M05-2X [Zhao *et al.* 2006] and M06-2X [Zhao and Truhlar 2008b] density functionals by Zhao and Truhlar have been tested by Sherrill and co-

workers [Hohenstein *et al*. 2008]. They have also compared the performance of these functionals with that of the non-empirical DFT method, PBE [Perdew *et al.* 1996; Perdew *et al.* 1997] and also with PBE-D, in which, Grimme's empirical dispersion correction [Grimme 2006a] is also included. They found a better performance for PBE-D on an average for the entire database and for M06-2X when only stacking interactions are considered.

Eshuis and Furche carried out a benchmark study and showed that the random phase approximation (RPA), a parameter free density functional, is a promising method for thermochemical applications, especially if non-covalent interactions are involved [Eshuis and Furche 2011]. S22 database was used by Gkionis *et al* [Gkionis *et al.* 2009] for the study of the performance of Becke's half-and-half (BHandH) functional in studying non-covalent interactions. BHandH performed well for dispersion dominated systems while overestimated the energies of hydrogen bonded complexes. The performance of several commonly used low-order scaling density functionals and wave function methods in studying dispersion interactions (the most difficult class of non covalent complexes to be studied accurately) is studied by Granatier *et al* [Granatier *et al.* 2012]. The dimers of unsaturated systems (such as $\pi\cdots\pi$ interacting systems) are described more accurately by the methods they have studied.

Several studies were conducted for improving DFT methods to facilitate the calculation of weak interactions. Several early works attempted to include long range dispersion correction to DFT [Aiga *et al.* 1999; Görling *et al.* 1999; van Gisbergen *et al.* 1998; Ylva and Henrik 1999]. Wu *et al* [Wu *et al.* 2001] analysed the applicability of several GGA functionals in calculating the interaction energy of weakly interacting systems of different kinds including dispersion dominated (dimers of Ar, Kr and benzene), electrostatic (water dimer) and metal carbonyls. The results showed a dependence on the choice of the functional for dispersion dominated systems and carbonyls whereas for water dimer, DFT gave relatively accurate results. They also used a hybrid approach in which, the dispersion component of the interaction energy is obtained using a multi polar expansion of the dispersion energy while the remaining part is calculated using different DFT approximations, which gave better results. Benighaus *et al* [Benighaus *et al.* 2008], in an attempts to improve the calculation of dispersion interactions by double hybrid density functionals, introduced two new functionals namely B2-P3LYP and B2-OS3LYP, obtained by modifying B2-PLYP. These functionals were parameterized using the S22

database for non-covalent interactions and gave better results for dispersion complexes compared to the B2-PLYP functional. Steinmann and Corminboeuf introduced a dispersion correction [Steinmann and Corminboeuf 2010], which can be combined with electronic structure method without appropriate dispersion correction and applicable to any elements of the periodic table. The dispersion term they introduced was according to Becke and Johnson's exchange-hole dipole moment (XDM) formalism. Introduction of this dDXDM correction dramatically improved the results of many popular functionals. The functionals PBE0-dDXDM and PBE-dDXDM outperformed M06-2X and B2PLYP-D methods in their study. Grimme introduced the dispersion correction, which is described by a sum of damped inter atomic potentials and added to usual DFT energy. This, applied to the GGA functionals PBE and BLYP could be applied for the accurate description of several van der Waals complexes [Grimme 2004]. Both DFTD-BLYP and DFTD-PBE, despite having different behaviours with respect to closed-shell interactions gave better results, which is desirable. Later, the dispersion corrected GGA functional B97-D was introduced, which contained an improved version of the dispersion correction [Grimme 2006a]. The performance of B97-D was tested against several benchmark databases including those of non-covalent complexes. The results were found to be very good and comparable even to the CCSD(T) accuracy. Also, this dispersion correction is applicable to many commonly used density functionals. PW6B95 and PWB6K functionals were developed by Zhao and Truhlar [Zhao and Truhlar 2005b] and were benchmarked against several benchmark databases including the WI7/05 weak interaction database, which is a subset of the WI9/04 database [Zhao and Truhlar 2005a] developed by the same authors. A supplemental potential, with corrections for dispersion and hydrogen bond interactions and captures the difference between DFT and high accuracy methods was introduced by Song *et al* [Song *et al.* 2010]. The Van der Waals density functional, which depends on local density and its gradient is proposed by Dion et al [Dion *et al.* 2004]. The effective use of this functional along with Gaussian basis functions and revPBE exchange for the accurate estimation of weakly interacting systems is shown by Vydrov et al [Vydrov *et al.* 2008]. Two new functionals *viz*. M08-HX and M08-SO were introduced along with modified versions of M05-2X and M06-2X by Zhao and Truhlar [Zhao and Truhlar 2008b] of which, M08-HX showed better performance for non-covalent interaction energies. Burns *et al* [Burns *et al.* 2011] performed an extensive benchmark study on the performance of a number of density functionals, designed especially for the study of non-covalent interactions, such as dispersion corrected and exchange-hole dipole moment(XDM) theory

using CCSD/CBS databases such as S22 and JSCH as benchmark sets. They rated the performance of different types of functionals and basis sets for complexes with different types of non-covalent interactions such as hydrogen bonds and dispersion dominated interactions. Hobza *et al* [Marom *et al.* 2011] benchmarked the performance of different approaches for the treatment of dispersion correction including semi empirical meta-GGA and inter atomic pair wise correction methods using the S22 database. Their results show that the meta-GGA functionals count the dispersion correction to some extent, though long-range correction is missing. Zhang *et al* [Zhang *et al.* 2010] introduced a correction scheme named X1 to be applied to the popular B3LYP functional, which enables it to overcome its drawbacks such as size dependence and bad prediction of barrier heights, van der Waals systems and dissociation enthalpies. Torres and DiLabio [Torres and DiLabio 2012] introduced dispersion-correcting potentials (DCPs) for B3LYP, which is applicable to any computational packages. The B3LYP-DCP method was tested against S66, S22, and HSG-A benchmark databases and was found to outperform many other DFT methods designed for the study of non-covalent interactions. Since this approach was found to overestimate the dissociation energy of cumyloxyl radical due to an error in the carbon atom DCP, they developed a new C-DCP [DiLabio *et al.* 2013] which was proven to be very much efficient in the study of non-covalent interactions by studies using benchmark databases such as S66, S22B, HSG-A, and HC12.

Sun *et al* [Sun *et al.* 2010] compared the accuracy of nine density functionals in calculating the binding energy of complexes formed between dihydrogen and metal centres by using high accuracy CCSD(T) and MP2 results as benchmark values. Their studies have shown that the PBE and PW91 functionals reproduce the high accuracy values with a reasonable degree of accuracy whereas LDA functionals overestimate the binding energies. A benchmark study was conducted by Johnson *et al* [Johnson *et al.* 2013] to locate appropriate density functionals to be used with the exchange-hole dipole moment (XDM) dispersion model for larger systems with non-covalent interactions. According to their results, polarization-consistent 2 (pc-2) basis sets and its modified forms gave results that are comparable with aug-cc-pVTZ basis sets.

PART B: Computational Chemistry

1.2 Introduction to Computational Chemistry

Computational chemistry mainly deals with problems in chemistry such as predicting the feasibility of a reaction, tracking the mechanistic pathways of complicated reactions and understanding concepts such as molecular bonding, which cannot be studied using experimental techniques. Computational chemist use models, approximations such as perturbations, simplified functions and fitting parameters to solve chemical problems.

Computational chemistry methods can be broadly classified as quantum mechanical and molecular mechanical methods. In molecular mechanics, Newtonian force field is used. Here, molecules are represented by ball and spring model (atoms are considered as spherical balls and bonds are considered as springs) and deals with molecules containing thousands of atoms such as large biomolecules. The stretching, bending and torsion energies are calculated using the classical equations for spring motion. For calculating the non bonded interaction, the van der Waals attraction, repulsion and electrostatic interactions between each non bonded pair of atoms are taken into account. Molecular dynamics deals with motion of molecules such as vibrations and conformational transitions using Newton's laws of motion.

In quantum mechanics, any system can be represented by a wavefunction, which can be obtained by solving the Schrödinger wave equation. Any properties of the system can be obtained from the wavefunction, by using appropriate operators. However, the only wavefunction that could be exactly solved is that of hydrogen atom. For all other systems, we have to use some kind of approximations. In *ab initio* methods, no empirical parameters are used. It uses constants such as speed of light, mass and charge of electrons, Plank's constant etc. However, the *ab initio* methods (especially the high accuracy methods), though accurate, are highly computationally demanding and can only be used for small systems with a few atoms. Density functional theory (DFT) is another quantum mechanical method which expresses the total energy of a system as a functional of electron density. DFT keeps a good balance between accuracy and computational demand.

Semiempirical quantum chemical methods use approximations and use empirical parameters and are calibrated against dependable experimental and theoretical records.

Since these methods use approximations and hence require less computational power, these can be applied to large molecules. The methods mentioned here will be described in detail in the following sections.

1.2.1 Hartree - Fock (HF) Method

Getting an approximate solution for Schrödinger wave equation has been an important problem for the computation chemists. Hartree – Fock method is the most important type of *ab initio* calculation tried to solve this problem. In this method, the primary approximation is Born-Oppenheimer approximation. According to Born-Oppenheimer approximation, since the motion of electrons much is much faster compared to that of the nuclei, it is assumed that the nuclei are stationary compared to the electrons and hence electronic energy can be calculated separately by neglecting the nuclear kinetic energy and taking inter nuclear attraction to be constant. In HF approximation, in order to find out the total electronic energy of an N electronic system, if it is assumed that the electrons are non interacting and the total Hamiltonian can be expressed as a sum of one electron Hamiltonians as,

$$\mathscr{H} = \sum_{i=1}^{N} h(i) \qquad \text{(Eq. 1.3)}$$

Also, the wavefunction of the system can expressed as a simple product of single electron spin orbital wavefunctions as,

$$\Psi^{HP}(x_1, x_2 \ldots x_N) = \chi_i(x_1)\chi_j(x_2)\ldots\chi_k(x_N) \qquad \text{(Eq. 1.4)}$$

where x_i indicate spatial and spin coordinates of one electron wavefunctions, χ_i.

This N electron wavefunction will be an eigen function of the total Hamiltonian $\mathscr{H}$ given in Eq. 1.3 and the eigen value E is the sum of the energies of each of the spin orbitals in Ψ^{HP} (Eq. 1.5).

$$E = \varepsilon_i + \varepsilon_j + \ldots + \varepsilon_k \qquad \text{(Eq. 1.5)}$$

Such a many electron wavefunction is referred to as Hartree product. According the wave function $\Psi^{HP,}$ the probability of finding one electron at a position is independent of the position of other electrons. In other words, it is an un-correlated or independent electron

wavefunction. In reality, electrons repel each other due to Coulombic forces and their motion is correlated.

The Hartree product do not meet the requirement known as the antisymmetry principle (Pauli exclusion principle), according to which, a many electron wavefunction must be antisymmetric with respect to the interchange of the coordinates (both spatial and spin) of any two electrons. This requirement can be satisfied by expressing the wavefunction of an N electron system in the form of a Slater determinant as,

$$\Psi(\mathbf{x_1}, \mathbf{x_2}, ..., \mathbf{x_N}) = \frac{1}{\sqrt{N!}} \begin{vmatrix} \chi_i(\mathbf{x_1}) & \chi_j(\mathbf{x_1}) \dots & \chi_N(\mathbf{x_1}) \\ \chi_i(\mathbf{x_2}) & \chi_j(\mathbf{x_2}) \dots & \chi_N(\mathbf{x_2}) \\ . & . \quad \dots & . \\ \chi_i(\mathbf{x_N}) & \chi_j(\mathbf{x_N}) \dots & \chi_N(\mathbf{x_N}) \end{vmatrix} \qquad \text{(Eq. 1.6)}$$

where $(N!)^{-1/2}$ is a normalization factor. Interchanging the coordinates of any two electrons in this wavefunction will result in interchange of two rows of the determinant, which will alter the sign of the determinant. Hence, antisymmetry principle is satisfied. Also, two electrons occupying the same spin orbital will result in two columns being equal, which will make the determinant equal to zero and thus no more than one electron can occupy a spin orbital (the general statement of Pauli exclusion principle). In a Slater determinant, the motion of electrons with parallel spins is correlated (exchange correlation) but that of electrons with opposite spins is not. The antisymmetrized N electron wavefunction (the Slatter determinant) is represented using a short notation as,

$$|\Psi_0\rangle = |\chi_1 \chi_2 ..... \chi_N\rangle \qquad \text{(Eq. 1.7)}$$

where χ_i are different spin orbitals constituting the wavefunction (only the diagonal elements in the Slater determinant is used in the notation). According to the variational principle, the best wavefunction is the one giving the lowest possible energy.

$$E_0 = \langle \Psi_0 | \mathscr{H} | \Psi_0 \rangle \qquad \text{(Eq. 1.8)}$$

By the choice of appropriate spin orbitals χ_i, one can minimize the energy. By minimizing the energy, an eigen value equation called Hartree - Fock equation can be derived, which can be given as,

$$f(i)\chi(x_i) = \varepsilon\chi(x_i) \qquad \text{(Eq. 1.9)}$$

where *f(i)* is a one electron operator called the Fock operator, which has the form,

$$f(i) = -\frac{1}{2}\nabla_i^2 - \sum_{A=1}^{M}\frac{Z_A}{r_{iA}} + v^{HF}(i) \qquad \text{(Eq. 1.10)}$$

Here, $v^{HF}(i)$ is the average potential seen by the i^{th} electron due to the remaining electrons (Hartree – Fock potential). In HF approximation, the complicated many electron problem is replaced by a one electron problem, where, the potential due to other electrons is treated in an average way. The potential $v^{HF}(i)$ depends on the spin orbitals of the remaining electrons. That is, the Fock operator depends on its eigen function and hence can only be solved by an iterative procedure known as the Self Consistent Field (SCF) method. In this method, an initial guess of spin orbitals is taken from which $v^{HF}(i)$ is calculated, and then solving the eigen value equation (Eq. 1.9) for a new set of spin orbitals. Using this new set of spin orbitals, new field is calculated and the process is repeated until self consistency is reached. That is, until the field remains the same and the spin orbitals used to build the Fock operator remains same as its eigen functions.

Solving Eq. 1.9 gives a set of orthonormal spin orbitals $\{\chi_k\}$ (and a corresponding set of energies $\{\varepsilon_k\}$), of which, N lowest energy spin orbitals will be occupied (also known as hole spin orbitals) and the remaining are known as virtual, unoccupied or particle spin orbitals. The Slater determinant formed by N lowest energy spin orbitals forms the variational approach to ground state of the N electron system under consideration. Though infinite number of virtual orbitals is possible, the HF equation is usually solved by providing a finite set of K spatial basis functions $\{\phi_\mu(r)|\ \mu = 1, 2, \ldots, K\}$, corresponding to which, there will be 2K set of spin orbitals. Out of 2K spin orbitals, N will be occupied and 2K-N will be virtual orbitals. With increase in size of the basis set used, the energy expectation value of $E_0 = \langle\Psi_0|\hat{H}|\Psi_0\rangle$ decreases (comes closer to the actual ground state energy). With increase in the basis set size, the energy goes on decreasing, until a limit, called the Hartree – Fock limit is attained. A finite value of K usually gives energy above the Hartree – Fock limit [Szabo and Ostlund 1989].

1.2.2 Post Hartree-Fock Methods

An important limitation of the HF method is that it does not consider electron correlation (or considers the inter-electronic repulsion in an average way). There are several approaches for including electron correlation in HF method and these are collectively known as post Hartree-Fock methods. Configuration interaction (CI), multi-configurational self consistent field (MCSCF), Moller-Plesset perturbation theory (MPn, where n is the order of correlation), coupled cluster theory etc. are examples of post HF methods.

1.2.2.1 Møller-Plesset Methods

In this method, the difference between the exact Hamiltonian and the Fock operator is considered as a perturbation. The electron correlation effects are added by means of Rayleigh–Schrödinger perturbation theory. Møller-Plesset calculations are not variational. Some MP2 calculations give energies below the exact energy. A Møller-Plesset calculation of order n is denoted as MPn. Using a second order perturbation method (MP2), a minimal amount of correlation is added. MP3 and MP4 methods are also commonly used. The accuracy of an MP4 calculation is roughly similar to that of a CISD calculation. MP5 and higher order methods are not commonly used due to high computational demand (N^{10} complexity or even higher) [Young 2001].

The exact Hamiltonian operator, H can be written as,

$$H = H_0 + \lambda V \qquad \text{(Eq. 1.11)}$$

where H_0 is the Hartree-Fock Hamiltonian, V is the small perturbation and λ is a dimensionless parameter that controls the size of the perturbation.

The exact wavefunction and energy can be expanded in terms of HF wavefunction and energy as,

$$\Psi = \Psi_0 + \lambda\Psi^{(1)} + \lambda^2\Psi^{(2)} + \lambda^3\Psi^{(3)} + \ldots \qquad \text{(Eq. 1.12)}$$

$$E = E^{(0)} + \lambda E^{(1)} + \lambda^2 E^{(2)} + \lambda^3 E^{(3)} + \ldots \qquad \text{(Eq. 1.13)}$$

Substituting these expansions into the Schrödinger equation,

$$H_0\Psi_0 = E^{(0)}\Psi_0 \qquad \text{(Eq. 1.14)}$$

$$H_0\Psi^{(1)} + V\Psi_0 = E^{(0)}\Psi^{(1)} + E^{(1)}\Psi_0 \quad \text{(Eq. 1.15)}$$

$$H_0\Psi^{(2)} + V\Psi^{(1)} = E^{(0)}\Psi^{(2)} + E^{(1)}\Psi^{(1)} + E^{(2)}\Psi_0 \quad \text{(Eq. 1.16)}$$

and so on. Multiplying each of the above equations by Ψ_0 and integrating over all space gives the expression for n^{th} order perturbation theory (MPn) as follows

$$E^{(0)} = \langle \Psi_0 | H_0 | \Psi_0 \rangle \quad \text{(Eq. 1.17)}$$

$$E^{(1)} = \langle \Psi_0 | V | \Psi_0 \rangle \quad \text{(Eq. 1.18)}$$

$$E^{(2)} = \langle \Psi_0 | V | \Psi^{(1)} \rangle \quad \text{(Eq. 1.19)}$$

Thus, the Hartree-Fock energy, which can be written as

$$E_0 = \langle \Psi_0 | H_0 + V | \Psi_0 \rangle \quad \text{(Eq. 1.20)}$$

is actually the sum of the zeroth and first order energies

$$E_0 = E^{(0)} + E^{(1)} \quad \text{(Eq. 1.21)}$$

And the correlation energy can be written as,

$$E_{corr} = E_0^{(2)} + E_0^{(3)} + E_0^{(4)} + \ldots \quad \text{(Eq. 1.22)}$$

of these, the first term is the MP2 energy.

In terms of spin orbitals, a, b, i and j and their energy values ε_a, ε_a, ε_i and ε_j, the MP2 energy can be written as,

$$E_0^{(2)} = -\frac{1}{4} \sum_{ab}^{virt} \sum_{ij}^{occ} \frac{\left| \langle ab \| ij \rangle \right|^2}{\varepsilon_a + \varepsilon_b - \varepsilon_i - \varepsilon_j} \quad \text{(Eq. 1.23)}$$

The MP2 method is the most widely used MPn method. It gives satisfactorily accurate results and is computationally less demanding compared to other higher order methods. The MP4 and higher methods, though highly accurate, are computationally demanding and are not widely used.

1.2.2.2 Configuration Interaction (CI) Method

In this method, a multiple determinant wavefunction is used. A CI wavefunction considers determinants corresponding to excitation of electrons from occupied to unoccupied orbitals along with the ground state HF wavefunction. The CI methods are classified according to the number of excitations made to construct each new determinant. Configuration interaction single-excitation (CIS) calculation gives an approximation to the excited states of the molecule, not changing the ground-state energy. Single and double excited CI method (CISD) provides a ground state energy that has been corrected for correlation. Triple (CISDT) and quadruple (CISDTQ) excitation calculations are used only when very high accuracy is required. CI calculations are very accurate, but require very high CPU time (N^8 times complexity or worse). A CI calculation which considers all possible excitations is known as a full CI. This is rarely done due to the demand of immense amount of computational resources. A full CI calculation can yield exact quantum mechanical results [Young 2001].

The CI method is generally represented as a linear combination of the ground state and excited state determinants as,

$$\left|\Phi_0\right\rangle = c_0\left|\Psi_0\right\rangle + \sum_{ar} c_a^r \left|\Psi_a^r\right\rangle + \sum_{\substack{a<b \\ r<s}} c_{ab}^{rs} \left|\Psi_{ab}^{rs}\right\rangle + \sum_{\substack{a<b<c \\ r<s<t}} c_{abc}^{rst} \left|\Psi_{abc}^{rst}\right\rangle + ... \quad \text{(Eq. 1.24)}$$

In Eq. 1.24, the first term represents the HF wavefunction and rest of the terms represent singly, doubly, triply... n-tuply excited determinants with corresponding expansion coefficients. The indices a, b, c etc. signify the occupied and r, s, t etc. represent the virtual orbitals involved in the electron excitations.

1.2.2.3 Coupled Cluster

The couple cluster method is among the most robust levels of theory that can describe dynamic electron correlation. In a coupled cluster calculation, the total wavefunction is a linear combination of several determinants similar to CI. However, the method for choosing the wavefunction is different compared to CI. The various orders of CC expansion are CCSD, CCSDT etc. If the excitations are included successively, the energy provided by a coupled cluster method will be variational. Thus, CCSD calculations give variational energy, but CCD calculations do not [Young 2001].

In this method, the electron correlation is accounted by taking the HF molecular orbital method and constructing multi-electron wavefunctions using the exponential cluster operator

$$\psi_{CC} = e^{T} \psi_{HF} \quad \text{(Eq. 1.25)}$$

Here, Ψ_{HF} is a Slater determinant constructed from Hartree-Fock molecular orbitals and

$$e^{T} = 1 + T + \frac{1}{2}T^{2} + \frac{1}{6}T^{3} + \ldots = \sum_{k=0}^{\infty} \frac{1}{k!}T^{k} \quad \text{(Eq. 1.26)}$$

T is known as cluster operator which when acting on Ψ_{HF} produces a linear combination of excited Slater determinants and can be given as,

$$T = T_1 + T_2 + T_3 + \ldots + T_n \ldots \quad \text{(Eq. 1.27)}$$

where n is the total number of electrons and various T_i operators generate all possible determinants having i excitations.

1.2.3 Semiempirical Methods

Semiempirical methods are similar to *ab initio* methods in that they also use a Hamiltonian and a wavefunction. However, these methods do not use all the information available for a system for calculations. Usually, the semiempirical methods avoid the use of core electrons in the calculation. The correction for the avoided data is done by fitting some empirical parameters that are obtained either experimentally or from *ab initio* calculations. Semiempirical methods are much faster compared to *ab initio* methods. However, the results may not be very accurate and a very few properties can be predicted with accuracy. The empirical parameters for a particular set of compounds (for example amino acids) will give absurd results for a different set of compounds. Most of the semiempirical methods calculate a few properties such as geometry and energy. Some of them provide information on dipole moments, heats of reaction, ionization potentials, NMR chemical shifts, electronic spectra etc. in addition. A variety of semiempirical methods that use different approximations and are applicable to different classes of compounds are available. They vary from the simple Hückel theory to the most modern methods such as PM6, PM7 and dispersion included methods [Young 2001].

1.2.4 Molecular Mechanics (MM)

The molecules that are too big to be handled by *ab initio* or semiempirical methods can be modelled using molecular mechanics method where quantum mechanics is totally avoided. This method does not use a wavefunction or electron density in calculations. Instead, it uses force fields. A set of equations with their associated constants is called a force field. The constants are obtained either from *ab initio* calculations or from experimental data. The expression for energy in these methods consists of sum of simple classical equations describing different physical phenomena of the molecule such as bond stretching, bending, torsion, van der Waals and hydrogen bonding interaction, electrostatic interaction etc. Bond stretching is usually described as a harmonic oscillator, and sometimes by a Morse potential. For describing bond bending, a harmonic equation is used. Intermolecular forces (for e.g. van der Waals forces or hydrogen bonds) are often described using Leonard-Jones equations and bond rotation. Coulomb's law is used in most of the terms in calculating the energy of attraction or repulsion between charged centres (electrostatic term). Solvation effects are usually modelled using a dielectric constant.

The success of molecular mechanics force field method depends on the energy expression, data used for parameterization, and the experience and ability of the user with the strengths and weaknesses of each method. There are different kinds of force fields. Some of them are parameterized for a particular class of molecules (like nucleotides or proteins) and cannot give reasonable results for a different class of molecules. Some other classes of force fields are parameterized to give reasonable results for a wide variety of organic compounds. A few of them are parameterized for all the elements. Some commonly used force fields have been used in more than one software packages. AMBER (Assisted model building with energy refinement) and CHARMM (Chemistry at Harward molecular mechanics) are examples where the force field and the software package bear the same name [Young 2001].

1.2.5 Molecular Dynamics (MD)

Molecular dynamics method is used for modelling the time dependent behaviour (e. g. Brownian motion) of a molecular system. The energy of the system at a particular point of time is usually obtained using a molecular mechanics force field. In an MD

simulation, the first step is to select the initial geometry (not necessarily the optimized geometry) and initial velocities of the atoms (usually according to the Boltzman distribution at a particular temperature). The velocity distribution is normalized so that the net momentum of the entire system is zero. After that, the momentum (from mass and velocity) and forces (using expression for energy) on each of the atoms is calculated, generally, using an MM force filed. Next is the time step in which a new position for each atom after a short time interval is calculated using Newton's equations for motion. The new velocity and forces on each atom are also calculated. These iterations are repeated till the system reaches equilibrium. After reaching equilibrium, the coordinates obtained after every 5 to 25 steps are saved. The list of coordinates over time thus obtained is called a trajectory. The iterations are continued until data with enough accuracy is obtained. Information such as diffusion coefficients, vibrational motions and radial distribution can be obtained from the trajectory of the system obtained from the iterations.

A force field suitable for the problem under study is usually used (e. g. GROMOS or OPLS force fields for bulk systems). The choice of time step also plays an important role in the accuracy of the simulations. A time step that is too large or too small is not acceptable. Usually, a time step that is one order of magnitude less than the time period of the shortest motion (period of vibration or time between successive collisions) is used. The degree of accuracy of the methods selected can be predicted by comparison with experimental values for the properties studied [Young 2001].

1.2.6 Density Functional Theory (DFT)

For a system consisting of N electrons, the total wavefunction will be a function of 3N coordinates. As the number of electrons increases, the wavefunction becomes too complicated to work with. The calculations would be simpler if we could use a physically observable quantity than using the wavefunction of a molecule. In DFT, electron density is the physically observable quantity that makes this possible. Electron density, ρ, can be defined as the number of electrons in the unit volume around a point in space around r. Electron density, when integrated over all space, gives the total number of electrons, N.

$$\mathrm{N} = \int \rho(\mathbf{r})\mathrm{d}\mathbf{r} \qquad \text{(Eq. 1.28)}$$

The total Hamiltonian depends on the positions and atomic numbers of nuclei and the total number of electrons. The nuclear positions correspond to the maxima in electron

density. Information on nuclear atomic number can also be obtained from electron density using the expression,

$$\left.\frac{\partial\overline{\rho}(r_A)}{\partial r_A}\right|_{r_A=0} = -2Z_A\rho(r_A) \qquad \text{(Eq. 1.29)}$$

for any nucleus A located at an electron density maximum, $r_{A,}$

Here, Z_A is the atomic number of the nucleus A, r_A is the radial distance from A and $\overline{\rho}$ is the spherically averaged density. Thus, the number of electrons, nuclear positions and the atomic numbers can be obtained from the electron density. This suggests that electron density could be used for predicting the energy and other properties of a system [Cramer 2004].

1.2.6.1 Thomas-Fermi DFT

The total energy can be separated into kinetic and potential energy components. The potential energy can be calculated using the classical mechanics. The electron-nuclear attraction,

$$V_{ne}[\rho(\mathrm{r})] = \sum_{\mathrm{k}}^{\text{nuclei}} \int \frac{\mathrm{Z_k}}{|\mathrm{r} - \mathrm{r_k}|}\rho(\mathrm{r})d\mathrm{r} \qquad \text{(Eq. 1.30)}$$

The self-repulsion of a classical charge distribution,

$$V_{ee}[\rho(r)] = \frac{1}{2}\iint \frac{\rho(r_1)\rho(r_2)}{|r_1 - r_2|} \qquad \text{(Eq. 1.31)}$$

where r_1 and r_2 are dummy integration variables running over all space.

Kinetic energy of a continuous charge distribution can be found out by introducing the concept of 'Jellium.' Jellium is a system composed of an infinite number of electrons moving in an infinite volume of space with a uniformly distributed positive charge. This distribution of electrons is also known as uniform electron gas. This possesses a constant non-zero density. In 1927, Thomas and Fermi, using fermion statistics, derived the kinetic energy of this system as,

$$T_{ueg}[\rho(r)] = \frac{3}{10}(3\pi^2)^{2/3} \int \rho^{5/3} dr \qquad \text{(Eq. 1.32)}$$

The T and V terms given in Eq. 1.30 - 1.32 are functions of ρ(r), which itself is a function of three dimensional spacial coordinates. Hence, T and V are 'functionals' of electron density and are called as 'density functionals.'

The Thomas-Fermi equations, together with a variational principle represent the first attempt to define density functional theory. Here, the energy is computed without using a wavefunction. However, these assumptions are inaccurate and find no use in modern chemistry. The main disadvantage is that Eq. 1.31 for calculating inter-electronic repulsion ignores electronic exchange and correlation. A concept called 'hole function' is used for correcting the energetic errors caused by the assumption of classical behaviour.

$$\left\langle \psi \left| \sum_{i<j}^{electrons} \frac{1}{r_{ij}} \right| \psi \right\rangle = \frac{1}{2} \iint \frac{\rho(r_1)\rho(r_2)}{|r_1 - r_2|} dr_1 dr_2 + \frac{1}{2} \iint \frac{\rho(r_1)h(r_1; r_2)}{|r_1 - r_2|} dr_1 dr_2 \qquad \text{(Eq. 1.33)}$$

In Eq. 1.33, LHS is the exact quantum mechanical inter-electronic repulsion. The second term in RHS is the correction term using hole function h associated with ρ ($h(r_1;r_2)$). The notation $h(r_1;r_2)$ implies that the hole is concentrated on the position of electron 1 and is evaluated from there as a function of the coordinates of r_2. Hence, h is a function of r_2 and r_1.

By construction, HF theory exactly evaluates the exchange energy. But the calculation of these four-index integrals is time consuming. In an attempt to speed up the HF calculation, Slater proposed to ignore the correlation correction to classical inter-electronic repulsion and consider only the exchange corrections since the latter is larger compared to the former. Slater proposed the exchange hole about any position as a sphere of constant potential with its radius depending on the magnitude of the density at that position. Within this approximation, exchange energy, E_x is determined as,

$$E_x\rho(r) = -\frac{9\alpha}{8}\left(\frac{3}{\pi}\right)^{1/3} \int \rho^{4/3}(r) dr \qquad \text{(Eq. 1.34)}$$

In 'Slater exchange', the value for the constant α is 1

Bloch and Dirac, in 1930 derived a similar expression starting from the uniform electron gas, with α = 2/3. This expression, along with Eq. 1.30 - 1.32 forms the Thomas-Fermi-Dirac model. This model also fails to see any modern use.

Using different derivations, different values for α were calculated for Eq. 1.34. These computations are termed as X_α calculations or Hartree-Fock-Slater calculations in the older literature. Empirical analysis in different systems suggest that α = 3/4 is more accurate than either α = 1 or α = 2/3. Though not used widely, this particular DFT methodology finds occasional use, particularly within the inorganic chemistry. Though the above mentioned methods were too simple compared to wavefunction methods and were widely used, especially in solid state physics, they produced large errors in molecular calculations and hence could produce no impact on chemistry. This situation was changed when Hohenberg and Kohn proved two theorems critical for establishing DFT as an important quantum chemical methodology [Cramer 2004].

1.2.6.2 The Hohenberg-Kohn Existence Theorem

The electrons interact with one another and with an 'external potential' that is, the nuclei. The Hohenberg-Kohn theorem assumes a dependence of energy on the ground state electron density of a system. Since the total number of electrons can be obtained by integrating the electron density, the quantity that remains to be found out is the external potential. The electron density determines the external potential, and thus, the Hamiltonian and thus, the wavefunction. Since the Hamiltonian determines all the excited state wave functions along with the ground state wave function, there is a tremendous amount of information coded in the density [Cramer 2004].

1.2.6.3 The Hohenberg-Kohn Variational Theorem

Hohenberg and Kohn showed that the electron density obeys a variational principle. Consider a candidate density which integrates to give the total number of electrons N and is related to a candidate wave function ψ_{cand} and a candidate Hamiltonian H_{cand}. Then, the energy expectation value can be calculated as given in Eq. 1.35, which, according to the variational principle, must be greater than or equal to the true ground state energy, E_0.

$$\langle \psi_{cand} | H_{cand} | \psi_{cand} \rangle = E_{cand} \geq E_0 \qquad \text{(Eq. 1.35)}$$

Thus, we have to choose different densities, with the one providing the lowest one being the closest to the correct. This method has two limitations. First, there is no prescription on how to choose an improved density and second, this method does not avoid the complicated process of solving the Schrödinger wave equation. An attempt for directly obtaining energy from density without using the wave function was first made in 1965 [Cramer 2004].

1.2.6.4 Kohn-Sham Self Consistent Field Methodology

A practically applicable form of DFT was developed by Kohn and Sham (1965) who developed it similar to HF method. They took the assumption that the electrons are non interacting in nature. Then, the Hamiltonian could be expressed as a sum of one electron operators. The eigen functions will be Slater determinants of individual one electron orbitals and the eigen values will be the sum of one electron eigen values.

A fictitious density of non interacting electrons is taken as starting point. The initial density chosen should be similar to that of a real system where the electrons do interact. Next, total energy functional is divided into specific components as,

$$E[\rho(r)] = T_{ni}[\rho(r)] + V_{ne}[\rho(r)] + V_{ee}[\rho(r)] + \Delta T[\rho(r)] + \Delta V_{ee}[\rho(r)] \qquad \text{(Eq. 1.36)}$$

where the terms on RHS represent respectively the kinetic energy of non interacting electrons, nuclear electron interaction, classical electron-electron repulsion, the correction to the kinetic energy due to the interacting nature of the electrons and all non classical corrections to the electron-electron repulsion energy.

The total kinetic energy will be the sum of individual kinetic energies, if the electrons are non interacting. Then, Eq. 1.36 can be rewritten as,

$$E[\rho(r)] = \sum_{i}^{N}\left(\left\langle \chi_i\left|-\frac{1}{2}\nabla_i{}^2\right|\chi_i\right\rangle - \left\langle \chi_i\left|\sum_{k}^{nuclei}\frac{zk}{|r_i - r_k|}\right|\chi_i\right\rangle\right) + \sum_{i}^{N}\left\langle \chi_i\left|\frac{1}{2}\int\frac{\rho(r')}{r_i - r'}dr'\right|\chi_i\right\rangle + E_{xc}[\rho(r)] \qquad \text{(Eq. 1.37)}$$

where, N is the number of electrons.

The density for a Slater determinantal wave function is

$$\rho = \sum_{i=1}^{N}\langle \chi_i|\chi_i\rangle \qquad \text{(Eq. 1.38)}$$

In Eq. 1.37, the terms ΔT and ΔV_{ee} are represented by the term E_{xc}, known as the exchange-correlation energy. This term also includes the correction for the classical self interaction energy along with the effects of quantum mechanical exchange and correlation.

The orbitals χ that minimize the value of E in Eq. 1.37 satisfy the pseudo eigen value equations.

$$h_i^{KS}\chi_i = \varepsilon_i\chi_i \qquad \text{(Eq. 1.39)}$$

where the Kohn-Sham one electron operator is defined as,

$$h_i^{KS}\chi_i = -\frac{1}{2}\nabla_i^2 - \sum_k^{nuclei}\frac{z_k}{|r_i - r_k|} + \int\frac{\rho(r')}{r_i - r'}dr' + V_{xc} \qquad \text{(Eq. 1.40)}$$

and

$$V_{xc} = \frac{\delta E_{xc}}{\delta\rho} \qquad \text{(Eq. 1.41)}$$

Vxc is a functional derivative. It is the one electron operator for which the expectation value of the KS Slater determinant is Exc. The orbitals χ must give the exact density. That is, the minimum must correspond to reality. These orbitals form the Slater determinantal eigenfunctions for the separable non interacting Hamiltonian defined as the sum of the Kohn Sham operators as given in Eq. 1.42.

$$\sum_i^N h_i^{KS}\left|\chi_1\chi_2.....\chi_N\right\rangle = \sum_i^N \varepsilon_i\left|\chi_1\chi_2.....\chi_N\right\rangle \qquad \text{(Eq. 1.42)}$$

Kohn Sham (KS) orbitals are determined by expressing them within a basis set of functions $\{\varphi\}$, and determining the individual orbital coefficients by a solution of a secular equation analogous to that employed for HF theory [Cramer 2004].

1.2.6.5 Exchange Correlation Functionals

The exchange correlation term E_{xc}, includes the correction for classical electron-electron repulsion and the kinetic energy difference between the fictitious non interacting system and the real system. Most of the modern functions compute this term explicitly, by an attempt to construct a hole function or use some empirical parameters which include

some kinetic energy correction if they are based on experiment. The functional dependence of E_{xc} on the electron density is expressed in terms of 'energy density ε_{xc}', which depends on the electron density as

$$E_{xc}[\rho(r)] = \int \rho(r)\varepsilon_{xc}[\rho(r)]dr \qquad \text{(Eq. 1.43)}$$

E_{xc} is the sum of individual exchange and correlation contributions. Whereas electron density is a per unit volume density, energy density is a per particle density. For e.g. the Slater exchange energy density is (comparing with Eq. 1.34)

$$\varepsilon_x [\rho(r)] = -\frac{9\alpha}{8}\left(\frac{3}{\pi}\right)^{1/3} \rho^{1/3}(r) \qquad \text{(Eq. 1.44)}$$

Effective radius,

$$r_s(r) = \left(\frac{3}{4\pi\rho(r)}\right)^{1/3} \qquad \text{(Eq.1.45)}$$

which is defined such that exactly one electron would be contained within the sphere defined by the effective radius [Cramer 2004].

1.2.6.6 Local Density Approximation (LDA)

Initially, the term LDA was used to denote any DFT where the value of ε_{xc} at any position could be computed from the value of ρ at that position. Functionals derived from uniform electron gas fit to that concept. For LDA method, value of empirical constant α in Eq. 1.34 is 2/3, for Slater (S) is 1 and for X_α is 3/4.

Calculation of the correlation energy density functional was difficult even for the uniform electron gas. Alder, in 1980, calculated the total energy for uniform electron gas using quantum Monte Carlo methods with high accuracy for several systems. They calculated the correlation energy of these systems by subtracting the analytical exchange energy from the total energy. Vosko, Wilk and Nusair (1980) developed local density functionals fitting to these results.

Among the various fitting schemes proposed by Vosk, Wilk and Nusair, VWN and VWN5 are the most widely used methods. LSDA (expanded as 'local spin density approximation', denotes LDA functionals in which spin polarization is also included) functionals using Slater exchange and VWN correlation are referred to as SVWN method.

None of the terms in the equation suggested by them can be assigned to a physical meaning and this shows the complexity of correlation energy term. It also shows the extent to which some of the DFT methods that include empirically optimized constants and functional forms can be described as semiempirical methods.

The first step involve in an LDA calculation is to choose a basis set. There are different basis sets involved in a DFT calculation. The Kohn Sham orbitals are formed from a basis set. The density ρ(r) is expanded in terms of another 'auxiliary' basis set, i.e.,

$$\rho(\mathrm{r}) = \sum_{\mathrm{i=1}}^{\mathrm{M}} ci\Omega i(\mathrm{r}) \qquad \text{(Eq. 1.46)}$$

After choosing the molecular geometry, the kinetic energy, nuclear attraction and the overlap integrals are evaluated. From the guess density, V_{xc} is constructed, and the remaining integrals are evaluated in each KS matrix element. After this point, the KS and HF SCF procedures are identical. The secular equation is solved and the new orbitals are determined from the solution. The density, which is obtained from these orbitals, is compared to the density from the preceding iteration. After achieving the convergence of SCF, the energy is calculated from the final density. If geometry optimization is required, it is checked whether the structure corresponds to a stationary point [Cramer 2004].

1.2.6.7 Density Gradient and Kinetic Energy Density Corrections

1.2.6.7.1 *Exchange Corrections*

In these methods, in order to improve the results, the correction energy is calculated in terms of electron density as well as its gradient. Density functionals that depend on both the density and the gradient of density are known as generalized gradient approximation (GGA). In most of the cases, correction term is added to the LDA functional.

$$\varepsilon_{\mathrm{x/c}}^{\mathrm{GGA}}[\rho(\mathrm{r})] = \varepsilon_{\mathrm{x/c}}^{\mathrm{LSD}}[\rho(\mathrm{r})] + \Delta\varepsilon_{\mathrm{x/c}}\left[\frac{|\nabla\rho(\mathrm{r})|}{\rho^{4/3}(\mathrm{r})}\right] \qquad \text{(Eq. 1.47)}$$

The first popular GGA exchange functional was developed by Becke and is abbreviated as 'B'. CAM, FT97, O, PW, mPW and X (which is a combination of B and PW) are some other GGA exchange functionals similar to B functional. The 'B' exchange functional contains an empirical parameter optimized by fitting to the exactly known

exchange energies of the noble gas atoms. P, PBE, mPBE, LG and B86 are some GGA functionals with no empirically optimized parameters [Cramer 2004].

1.2.6.7.2 Correlation Corrections

The popular GGA correlation functional LYP by Lee, Yang and Parr does not correct the LDA expression. This functional calculates the correlation energy as a whole and contains four empirical parameters that fit to the He atom. B86, P86 and PW91 correlation functionals contain corrections to correlation energy density following Eq. 1.47 and contain no empirical parameters. Specification of an exchange-correlation correction is done by interconnecting the two acronyms in that order. Thus, BLYP method combines Becke's exchange and LYP correlation [Cramer 2004].

1.2.6.8 Meta-GGA Functionals

For further improvement of the functionals, second derivative (the Laplacian) of the density is taken into account. Such functionals are termed as meta-GGA functionals. Exchange functional by Becke and Roussel was the first to have such dependence. Proynov, Salahub and co-workers developed meta-GGA correlation functional (LAP). Though it is difficult to calculate the Laplacian of the density, the meta-GGA functionals give somewhat improved results over GGA analogues. A meta-GGA formalism that is numerically more stable is to include a dependence on the kinetic energy density, τ in the exchange-correlation potential, which is defined as,

$$\tau(r) = \sum_{i}^{occupied} \frac{1}{2}\left|\nabla\psi_i(r)\right|^2 \qquad \text{(Eq. 1.48)}$$

where the ψ_i are self-consistently determined from Kohn-Sham orbitals

The BR functional includes dependence on both Laplacian of density and τ. However, most of the developers tend to include only the dependence of τ in their functionals. B95, B98, τHCTH, PKZB, KCIS, VSXC and TPSS are some meta-GGA (exchange, correlation or both) functionals including dependence on τ. For a pure density functional, the performance of meta-GGA functional is better compared to that of a GGA functional, with the computational coast for both being almost the same [Cramer 2004].

1.2.6.9 Inclusion of HF Exchange in Density Functionals (Hybrid Density Functionals)

Using Hellman-Feynman theorem, the exchange-correlation energy can be computed as,

$$E_{xc} = \int_0^1 \langle \Psi(\lambda) | V_{xc}(\lambda) | \Psi(\lambda) \rangle d\lambda \qquad \text{(Eq. 1.49)}$$

where λ is the extend of inter electronic interaction. λ changes between 0 (none) to 1 (exact). If we assume that the electrons are non interacting, then, the total exchange-correlation energy, V_{xc}, will have only the exchange-energy component, which is derived from anty-symmetry of the wavefunction.

Since Slater determinant of KS orbitals is the exact wavefunction for the Hamiltonian operator of non interacting systems, its expectation value is the exact exchange for such a system. The calculation of this exchange energy is similar to that in HF calculation except that KS orbitals are used. Also, we do not know the exchange correlation energy of a fully interacting system. Hence, we take the approximation that E_{xc} is computed directly by some choice of DFT functional. Then, the total expectation value for E_{xc} (Eq. 1.49) can be given as,

$$E_{xc} = E_x^{HF} + z(E_{xc}^{DFT} - E_x^{HF}) \qquad \text{(Eq. 1.50)}$$

where z is a fractional number.

Usually, Eq. 1.50 is written using another variable, defined as 1-a, providing

$$E_{xc} = (1-a)E_{xc}^{DFT} + aE_x^{HF} \qquad \text{(Eq. 1.51)}$$

This analysis is the basis of so called ‘adiabatic connection method (ACM)’, since it connects between non interacting and fully interacting states.

If we assume z = 0.5, it is called ‘half-and-half (H&H)’ method. This method is shown to have an error of 6.5 kcal/mol, using LDA exchange-correlation. Whereas in KS-SCF scheme, a large portion of the exact kinetic energy is calculated exactly and then worries about the small reminder, in ACM approach, a large portion of the total exchange-

correlation energy is calculated and then takes into account the difference between the total and exact (HF) exchange.

The value of constant 'a' is taken so as to get most accurate results. For the improvement of these methods, additional empirical parameters are also added. Becke used three parameters *viz*. a, b and c in the B3PW91 functional as,

$$E_{xc}^{B3PW91} = (1-a)E_x^{LSDA} + aE_x^{HF} + b\Delta E_x^{B} + E_c^{LSDA} + c\Delta E_c^{PW91} \quad \text{(Eq. 1.52)}$$

where a, b and c are optimized to be 0.20, 0.72 and 0.81 respectively.

Subsequently, Stevens *et al* modified this method to use LYP functional, which is designed to compute the full correlation energy instead of adding a correction term to LSDA. This is known as the B3LYP model, defined as

$$E_{xc}^{B3LYP} = (1-a)E_x^{LSDA} + aE_x^{HF} + b\Delta E_x^{B} + (1-c)E_c^{LSDA} + cE_c^{LYP} \quad \text{(Eq. 1.53)}$$

where the values of a, b and c are similar to those in B3PW91. B3LYP is one of the popular density functionals at present.

For O3LYP, a = 0.1161, b = 0.9262 and c = 0.8133. Whereas B3LYP uses VWN3 version, O3LYP uses VWN5 version of LSDA correlation functional. X3LYP also uses a similar equation with a = 0.218, b = 0.709 and c = 0. 129. In this method, b is multiplied with a combination of B and PW exchange. Since HF and DFT exchange are combined, ACM methods are also known as 'hybrid methods'.

Examples of one parameter methods are B1PW91, B1LYP, B1B95, mPW91, PBE1PBE etc. in these methods, the percentage of HF method included in the functional is adjusted according to the value of a. In meta-GGA functionals, the improvement of performance with the inclusion of HF exchange appear to be lesser compared to GGA functionals, but still noticeable [Cramer 2004].

1.2.6.10 Perdew's Jacob's Ladder of Density Functionals

In 2001, Perdew and Schmidt [Perdew and Schmidt 2001] introduced the concept of the Jacob's ladder of density functionals, which is placed in the ground of the Hartree world and ends in the heaven of chemical accuracy. Different rungs of the ladder indicate different types of density functionals, with the accuracy (and also the complexity) of the

functional (the exchange correlation part) increasing with going upwards the ladder. In this way, the lowest rung represents the simplest form of DFT, *viz*. the local density approximation (LDA) where only the electron density, ρ(r) is used. The second rung represents the generalized gradient approximation (GGA) functionals which considers the gradient of electron density ∇ρ(r) along with ρ(r). Meta-GGA functionals which consider the second derivative of electron density, $\nabla^2\rho(r)$, is represented by the third rung of the Jacob's ladder. The fifth rung represents the hybrid GGA functionals, also known as hyper-GGA (exact exchange and compatible correlation). The sixth rungs represent generalized random phase approximation, which uses occupied and unoccupied orbitals in the calculation. The authors also discuss about the investigations that remain to be done to reach their dream of a final theory. Representation of the Jacob's ladder is given in Figure 1.12.

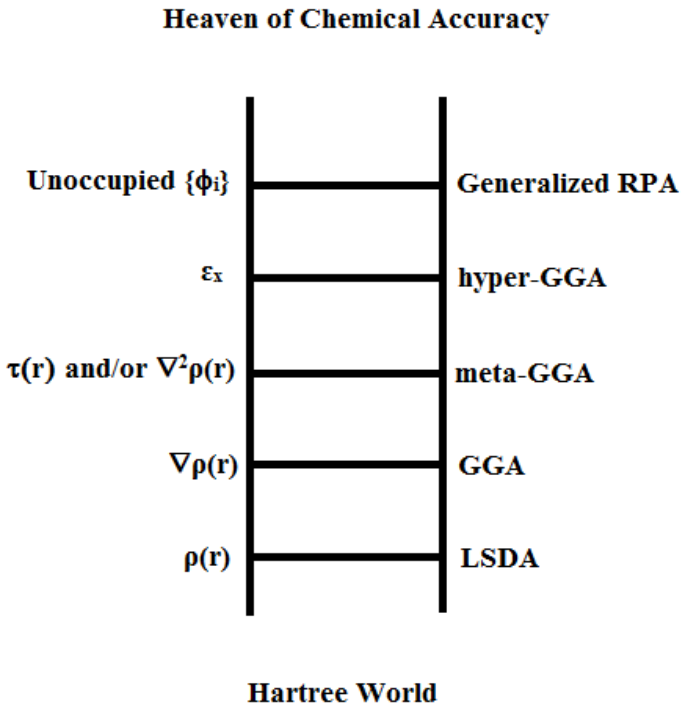

Figure 1.12 Jacob's ladder of density functionals described by Perdew and Schmidt.

Janesco in 2013 introduced a new class of density functional, described as rung 3.5 of the Jacob's ladder, which includes a linear dependence on the non-local one particle density matrix [Janesko 2013]. These functionals, according to the author, are more efficient than the first three rungs of local/semi-local functionals and less computationally demanding than the hybrid functionals of fourth rung and above.

1.2.7 Basis Sets

The sets of one-particle functions used to build molecular orbitals (MOs) are known as basis sets. The method of constructing MOs by a linear combination of atomic orbitals (AOs) is known as the LCAO method. The computer programs calculate the MO expansion coefficients in terms of basis sets. The merit of this method is that it can be used for any molecule with any number of atoms. Taking a larger set of AOs, for instance considering *p* and *d* orbitals in the case of hydrogen atoms, increases the flexibility of resultant MOs and hence, give more accurate results. A minimal basis set considers only the most basic aspects of a molecule. Minimal basis sets are hardly used in present days due to very low accuracy of results. Extended basis sets use a detailed description of molecules. J. C. Slater was the first to develop basis sets. The expression for a Slater type orbital (STO) can be given as,

$$\Phi_{abc}^{STO}(x,y,z) = Nx^a y^b z^c e^{-\varsigma r} \qquad \text{(Eq. 1.54)}$$

where N is a normalization constant, a, b, c are the components of angular momentum (L = a+b+c), r is the radius in angstrom and ς is the orbital exponent.

Since use of STOs includes tedious calculations, an easier to compute type of orbitals known as Gaussian type orbitals (GTOs) were introduced by S. F. Boys. GTOs can be represented as,

$$\Phi_{abc}^{GTO}(x,y,z) = Nx^a y^b z^c e^{-\varsigma r^2} \qquad \text{(Eq. 1.55)}$$

The difference between STO and GTO is that GTO squares the ‘r’ term. Thus, the product of two primitive Gaussians gives rise to another Gaussian. Since GTOs use simpler formulae and easier calculations, these are almost universally used by computational chemists. However, though calculations are easier, use of GTOs result in less accuracy of results. In order to overcome this limitation, linear combinations of primitive gaussians are usually used, which can mimic or approximate an STO. These types of functions are known as contracted Gaussian type orbitals (CGTOs). A CGTO formed by the linear combination of n primitive gaussians is referred to as STO-nG. STO-nG basis sets are considered as minimal basis sets. Different types of extended basis

include split valence, polarized, diffuse, double zeta, triple zeta and quadruple zeta basis sets.

The double, triple and quadruple zeta basis sets use more than one (two in the case of double, three in the case of triple etc.) basis functions for each of the AOs. In order to simplify this tedious effort to represent each of the AOs with more than one basis functions, the split valence basis sets were introduced. In split valence basis sets, only the valence orbitals are represented as multiple zeta while the core orbitals are represented by a single basis function. 3-21G basis set is a double zeta split valence basis set in which the core electrons are a represented as a sum of three gaussian functions and the valence orbitals are represented by two basis functions of which one is a sum of two primitive gaussians and the second is a gaussian function. Thus, in carbon, 1s orbital is represented by a basis function, which is a combination of three GTOs and 2s and the three 2p orbitals (2px, 2py, 2pz) are represented by two basis functions each, of which, one being a combination of two GTOs and the other formed from one GTO. Thus, a carbon atom will be represented by a total of nine basis functions. Other examples of split valence basis sets are 4-21G (double zeta), 6-311G (triple zeta) etc.

In polarized basis sets, contracted gaussians corresponding to angular momentum higher than in the valence orbitals are added to each atom, since the characteristics of s and p orbitals or p and d orbitals are sometimes shared by orbitals. These polarization functions increase the flexibility of atoms in forming chemical bonds in different directions and hence will give better geometries. Thus, the polarized basis set 6-31G* (also written as 6-31G(d)) adds a little ‘d’ character to the valence p orbitals and 6-31G** (also written as 6-31G(d,p))adds some ‘p’ character to the valence s orbitals as well as ‘d’ character to the valence p orbitals.

Diffuse functions are used for describing electrons that are held far away from the nucleus. These functions have low ς exponent. The use of diffuse functions is necessary in cases like anions, highly electronegative atoms with high electron density, Rydberg states, and van der Waals complexes bound by dispersion. Calculations on anions without using diffuse functions can result in unrealistic results. Diffuse functions are represented using ‘+’ signs. For example, 6-31+G basis set adds s and p diffuse functions to non hydrogen atoms and 6-311++G adds diffuse functions to both non-hydrogen and hydrogen atoms. A

basis set consisting of both polarization and diffuse function is considered to be 'balanced'. Examples are 6-31G* and 6-311G** basis sets.

1.2.8 Quantum Theory of Atoms in Molecules (QTAIM)

R. W. F. Bader introduced Quantum theory of Atoms in Molecules. According to this theory, information on molecular features such as bonds, atoms and molecular structure are derived from the spacial distribution of electronic charge in the field of the nuclei and its flow in the presence of external field. These concepts are derived from the topology of electron density, ρ(r). According to this theory, the topological distribution of electronic charge in the field of nuclei and its flow in the presence of external field serve as the carrier of physical information such as the presence of a bond. In topology of electron density of molecules, maxima are found at the nuclear positions.

A critical point in the electron density topology is a point in space at which the first derivative of density vanishes. That is,

$$\nabla\rho = i\frac{d\rho}{dx} + j\frac{d\rho}{dy} + k\frac{d\rho}{dz} \longrightarrow \begin{cases} = \vec{0} \text{ (at critical points and at } \infty) \\ \# \vec{0} \text{ (at all other points)} \end{cases} \qquad \text{(Eq. 1.56)}$$

A critical point may be a maximum, minimum or a saddle point. The maxima of electron density at the nuclei, though not maxima in true mathematical sense, are actually topological maxima. The electron density, ρ(r) is a scalar quantity, whereas its gradient ∇ρ, is a vector. The gradient of ρ(r) at a point in space points in the direction in which ρ(r) undergoes the highest rate of increase and its magnitude is equal to the rate of increase in that direction.

A local minimum, a local maximum or a saddle point can be distinguished by considering the second derivative, ∇∇ρ. The 'Hessian matrix' consists of the nine second derivatives. At a critical point located at rc, the Hessian matrix can be evaluated as,

$$A(r_c) = \begin{pmatrix} \frac{\partial^2\rho}{\partial x^2} & \frac{\partial^2\rho}{\partial x\partial y} & \frac{\partial^2\rho}{\partial x\partial z} \\ \frac{\partial^2\rho}{\partial y\partial x} & \frac{\partial^2\rho}{\partial y^2} & \frac{\partial^2\rho}{\partial y\partial z} \\ \frac{\partial^2\rho}{\partial z\partial x} & \frac{\partial^2\rho}{\partial z\partial y} & \frac{\partial^2\rho}{\partial z^2} \end{pmatrix}_{r=rc} \qquad \text{(Eq. 1. 57)}$$

Since a Hessian matrix is real and symmetric, it can be diagonalized. The diagonalization of *A(rc)* is equivalent to a rotation of the coordinate system r(x,y,z) ⟶ r(x',y',z'), where the new axes x', y', z' superimposes with the principal curvature axes of the critical point. The diagonal form of the Hessian matrix is obtained via similarity transformation ($U^{-1}AU = \Lambda$), which is given as,

$$\Lambda(r_c) = \begin{pmatrix} \frac{\partial^2\rho}{\partial x'^2} & 0 & 0 \\ 0 & \frac{\partial^2\rho}{\partial y'^2} & 0 \\ 0 & 0 & \frac{\partial^2\rho}{\partial z'^2} \end{pmatrix}_{r=rc} = \begin{pmatrix} \lambda_1 & 0 & 0 \\ 0 & \lambda_2 & 0 \\ 0 & 0 & \lambda_3 \end{pmatrix} \qquad \text{(Eq. 1.58)}$$

Here, λ_1, λ_2 and λ_3 are the curvatures of the density with respect to the three principal axes, x', y', z'. Diagonalization of Hessian matrix provides a set of eigen values and eigen vectors. The eigen values λ_1, λ_2 and λ_3 give the curvatures of ρ with respect to the three principal axes, which are positive at minima and negative at maxima. The eigen vectors denote the corresponding axes.

The trace of a Hessian matrix (the sum of the diagonal elements of an n×n matrix is known as its trace) is invariant to the rotation of the coordinate system. The trace of the Hessian matrix is known as the Laplacian of density, $\nabla^2\rho$, and is defined as,

$$\nabla^2\rho(r) = \frac{\partial^2\rho}{\partial x'^2} + \frac{\partial^2\rho}{\partial y'^2} + \frac{\partial^2\rho}{\partial z'^2} = \lambda_1 + \lambda_2 + \lambda_3 \qquad \text{(Eq. 1.59)}$$

When x = x', y = y' and z = z'

The three terms on RHS are λ_1, λ_2 and λ_3 respectively.

A critical point is denoted as (ω, σ), where ω is the rank (the number of non-zero curvatures of ρ at the critical point) and σ is the signature (the algebraic sum of the signs of curvature). Usually, the value of ω is equal to 3 for cp of molecules with energetically stable nuclear configurations, since rank less than 3 indicate a change in the topology of ρ and hence a change in the molecular structure. Each of the three curvatures contributes ±1 to the value of σ depending on whether it is positive or negative.

The four types of critical points with rank 3 are

1) (3,-3) critical points: three negative curvatures. Here, ρ is a local maximum. Also known as nuclear critical point (NCP).
2) (3,-1) critical point: two negative curvatures. ρ is a maximum in the plane defined by these two eigen vectors. Minimum along the third axis, which is perpendicular to this plane. Also known as bond critical point (BCP).
3) (3,+1) critical point: two positive curvatures. ρ is a minimum along the plane defined by the corresponding eigen vectors. ρ is a maximum along the third axis, which is perpendicular to this plane. Also known as ring critical point (RCP) and are found in the interior of a ring of chemically bonded atoms.
4) (3,+3) critical point: three positive curvatures. ρ is a local minimum. Also known as cage critical point (CCP). Found in the interior of an interstitial space enclosed by several rings.

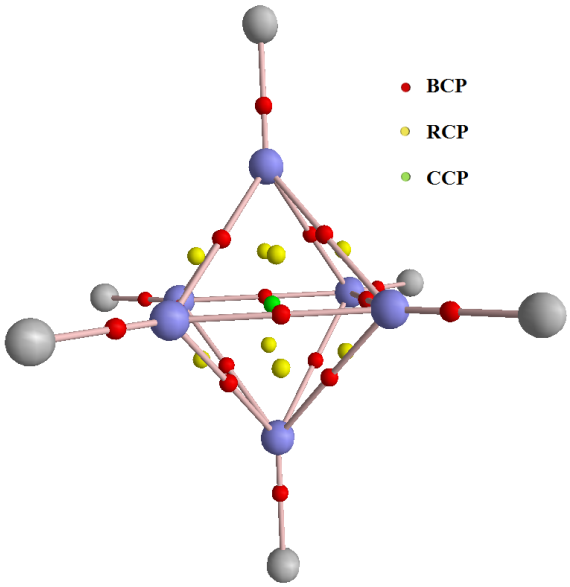

Figure 1.13 QTAIM molecular graph of *closo*-$[B6H6]^{2-}$ showing bond paths, BCPs, RCPs and CCPs.

A topological relationship governs the number and type of critical points that can coexist in a crystal or in a molecule. i.e.,

$$n_{NCP} - n_{BCP} + n_{RCP} - n_{CCP} = \begin{cases} 1 & \text{(Infinite crystals)} \\ 0 & \text{(Isolated molecules)} \end{cases} \qquad \text{(Eq. 1.60)}$$

where n is the number of subscripted type of CP. The equation that applies to isolated molecules is known as Poincaŕe - Hopf (HP) relationship. The second equality that applies to infinite periodic lattices of crystals is known as Morse equation. The characteristic set for a given system is defined as the set $\{n_{NCP}, n_{BCP}, n_{RCP}, n_C\}$. If the above equation is not satisfied, then, it is said to be an inconsistent characteristic set.

Figure 1.13 gives the molecular graph of the closo-borane *closo*-$[B_6H_6]^{2-}$ with different kinds of CPs and bond paths. A bond path is a line of maximum electron density that connects the nuclei of two atoms that are bonded to each other. From Figure 1.13, it can be seen that *closo*-$[B6H6]^{2-}$ contains eighteen BCPs, eight RCPs and one CCP.

The maxima of electro density at the nuclear positions separate the molecular space into mononuclear regions, Ω. Such a surface, which is identified as atoms in a molecule, is of zero flux in the gradient vector field of electron density (i.e., it is not crossed by any of the gradient vectors, $\Delta\rho$ (r)). Mathematically,

$$\nabla\rho(r).n(r) = 0 \qquad \text{(Eq. 1.61)}$$

where r is the position vector and n(r) is the unit vector normal to the surface S(Ω).

In a plot of the gradient vector field of electron density, the zero flux surfaces of $\Delta\rho$ separate each nucleus into 'atomic basins' and an arbitrary surface cutting through the density. Nuclei act as attractors of these gradient paths. That is, all paths belonging to an atom basin converge into the corresponding nucleus. The region of space enclosed by all trajectories of $\rho(r)$ terminating at the nuclear attractor form the basin of attractors. An atom in a molecule consists of a nucleus and its associated basin. Atoms can be alternatively defined in terms of a zero flux surface which is not crossed by any of the trajectories. This surface forms the boundary of an atom in a molecule. If there exists such a boundary between two atoms, it also indicate the presence of a (3,-1) critical point. Sometimes, maxima of electron density occur in positions other than those corresponding to atomic nuclei, and are known as non-nuclear attractors (NNA) and cannot be distinguished from

nuclear maxima. NNAs show atomic basins bound by zero flux surfaces and they are referred to as 'pseudo atoms' and may show BCPs corresponding to bonding interaction with other atoms or other NNAs. These are important in characterizing metallic bonding.

The line of locally maximum electron density connecting two bonded atoms in equilibrium geometry is known as bond path ('atomic interaction lines' in the case of a non-equilibrium geometry). Bond critical point is the point of lowest electron density along the bond path. A 'molecular graph' is a collection of bond paths connecting the nuclei and the various types of critical points. Molecular graph defines the structure of a molecule. A line of largest negative potential energy density connecting the attractors is known as virial path and a collection of virial path and associated critical points is known as virial graph, which also defines the molecular structure.

1.2.8.1 Characterization of Atomic Interactions in QTAIM Analysis

Properties of electron density at a BCP can be used for the characterization of the bonding interaction. The extent of charge accumulation in the inter atomic surface and along the bond path increases with the assumed number of electron pair bonds and this increase can be examined by the value of electron density, ρ at the BCP. The bond orders can be obtained from AIM analysis. For instance, the C-C bond orders for ethane, benzene, ethylene and acetylene can be obtained as 1.0, 1.6, 2.0, and 3.0 respectively. The value of ρ at an intermolecular BCP such as that for a hydrogen bond is usually taken as a measure of the strength of such an interaction [Bader 1990].

1.2.9 Molecular Electrostatic Potential (MESP)

Charles Augustin de Coulomb in 1784 described the most fundamental law in electrostatics, known as the Coulomb's law. According to the Coulomb's law, the force of attraction or repulsion, F between two point charges q_1 and q_2 separated by a distance r is given by an inverse square law as,

$$F = \frac{q_1 q_2 \hat{\mathbf{r}}}{4\pi\varepsilon_0 r^2} \qquad \text{(Eq. 1.62)}$$

where $4\pi\varepsilon_0$ is the proportionality constant and $\hat{\mathbf{r}}$ is a unit vector joining the position vectors of q_1 and q_2. The electric field produced at a distance r by a fixed point charge q is given as,

$$\mathbf{E} = \frac{q\mathbf{r}}{4\pi\varepsilon_0|\mathbf{r}|^3} \qquad \text{(Eq. 1.63)}$$

The force acting on a unit test charge placed at a reference point in the field is called the intensity E of the field and is expressed in Newton per Coulomb (NC^{-1}). If a system contains two or more charges $\{q_\alpha\}$, then, according to the superposition principle, the electric field is given by the vector sum of the fields produced by individual charges as,

$$\mathbf{E}(\mathbf{r}) = \sum_\alpha \mathbf{E}_\alpha(\mathbf{r}) = \frac{1}{4\pi\varepsilon_0} \sum_\alpha \frac{q_\alpha(\mathbf{r}-\mathbf{r}_\alpha)}{|\mathbf{r}-\mathbf{r}_\alpha|^3} \qquad \text{(Eq. 1.64)}$$

If a positive charge q is moved in the electric field E, a force qE is exerted on the charge by the electric field. Thus, the total work done by an external agent in moving the charge q from a point A to point B is given by a line integral as,

$$W_{AB} = -q\int_A^B \mathbf{E}.d\mathbf{l} \qquad \text{(Eq. 1.65)}$$

Where $d\mathbf{l}$ is an infinitesimal displacement vector along AB. if a unit positive charge is moved from A to B, then the work done will be equal to the potential difference, V_B-V_A. In the field of a point charge q_0, the work done is given by,

$$q(V_B - V_A) = -q\int_A^B \mathbf{E}.d\mathbf{l} = -q\int_{r_A}^{r_B} \frac{q_0 dr}{4\pi\varepsilon_0 r^2} = \frac{qq_0}{4\pi\varepsilon_0}\left\{\frac{1}{r_B} - \frac{1}{r_A}\right\} \qquad \text{(Eq. 1.66)}$$

This equation implies that the electrostatic field is conservative. That is, both W_{AB} and (V_B-V_A) are path independent. If a vector field A satisfies the condition $\nabla\times A = 0$, then, it is known as an irrotational vector field. If A is the gradient of a scalar function ϕ ($A = \nabla\phi$), then it will readily follow the equation $\nabla\times A = 0$. Here, ϕ is called the potential of the vector function A. Since the electrostatic field E is expressible as the gradient of a scalar quantity V ($E = \pm\nabla V$), the latter is known as electrostatic potential. V at a reference point can also be defined as the work done in bringing a unit positive charge from infinity to that reference point. Thus, the electrostatic potential at a point r_0 in the field produced by a point charge q_0 can be given as,

$$V = \frac{q_0}{4\pi\varepsilon_0 r} \qquad \text{(Eq. 1.67)}$$

Applying the principle of superposition, the potential produced by a set of fixed point charges $\{q_\alpha\}$ located at $\{r_\alpha\}$ at point r is given as,

$$V = \frac{1}{4\pi\varepsilon_0} \sum_\alpha \frac{q_\alpha}{|\mathbf{r} - \mathbf{r}_\alpha|} \qquad \text{(Eq. 1.68)}$$

If the electric filed is produced by a continuous distribution of charges and not by discrete point charges, then, the charge distribution is described by a function $\rho(r)$ and the summation will be replaced by integration in the expression for potential, which can be given as,

$$V(\mathbf{r}) = \frac{1}{4\pi\varepsilon_0} \int \frac{\rho(\mathbf{r}')\mathrm{d}^3\mathrm{r}'}{|\mathbf{r} - \mathbf{r}'|} \qquad \text{(Eq. 1.69)}$$

The electrostatic potential produced by a combination of both discrete charges $\{q_\alpha\}$ placed at $\{r_\alpha\}$ and a smeared distribution of charges $\rho(r)$ can be written as,

$$V(\mathbf{r}) = \frac{1}{4\pi\varepsilon_0} \left\{ \sum_\alpha \frac{q_\alpha}{|\mathbf{r} - \mathbf{r}_\alpha|} + \int \frac{\rho(\mathbf{r}')}{|\mathbf{r} - \mathbf{r}'|} d^3\mathrm{r}' \right\}$$

(Eq. 1.70)

Eq. 1.70 is applicable to the charge distribution in any molecule, which is a collection of discrete positive nuclear charges $\{Z_\alpha\}$ and a continuous negative chare density of electrons $\{\rho(r)\}$. Thus, MESP in atomic units is given as,

$$V(\mathbf{r}) = \sum_\alpha \frac{Z_\alpha}{|\mathbf{r} - \mathbf{r}_\alpha|} - \int \frac{\rho(\mathbf{r}')}{|\mathbf{r} - \mathbf{r}'|} d^3\mathrm{r}' \qquad \text{(Eq. 1.71)}$$

In Eq. 1.71, the first term in RHS is known as bare nuclear potential, and is always positive. The second term is the negative potential produced due to continuous distribution of electrons. If the first term in the RHS of Eq. 1.71 dominates, the value of MESP will be positive. On the other hand, domination of the second term gives rise to a negative MESP value. The second term dominates at electron rich regions resulting in negative values of MESP while the first term dominates near the nuclei. A zero-valued MESP isosurface is the characteristic feature of a molecular system. A collection of points in space at which the electrostatic potential value is the same is known as an equipotential surface. The MESP features of a molecule can be visualized by viewing equipotential surfaces. Figure

1.14 (a) shows MESP mapped at 0.01 au isodensity surface of water molecule. This can be constructed with the help of visualization softwares such as Chemcraft, Gaussview, SPARTAN, HyperChem etc.

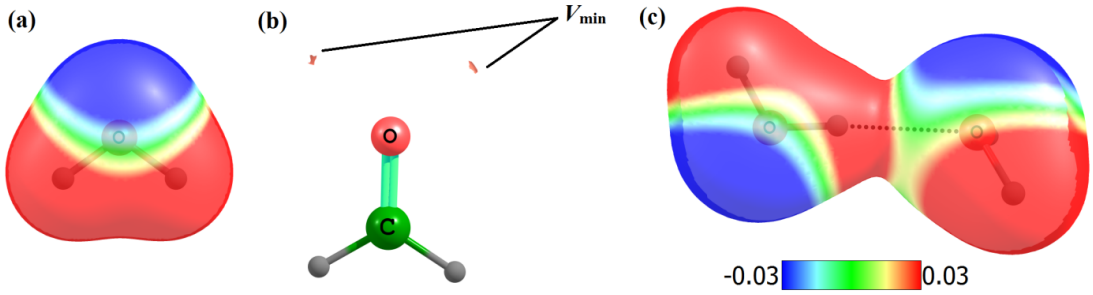

Figure 1.14 (a) MESP mapped at 0.01 au isodensity surface of water molecule (b) V_{min} of acetaldehyde located at either side of the oxygen corresponding to the lone pairs and (c) MESP mapped at 0.01 au isodensity surface of water dimer where the hydrogen with a positive MESP value interacts with the electron rich oxygen.

The most negative value of MESP in a molecule is known as its V_{min}. When a positive charge interacts with the molecule, the position of V_{min} corresponds to its possible equilibrium position, if the static charge distribution of the molecule is not allowed to relax. Figure 1.14 (b) shows the position of V_{min} in acetaldehyde molecule, which is located on either sides of the oxygen atom, corresponding to the two lone pairs on oxygen. Apart from interaction with cations, the position and magnitude of V_{min} also helps in understanding the interaction of a molecule with other nucleophiles such as a hydrogen bond donor. Also, in the study of non-covalent interactions, a map of MESP distribution can help in understanding the nature of weak interactions. For example, in Figure 1.14 (c), the electron deficient hydrogen on one of the water molecules (hydrogen bond donor) forms a bonding interaction with the electron rich oxygen atom of the second water molecule [Gadre and Shirsat 2000].

1.3 Conclusions

Non-covalent interactions are important in various fields of study such as biology, material science, catalysis, crystallography etc. Apart from the most widely studied hydrogen bonds, several types of interactions such as π···π stacking, cation···π, anion···π etc. have been widely analyzed for their nature, strength and effects. With the development of novel theoretical and experimental methods, interactions involving main group elements

such as halogen bonds, chalcogen bonds, pnicogen bonds tetrel bonds and carbon bonds have been discussed relatively recently. This also points to the possibility of exploring new types of intermolecular interactions and clarification of unsolved physical or chemical phenomena. Cooperativity of non-covalent interactions is the phenomenon which drives the formation of molecular clusters. The cooperativity of non-covalent interactions in several fields study, especially in biological systems has been widely analyzed. The accurate and computationally efficient assessment of the nature and strength of these interactions has been a challenge for the computational chemists. Having a good balance between accuracy and computational cost, density functional theory methods are good candidate for this purpose. Attempts to improve the applicability of DFT method to non-covalent interactions include long range correction, different versions of dispersion correction etc. Several high accuracy databases of non-covalently interacting systems are available in the literature. Before selecting a method for the study of non-covalent interactions, proper benchmark studies utilizing the high accuracy databases need to be conducted for testing its applicability to the problem.

The computational chemistry methods have been widely used nowadays in the several areas of research including non-covalent interactions. The second part of this chapter gives a brief introduction to these methods, with emphasis being given to the methods that have been used in the thesis. Various molecular mechanical and quantum mechanical methods have been discussed in this chapter. An account of the Hartree-Fock methods followed by a brief discussion on post Hartree-Fock methods is given. Different features of the semi-empirical methods are also discussed, followed by a brief account of the molecular mechanical and molecular dynamical methods. The DFT methods have gained wide popularity nowadays since it gives a good balance between accuracy and computational coast. Various DFT methods are used in the thesis for solving problems in non-covalently interacting systems. A detailed discussion on different aspects of DFT including its origin, theorems, SCF methodology and classification is given in this chapter. MESP and QTAIM methods have been discussed along with their applicability in the study of non-covalent interactions.

CHAPTER 2

A Benchmark Study on Density Functional Theory Methods to Describe Geometry and Interaction Energy of Non-Covalent Dimers

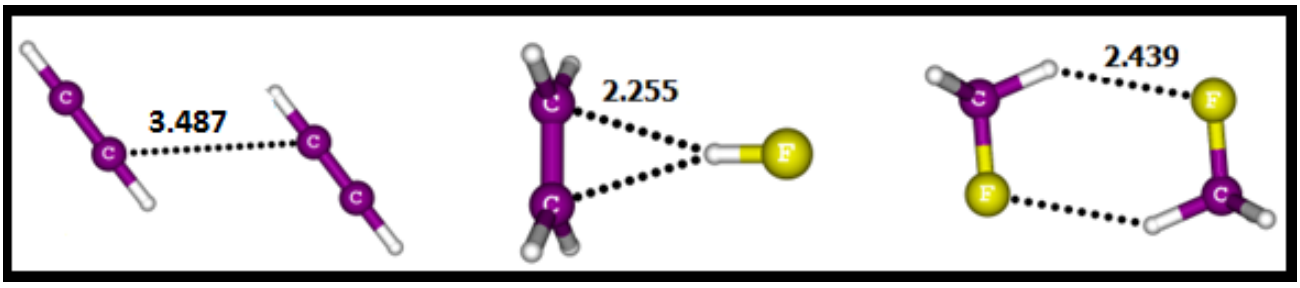

2.1 Abstract

A benchmark study on all possible DFT methods in Gaussian09 is done to locate functionals that agree well with CCSD/aug-cc-pVTZ geometry and Ave-CCSD(T)/(Q-T) interaction energy (E_{int}) for small non-covalently interacting molecular dimers in 'dispersion-dominated' (class 1), 'dipole-induced dipole' (class 2), and 'dipole-dipole' (class 3) classes. A DFT method is recommended acceptable if the geometry showed close agreement to CCSD result (RMSD < 0.045) and E_{int} was within 80 - 120% accuracy. Among 382 tested functionals, 1- 46% gave good geometry, 13 - 44% gave good E_{int} while 1 - 33 % satisfied geometry and energy criteria. Among the list of 'recommended' functionals, exchange-correlation functionals and long-range corrected exchange-correlation functionals dominated along with small population of 0-5 pure functionals, 0-27 hybrid functional and 0-4 double hybrid functionals. No functional was found to be common for satisfying both energy and geometry criteria in 1 and 3 classes while two exchange-correlation functionals (mPWB95, and TPSSB95) gave good geometry and energy for all the dimers in class 2. Further screening to locate the best performing functionals for all the three classes was made by counting the acceptable values of energy and geometry given by each functionals. The meta-GGA functional M06L was the best performer with total 14 hits; 7 acceptable energies and 7 acceptable geometries. This was the only functional 'recommended' for at least two dimers in each class. The remaining functionals in the best performing list are M05, B2PLYPD, B971, mPW2PLYPD, PBEB95 and CAM-B3LYP giving 11 hit counts and PBEhB95, PW91B95, Wb97x, BRxVP86, BRxP86, HSE2PBE, HSEh1PBE, PBE1PBE, PBEh1PBE, and PW91TPSS giving 10 hit counts. Among these, M05, B971, mPW2PLYPD (recommended for 5 dimers), Wb97x (long-range corrected hybrid functional of Head-Gordon and co-workers), and PW91TPSS (recommended for 4 dimers) were among the 'recommended' list of at least one dimer from each class. Long-range correction (LC) of Hirao and coworkers to exchange-correlation functionals showed massive improvement in geometry and E_{int} and some of them even appeared among the 'recommended' list of functionals. The best performing LC- incorporated functionals were LC-G96KCIS and LC-PKZBPKZB. Exchange-correlation functionals, especially those with S, O, G96, and XA exchange if used for the study of non-covalently interacting system must be always used with the long-range correction. This extensive study predicts that M06L is the most trustworthy DFT method in Gaussian09 to study small non-covalently interacting systems.

2.2 Introduction

Non-covalent interactions are very important in the field of biology, nano-materials and supra molecular chemistry. These interactions play a crucial role in deciding the structure and function of bio-molecules like DNA, proteins etc [Lehn 2002]. In the bottom-up approach for the synthesis of nano-materials, molecular aggregates are formed by these interactions. The molecular constituents in a supra-molecule are bound together by non-covalent interactions. These interactions are also important in catalysis (catalyst interaction with surfaces), drug discovery and even in some chemical reactions. For computational study of non-covalently interacting systems, Kohn-Sham density functional theory (DFT) methods are attractive for a good balance between computational demand and accuracy [Goerigk and Grimme 2011b; Grimme 2006a]. A large number of density functionals applicable to different kinds of systems have been developed so far and are assigned to different rungs of "Jacob's ladder" [Perdew *et al.* 2009; Perdew *et al.* 2005; Tao and Perdew 2003] wherein the first three rungs describes LDA, GGA, and meta-GGA density functionals. LDA indicate the local electron spin density calculations while GGA functionals consider the electron spin density gradient $\Delta\rho$ along with the density, ρ. The meta-GGA functionals include the spin kinetic energy density (Laplacian of ρ) in addition to these two factors. The next two rungs, the hybrid and double hybrid functionals, add some amount of Hartree-Fock exchange to the density functionals and consider virtual Kohn-Sham orbitals [Perdew *et al.* 2009; Perdew *et al.* 2005; Tao and Perdew 2003; Zhao and Truhlar 2008a]. Many of these DFT methods are very good in describing the strong interactions among atoms and molecules, but many of them cannot give accurate descriptions of weak interactions like dispersion and van der Waals interactions. Several groups have conducted efforts to find out proper density functionals giving accurate energy, geometry and thermo chemical properties of non-covalently interacting systems [Burns *et al.* 2011; Eshuis and Furche 2011; Gkionis. *et al.* 2009; Goerigk and Grimme 2011b; Hujo and Grimme 2011; Sherrill *et al.* 2009; Sun *et al.* 2010; Wu *et al.* 2001; Zhao and Truhlar 2005b; Zhao and Truhlar 2008a; Zhao and Truhlar 2008b]. Some typical weakly bound systems were studied by Wu *et al.* using both pure and hybrid DFT methods. These include four systems of increasing binding strength, namely the Ar_2 and Kr_2 dimers, the benzene dimer, the water dimer, and a few metal carbonyls. The dispersion dominated systems (noble gases and benzene dimers) and carbonyls showed a strong dependence of results on the choice of functionals in the case of pure functionals.

Relatively precise, functional independent results were obtained for systems dominated by electrostatic interaction such as water dimers [Wu *et al.* 2001]. Four benchmark databases on binding energies of hydrogen bonding, charge transfer, dipole interactions, and weak interactions were presented by Zhaho and Truhlar. Among the 44 density functionals tested by them, the best performance for dipole interactions was given by MPW3LYP, B97-1, PBE1KCIS, B98, and PBE1PBE. B97-1, MPWB1K, PBE1KCIS, and MPW1B95 functionals gave the best results for weak interactions [Zhao and Truhlar 2005b]. Zhaho and Truhler also tested the performance of M05-2X and M06 class of functionals (M06L, M06, M06HF and M06-2X) created by them against some popular functionals to study non-covalent interactions and found the performance of M06-2X, M05-2X, M06-HF, M06, and M06L to be satisfactory [Zhao and Truhlar 2008a]. Gkionis *et al.* analyzed the performance of BHandH functional for the study of non-covalent interactions using high level *ab-initio* results as benchmarks [Gkionis. *et al.* 2009]. Though this method calculated the binding energies with a good degree of accuracy for dispersion dominated and 'mixed' systems, significant overestimation was found in the case of hydrogen bonded systems. Changing the proportion of exact and Slater exchange did not show improvement in the overall performance. The accuracy of nine exchange-correlation density functionals in calculating metal-dihydrogen binding energies have been analyzed by Sun *et al*. using MP2 and CCSD(T) results with high accuracy basis sets as benchmarks. They showed that PBE and PW91 functionals give good results while LDA functional overestimating the dihydrogen binding [Sun *et al.* 2010]. An extensive benchmark study for main group thermo chemistry, kinetics and non-covalent interactions of 47 density functionals, DFT-D3 corrected forms of most of them, the double hybrids, and the M05 and M06 class of functionals on GMTKN30 database have been carried out by Georigk and Grimme [Goerigk and Grimme 2011b]. B97-D3 and PBE-D3 in the GGA and TPSS-D3 in the meta-GGA class of functionals were recommended by them. Also, they have shown that PW6B95 in combination with DFT-D3 was the most robust hybrid functional [Goerigk and Grimme 2011b]. Random phase approximation (RPA), a parameter free 5th rung functional was assessed for its performance of for reaction energies governed by changes in medium and long-range non-covalent interactions was assessed by Eshuis and Furche. The results were found to be more accurate than those of PBE or B3LYP and more systematic than those of B2PLYPD or M06-2X [Eshuis and Furche 2011]. Burns *et al.* studied a variety of density functionals using at the CCSD(T)/CBS level interaction energies as benchmark values and concluded that the tested functionals

elicit the best performance among the double zeta or triple zeta basis set regimes. They have also recommended suitable model chemistries for different types of non-covalently interacting systems [Burns *et al.* 2011]. Hobza and coworkers have conducted extensive studies on non-covalently interacting systems [Černý *et al.* 2011; Gráfová *et al.* 2010; Granatier *et al.* 2012; Hobza 2012; Řezáč *et al.* 2012; Riley *et al.* 2010].

In the present study, the aim is to scan all the density functionals implemented in *Gaussian09* [Frisch *et al.* 2010] suite of programs - one of the most widely used quantum chemical programs - and locate those functionals giving a good value for both geometry and interaction energy for non-covalently bonded molecular dimers. The benchmark values used for the study are CCSD/aug-cc-pVTZ level geometries and Ave-CCSD(T)/(Q-T) level non-covalent interaction energies reported by Mackie and DiLabio [Mackie and DiLabio 2011] for nine non-covalently bonded systems as reference values. Tight screening parameters on geometry and interaction energy have been applied to evaluate the performance of the functionals. This kind of a wide screening of DFT methods based on a strategy that rely on the goodness of both geometry and energy is not yet discussed in the literature.

2.3 Computational Methods

A total of 382 density functionals have been selected which include LDA, GGA, meta-GGA, hybrid and double hybrid functionals as well as long-range corrected and some dispersion-corrected functionals. The exchange-correlation functionals are made by the combinations between any of the 13 exchange functionals *viz*. S, XA [Hohenberg and Kohn 1964; Kohn and Sham 1965; Slater 1974], B [Becke 1988], PW91 [Burke *et al.* 1998; Perdew 1991; Perdew *et al.* 1996b; Perdew *et al.* 1992; Perdew *et al.* 1993], mPW [Adamo and Barone 1998], G96 [Adamo and Barone 1998; Gill 1996], PBE [Perdew *et al.* 1996a; Perdew *et al.* 1997], O [Handy and Cohen 2001; Hoe *et al.* 2001], TPSS [Tao *et al.* 2003], BRx [Becke and Roussel 1989], PKZB [Perdew *et al.* 1999], wPBEh [Henderson *et al.* 2009; Heyd *et al.* 2003; Izmaylov *et al.* 2006], and PBEh [Ernzerhof and Perdew 1998] and any of the thirteen correlation functionals *viz*. VWN [Vosko *et al.* 1980], VWN5 [Vosko *et al.* 1980], LYP [Lee *et al.* 1988; Miehlich *et al.* 1989], PL [Perdew and Zunger 1981], P86 [Perdew 1986], PW91, B95 [Becke 1996], PBE, TPSS, KCIS [Krieger *et al.* 1999; Krieger *et al.* 2001; Rey and Savin 1998; Toulouse *et al.* 2002], PKZB, VP86, and V5LYP) (total 169 combinations). Further, long-range

correction (LC) of Hirao and co-workers [Iikura *et al.* 2001] is applied to 156 out of these 169 exchange-correlation functionals (the functionals with wPBEh exchange cannot be done). The prefix notation LC is used exclusively for long-range correction of Hirao and coworkers. Pure functionals B97D [Grimme 2006a], HCTH, HCTH147, HCTH407, HCTH93 [Boese *et al.* 2000; Boese and Handy 2001; Hamprecht *et al.* 1998], M06L [Zhao and Truhlar 2006b], tHCTH [Boese and Handy 2002], and VSXC [Voorhis and Scuseria 1998] are also included in the study. LC of Hirao and co-workers is applied for six pure functionals (LC cannot be applied for VSXC and HCTH). The hybrid functionals selected for the study are B1B95 [Becke 1996], B1LYP [Adamo and Barone 1997; Becke 1996], B3LYP, B3P86, B3PW91 [Becke 1993], B971 [Hamprecht *et al.* 1998], B972 [Wilson *et al.* 2001], B98 [Becke 1997; Schmider and Becke 1998], BHandH, BhandHLYP [Becke 1993], BMK [Boese and Martin 2004], HSE2PBE, HSEh1PBE [Henderson *et al.* 2009; Heyd *et al.* 2005; Heyd and Scuseria 2004a; Heyd and Scuseria 2004b; Heyd *et al.* 2006; Izmaylov *et al.* 2006; Krukau *et al.* 2006], M05 [Zhao *et al.* 2005], M052X [Zhao *et al.* 2006], M06, M062X [Zhao and Truhlar 2008c], M06HF [Zhao and Truhlar 2006a], mPW1LYP, mPW1PBE, mPW1PW91 [Adamo and Barone 1997; Adamo and Barone 1998; Becke 1996], mPW3PBE, O3LYP [Cohen and Handy 2001], PBE1PBE [Adamo and Barone 1999], PBEh1PBE [Ernzerhof and Perdew 1998], tHCTHhyb [Boese and Handy 2002], TPSSh [Tao *et al.* 2003], and X3LYP [Xu and III 2004]. The long range-corrected hybrid functionals LC-wPBE [Krukau *et al.* 2006; Tawada *et al.* 2004; Vydrov and Scuseria 2006; Vydrov *et al.* 2007], CAM-B3LYP [Yanai *et al.* 2004] (long-range corrected version of B3LYP by Handy and coworkers), wB97, wB97X [Chai and Head-Gordon 2008b] and wB97XD [Chai and Head-Gordon 2008a] (functionals with long-range correction from Head-Gordon and co-workers) available in *Gaussian09* [Frisch et al. 2010] are also analyzed for their performance. Also included in the study are three exchange only functionals (HFB [Becke 1988], HFS, and Xalpha [Hohenberg and Kohn 1964; Kohn and Sham 1965; Slater 1974]), their LC-corrected forms and the double hybrid functionals B2PLYP, B2PLYPD, mPW2PLYP, and mPW2PLYPD [Grimme 2006b; Schwabe and Grimme 2006; Schwabe and Grimme 2007].

The high accuracy energies and geometries of nine non-covalent molecular complexes given by Mackie and DiLabio [Mackie and DiLabio 2011] are used as benchmark values for the study. The nine dimers are categorized in to three classes in which, the Class 1 includes 'dispersion' dominated systems ($(C_2H_2)_2$, $(C_2H_6)_2$, and $(CO_2)_2$). Class 2 systems (CH_4-NH_3, CH_4-HF, and C_2H_4HF) are characterized by 'dipole-induced

dipole' interactions while class 3 dimers ($(CH_3CN)_2$, $(HCHO)_2$, and $(CH_3F)_2$) possess 'dipole-dipole' interactions. Mackie and DiLabio [Mackie and DiLabio 2011] have done the optimization of these systems using the high accuracy *ab initio* method CCSD with aug-cc-pVTZ basis sets while the interaction energies were computed using a rigorous procedure, the Ave-CCSD(T)/(Q-T) level. All the nine dimers belonging to the three classes were optimized using the 382 density functionals selected for the study. The RMSD of the dimers optimized at different DFT levels from the CCSD/aug-cc-pVTZ geometry as well as the percentage deviation of the DFT interaction energy from the Ave-CCSD(T)/(Q-T) interaction energy were calculated. To calculate RMSD, one dimer is superimposed on the other in the best possible way and this accounts for the deviations of both inter and intramolecular geometry parameters. An RMSD value less than 0.045 was selected as a criterion for "good geometry" and interaction energy (E_{int}) satisfying the condition that $0.8E_{int0} < E_{int} < 1.2E_{int0}$, (ie, within 80-120% accuracy) where E_{int0} is the Ave-CCSD(T)/(Q-T) level interaction energy, was considered as "good interaction energy". Functionals satisfying both the criteria were listed as 'recommended' for each of the nine the non-covalent dimers. E_{int} is calculated using the supermolecule approach, where the interaction energy is obtained by subtracting the energy of the constituent monomers from that of the dimer ($E_{int} = E_{dimer} - (E_{monomer1} + E_{monomer2})$). BSSE correction to the interaction energy was found to be very small (0.0 – 0.4 kcal/mol) for all the systems at all the DFT levels and hence it is not included in further discussions.

2.4 Results and Discussion

2.4.1 Dispersion Dominated Systems

2.4.1.1 Acetylene Dimer

The Ave-CCSD(T)/(Q-T) value of E_{int} reported by Mackie and DiLabio [Mackie and DiLabio 2011] (E_{int0}) for acetylene dimer is -1.38 kcal/mol. Among the 382 DFT methods considered, 129 satisfied the geometry criterion (root-mean-square-deviation (RMSD) < 0.045) and 104 satisfied the E_{int} criterion ($0.8E_{int0} < E_{int} < 1.2E_{int0}$). 49 of them gave both good geometry and good E_{int} and are recommended for acetylene dimer. These 48 functionals include 23 exchange-correlation functionals, 22 LC-exchange-correlation functionals, 2 pure functionals (M06L, B97D), and 2 hybrid functionals (M05, B971) (Figure 2.1). An interesting fact is that the correlation part of 20 out of 22 recommended

LC-functionals were either LYP (10 cases) or V5LYP (10 cases). Among the 'recommended' functionals, the best geometry was given by M06L (RMSD = 0.002, Figure 2.2). The best E_{int} value was given by two LC-functionals *viz*. LC-OLYP and LC-OV5LYP (-1.376 kcal/mol for both). Further the functionals PBELYP, PBEV5LYP, PBEhLYP, PBEhV5LYP, wPBEhLYP and wPBEhV5LYP performed exceedingly well for reproducing both the CCSD geometry and E_{int} (Figure 2.1). The E_{int} value given by PBEhV5LYP, PBEhLYP, wPBEhV5LYP and wPBEhLYP is -1.362 kcal/mol and that given by PBEV5LYP and PBELYP is -1.375 kcal/mol.

In general, among the recommended functionals, most of the exchange-correlation functionals performed well for geometry than the LC-functionals while most of the LC-functionals gave better values of E_{int} than the exchange-correlation functionals. A notable observation is that many of the functionals having poor performance on both geometry and E_{int} showed massive improvement with the incorporation of LC and many of them even satisfied the recommended criteria with LC (Figure 2.1). Notable among them are exchange-correlation functionals with LDA exchange S and GGA exchanges B, BRx, G96, O and XA. For example, the OLYP and OV5LYP functionals showed E_{int} = -0.504 kcal/mol and RMSD = 0.370 while their LC-incorporated forms gave the best value for E_{int} among all the recommended functionals as well as a good RMSD (0.044). But such strong improvement was not shown by exchange-only and pure functionals. With LC, the poor results given by the exchange only functionals Xalpha and HFS became even worse and those given by HFB showed only a slight improvement. Among the pure functionals, the results calculated by the HCTH functionals with LC and without LC were poor except the fact that HCTH407 gave a good value for E_{int} (-1.355 kcal/mol). The pure functionals M06L (which gave the best E_{int}) and B97D gave very good results for both geometry and energy while with LC, they gave the worst results for E_{int}.

2.4.1.2 Ethane and Carbon Dioxide Dimers

E_{int0} of ethane dimer is -1.36 kcal/mol and that of CO_2 dimer is -1.48 kcal/mol. In the case of ethane dimer, 83 functionals gave RMSD < 0.045, 64 satisfied the condition $0.8E_{int0} < E_{int} < 1.2E_{int0}$ while only 19 satisfied both geometry and energy criteria (Figure 2.3A). Among these 19 recommended functionals, 2 were exchange-correlation (PW91P86, PW91VP86), 16 were LC-exchange-correlation, and 1 was a pure functional (M06L). The correlation part of all the sixteen LC-exchange-correlation functionals were either LYP (8 cases) or V5LYP (8 cases).

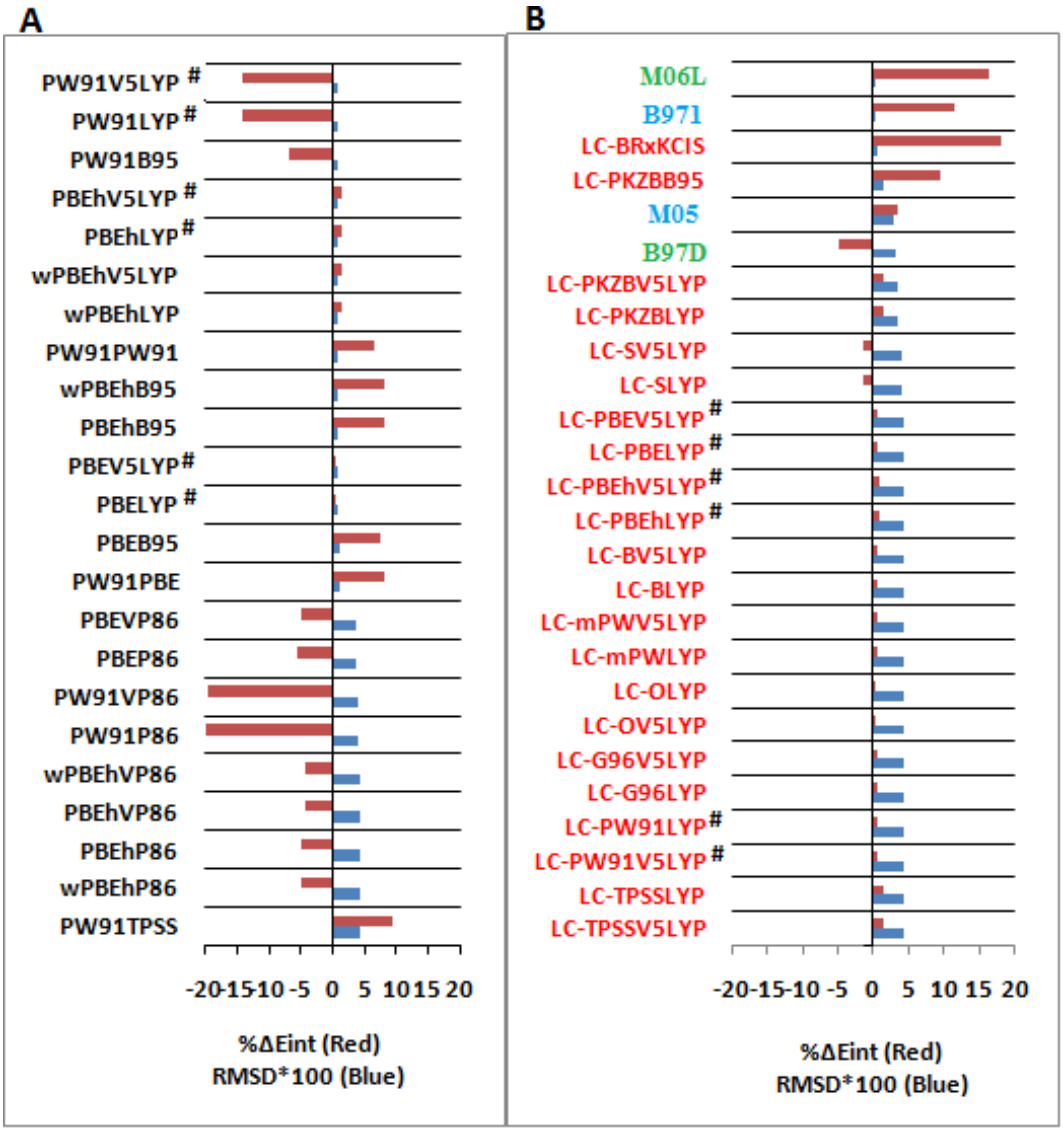

Figure 2.1 (A) and (B) The recommended functionals given in the increasing order of RMSD for acetylene dimer. Exchange-correlation (black), LC-corrected exchange-correlation (red), pure (green) and hybrid (blue) functionals are also indicated. # indicates recommended functionals common for with and without LC.

In the case of CO_2 dimer, 26 showed RMSD < 0.045 and 53 satisfied the E_{int} criterion while only 14 functionals satisfied both the criteria. Among these 14 methods, 1 exchange-correlation (PW91B95), 10 LC-exchange-correlation, 1 hybrid (M052X), 1 hybrid with long-range correction of Head-Gordon (Wb97x) and 1 double hybrid (mPW2PLYPD) functionals were found. Interestingly, all the recommended LC-functionals and one exchange-correlation functional had the same correlation part *viz*. B95.

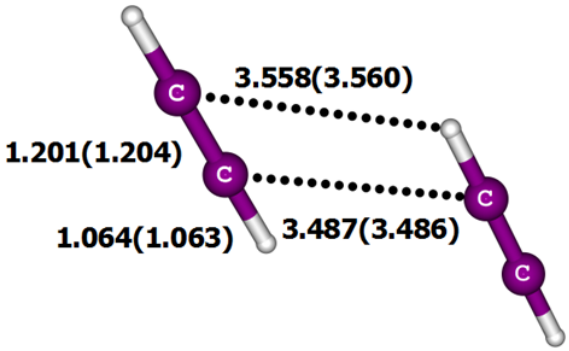

Figure 2.2 Geometry of acetylene dimer optimized at M06L/6-311++g(d,p) level. Distances are given in Å. Corresponding CCSD/aug-cc-pVTZ level values are in parenthesis [Remya and Suresh 2013].

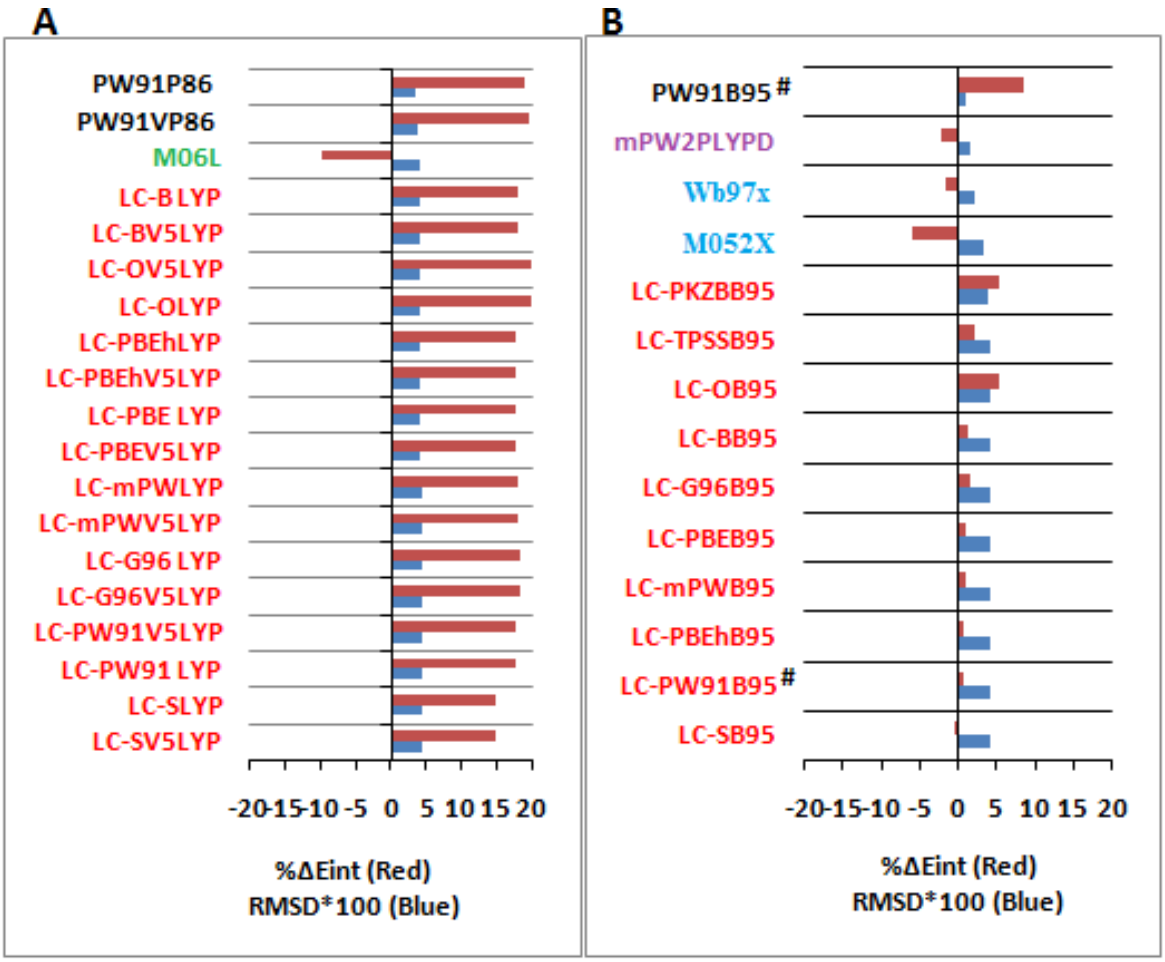

Figure 2.3 The recommended functionals given in the increasing order of RMSD for (A) ethane dimer and (B) CO_2 dimer. Exchange-correlation (black), LC-exchange-correlation (red), pure (green), hybrid (blue) and double hybrid (purple) functionals are also indicated. # indicates recommended functionals common for with and without LC.

Among the recommended functionals for ethane dimer, PW91P86 (RMSD = 0.035, Figure 2.4 a) gave the best geometry and M06L (E_{int}= -1.492 kcal/mol) gave the best value for E_{int}. For CO_2 dimer, PW91B95 (RMSD = 0.010, Figure 2.4 b) gave the best geometry and LC-SB95 functional (E_{int} = -1.488 kcal/mol) gave the best E_{int} among those recommended.

The results for both geometry and energy were improved with the incorporation of LC in the case of functionals with B, G96, O, S, and XA exchange than their pure forms for ethane dimer. Though the functionals with S and XA exchange gave the worst energies, considerable improvement was observed with LC. For instance, the RMSD and E_{int} values given by SLYP functional were 0.295 and -6.628 kcal/mol respectively while those of LC-SLYP were 0.045 and -1.161 kcal/mol respectively, satisfying both geometry and energy criteria. Similarly functionals with BRx, mPW, and TPSS exchange, with few exceptions, reproduced the CCSD results extremely well in their LC forms. The functionals with PBE, PBEh, PKZB and PW91 exchange parts showed uneven trends. In some cases, LC forms performed better whereas in some other cases, non-LC forms gave better results. Exchange-only functionals gave poor results in LC and non-LC forms for both geometry and energy. Among the pure functionals, M06L performed well to reproduce both energy and geometry close to the CCSD level accuracy. However, with LC, all pure functionals showed bad results for energies.

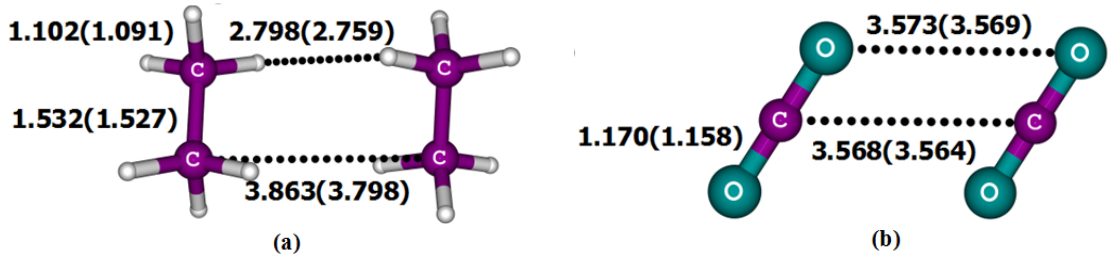

Figure 2.4 (a) Geometry of ethane dimer optimized at PW91P86/6-311++g(d,p) level (b) geometry of carbon dioxide dimer optimized at PW91B95/6-311++g(d,p) level. Corresponding CCSD/aug-cc-pVTZ level values are in parenthesis. Distances are in Å [Remya and Suresh 2013].

In the case of CO_2 dimer, functionals with B, BRx, G96, O, mPW, PKZB, S, TPSS and XA exchange with all types of correlation gave good results in the LC forms. The geometries and energies given by some of them without LC were very poor, but after LC incorporation they gave better results and some of them (BB95, G96B95, OB95, mPWB5,

PKZBB95, SB95 and TPSSB95) appeared in the list of recommended functionals. Functionals with PBE, PBEh, and PW91 exchange gave comparable results in LC and non-LC forms and in many cases; functionals without LC gave better results. Exchange-only functionals, neither with nor without LC gave acceptable results. Some of the pure functionals gave very good results without LC while they performed poorly in the LC forms.

2.4.2 Dipole-Induced Dipole Systems

2.4.2.1 Ammonia - Methane Complex

Ammonia-methane complex has the weakest interaction among all the complexes studied with E_{int0} = -0.76 kcal/mol. Out of the 382 functionals, 68 gave RMSD < 0.045, and 68 satisfied the energy criterion and 25 gave both (Figure 2.5). 14 exchange-correlation, 10 LC- exchange-correlation and 1 pure density functionals (HCTH147) were included in these 25 recommended functionals. All the 10 recommended LC-exchange-correlation functionals have VWN as their correlation part. The best geometry was given by PBEVWN (RMSD = 0.005, Figure 2.6) and the best value of interaction energy was given by mPWB95 (E_{int} = -0.769 kcal/mol). Almost all the recommended functionals gave excellent geometry while the functionals PBEhVWN, PBEVWN, wPBEhVWN, wPBEhPL, PBEhPL, PBEVWN5, mPWB95, PBEPL, TPSSB95 and mPWKCIS performed very well for both geometry and interaction energy.

Similar to the case of acetylene dimer, very poor results were obtained for both geometry and E_{int} for functionals with B, BRx, G96, S, O, and XA as exchange in many cases while they all showed massive improvement, particularly on the E_{int} with LC incorporation and some of them with VWN correlation (LC-OVWN, LC-BVWN, LC-G96VWN, LC-SVWN, LC-BRxVWN) even qualified to the recommended levels (Figure 2.5). All the pure functionals showed poor behavior with LC incorporation, particularly the values for E_{int} were very bad compared to other methods. In many cases, functionals with PW91, PBE and PBEh exchange gave good geometries compared to many other functionals. In general, a good geometry given by an exchange-correlation functional was not improved by further incorporation of LC. However, with LC-incorporation, overall the estimation of E_{int} was significantly improved in many cases. In the case of exchange only functionals, some improvement in geometry and energy was observed with LC, though not to the recommended levels.

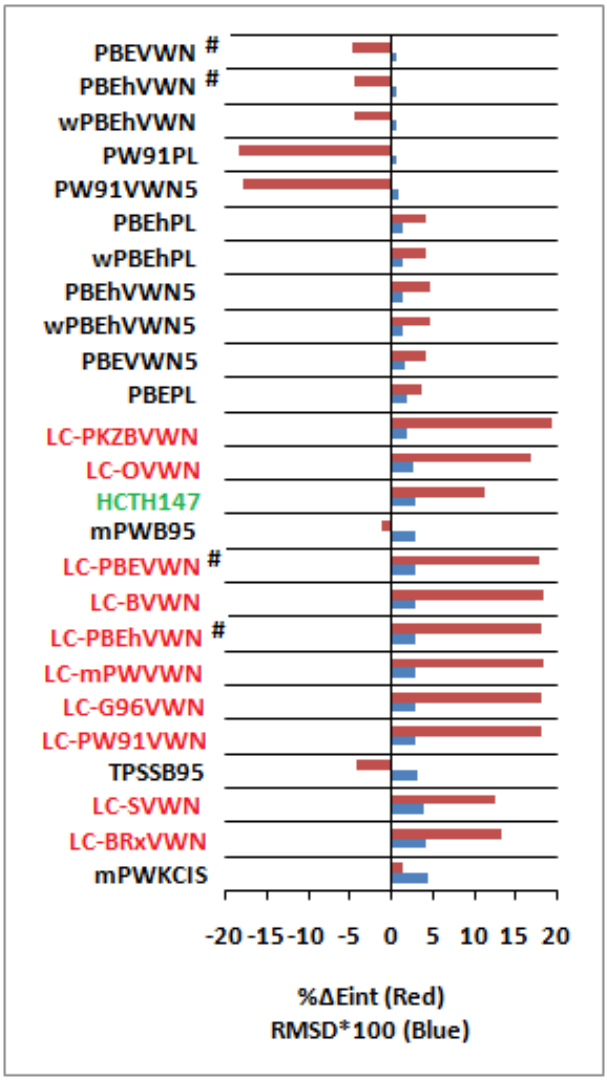

Figure 2.5 The recommended functionals given in the increasing order of RMSD for ammonia-methane complex. Exchange-correlation (black), LC-corrected exchange-correlation (red) and pure (green) functionals are also indicated. # indicates recommended functionals common for with and without LC.

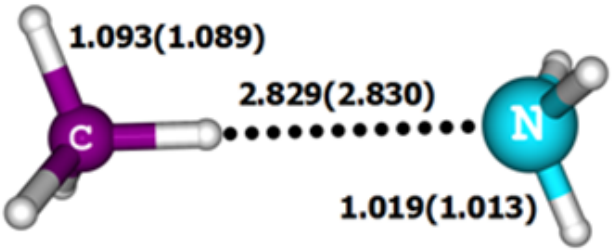

Figure 2.6 Geometry of ammonia-methane dimer optimized at PBEVWN/6-311++g(d,p) level. Corresponding CCSD/aug-cc-pVTZ level values are in parenthesis. Distances are in Å [Remya and Suresh 2013].

2.4.2.2 $CH_4\cdots HF$ and $C_2H_4\cdots HF$ Complexes

E_{int0} for $CH_4\cdots HF$ and $C_2H_4\cdots HF$ are -1.64 kcal/mol and -4.50 kcal/mol respectively. For $CH_4\cdots HF$, 121 functionals gave RMSD < 0.045, 113 gave E_{int} in the range $0.8E_{int0} < E_{int} < 1.2E_{int0}$ and 54 satisfied both criteria (Figure 2.7). 32 exchange-correlation, 3 LC-exchange-correlation, 1 pure (M06L), 16 hybrid, and 2 double hybrid functionals (B2PLYPD and mPW2PLYPD) are included in these 54 recommended functionals. In the case of $C_2H_4\cdots HF$, 177 functionals gave a good geometry, 131 gave a good energy and 127 satisfied both criteria (Figure 2.8), which include 54 exchange-correlation, 36 LC-exchange-correlation, 5 pure, 28 hybrid, and 4 double hybrid functionals. The correlation part of the LC-exchange-correlation functionals was PL (12 out of 36), VWN (11 out of 36) or VWN5 (13 out of 36).

The best geometry in the case of $CH_4\cdots HF$ was given by the hybrid functional mPW1LYP (RMSD = 0.002, Figure 2.9 a) while the best E_{int} in this case was given by LC-TPSSKCIS (E_{int} = -1.634 kcal/mol). In the case of $C_2H_4\cdots HF$ B1B95 method (RMSD = 0.002, Figure 2.9 b) gave the best geometry whereas the best E_{int} was given by wPBEhVWN and PBEhVWN (E_{int} = -4.495 kcal/mol for both) methods. In the case of $C_2H_4\cdots HF$, several LC methods performed remarkably well for reproducing both the geometry and E_{int} at the CCSD level accuracy while in the case of $CH_4\cdots HF$, only three LC methods (LC-PKZBKCIS, LC-PKZBKCIS, and LC-TPSSKCIS) performed to the recommended levels of accuracy.

In the case of $CH_4\cdots HF$, exchange-correlation functionals with B (with few exceptions), G96, O, S, and XA exchange showed very good improvement with LC for reproducing the benchmark values of both geometry and energy. Functionals having BRx, mPW, PBE, PBEh PW91 and TPSS exchange, except with PL, VWN and VWN5 correlation, gave better geometries without LC. But energies showed dissimilar and irregular trends. LC-functionals gave good energies in some cases whereas in some other cases non LC forms gave better results. For PBE and PBEh exchange, both LC and non-LC forms showed similar results. Exchange-only functionals showed small improvement with LC incorporation, but not to the 'recommended' levels. Pure functionals, especially M06L gave good results while all of them gave bad results with LC incorporation.

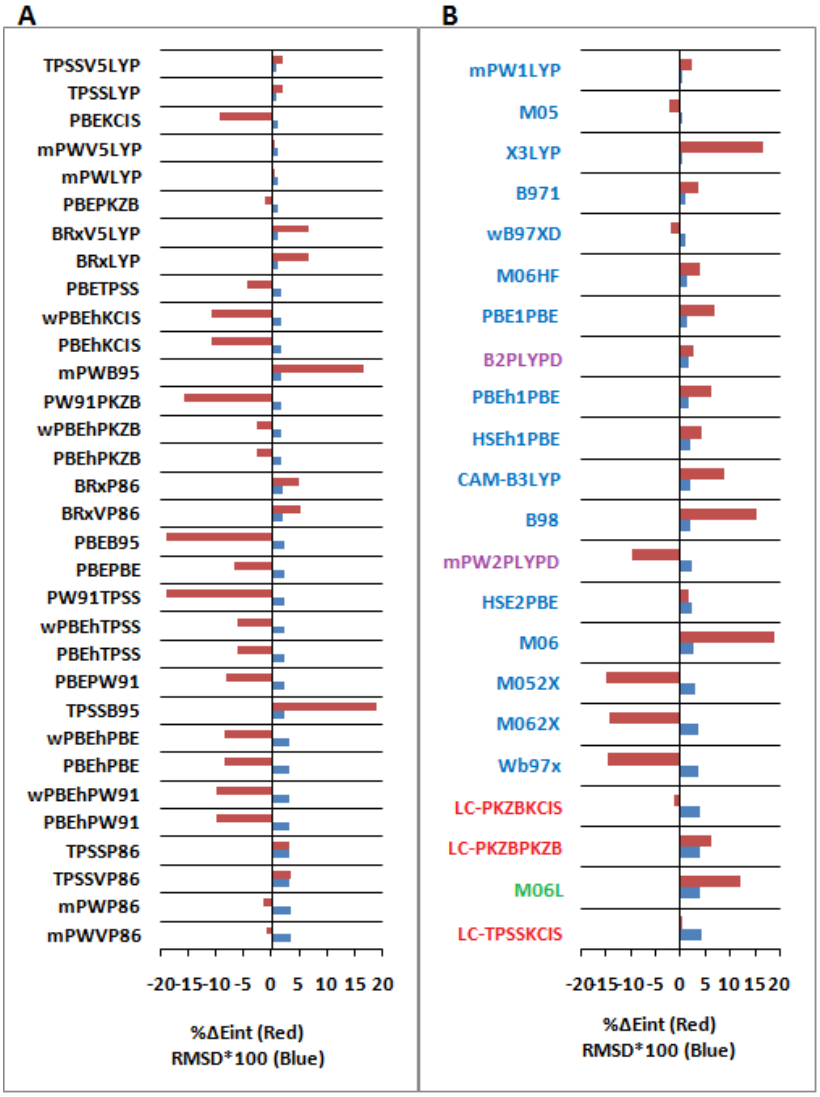

Figure 2.7 The recommended functionals given in the increasing order of RMSD for $CH_4\cdots HF$. Exchange-correlation (black), LC-corrected exchange-correlation (red) and pure (green), hybrid (blue) and double hybrid (purple) functionals are also indicated.

Many exchange-correlation functionals with and without LC gave very good results for both geometry and energy in the case of $C_2H_4\cdots HF$ (Figure 2.8). The exchange-correlation functionals made up of B, BRx, G96, mPW, PBE, PBEh, PW91, and TPSS exchange and PL, VWN, and VWN5 correlation are remarkable as they showed very good improvement in geometry with LC incorporation while the non-LC forms performed better when these exchange functions where combined with other correlation functions. Though the energies did not show a regular trend, the difference between the LC and non-LC functionals were not very high compared to other dimers. Functionals with S and XA exchange gave very poor results while their LC-forms showed acceptable values. Similarly, the exchange-only functionals showed bad results but good improvement for

geometry and E_{int} with LC. However, none of them satisfied the recommended values. The good results given by pure functionals became worse with LC, particularly for E_{int} values.

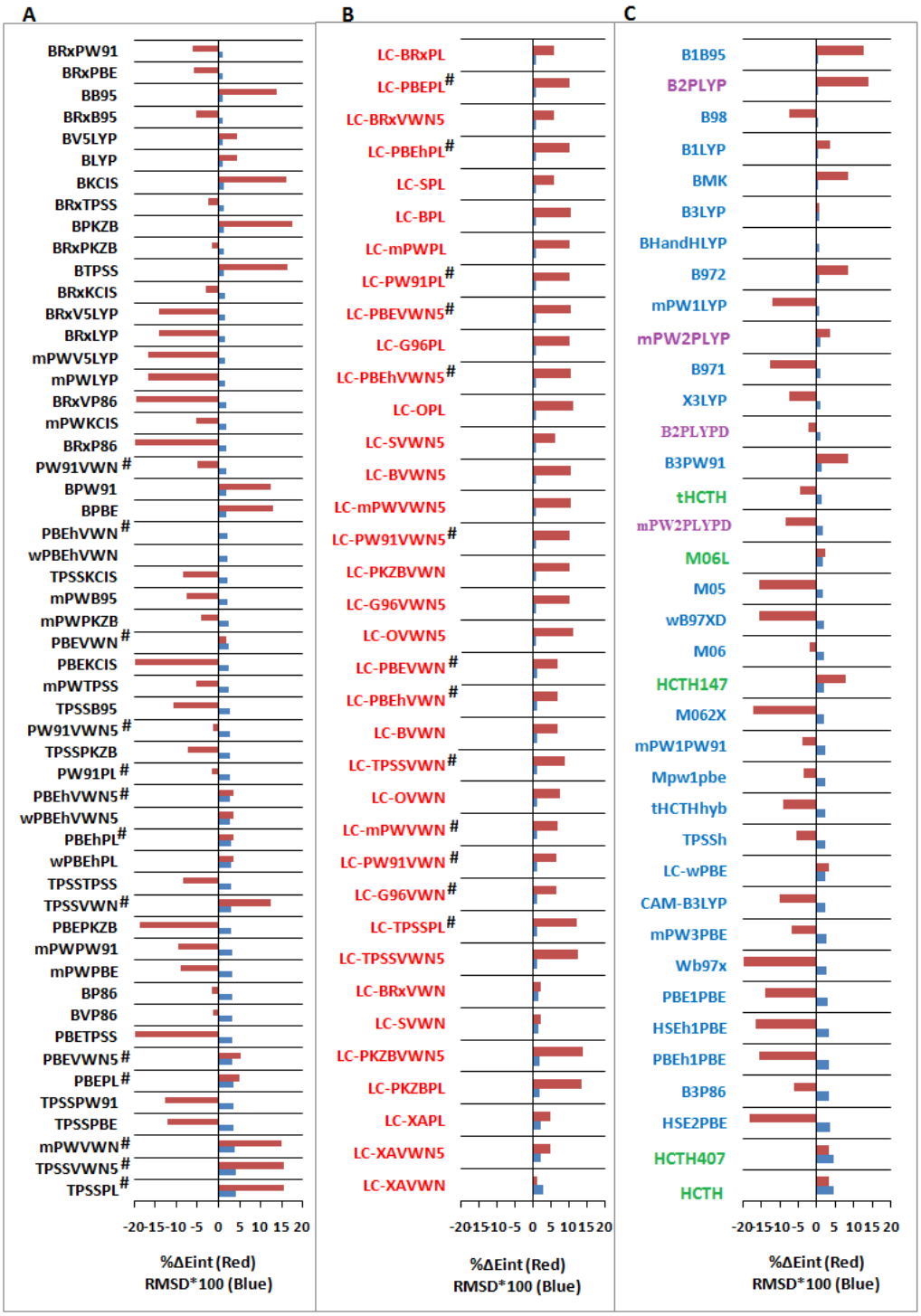

Figure 2.8 The recommended functionals given in the increasing order of RMSD for $C_2H_4\cdots HF$. Exchange-correlation (black), LC-corrected exchange-correlation (red) and pure (green), hybrid (blue) and double hybrid (purple) functionals are also indicated. # indicates recommended functionals common for with and without LC.

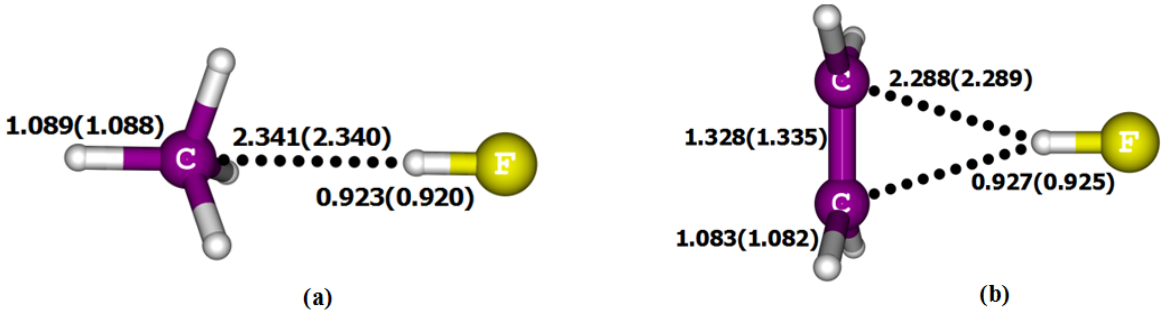

Figure 2.9 (a) Geometry of $CH_4\cdots HF$ complex optimized at mPW1LYP/6-311++g(d,p) level and (b) Geometry of $C_2H_4\cdots HF$ complex optimized at B1B95/6-311++g(d,p) level. Distances are in Å [Remya and Suresh 2013].

2.4.3 Dipole-dipole Systems

2.4.3.1 Acetonitrile Dimer

Among all the nine systems considered, acetonitrile has the highest value for E_{int0} (-6.28 kcal/mol). For this systems, 159 gave good geometry (RMSD < 0.045) and 170 gave good E_{int} ($0.8E_{int0} < E_{int} < 1.2E_{int0}$) while 104 gave both. Among these 104 recommended functionals, 31 exchange-correlation, 58 LC-exchange-correlation, 2 pure (B97D and M06L), 11 hybrid and 2 double hybrid functionals (wPW2PLYPD and B2PLYPD) were found (Figure 2.10). The best geometry was given by the long range-corrected version of the hybrid functional B3LYP *viz*. CAM-B3LYP (RMSD = 0.014, Figure 2.11) and the best value for E_{int} was given by the pure *meta*-GGA M06L (E_{int} = -6.242 kcal/mol) functional.

Among the recommended methods given in Figure 2.10, many of the methods without LC gave better geometries (Figures 2.10A and D) than those with LC (Figures 2.10B and C). However, the bad results given by the functionals with G96, O, PKZB, S, TPSS, and XA exchange showed massive improvement with LC. For instance, the (RMSD, E_{int}) for G96LYP, OLYP, PKZBLYP, XALYP and SLYP were (0.253 -1.277 kcal/mol), (0.290 -2.766 kcal/mol), (0.157 -4.322 kcal/mol), (0.206 -14.460 kcal/mol) and (0.177 -13.572 kcal/mol) respectively while in their LC forms, these were improved to (0.032 -6.681 kcal/mol), (0.037 -6.628 kcal/mol), (0.021 -6.481 kcal/mol), (0.050 -11.142 kcal/mol), and (0.034 -6.849 kcal/mol) respectively. Some of these methods, especially SLYP satisfied the criteria for both geometry and E_{int}.

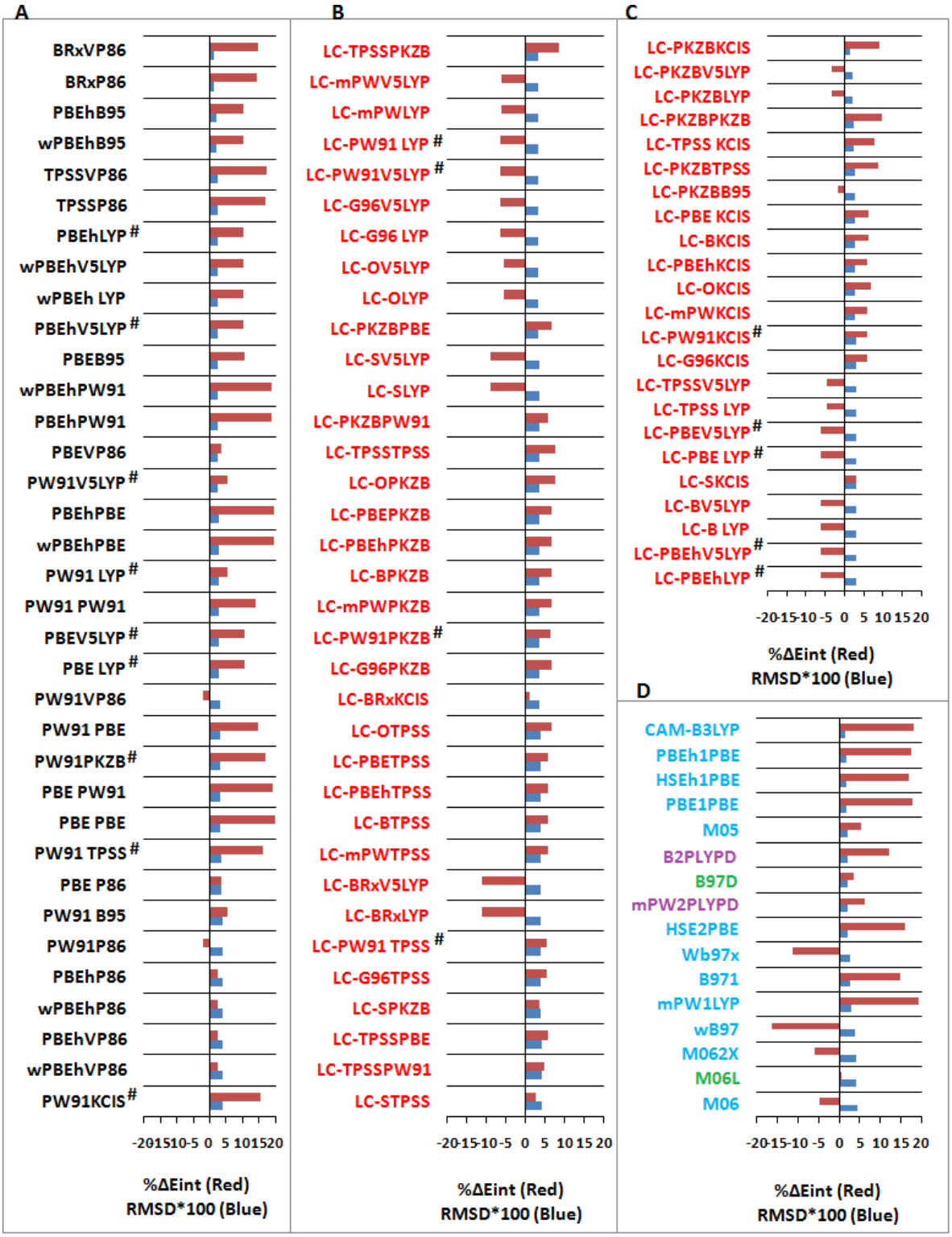

Figure 2.10 The recommended functionals given in the increasing order of RMSD for acetonitrile dimer. Exchange-correlation (black), LC-corrected exchange-correlation (red), pure (green), hybrid (blue) and double hybrid (purple) functionals are also indicated. # indicates recommended functionals common for with and without LC.

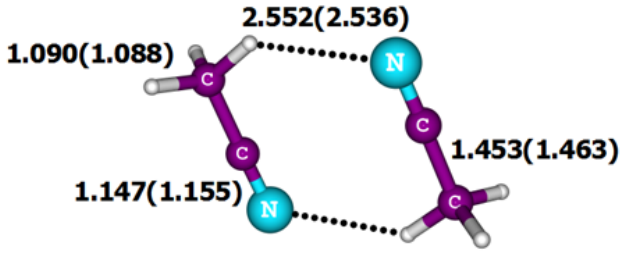

Figure 2.11 Geometry of acetonitrile dimer optimized at CAM-B3LYP/6-311++g(d,p) level. Corresponding CCSD/aug-cc-pVTZ level values are in parenthesis. Distances are in Å [Remya and Suresh 2013].

Similarly, the bad geometries and bad interaction energies given by functionals with B and mPW exchange showed improvement with LC. In many cases, the functionals with BRx, PBE, and PBEh exchange gave good values for E_{int} and they were only slightly improved with LC.

2.4.3.2 Formaldehyde and Fluoromethane Dimers

The value of E_{int0} is -3.72 kcal/mol in the case of $(HCHO)_2$ and -2.43 kcal/mol in the case of $(CH_3F)_2$. For $(HCHO)_2$, 108 functionals gave good geometry, 159 gave good E_{int} and 75 gave both (Figures 2.12A, B and C). These 75 recommended functionals include 25 exchange-correlation, 35 LC-exchange-correlation, 12 hybrid, and 3 double hybrid functionals. The correlation part of the LC-functionals had some similarities; 13 out of 35 had VWN as their correlation part while others had VWN5 (11 cases) and PL (11 cases). In the case of $(CH_3F)_2$, a large number of functionals (181) gave E_{int} in the range $0.8E_{int0} < E_{int} < 1.2E_{int0}$ while only 5 gave RMSD < 0.045 and 4 functionals among them satisfied both geometry and energy criteria (Figure 2.12 D). These 4 functionals include one exchange-correlation (mPWP86), two hybrid (wB97XD and M06), and one pure (M06L) density functionals. The (RMSD, E_{int}) values given by mPWP86, wB97XD, M06 and M06L for $(CH_3F)_2$ are (0.045, -2.204 kcal/mol), (0.015, -2.758 kcal/mol), (0.043, -2.290 kcal/mol) and (0.005, -1.992 kcal/mol) respectively.

The best geometry for formaldehyde dimer was given by mPW2PLYP (RMSD = 0.002, Figure 2.13 (a)) and the best interaction energy was given by PBELYP and PBEV5LYP (E_{int} = -3.707 kcal/mol). For fluoromethane dimer, the best geometry was

given by M06L (RMSD = 0.005, Figure 2.13 (b)) and the best interaction energy was given by M06 functional (E_{int} = -2.290 kcal/mol).

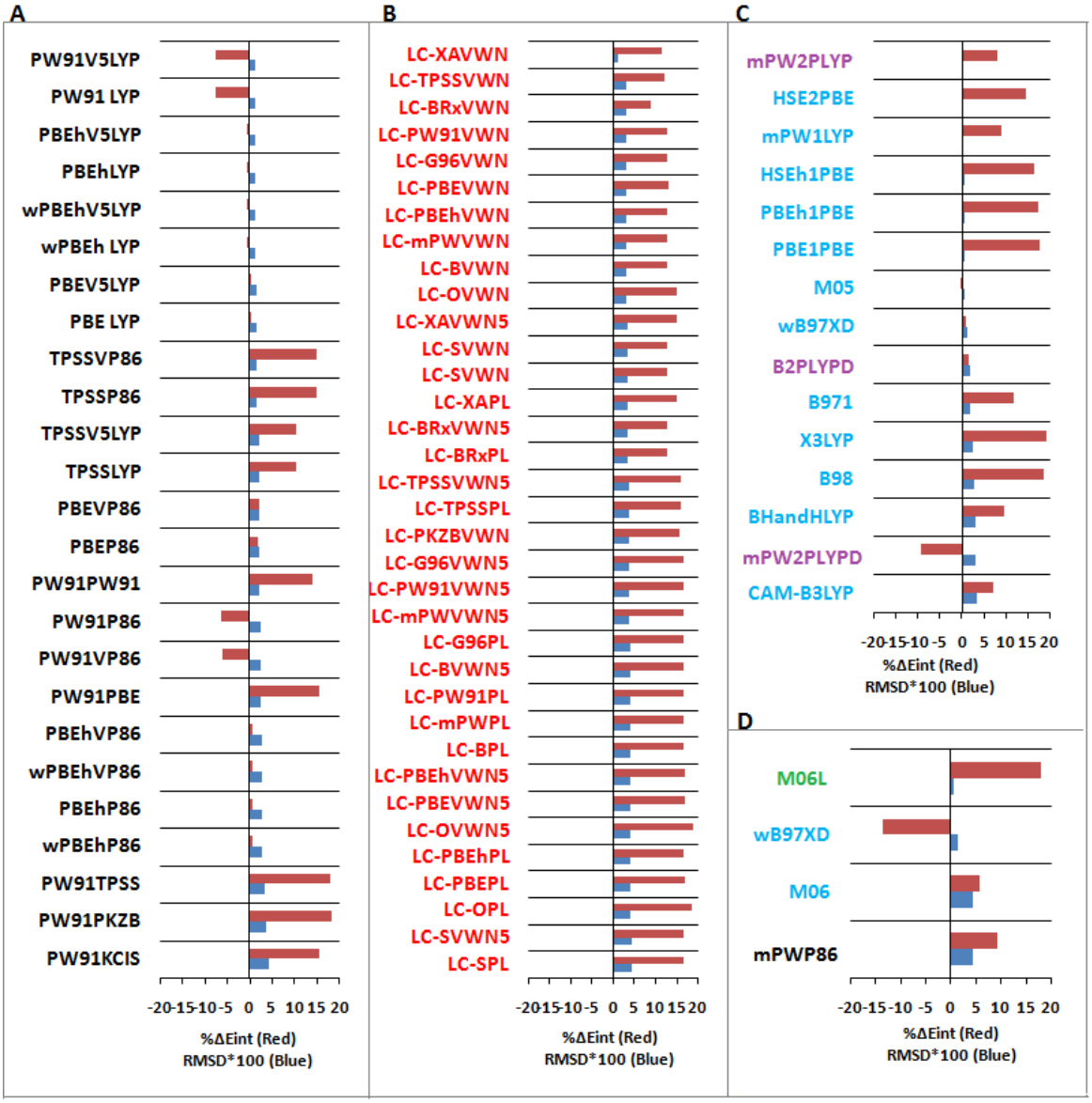

Figure 2.12 The recommended functionals given in the increasing order of RMSD. (A), (B) and (C) for formaldehyde dimer and (D) for fluoromethane dimer. Exchange-correlation (black), LC- exchange-correlation (red), pure (green), hybrid (blue) and double hybrid (purple) functionals are also indicated.

Functionals with G96, O, PKZB, S, and XA exchange gave poor results for formaldehyde dimer. LC incorporation showed great improvement in geometry and energy and some LC forms even appeared in the recommended list of functionals (Figure 2.12). The remaining functionals showed mixed trends. Functionals with PBE, PBEh, and PW91 exchange gave good geometries without LC in most of the cases. Exchange-only functionals neither with nor without LC showed good results.

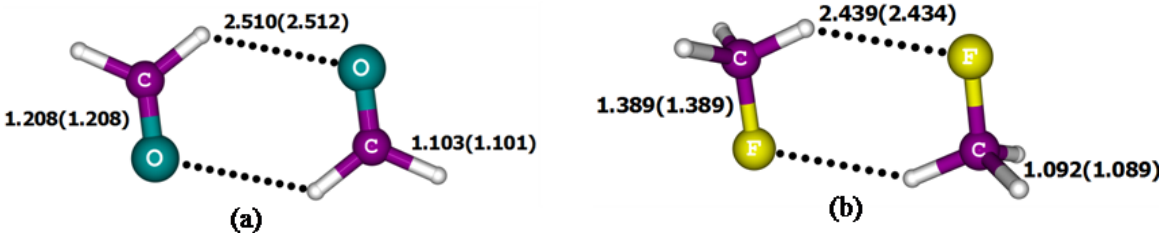

Figure 2.13 (a) Geometry of formaldehyde dimer optimized at mPW2PLYP/6-311++g(d,p) level. (b) Geometry of fluoromethane dimer optimized at M06L/6-311++g(d,p) level. Corresponding CCSD/aug-cc-pVTZ level values are in parenthesis. Distances are in Å [Remya and Suresh 2013].

In the case of fluoromethane dimer, exchange-correlation functionals with G96, O, S, and XA exchange showed very good improvement with LC. With PBE, PBEh, and PW91 exchange, the difference between LC and non-LC values were not very significant. Others showed irregular tendencies for both energies and geometries. Similarly, the exchange-only functionals showed irregular trends and none of them appeared among the recommended functionals. Pure functionals gave good values for energy and geometry without LC.

2.4.4 Best Performing Density Functionals for All the Nine Dimers

The number of acceptable energies and geometries given by each of the functionals were counted separately to find out the 'best performing' functionals. Functionals providing at least five hits for acceptable geometry and five hits for acceptable energy out of the nine geometries and nine interaction energies evaluated were included in the best performing list. 17 functionals satisfied these criteria (Table 2.1). In this list M06L functional came out as the most outstanding one with a total hit count of 14 out of a maximum of 18. Also, this was the only functional which gave good geometry as well as energy for at least two systems in each class. Moreover, this was the functional recommended for the highest number of dimers (6 dimers). None out of the nine energies given by this functional showed an error greater than 25% compared to the Ave-CCSD(T)/(Q-T) value and the highest RMSD value given by an M06L optimized geometry was 0.109. Other functionals in the best performing category were PBEB95, M05, B971, B2PLYPD, mPW2PLYPD, and CAM-B3LYP giving 11 hit counts. Out of these, mPW2PLYPD, M05, and B971were recommended for five dimers and there were at least 1 dimer from each class. Remaining

Table 2.1 The list of best performing DFT methods.

	No. of acceptable RMSD	No. of acceptable E_{int}	Total hit counts	Ave. RMSD (of all 9 systems)	Ave. $\%\Delta E_{int}$ (of all 9 systems)
M06L	7	7	14	0.042	13
M05	5	6	11	0.040	-5
B2PLYPD	6	5	11	0.043	22
B971	5	6	11	0.051	12
mPW2PLYPD	5	6	11	0.046	16
PBEB95	5	6	11	0.049	20
CAM-B3LYP	5	6	11	0.055	25
PBEhB95	5	5	10	0.049	21
PW91B95	5	5	10	0.052	24
Wb97x	5	5	10	0.056	21
BRxVP86	5	5	10	0.049	32
BRxP86	5	5	10	0.051	32
HSE2PBE	5	5	10	0.069	26
HSEh1PBE	5	5	10	0.071	26
PBE1PBE	5	5	10	0.071	27
PBEh1PBE	5	5	10	0.072	27
PW91TPSS	5	5	10	0.087	28

functionals in the best performing list were PW91B95, PBEhB95, Wb97x, BRxVP86, HSE2PBE, BRxP86, PBE1PBE, HSEh1PBE, PW91TPSS and PBEh1PBE giving 10 hit counts. Among these, PW91TPSS and Wb97x were recommended for four dimers and there were at least one dimer from each class. CAM-B3LYP, HSEh1PBE, HSE2PBE, PBEh1PBE and PBE1PBE functionals were also recommended for 4 systems but they did not appear among the 'recommended' functionals of any of the class 1 dimers. We also

note that functionals such as BRxVP86, BRxP86 PW91B95 and PBEhB95 have never been discussed in the literature and hence further studies may be required to validate their use as recommended methods for non-covalent interactions.

Table 2.2 The list of best performing LC-exchange-correlation functionals.

Functional	No. of acceptable RMSD	No. of acceptable E_{int}	Total hit counts	Ave. RMSD (of all 9 systems)	Ave.%ΔE_{int} (of all 9 systems)
LC-G96KCIS	4	6	10	0.048	18
LC-PKZBPKZB	4	6	10	0.045	21
LC-PKZBKCIS	4	5	9	0.045	19
LC-OKCIS	4	5	9	0.046	20
LC-TPSSKCIS	4	5	9	0.047	19
LC-BRxVWN	5	4	9	0.077	27
LC-G96VWN	5	4	9	0.082	31
LC-PW91VWN	5	4	9	0.083	31
LC-PBEhVWN	5	4	9	0.083	31
LC-mPWVWN	5	4	9	0.083	31
LC-BVWN	5	4	9	0.083	31
LC-SVWN	5	4	9	0.084	29
LC-PBEVWN	5	4	9	0.084	31
LC-OVWN	5	4	9	0.084	32

Thus, 6 exchange-correlation functionals, 1 pure functional (M06L), 6 hybrid functionals, long-range corrected version of B3LYP by Handy and coworkers (CAM-B3LYP), 1 long-range corrected functional from Head-Gordon and coworkers (Wb97x), and 2 double hybrid functionals with dispersion correction (B2PLYPD, mPW2PLYPD) are included in the best performing list. It may be noted that these functionals were screened from a total of 169 exchange-correlation, 8 pure, 33 hybrid, and 4 double hybrid functionals.

Even though the long-range correction of Hirao and co-workers applied on exchange-correlation functionals (LC-forms) showed massive improvement in describing the geometry and E_{int} in all the cases, none of them appeared in the list of best performing functionals since none of LC functionals were consistently good performing to give at least 5 good geometries along with 5 good E_{int}. Hence we considered the LC-methods which give at least 4 acceptable geometries, 4 acceptable energies and a total hit count 9 to make the list of the best performing LC-methods (Table 2.2). Notable among them were LC-PKZBPKZB, LC-G96KCIS, LC-PKZBKCIS, LC-TPSSKCIS and LC-OKCIS whose ave. RMSD and ave. $\%\Delta E_{int}$ were close to the acceptable values. Among these, LC-PKZBPKZB and LC-G96KCIS gave 10 hit counts with 4 acceptable geometries and 6 acceptable energies.

2.5 Conclusions

Among the 382 density functionals studied, M06L outperformed all the others in calculating the geometry and E_{int} of the nine dimers with accuracy close to that of CCSD. The functionals mPW2PLYPD, M05, B971, PW91TPSS and Wb97x also performed well and gave acceptable energy and geometry for at least one system from each class. The effect of LC on exchange-correlation functionals, especially on those with S, G96, O, and XA exchange was significant. The use of LC is highly advisable for almost all exchange-correlation functionals. Among dispersion dominated dimers (class 1), exchange-correlation and LC-exchange-correlation functionals along with a few pure, hybrid, and double hybrid functionals showed a good performance. Only a few functionals were recommended for the CO_2 dimer while many functionals could reproduce correct geometry for the C_2H_2 dimer. For $C_2H_4\cdots HF$, a member of the 'dipole-induced dipole' class 2, several functionals could give very good results. This was the only system for which most of the functionals with B and BRx exchange gave good geometry as well as good energy. Generally, exchange-correlation functionals showed good performance for all the dimers of this class. The CH_3F dimer in the 'dipole-dipole' class 3 was the toughest to deal with as only 5 functionals could give an acceptable geometry for it. The functionals mPWB95 and TPSSB95 gave acceptable geometry as well as energy for all the three dimers of class3 with 'dipole-induced dipole' interaction between them. In all the three classes, some functionals gave acceptable E_{int} while some others gave acceptable geometry for all the three dimers. Although, a functional that satisfies geometry and energy criteria for all the

nine molecules in three classes was not found, M06L gave the most satisfactory results with seven acceptable geometries and seven acceptable energies. Moreover, the average RMSD and $\%\Delta E_{int}$ values given by this functional were in the acceptable range.

Among the 'recommended' LC-exchange-correlation functionals, a dominance of functionals with LYP and V5LYP correlation is observed for $(C_2H_2)_2$ and $(C_2H_6)_2$ while B95 correlation showed good performance for $(CO_2)_2$. Those with VWN and VWN5 exchange came out to be the best among LC-exchange-correlation functionals to describe CH_4-NH_3 and C_2H_4-HF in class 2 and $(HCHO)_2$ in class 3. Functionals with PBE, PBEh, and PW91 exchange were not much influenced by LC whereas S, G96, O, and XA exchange-correlation functionals must always be used along with LC to get good values for geometry and interaction energy. On the basis of this study, we recommend that M06L is the best DFT method in *Gaussian09* for the study of small non-covalently interacting systems. CAM-B3LYP, B971, B2PLYPD, mPW2PLYPD, M05 and PBEB95 can also be recommended on the basis their total number of hit counts and the average of RMSD and $\%\Delta E_{int}$. The best among the LC-exchange-correlation methods are LC-PKZBPKZB and LC-G96KCIS.

CHAPTER 3

Non-Covalent Interactions and Cooperativity in Molecular Clusters

Part A – Growth Patterns of Acetonitrile Clusters and Cooperativity

&

Part B - Intermolecular C···C, N···N and O···O Bonding in Dipolar Organic Molecules

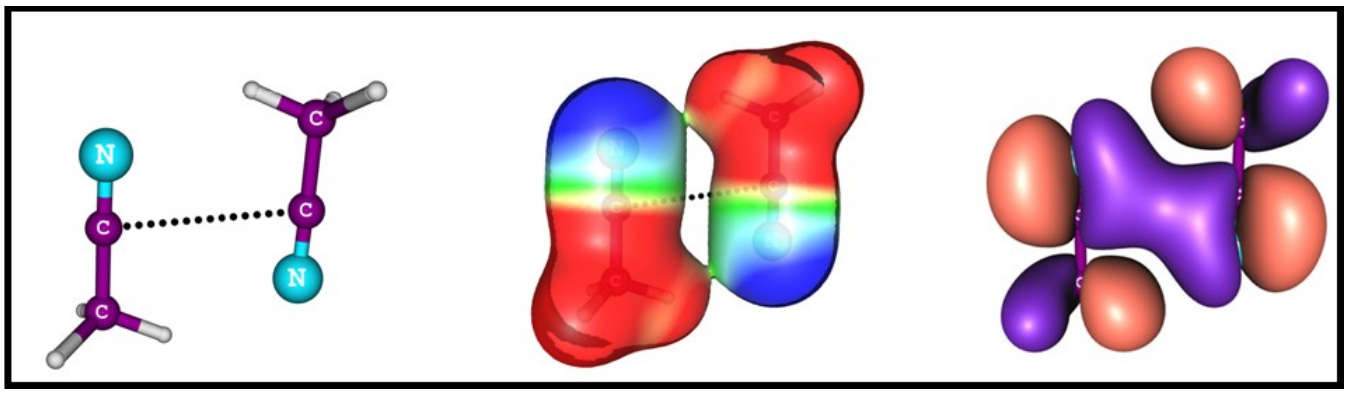

3.1 Abstract

*In part A of this chapter, a study on different growth patterns of acetonitrile clusters viz. cyclic, ladder type, stacked, cross-stacked and mixed patterns is performed with M06L/6-311++g(d,p) DFT method. The selected DFT method is the best performing DFT method to describe the non-covalent interactions (Chapter 2). The basis set superposition error (BSSE)-corrected interaction energy (E_{int}) and interaction energy per monomer (E_m) data for clusters containing up to 27 monomers (**27mer**) have been obtained. The cooperativity of intermolecular interactions in the growth patterns is studied by analyzing their E_m values. The magnitude of E_{int} shows a steady increase from the antiparallel dimer (-5.93 kcal/mol) to **27mer** (-211.72 kcal/mol). Also, a 2.6 fold increase in the value of E_m from dimer to **27mer** indicated a strong cooperativity of intermolecular interactions. The E_{int} and E_m values indicate the highest stability and cooperativity in stacked clusters followed by cross-stacked ones. The highest number and strength of inter-molecular interactions explain the maximum stability and cooperativity of the stacked clusters, which is also supported by quantum theory of atoms in molecules (QTAIM) and molecular electrostatic potential (MESP) data. Sum of electron density (ρ) at intermolecular bond critical points (BCPs) is the highest for stacked followed by cross-stacked clusters. Also, area of negative-valued MESP shows the lowest value in stacked clusters, indicating maximum utilization of lone pair density and maximum cooperativity in stacking growth pattern. Further, based on the observation that the **hexadecamer1** (the cluster with 16 monomers) is more stable than α and β crystal patterns of acetonitrile with 16 monomer units, we predict a new crystal structure for acetonitrile that is more stable and ordered than the existing (α and β) forms.*

In the Part B of this chapter, the inter-molecular C···C interaction between the nitrile carbon atoms of two antiparallelly oriented acetonitrile molecules, observed in the most stable acetonitrile clusters showing C···C distance 3.2 – 3.4 Å is studied in detail. The carbon atoms responsible for such interactions belong to similar chemical environments is a noteworthy feature as typical intermolecular interactions occur between two atoms in different chemical environments (usually one donor atom and one acceptor atom). This type of C···C interactions has been studied for the first time. In order to obtain further evidence for such C···C interactions, homogeneous dimers of several dipolar organic molecules have been investigated on the basis of molecular orbital (MO), natural

bond orbital (NBO), MESP, energy decomposition (EDA) and QTAIM electron density analyses. Apart from C···C interactions, evidence for N···N and O···O interactions between atoms in similar chemical environments is also obtained. MESP analysis is used to characterise the electron rich and electron deficient regions of the interacting monomers and suggested that these X···X (X = C, N and O) interactions result from complementary electrostatic interactions between electron rich region on one monomer with electron deficient region of the second. NBO analysis provides evidence for charge transfer between the two X atoms. The strength of this type of interaction depends directly on the dipole moment of the interacting monomers. The EDA analysis shows that interaction energy of these monomers is mainly electrostatic in nature. The C···C interaction between similar carbon atoms is located for several crystal structures obtained from the literature. A rigorously tested QSAR (quantitative structure-activity relationship) equation is derived to predict E_{int} for all dimer systems from their sum of electron density at the intermolecular bond critical points ($\sum\rho$) and monomer dipole moment (μ). This equation suggests that polarization induced bonding interaction between atoms in similar chemical environment could be a general phenomenon in chemistry. Further validation of the geometries and binding energies is done using the high accuracy G3MP2 method and also with other DFT methods.

PART A: Growth Patterns of Acetonitrile Clusters and Cooperativity

3.2 Introduction

The phenomenon of cooperativity arises when different types of interactions exist together and the properties of the system are the result of interplay between these interactions [Hunter and Anderson 2009]. This interplay between different interactions can result in positive or negative cooperativity, depending on whether one interaction strengthens the other or not. Understanding cooperativity of intermolecular interactions, especially hydrogen bonds in molecular cluster is particularly important in studying chemical as well as biological processes [Cabaleiro-Lago and Ríos 1999a] since it affects various molecular properties such as geometries and vibrational frequencies [King and Weinhold 1995; Wieczorek and Dannenberg 2003a; Wieczorek and Dannenberg 2003b] as well as physical properties of materials such as solvation behaviour of liquids [Richardi *et al.* 1998] and tertiary and quaternary structures of proteins [Esrafili *et al.* 2011]. Cooperativity drives the individual molecules towards the formation of clusters. This phenomenon is non-additive in nature [Del Bene and Pople 1969] due to which, intermolecular interactions such as hydrogen bonds will be stronger in a large cluster compared to that in an isolated dimer [Parra and Ohlssen 2008] and hence many molecules inherently possess a tendency to exist together as large clusters and in bulk, as liquids or solids.

Study of cooperative the intermolecular associations of liquid molecules in gas phase [C. P. Schullz 1994] and their structural ordering in liquid phase [Castleman and Bowen 1996] is important in understanding the process of solvation. Detailed understanding of the phenomenon of solvation is important since it influences the functioning of several biological macromolecules [Antony *et al.* 2009] and the chemical behaviour of compounds [Bacelo 2002]. Also, by studying large molecular clusters, the transition between gas and solid phases can be understood in detail. [Cabaleiro-Lago and Ríos 1999a] Systems of chemically as well as biologically relevance such as clusters of water, [Clementi *et al.* 1980; Del Bene and Pople 1969; Deshmukh *et al.* 2008; Liu *et al.* 1996; Ludwig and Appelhagen 2005; Maheshwary *et al.* 2001; Suhai 1994; Xantheas

2000] amides, [Esrafili *et al.* 2008; Jiang and Wang 2009; Kobko and Dannenberg 2003a; Kobko and Dannenberg 2003b; Kobko *et al.* 2001; Ludwig 2000; Ludwig *et al.* 1997; Mahadevi *et al.* 2011; Tan *et al.* 2005] urea, [Esrafili *et al.* 2011] amino acids and their oligomers [Ireta *et al.* 2003; Viswanathan and Dannenberg 2008; Wieczorek and Dannenberg 2003a; Wieczorek and Dannenberg 2003b; Wu and Zhao 2001; Zhao and Wu 2002] and numerous other systems have been extensively studied using different theoretical approaches.

Here, acetonitrile, a widely used aprotic solvent with a high dipole moment (3.92 D) [Alston Steiner and Gordy 1966] is analyzed for the relative stability of its cluster growth patterns and the cooperativity of intermolecular interactions in them. The high boiling point of acetonitrile (82°C) compared to that of hydrogen cyanide is (25.6°C) despite the presence of much less polarized methyl hydrogen atoms in the former indicates strong cooperativity in its intermolecular interactions in it. At the same time, the melting point of acetonitrile is very low (-45°C) compared to that of hydrogen cyanide (-13.4°C) indicating inefficient solid state packing in the former. Thus, it will be interesting to study the patterns of cluster formation in acetonitrile as well as their cooperativity. In general, increase in alkyl substitution leads to increase in the melting point of a compound. But the melting point -45°C, -93°C and -72°C observed respectively for CH_3CN, CH_3CH_2CN and $(CH_3)_2CHCN$ is a clear exception to this common trend. This remarkably high melting point of CH_3CN compared to other two higher alkyl derivatives are difficult to explain. In the formation of acetonitrile clusters, it is believed that the intermolecular interaction is mainly governed by electrostatics rather than hydrogen bond (HB) interactions. [Cabaleiro-Lago and Ríos 1999b] The C-H**...**N hydrogen bonding interactions should be considered while discussing the stability of acetonitrile clusters [Mata and Costa Cabral 2004], even though the possibility of C-H bond acting as a hydrogen bond donor is still controversial, [Scheiner 1997].

Different growth patterns of acetonitrile have been studied by many theoretical groups using semi empirical potential functions, density functionals and ab initio methods. [Böhm *et al.* 1984; Cabaleiro-Lago *et al.* 2000; Cabaleiro-Lago and Ríos 1997; Cabaleiro-Lago and Ríos 1999b; Defranceschi *et al.* 1993; Edwards and Madden 1984; Ford and Glasser 2001; Jorgensen and Briggs 1988; Kharat *et al.* 2013; La Manna 1983; Mata and Costa Cabral 2004; Mathieu *et al.* 1993; Nigam and Majumder 2008; Siebers *et al.* 1998] Experimental groups have also worked for identifying the ordering in the

structure of both liquid and solid acetonitrile. [Barrow 1981; Bertagnolli *et al.* 1976; Bertagnolli and Zeidler 1978; Enjalbert and Galy 2002; Torrie and Powell 1992] Some of the studies used both theory and experiment. [Al-Mubarak *et al.* 1988] Most of the studies propose that acetonitrile prefer an antiparallel dimer structure and bigger clusters consisting of antiparallel dimer units. In this work, our aim is to explore the structural ordering and cooperativity of intermolecular interactions in acetonitrile clusters in terms of different types of intermolecular interactions including dipolar and C-H**...**N interactions. Pair wise interaction energies, MESP and electron density at intermolecular BCP's obtained using QTAIM analyses are used in comparing and explaining the relative stability of the patterns studied. Structural, vibrational, and energetic features of the clusters are also described.

3.3 Computational Methods

Types of acetonitrile clusters studied include those with stacked, cross-stacked, ladder type, cyclic and mixed arrangements. These patterns are studied for their relative stability up to six monomers (hexamers) and on the basis of the most stable configuration, the study is extended to bigger clusters such as two octamers, four dodecamers one hexadecamer and one 27mer. Molecular patterns in the two crystal structures of acetonitrile (α and β patterns) [Enjalbert and Galy 2002] with sixteen monomers are also optimized. All the structures are confirmed to be local minima by frequency calculations. The density functional M06L with 6-311++G(d,p) basis set is used for clusters containing up to eight monomers. For clusters containing more than eight monomers, M06L/6-311++G(d,p)//M06L/6-31G(d,p) method was chosen to reduce the computational cost. The model chemistry M06L/6-311++G(d,p) is shown to yield geometry as well as interaction energy with accuracy close to that of CCSD levels, as shown in the extensive benchmark study described in Chapter 2 [Remya and Suresh 2013]. All the calculations are done using *Gaussian09* [Frisch *et al.* 2010] suite of programs.

The results are further verified using two more density functionals from the list of best performing functionals from our benchmark study (Chapter 2) *viz*. CAM-B3LYP (the long range corrected version of B3LYP by Handy and co-workers [Yanai *et al.* 2004]) and Grimme's dispersion corrected functional B2PLYPD [Grimme 2006b]. Clusters up to tetramers are also optimized using these functionals and the results are compared with those given by M06L.

The total interaction energy (E_{int}) of a cluster M_n, where M is the monomer and n is the number of monomers, is calculated by the super molecule approach given in Eq. (3.1).

$$E_{int} = E_{cluster} - n \times E_{monomer} + E_{BSSE} \quad \text{(Eq. 3.1)}$$

Where $E_{cluster}$ is the energy of the cluster M_n and $E_{monomer}$ is the energy of isolated monomer. E_{BSSE} is the correction factor for the basis set super position error which is calculated using the counterpoise correction method of Boys and Bernardi [Boys and Bernardi 1970] as implemented in *Gaussian09*.

Counterpoise corrected pair-wise interaction energies in the clusters were calculated up to hexadecamer. This helps to quantify the effects of relative orientation of the dimers in deciding the interaction energy and hence the stability of each type of clusters.

The nature of intermolecular interactions was analyzed using AIM2000 software package [Biegler-König and Schönbohm 2002; Biegler-König *et al.* 2001; Biegler-König *et al.* 2000], which applies Bader's [Bader 1990] QTAIM theory. The value of electron density (ρ) at the BCP's corresponding to intermolecular interactions in QTAIM topology is often used as a direct measures of the strength of such interaction [Mahadevi *et al.* 2011]. More insights on the intermolecular interactions and cooperativity are obtained from the analysis of molecular electrostatic potential. The theory and applications of MESP in chemical systems are explained in detail elsewhere [Gadre and Shirsat 2000; Murray and Sen 1996; Politzer and Truhlar 1981]. In the formation of acetonitrile clusters, several C-H**...**N interactions arise which modifies the MESP distribution in the cluster. These changes in MESP isosurface is monitored to obtain information on the relative stability and cooperativity of the clusters.

3.4 Results and Discussion

3.4.1 Geometries and Interaction Energies of the Clusters

The calculated values of E_{int}, E_{BSSE}, interaction energy per monomer (E_m) and interaction energy without BSSE correction (E_{int_noBSSE}) are depicted in Table 3.1. The stability of a cluster is mainly determined by three factors. First one is the C-H**...**N hydrogen bonding interaction, which is of two types. First type of C-H**...**N interaction is found in systems with antiparallelly arranged monomers, which show C-H**...**N angle in the

range 125-135° and C-H**...**N distance in the range 2.45 - 3.00 Å while a second category of systems having cyclic arrangement of monomers show a wider C-H**...**N angle (150-175°) and a shorter interaction distance (2.25 – 2.27 Å). The second factor that influences the stability of a cluster is the dipolar interaction. Previous theoretical studies [Cabaleiro-Lago *et al.* 2000; Cabaleiro-Lago and Ríos 1997; Cabaleiro-Lago and Ríos 1999b; Defranceschi *et al.* 1993; Mata and Costa Cabral 2004] suggest that antiparallel orientation of the molecular dipoles is favoured in acetonitrile clusters. The third factor is a destabilizing interaction arising from parallel alignment of the dipoles in the cluster.

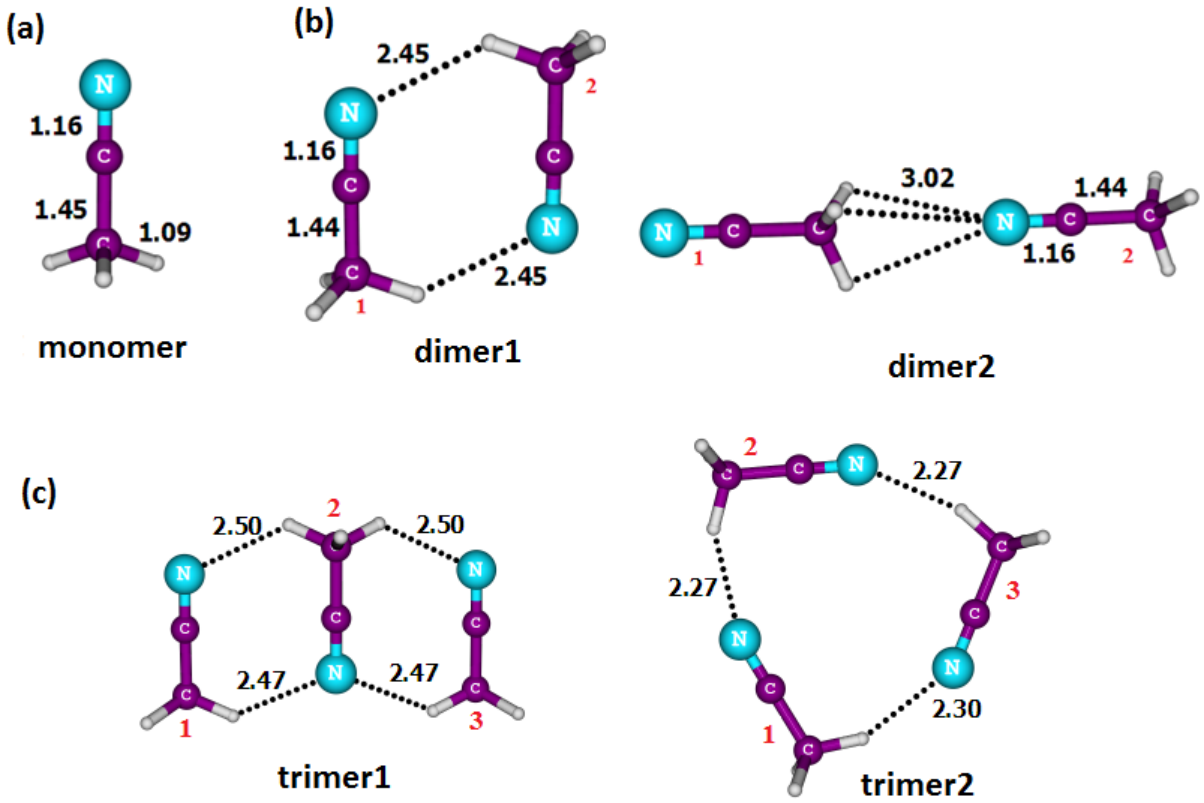

Figure 3.1 Optimized geometries of (a) acetonitrile monomer, (b) antiparallel (**dimer1**) and linear (**dimer2**) dimers and (c) ladder type (**trimer1**) and cyclic (**trimer2**) trimers optimized at M06L/6-311++G(d,p) level [Remya and Suresh 2014].

In Figure 3.1, acetonitrile monomer geometry is given along with an antiparallel (**dimer1**) and a linear (**dimer2**) dimer structures. From Table 3.1, it can be seen that E_{int} of **dimer2** (-2.63 kcal/mol) is less than half that of **dimer1** (-5.93 kcal/mol). The latter, with a C_{2h} symmetry was located as the minimum in previous studies using potential functions [Cabaleiro-Lago *et al.* 2000; Cabaleiro-Lago and Ríos 1997] and B3LYP/6-31++G(d,p) level of DFT. [Nigam and Majumder 2008] E_{int} of **dimer1** shows a good

agreement with the E_{int} value reported by Mackie and DiLabio [MacKie and DiLabio 2011] at Ave-CCSD(T)/(Q-T) level of theory (-6.28 kcal/mol). The **dimer1** possesses two

Table 3.1 The values of interaction energies (E_{int}), BSSE values (E_{BSSE}) and interaction energy per monomer (E_m) in kcal/mol of different types of acetonitrile clusters studied.

Cluster name	E_{int}	E_{BSSE}	E_m	E_{int_noBSSE}
dimer1	-5.93	0.30	-2.97	-6.24
dimer2	-2.63	0.35	-1.32	-2.98
trimer1	-10.88	0.61	-3.63	-11.49
trimer2	-10.99	0.66	-3.66	-11.65
tetramer1	-14.73	1.02	-3.68	-15.75
tetramer2	-14.82	0.53	-3.71	-15.36
tetramer3	-15.41	0.98	-3.85	-16.39
tetramer4	-16.07	0.92	-4.02	-16.99
tetramer5	-20.93	1.51	-5.23	-22.43
tetramer6	-21.18	1.48	-5.29	-22.66
pentamer1	-25.56	2.07	-5.11	-27.64
pentamer2	-26.17	2.05	-5.23	-28.22
hexamer1	-34.71	2.71	-5.78	-37.42
hexamer2	-35.57	2.8	-5.93	-38.37
octamer1	-48.97	4.03	-6.12	-53.00
octamer2	-50.15	4.16	-6.27	-54.31
dodecamer1	-76.58	6.75	-6.38	-83.33
dodecamer2	-77.73	6.93	-6.48	-84.66
dodecamer3	-82.17	7.53	-6.85	-89.70
dodecamer4	-82.27	7.73	-6.86	-90.00
hexadecamer1	-115.11	10.84	-7.19	-125.95
α form (16 monomers)	-95.72	8.50	-5.98	-104.22
β form (16 monomers)	-96.05	10.00	-6.00	-106.05
27mer	-211.72	20.52	-7.84	-232.23

C-H**...**N hydrogen bonds of length 2.45 Å and a stabilizing dipolar interaction. Linear **dimer2** is not energetically favourable and the extension of such structures to higher order clusters is not considered.

Two types of trimers, *viz*. ladder type (**trimer1**) and cyclic (**trimer2**) (Figure 3.1) have been studied. The **trimer2** is more stable than **trimer1** by 0.11 kcal/mol. **trimer2** was previously reported as the most stable structure of an acetonitrile trimer [Cabaleiro-Lago and Ríos 1999b; Nigam and Majumder 2008]. The destabilizing parallel arrangement of monomers '1' and '3' causes **trimer1** to be slightly less stable. Counterpoise corrected pair-wise interaction energy (E_{pw}) calculation suggests that this destabilization due to parallelly arranged monomers is 0.98 kcal/mol (Table 3.2). Compared to **trimer1**, **trimer2** has shorter hydrogen bonds. Stronger hydrogen bonds and the absence of destabilizing dipolar interactions make **trimer2** more stable than **trimer1** despite of the higher number of hydrogen bonds in the latter.

For tetramer clusters, a total of six conformations have been studied. These are named in the increasing order of stability starting from the least stable **tetramer1** to the most stable **tetramer6** (Figure 3.2). In the cyclic **trimer2**, if an acetonitrile molecule is inserted to any of the C-H**...**N hydrogen bonds, it gives rise to the cyclic **tetramer1**. Absorption of a CH_3CN on monomer '2' of **trimer1** yields **tetramer2**. The **tetramer3** configuration can be obtained by the 'adsorption' of a CH_3CN to **trimer2**. The ladder type **tetramer4** is the antiparallel extension of **trimer1** while **tetramer5** can be described as a pair of stacked **dimer1** structures. The **tetramer6** can be considered as formed from cross-stacking of a pair of **dimer1** structures. Cross-stacking indicates that the orientation of the molecules in one dimer unit is almost perpendicular to that of the second dimer unit.

In cyclic **tetramer1,** even though there are no destabilizing E_{pw}, the presence of only four C-H**...**N interactions suggests the lowest cooperativity among the monomers and hence the lowest stability. The lower stability of **tetramer2** despite the presence of six C-H**...**N hydrogen bonding interactions and three antiparallell dipolar interactions can be explained on the basis of destabilizing effect from parallelly oriented monomer pairs *viz*. (1,3), (1,4) and (3,4) which give E_{pw} 1.23, 1.11 and 1.10 kcal/mol, respectively (Table 3.2). **tetramer2** contains lesser destabilizing interactions compared to **tetramer3** i.e., of (1,4) and (2,4) pairs with E_{pw} value of 0.63 and 0.64 kcal/mol respectively. The ladder type **tetramer4** has six C-H**...**N interactions which indicate a further enhancement in

cooperativity in it. The stabilizing interactions in **tetramer4** are from the antiparallel (1,2), (2,3), (3,4) and (1,4) monomer pairs while (1,3) and (2,4) monomer combinations are destabilizing it. The most stable tetramer structures are the stacked **tetramer5** and the cross-stacked **tetramer6**, with the latter being slightly more stable by 0.25 kcal/mol. Both these structures show eight CH**...**N interactions and this explains the high cooperativity in them. It is remarkable that **tetramer5** is more stable by 4.86 kcal/mol than the most stable non-stacked structure, **tetramer4**.

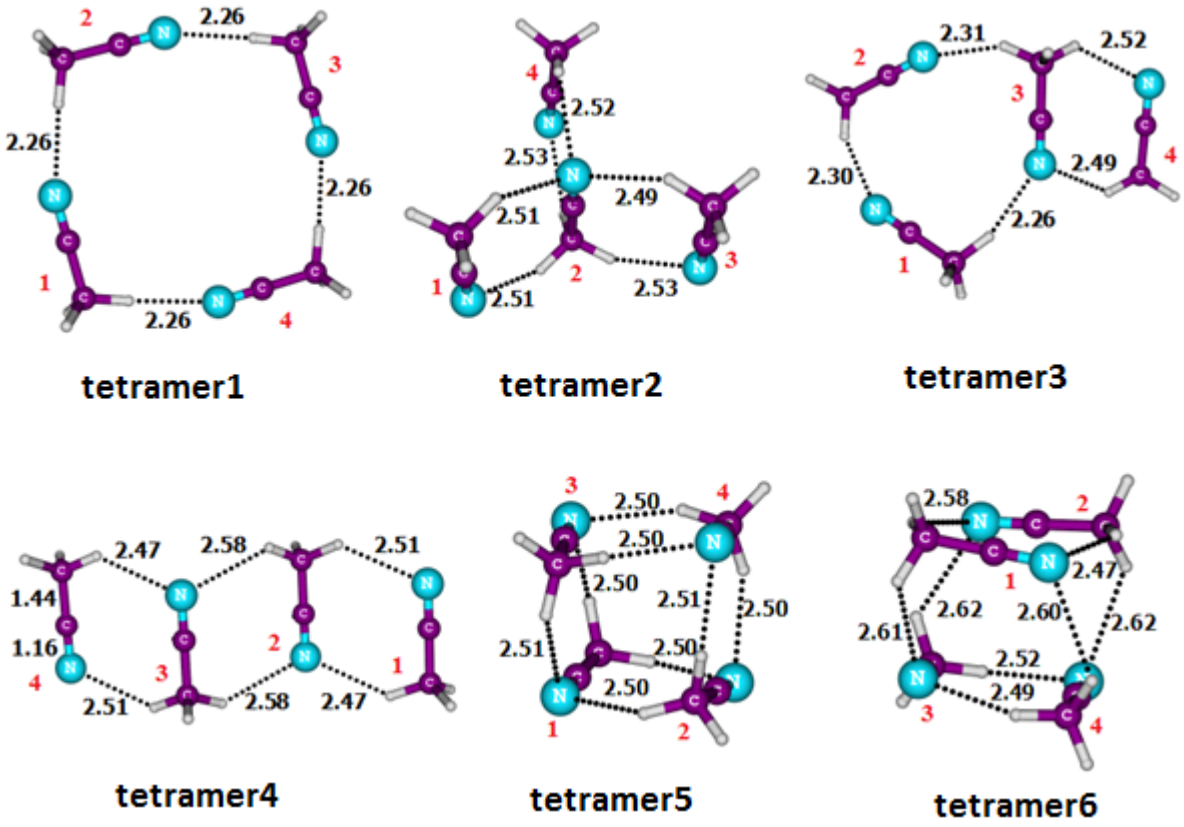

Figure 3.2 Optimized geometries of acetonitrile tetramers at M06L/6-311++G(d,p) level [Remya and Suresh 2014].

In the case of **tetramer6**, all E_{pw} values are negative and there are no repulsive dipolar interactions. The large stabilizing dipolar interactions from monomer pairs (1, 2), (2, 4), (3, 4) and (1, 3) mainly accounts for the strong cooperativity effect in **tetramer5**,which override the destabilizing effect from parallelly oriented monomer pairs *viz.* (1,4) and (2,3). It may be noted that most of the previous studies using *ab initio* [Cabaleiro-Lago *et al.* 2000; Cabaleiro-Lago and Ríos 1997; Cabaleiro-Lago and Ríos 1999b] and semiempirical potential functions [Siebers *et al.* 1998] have shown that stacked and cross-stacked structures are the most stable among acetonitrile tetramers. All

these studies except one [Cabaleiro-Lago and Ríos 1997] rated cross-stacked as the most stable tetramer pattern. Some DFT studies found cyclic tetramer to be the most stable among all the limited types of patterns studied [Kharat *et al.* 2013; Mata and Costa Cabral 2004; Nigam and Majumder 2008]. E_{int} values of clusters up to tetramers obtained using two more DFT methods from the list of best performing functional (Chapter 2) *viz*. CAM-B3LYP and B2PLYPD are given Table 3.2. Order of stability of dimer and trimer clusters given by CAM-B3LYP and B2PLYPD are similar to that given by M06L. In the case of tetramers, the results given by B2PLYPD method is almost similar to that obtained with M06L, except for **tetramer1**. This method rates cyclic **tetramer1** to be more stable than **tetramer2** and **tetramer3**. CAM-B3LYP method shows minor deviation in the order of stability of **tetramer1**-**tetramer4** clusters. According to all the three functionals, most stable tetramer is **tetramer6** followed by **tetramer5**, justifying the study of larger clusters of this type using M06L.

Table 3.2 Counterpoise corrected interaction energies (kcal/mol) of dimers, trimers and tetramers obtained using B2PLYPD and CAM-B3LYP density functionals.

Cluster	B2PLYPD	CAM-B3LYP
dimer1	-6.07	-5.01
dimer2	-3.24	-2.55
trimer1	-11.23	-9.05
trimer2	-11.99	-10.75
tetramer1	-14.42	-15.14
tetramer2	-11.63	-11.77
tetramer3	-13.78	-14.26
tetramer4	-16.65	-13.32
tetramer5	-20.71	-15.70
tetramer6	-20.79	-15.78

It is evident that the number of patterns possible for pentamer, hexamer and higher order clusters could be much higher than that we have found for the tetramer. However, we have considered only the stacked and cross-stacked conformations for the extension to higher order clusters since highest stability and cooperativity is observed in them so far.

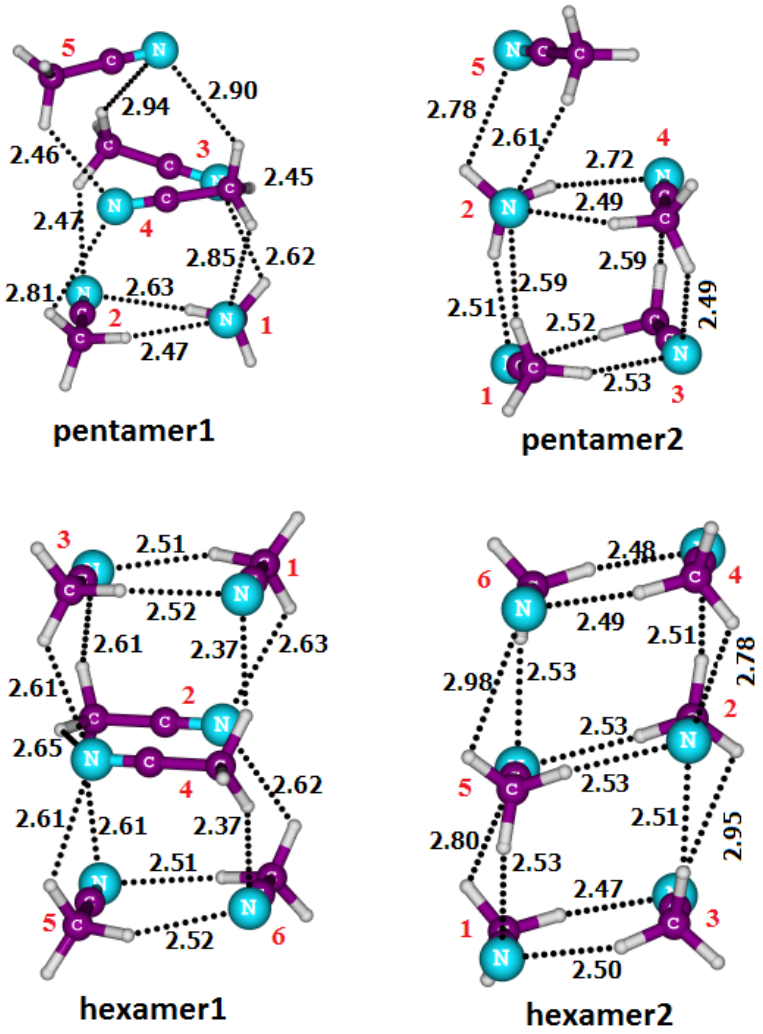

Figure 3.3 Optimized geometries of stacked and cross-stacked pentamers and hexamers at M06L/6-311++G(d,p) level [Remya and Suresh 2014].

The stacked **pentamer2** (Figure 3.3) is more stable by 0.61 kcal/mol compared to the cross-stacked **pentamer1**. In **pentamer1** there exists ten C-H**...**N stabilizing interactions and three antiparallel pairs along with destabilizing (almost parallel) orientations of (1,5), (2,5), and (3,5) pairs. The stacked form consists of eleven C-H**...**N interactions and five antiparallel pairs along with the destabilizing effect of (1,4), (1,5), (2,3) and (4,5) monomer pairs. Pair-wise interaction energies (E_{pw}) of different types of trimers, tetramers and pentamers are given in Table 3.3. According to the data given in

Table 3.3, the total destabilizing effect in **pentamer1** is very small (0.91 kcal/mol) compared to that in **pentamer2** (4.38 kcal/mol). However, **pentamer2** is stabilized by more number of favourable antiparallel orientations of the molecular dipoles, despite this higher value of destabilizing energy.

The E_{int} value of stacked **hexamer2** is -35.57 kcal/mol, which is more stable than the cross-stacked **hexamer1** by 0.86 kcal/mol (Figure 3.3). **hexamer1** has thirteen C-H**...**N interactions, three antiparallel pairs, and destabilizing orientations of two monomer pairs while **hexamer2** has fourteen C-H**...**N interactions, seven antiparallel pairs, and destabilizing orientations of five monomer pairs. The individual E_{pw} values of the pair wise interactions are listed in Table 3.4. Interaction energy per monomer, E_m for **hexamer1** and **hexamer2** is -5.78 and -5.93 kcal/mol, respectively and these values are significantly higher than all the other smaller clusters (Table 3.1), which implies that cooperativity is considerably improved in the hexamer cluster.

Table 3.3 Counterpoise corrected pair-wise interaction energies (kcal/mol) of the trimer, tetramer and pentamer complexes of acetonitrile studied.

Cluster	1,2	1,3	1,4	1,5	2,3	2,4	2,5	3,4	3,5	4,5
trimer1	-5.87	0.98	-	-	-5.87	-	-	-	-	-
trimer2	-3.07	-3.30	-	-	-3.10	-	-	-	-	-
tetramer1	-2.80	-0.52	-2.80	-	-2.80	-0.52	-	-2.80	-	-
tetramer2	-5.84	1.23	1.11	-	-5.83	-5.80	-	1.10	-	-
tetramer3	-3.33	-2.82	0.63	-	-3.05	0.64	-	-5.84	-	-
tetramer4	-5.87	0.95	-0.18	-	-5.68	0.95	-	-5.87	-	-
tetramer5	-5.74	-5.73	1.65	-	1.53	-5.73	-	-5.74	-	-
tetramer6	-5.76	-1.79	-1.69	-	-1.78	-1.72	-	-5.78	-	-
pentamer1	-5.51	-1.73	-1.53	0.04	-1.87	-1.57	0.46	-4.98	0.42	-5.30
pentamer2	-5.69	-5.75	1.55	0.83	1.69	-5.48	-5.12	-5.64	-0.52	0.31

Table 3.4 Counterpoise corrected pair-wise interaction energies (kcal/mol) of the hexamers.

Pair	**hexamer1**	**hexamer2**
1,2	-1.38	1.42
1,3	-5.82	-5.87
1,4	-1.90	-0.26
1,5	-0.44	-5.67
1,6	1.01	0.90
2,3	-1.97	-5.66
2,4	-5.32	-5.68
2,5	-1.97	-5.72
2,6	-1.37	2.05
3,4	-1.43	0.91
3,5	0.94	-0.71
3,6	-0.43	-0.71
4,5	-1.42	1.42
4,6	-1.91	-5.89
5,6	-5.82	-5.61

The ladder-type clusters came next in the stability order after the stacked and cross stacked clusters. The mixed clusters (formed by a combination of cyclic and antiparallel structures) showed lower stability than ladder-type clusters. These combined clusters showed higher stability than the fully cyclic structures. In combined clusters, the stability increased with decrease in size of cyclic part and increase in size of antiparallel part. Also, the cyclic structures showed an increase in stability with decrease in size and cyclic trimer

was the only structure that could exceed the stability of the antiparallel ladder-type orientation.

The stacked and cross-stacked forms of octamers and dodecamers are given in Figure 3.4. The stacked form shows slightly higher stability in both octamers and dodecamers. Both stacked and cross-stacked octamers possess twenty C-H**...**N hydrogen bonding interactions. Also, there are ten and four antiparallel monomer pairs in stacked and cross-stacked octamers respectively. Despite the high value of total destabilizing E_{pw} in stacked octamer (13.65 kcal/mol) compared to that of the cross-stacked one (5.43 kcal/mol), the former is more stable by 1.18 kcal/mol, which is due to the larger number of antiparallel monomer pairs in it.

In the case of dodecamers, there are thirty two and thirty C-H**...**N interactions is in stacked and cross-stacked clusters respectively. The number of antiparallel monomer pairs in stacked and cross-stacked dodecamers is sixteen and six respectively. The higher stability of stacked dodecamer (by 1.15 kcal/mol) despite its higher value for total positive E_{pw} (35.38 kcal/mol) compared to that of the cross-stacked form (18.13 kcal/mol) can be attributed to this higher number of antiparallel monomer pairs.

The stacked and cross-stacked clusters described so far are simple axial (vertical) extension of stacked and cross-stacked tetramers. Sidewise extensions of the most stable stacked clusters (**dodecamer3** and **dodecamer4,** Figure 3.5**)**, result in higher number of intermolecular bonding interactions and hence higher stability. In **dodecamer3,** one stacked hexamer is arranged on top of another resulting in additional end-on interaction between nitrogen atom on one monomer and methyl group on another similar to that found in **dimer2**. In **dodecamer4**, one stacked hexamer unit is arranged on top of another to obtain more lateral antiparallel interactions. Both these dodecamers are stabilized by more than 4 kcal/mol compared to the **dodecamer2** (Table 3.1), which implies that the additional end-on and lateral interactions contribute considerably to the stability of the cluster. The **dodecamer4** is more stable than **dodecamer3** by 0.10 kcal/mol. Total positive E_{pw} for **dodecamer3 is** 36.45kcal/mol and that for **dodecamer4** is 38.82 kcal/mol. Among dodecamers studied, **dodecamer4** having the highest value of destabilizing E_{pw} is the most stable. This is because, along with the number of unfavourable parallel orientations, number of antiparallel orientations is also increasing and there is maximum cooperativity in cluster having **dodecamer4** pattern.

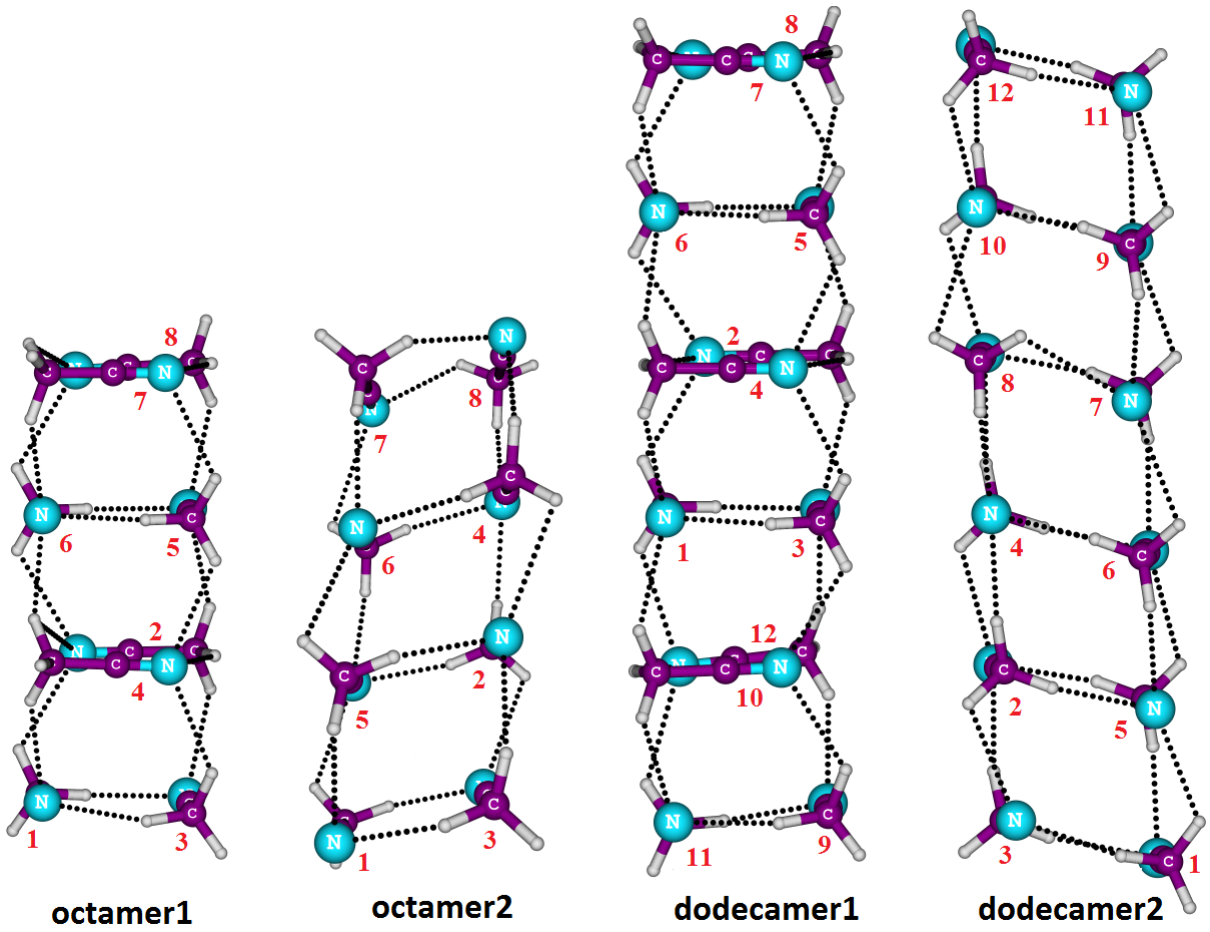

Figure 3.4 Optimized geometries of stacked and cross-stacked octamers and dodecamers at M06L/6-311++G(d,p) level [Remya and Suresh 2014].

Dodecamer4 being the most stable pattern, is extended by the adsorption of one layer of ladder-type tetramer, to obtain **hexadecamer1**, the cluster with 16 monomers (Figure 3.6). This resulted in a further increase in the number of sidewise interactions. This cluster, with forty eight C-H**...**N interactions, twenty four antiparallel pairs and total positive E_{pw} 64.25 kcal/mol shows a further enhancement in the value of E_m compared to **dodecamer4**. This increase in E_m shows a strong cooperativity in this growth pattern and can be attributed to the large number of stabilizing intermolecular interactions. From Figure 3.6, it is clear that all of the three methyl hydrogen atoms of inner monomers are involved in C-H**...**N interactions. The Nitrogen atoms of inner monomers are involved in a maximum of three C-H**...**N interactions. Also, highest number of favourable dipolar interactions is possible in this pattern.

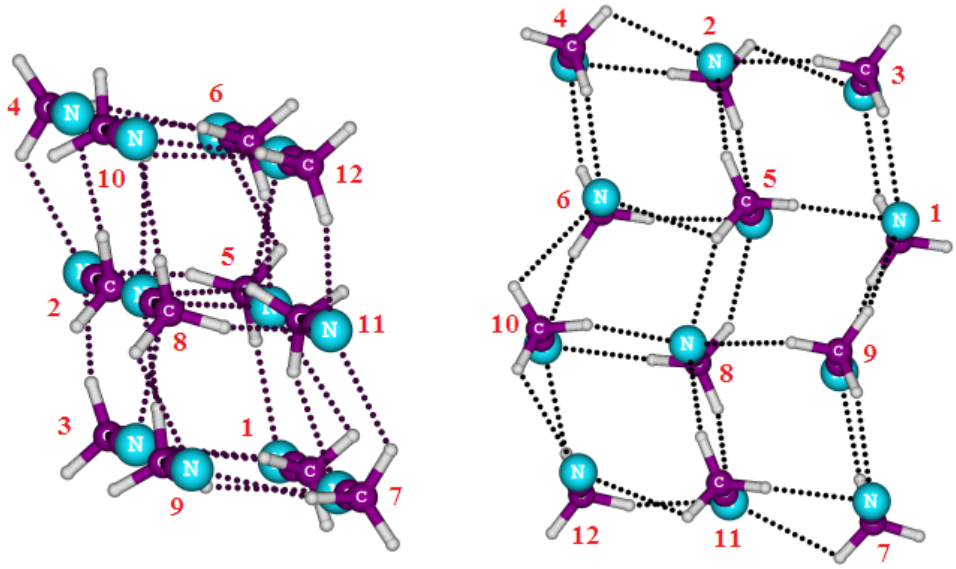

Figure 3.5 Optimized geometries of (a) **dodecamer3** and (b) **dodecamer4** at M06L/6-31G(d,p) level [Remya and Suresh 2014].

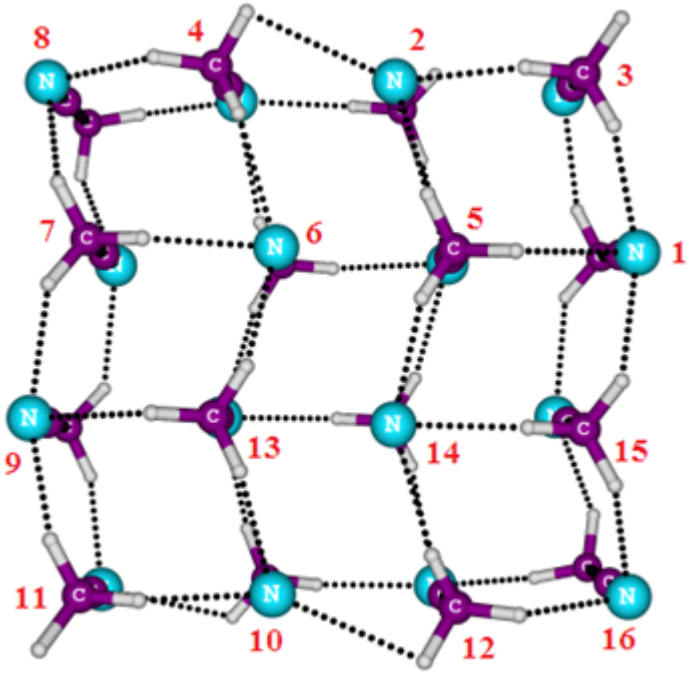

Figure 3.6 Optimized geometry of **hexadecamer1** at M06L/6-31G(d,p) level [Remya and Suresh 2014].

One large cluster with 27 monomers that contains lateral interaction similar to that in **dimer1** as well as end-on interactions similar to that in **dimer2** is also studied (Figure 3.7). This **27mer** is designed such that the central monomer molecule experiences lateral

interactions from all sides along with end-on interactions, from top as well as from bottom. This structure showed a further increase in the value of E_m showing a strong cooperativity in this growth pattern.

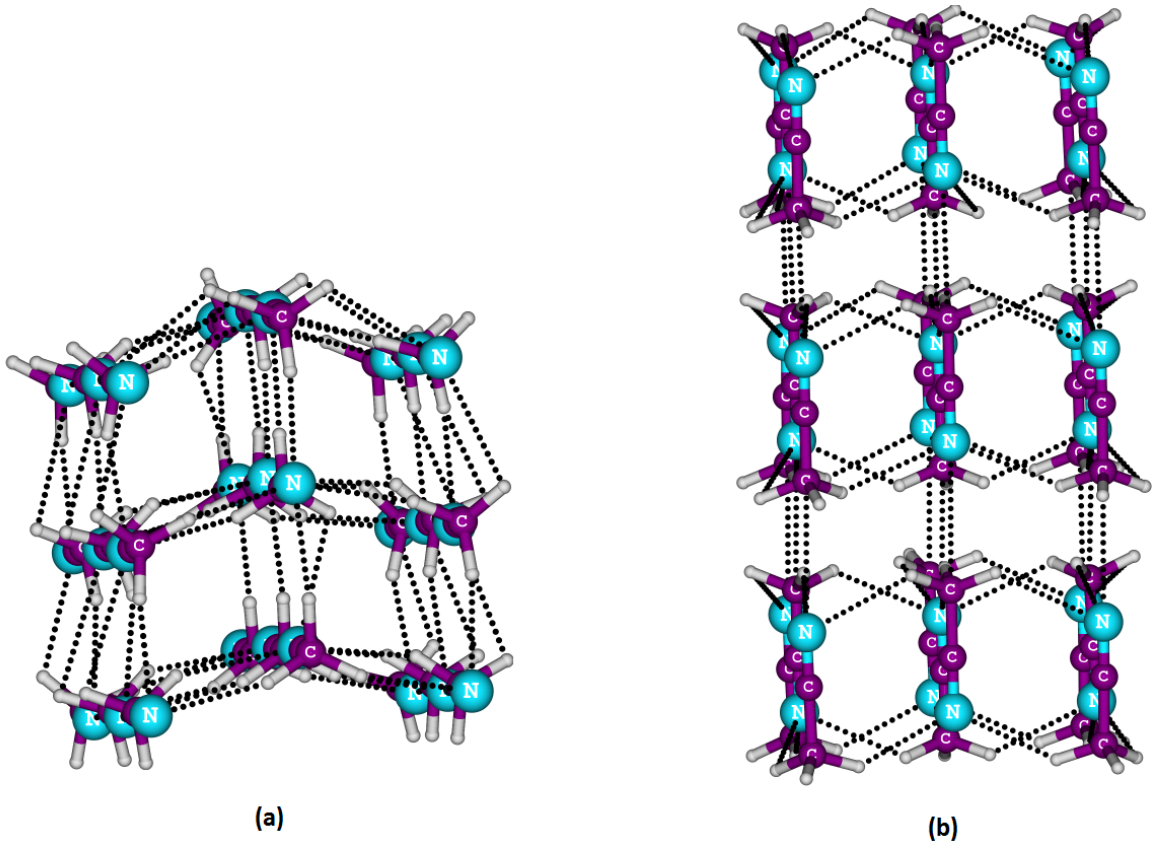

Figure 3.7 (a) View along the C-N axis and (b) the side-view of **27mer** in which the central monomer experiences all kinds of intermolecular interactions including lateral and end-on interactions [Remya and Suresh 2014].

There are two crystallization patterns reported in the literature [Enjalbert and Galy 2002] for acetonitrile. Both these crystallization patterns with sixteen monomers (Figure 3.8) are optimized and compared with the pattern (**hexadecamer1**) we have located. Frequency calculation confirmed the α-form to be a minimum. The β-form with sixteen monomers showed substantial distortion from the reported pattern. A small imaginary frequency of 37.45 cm^{-1} observed for this structure could not be eliminated even after repeated refinement of geometry optimization. This suggests that one layer of sixteen monomers may not be sufficient to stabilize the β-form. It can be seen from Table 3.1 that **hexadecamer1** is more stable than the hexadecamer crystal patterns by ~19 kcal/mol.

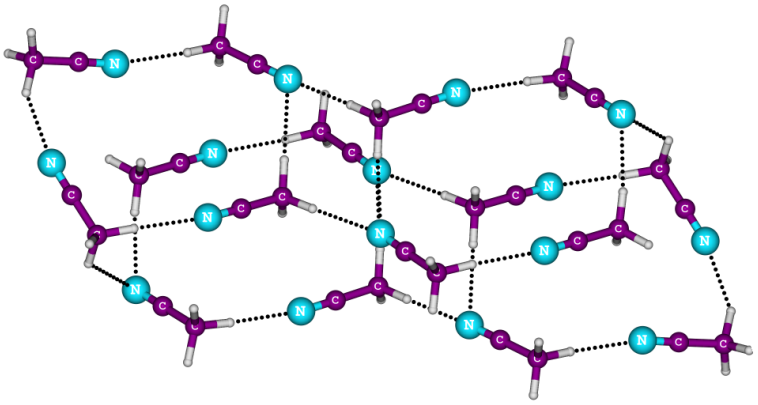

(a)

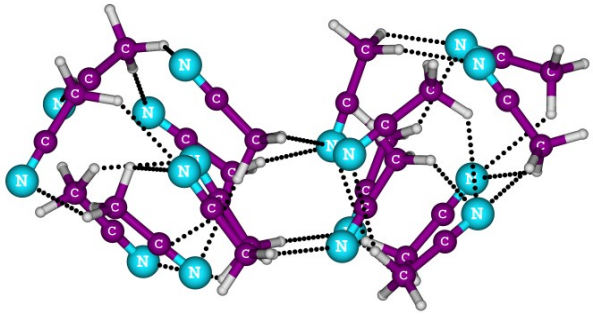

(b)

Figure 3.8 Optimized geometries of crystal patterns in the (a) α and (b) β forms at M06L/6-31G(d,p) level [Remya and Suresh 2014].

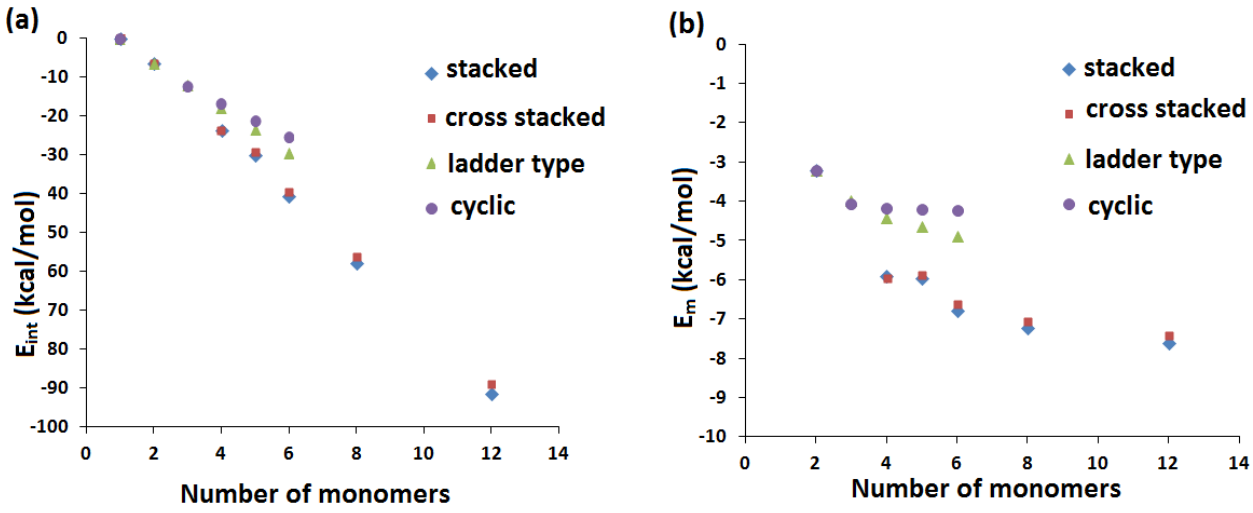

Figure 3.9 (a) Variation of interaction energy (E_{int}) with number of monomers and (b) Variation of interaction energy per monomer (E_m) with number of monomers in different types of clusters [Remya and Suresh 2014].

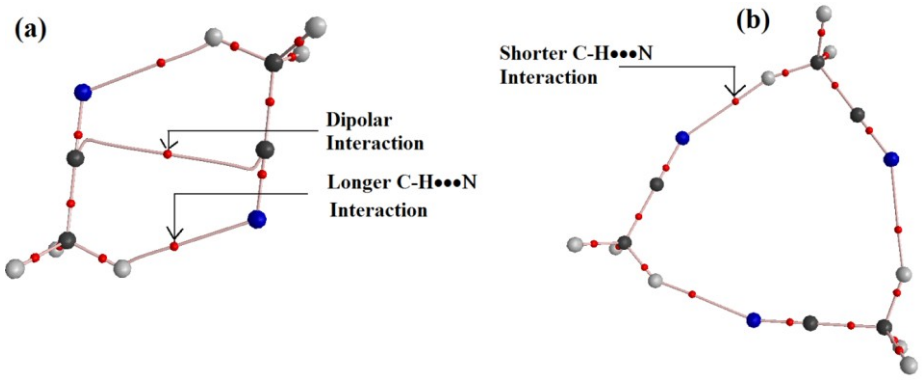

Figure 3.10 QTAIM plots of (a) **dimer1** and (b) **trimer2** showing different types of inter molecular interactions [Remya and Suresh 2014].

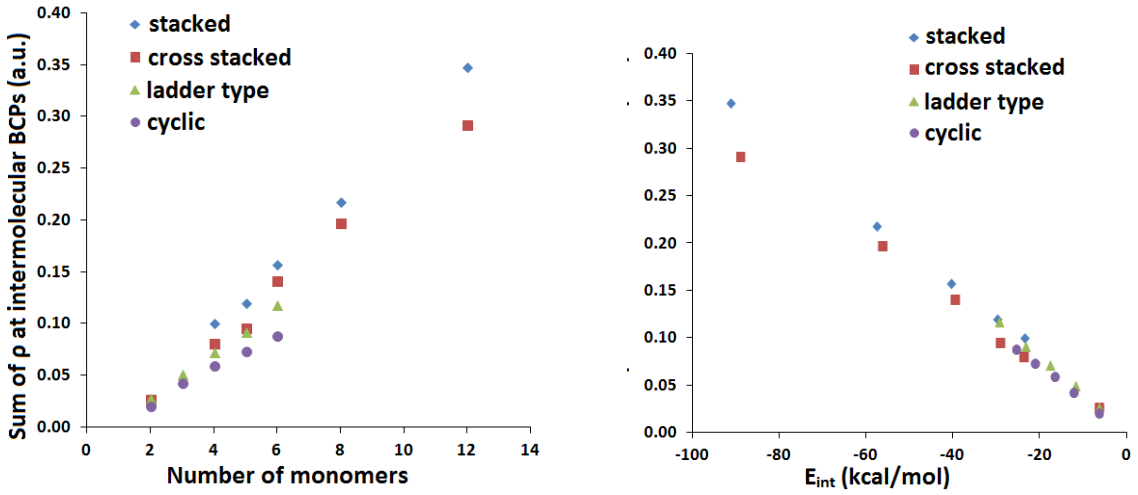

Figure 3.11 (a) Variation of the sum of electron density at intermolecular bond critical points with number of monomers (b) Correlation between interaction energy of clusters and sum of electron density at intermolecular BCPs [Remya and Suresh 2014].

The plot of E_{int} and number of monomers given in Figure 3.9 (a) clearly shows that E_{int} of all the growth patterns (stacked, cross-stacked, ladder type and cyclic) show an increase with increase in the number of monomers and the largest increase is found in stacked followed by cross stacked clusters. The values of E_m also show an increase with increase in the number of monomers as given in Figure 3.9 (b). The value of E_m shows a twofold increase on going from dimer to hexamer in the case of stacked and cross stacked clusters. But, in the case of ladder type clusters, the value of E_m shows only a small difference on going from dimer to hexamer and is almost constant in the case of cyclic clusters. The increase in the value of E_m indicates the increase in the strength of the intermolecular interactions with increase in number of monomers. This result gives a clear

evidence for strong cooperativity in acetonitrile clusters. The cooperativity is the highest in stacked followed by cross-stacked clusters.

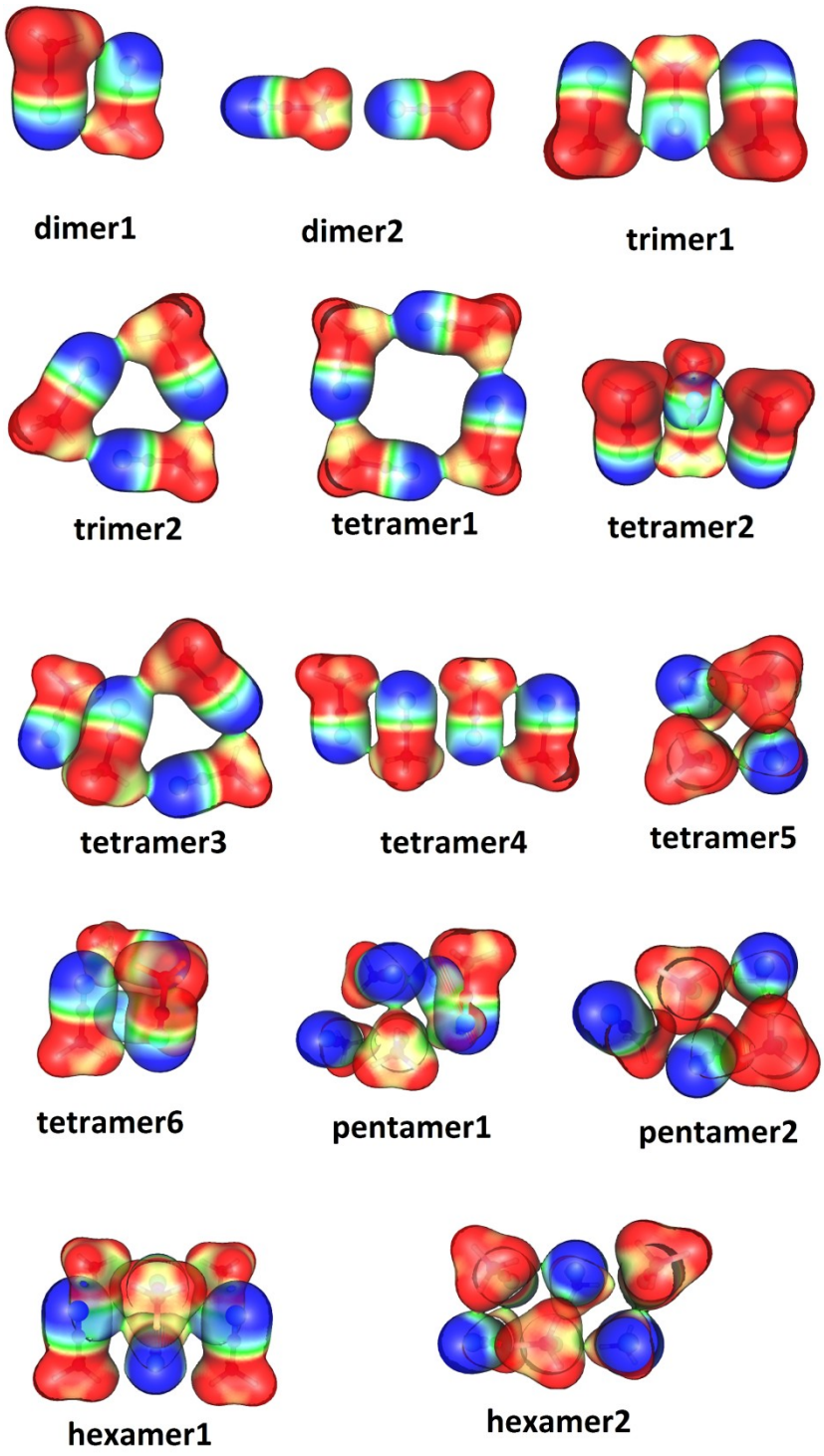

Figure 3.12 MESP of dimers, trimers, tetramers, pentamers and hexamers plotted on isodensity surface of 0.009 atomic units. Range: From-0.03 to 0.05 atomic units from blue to red [Remya and Suresh 2014].

3.4.2 QTAIM Analysis

The QTAIM analysis showed the largest number of bonding interactions in the stacked followed by the cross-stacked clusters suggestive of highest cooperativity in the former followed by the later. Two types of intermolecular interactions have been shown in the QTAIM bond critical point (BCP) analysis, *viz*. C-H**...**N interactions and the dipolar interactions between dimer pairs with an antiparallel orientation. The QTAIM plots of antiparallel dimer (**dimer1)** and the cyclic trimer (**timer2)** are shown in Figure 3.10 as typical examples to portray the BCPs corresponding to C-H**...**N and dipolar interactions. The largest increase in the sum of electron densities at intermolecular BCPs with increase in the number of monomers is shown by the stacked, followed by the cross-stacked clusters (Figure 3.11. (a)), indicating the highest number and strength of intermolecular interactions in them. The sum of electron densities at intermolecular bond critical points correlates well with the E_{int} in all types of clusters (Figure 3.11. (b)) verifying the fact that the stability of the clusters is directly dependent on the number and strength of intermolecular bonding interactions. These, along with the pair-wise interaction energies explain the highest stability observed in stacked clusters followed by cross-stacked ones.

3.4.3 Molecular Electrostatic Potential (MESP) Analysis

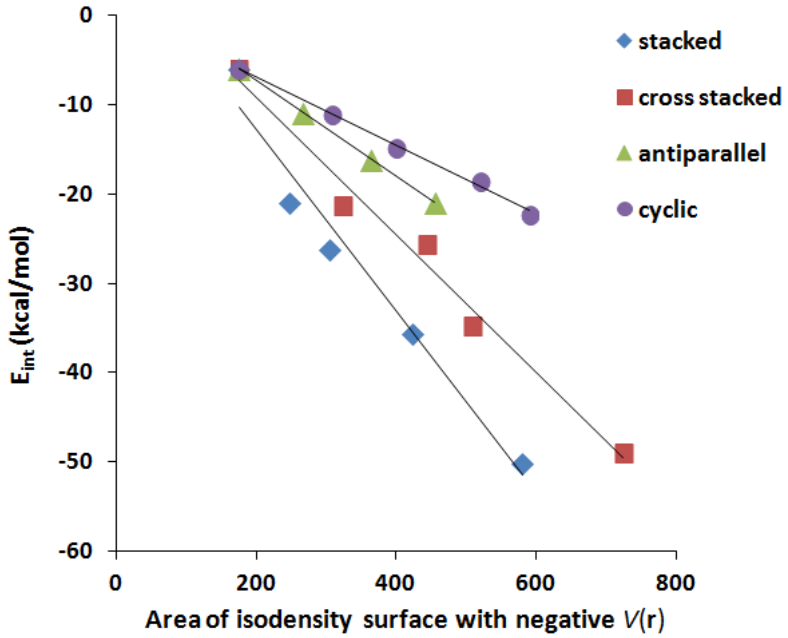

Figure 3.13 Correlation between area of isodensity surface with negative $V(r)$ and the interaction energy (E_{int}) in different types of clusters [Remya and Suresh 2014].

Table 3.5 Free energy of formation of **dimer1**, stacked and cross-stacked forms of tetramers, hexamers and octamers, all the four dodecamers, **hexadecamer1** and the **27mer** clusters at 298K, 227 K and 215 K.

Cluster	ΔG at 298 K (kcal/mol)	ΔG at 227 K (kcal/mol)	ΔG at 215 K (kcal/mol)
dimer1	2.15	0.46	1.48
tetramer5	9.31	2.84	4.34
tetramer6	6.89	0.98	2.57
hexamer1	17.35	6.35	8.38
hexamer2	17.28	6.07	8.07
octamer1	24.84	9.20	10.57
octamer2	23.94	8.18	10.70
dodecamer1	44.72	19.28	14.92
dodecamer2	45.72	19.58	15.10
dodecamer3	42.91	16.39	11.85
dodecamer4	44.77	17.86	13.24
hexadecamer1	57.64	20.96	14.67
27mer	95.22	29.76	18.54

MESP has been previously portrayed as a means for characterizing the nature of interactions of lone pairs with electron deficient systems [Mohan *et al.* 2013] as well as for distinguishing them from other electron rich regions [Kumar *et al.* 2041] in a molecule. There is always a negative MESP associated with the lone pair region of nitrogen atom of acetonitrile. The slight variations in the MESP as the acetonitrile forms a cluster can be examined and can be gainfully used for understanding the C-H**...**N hydrogen bond interactions. MESP plotted on electron density isosurface of the clusters up to hexamers is given in Figure 3.12. Blue colour indicates negative MESP regions (nitrogen lone pair regions) while red colour indicates the positive MESP regions (partial positive charge on the methyl hydrogen atoms). With the increase in number of CH···N interactions around a nitrogen atom, a decrease in the negative character of MESP is observed. In all types of clusters studied, the interaction energies are found to be in direct correlation with area of isodensity surface with negative potential (Figure 3.13). This indicates that the electron

density on nitrogen gets more and more involved in intermolecular bonding as the size of the clusters increases, which again indicates a strong cooperativity in cluster formation. The area of isodensity surface with negative potential is the lowest for stacked cluster which indicates that the highest amount of lone pair electron density is donated towards intermolecular bonding interactions and hence the highest cooperativity is shown by such clusters.

3.4.4 Study of Thermodynamic Parameters

Table 3.6 ΔG/n of dimer1, stacked and cross-stacked forms of tetramers, hexamers and octamers, all the four dodecamers, the **hexadecamer1** and the **27mer** clusters at 298K, 227 K and 215 K.

Cluster	ΔG/n at 298 K (kcal/mol)	ΔG/n at 227 K (kcal/mol)	ΔG/n at 215 K (kcal/mol)
dimer1	1.07	0.23	0.74
tetramer5	2.33	0.71	1.08
tetramer6	1.72	0.24	0.64
hexamer1	2.89	1.06	1.40
hexamer2	2.88	1.01	1.35
octamer1	3.11	1.15	1.32
octamer2	2.99	1.02	1.34
dodecamer1	3.73	1.61	1.24
dodecamer2	3.81	1.63	1.26
dodecamer3	3.58	1.37	0.99
dodecamer4	3.73	1.49	1.10
hexadecamer1	3.60	1.31	0.92
27mer	3.53	1.10	0.69

Free energies of the clusters at different temperatures are obtained from vibrational frequency calculations. Table 3. 5 lists the free energy of formation (ΔG) of **dimer1**, stacked and cross-stacked tetramers, hexamers and octamers, all the dodecamers, **hexadecamer1** and **27mer**. Corresponding values of ΔG/n are given in Table 3.6. A steady increase in ΔG values with increase in cluster size is observed at room temperature (298 K) and hence we assume that the smaller clusters are more stable at this temperature.

But at lower temperatures, ΔG values of the larger clusters show substantial decrease. The values of ΔG/n (Table 3.6) give a clearer insight into the stability of the clusters. At room temperature, ΔG/n shows a steady increase with cluster size up to dodecamer and then reaches a constant value around 3.6 kcal/mol. Even for **hexadecamer1**, ΔG/n is 3.6 kcal/mol while the **27mer** shows a slightly smaller value (3.53 kcal/mol). At 227 K, the **hexadecamer1** along with **27mer** also shows a smaller value for ΔG/n compared to the preceding cluster. At 215 K, the four types of dodecamer patterns also show decrease in ΔG/n compared to smaller clusters along with the **hexadecamer1** and **27mer**. From these results, we infer that these clusters become more and more stable as the temperature decreases and the size of the cluster increases. The preference towards larger clusters is again an indication of the stability and cooperativity of these growth patterns, especially at lower temperatures. ΔG/n value of the dimer at 215 K is more comparable to that of **27mer** than any other clusters. This can be an indication of 'all or nothing' [Hunter and Anderson 2009] behaviour in cluster formation of these molecules, which is a sign of positive cooperativity. We assume that the loss of entropy in the formation of these clusters can be overcome by the lowering of free energy. The thermodynamic data leads to the conclusion that, the antiparallel dimer is more likely to be observed at room temperature while at lower temperatures large clusters might exist.

PART B: Intermolecular C···C, N···N and O···O Bonding in Dipolar Organic Molecules

3.5 Introduction

Development of novel theoretical as well as experimental techniques has led to the discovery and understanding of several new types of inter molecular interactions involving halogens [Clark *et al.* 2007; Desiraju and Parthasarathy 1989; Legon 2010; Lommerse *et al.* 1996; Metrangolo and Resnati 2008; Metrangolo *et al.* 2008; Pedireddi *et al.* 1994; Politzer *et al.* 2013], chalcogens [Bleiholder *et al.* 2006; Gleiter *et al.* 2003; Iwaoka *et al.* 2002; Nagao *et al.* 1998; Wang *et al.* 2009b; Werz *et al.* 2002] and pnicogens. [Solimannejad *et al.* 2011; Zahn *et al.* 2011] Intermolecular chalcogen···chalcogen interactions are previously described in literature [Bleiholder *et al.* 2006; Row and Parthasarathy 1981] as leading to the formation of tubular structures [Gleiter *et al.* 2003; Werz *et al.* 2002] and crystals [Bai *et al.* 2013]. Recently, non covalent interactions involving group IV elements have also gained interest [Azofra *et al.* 2014; Bauzá *et al.* 2013; Bauzá *et al.* 2014; Bundhun *et al.* 2013; Grabowski 2014; Li *et al.* 2014; Mani and Arunan 2013; Mani and Arunan 2014; McDowell 2014; McDowell and Joseph 2014; Thomas *et al.* 2014; Varadwaj *et al.* 2014]. The non-covalent interaction of a covalently bonded group IV element with an electron donor site is explained based on the MESP features of the interacting atoms along with halogen, chalcogen and pnicogen bonds by Politzer *et al* as σ-hole interactions [Murray et al. 2007a; Murray et al. 2009; Murray et al. 2007b; Politzer et al. 2013]. The concept of σ-hole is defined by them as 'a region of positive electrostatic potential on the outermost portion of the atom's surface, centred on the R–X axis', where X is the interacting atom and R is the electronegative species attached to it [Clark *et al.* 2007; Murray *et al.* 2014]. The strength of a σ-hole interaction increases with increase in the polarizability of the X atom and the electronegativity of the species R attached to it. Also, these interactions are found to be highly directional (the direction is along the extension of the R-X bond axis), unlike hydrogen bonding interaction. A detailed study on the interaction of the σ-holes on group IV elements in F_3MX (M = C, Si, Ge and X = F, Cl, Br, I) with the lone pair on nitrogen of HCN is published by Bundhun *et al* [Bundhun *et al.* 2013]. The term 'carbon bond', which

denotes the interaction of an electron deficient carbon with electron rich donor sites in molecules like H_2O and H_2S is introduced by Arunan and Mani [Mani and Arunan 2013]. They stated that the 'carbon bonds' play important roles in hydrophobic interactions as well as in the stabilization of intermediate of S_N2 reaction. Bauzá *et al* [Bauzá *et al.* 2013] coined the term 'tetrel bonding' for describing the interaction of heavier group IV elements with nucleophilic centres. The concept of 'dicarbon bond' (similar to dihydrogen bond) between an electron deficient (donor) and an electron rich (acceptor) carbon atom in complexes of CO with CH_3-X is described by Varadwaj *et al* [Varadwaj *et al.* 2014].

In the study of acetonitrile growth patterns described in Part A of this chapter, [Remya and Suresh 2014] it was shown that the patterns with highest number of antiparallelly oriented monomers own maximum stability and cooperativity. QTAIM analysis showed bond critical points (BCPs) and bond paths between the nitrile carbon atoms of two acetonitrile molecules with antiparallel orientations along with those for hydrogen bonding interactions. These intermolecular C···C interactions were unusual, since they were observed between two carbon atoms of similar chemical environment. The studies on non-covalent interactions in the literature usually describe donor-acceptor type interactions where donor and acceptor atoms belong to different chemical environments. This led us to the search for molecules with intermolecular interaction between atoms in similar chemical environments in dimers of organic molecules with different functional groups.

A variety of organic molecules with different functionalities, rich in multiple bonds and most of them with an inherent dipole moment are shown to have such intermolecular C···C interaction between carbon atoms in similar chemical environment. Also, evidence for those C···C interactions is shown using QTAIM and molecular orbital (MO) analyses. Also, crystal structures of several organic compounds from literature are shown to have such C···C interactions using QTAIM analysis. Evidence for intermolecular N···N and O···O interactions between nitrogen and oxygen atoms of similar chemical environments are also given using QTAIM and MO analysis.

3.6 Computational Methods

All the molecules are optimized using the meta-GGA DFT method, M06L [Zhao and Truhlar 2006b] with 6-311++g(d,p) basis set, the best performing model chemistry among those tested in the benchmark study described in Chapter2 [Remya and Suresh

2013]. All the dimers are confirmed to be minima with no imaginary frequency. For Further validation of the results, the calculations are repeated using B3LYP, CAM-B3LYP [Yanai *et al.* 2004] - the long range corrected version of B3LYP [Becke 1993] - and B971 [Hamprecht *et al.* 1998] functionals. A measure of the effect of dispersion is obtained using B3LYP-D3 method, which uses Grimme's dispersion correction along with Becke-Johnson damping function [Grimme *et al.* 2011]. 6-311++g(d,p) basis set is used with all these functionals. Further, the high accuracy G3MP2 [Curtiss *et al.* 1999] method is used to obtain accurate binding energy values for the dimers. The calculations are done using *Gaussian09* [Frisch *et al.* 2010] suite of programs.

Interaction energy values of the homogeneous dimers (E_{int}) are calculated by the same method used in Part A of this chapter, by subtracting twice the energy of the constituent monomer from the energy of a dimer. The monomers are also optimized at the same level of theory as the dimers. Counterpoise correction by Boys and Bernardi [Boys and Bernardi 1970] method as implemented in *Gaussian09* is also applied.

QTAIM analysis [Bader 1990] as implemented in AIM2000 [Biegler-König and Schönbohm 2002; Biegler-König *et al.* 2001; Biegler-König *et al.* 2000] and AIMALL [Keith 2014] are used for identifying the intermolecular interactions through bond critical points (BCPs). The bonding interactions are illustrated using AIMALL generated molecular graphs. The intermolecular BCPs shown by the QTAIM topological analysis are also identified in MO analysis.

MESP, defined by Eq. 1.71 (Section 1.2.9) can be used as a tool for understanding intermolecular interactions [Gadre and Shirsat 2000; Mohan and Suresh 2014; Murray and Sen 1996; Politzer and Truhlar 1981]. It directly reflects the charge distribution in the system, based upon Coulomb's law [Politzer and Murray 2015]. Here, MESP features of the interacting molecules are used for understanding the X···X type interactions (X = C, N and O).

Energy Decomposition Analysis [Bickelhaupt and Baerends 2000; Ziegler and Rauk 1979a; Ziegler and Rauk 1979b] (EDA) is carried out using ADF software [E.J. Baerends 2010; Fonseca Guerra *et al.* 1998; te Velde *et al.* 2001] to understand the nature of intermolecular interactions. The total interaction energy will be split into Pauli, Electrostatic and orbital contributions in the Morokuma scheme of EDA [Kitaura and Morokuma 1976] used. For this, all the dimers were optimized at M06L/tzvp level of DFT and single point fragment analysis was done using M06L/tz2p method available in ADF. Intermolecular C···C interactions between carbon atoms in similar chemical environments

were shown to exist in the crystal structures of some molecules from literature located using Cambridge structural database [Allen 2002] with the help of QTAIM analysis. Dimers from their crystal structures were chosen and were subjected to QTAIM analysis for the presence of such interactions.

Natural bond orbital (NBO) analysis [Weinhold and Landis 2005] as implemented in *Gaussian09* is used for analyzing the nature of charge transfer between the two X atoms in the X···X interactions. In NBO analysis, the total electronic wavefunction of a molecular system is interpreted in terms of a set of filled Lewis and a set of empty non-Lewis localized orbitals. Interaction between these two sets of orbitals, which results in a donation of occupancy from the occupied Lewis to unoccupied non-Lewis set of orbitals is analyzed using a second order perturbation theory. This results in the departure from the idealized Lewis structure description. The stabilization energy E_2 associated with $i \rightarrow j$ delocalization, where i is the donor and j is the acceptor NBO, is calculated as,

$$E_2 = \Delta E_{ij} = qi \frac{F(i, j)^2}{\varepsilon_j - \varepsilon_i} \qquad \text{(Eq. 3.2)}$$

where qi is the donor orbital occupancy, εi, εj are diagonal elements (orbital energies) and $F(i,j)$ is the off-diagonal NBO Fock matrix element.

3.7 Results and Discussion

3.7.1 Intermolecular C···C Interactions between Carbon Atoms in Similar Chemical Environment

The dimer selected for this study include those of triple bonded molecules such as acetonitrile and its derivatives, cycloalkanes with cyanide functional group, dimethyl cyanamide, acetylene and its halogenated derivatives. Dimers of double bonded compounds such as ethylene derivatives, methyl thiocyanate and thioacetone are also included in the study. The optimized geometries of these dimers are given in Figure 3.14 - 3.15. One intermolecular C···C interaction distance is shown in these figures for every dimer. These C···C interactions are characterized as bonding interactions by locating bond critical points in the QTAIM analysis as well as identifying bonding molecular orbitals (MO), which will be described later. Some of the systems such as dimers of hydrogen cyanide, acetylene derivatives except acetylene chloride and ethylene derivatives show only C···C interactions between their monomers. Acetylene chloride dimer also shows

carbon-halogen interactions along with C···C interaction. Cyanides, cyanamides, thiocyanate and thioacetone has hydrogen bonding interactions together with C···C interactions.

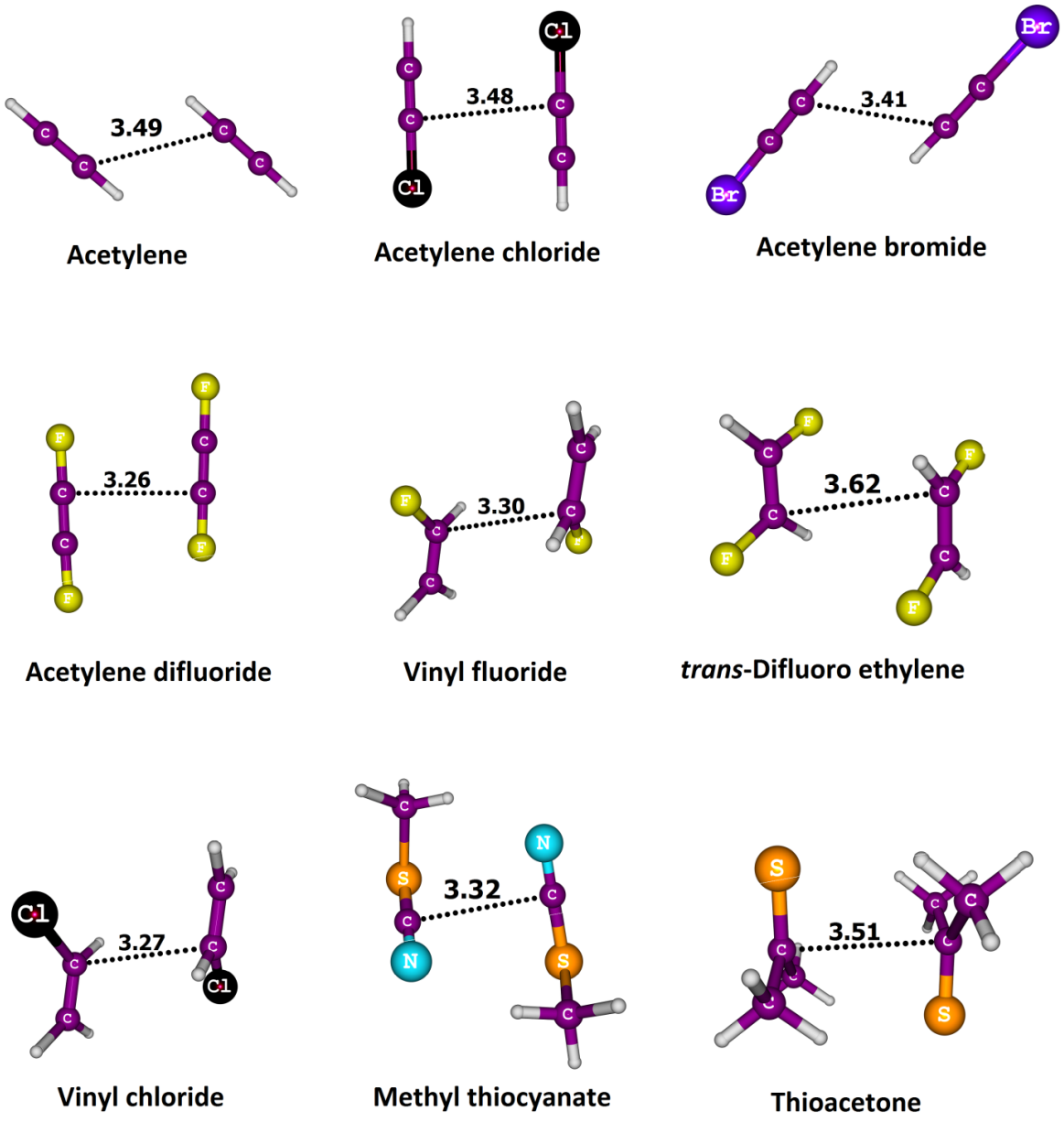

Figure 3.14 Dimers of acetylene, its halogenated derivatives, halides of ethylene, methyl thiocyanate and thioacetone showing C···C interactions (dotted lines) between carbon atoms in similar chemical environment. Distances are given in Å. Interactions other than C···C type are not shown in the figure for simplicity [Remya and Suresh 2015a].

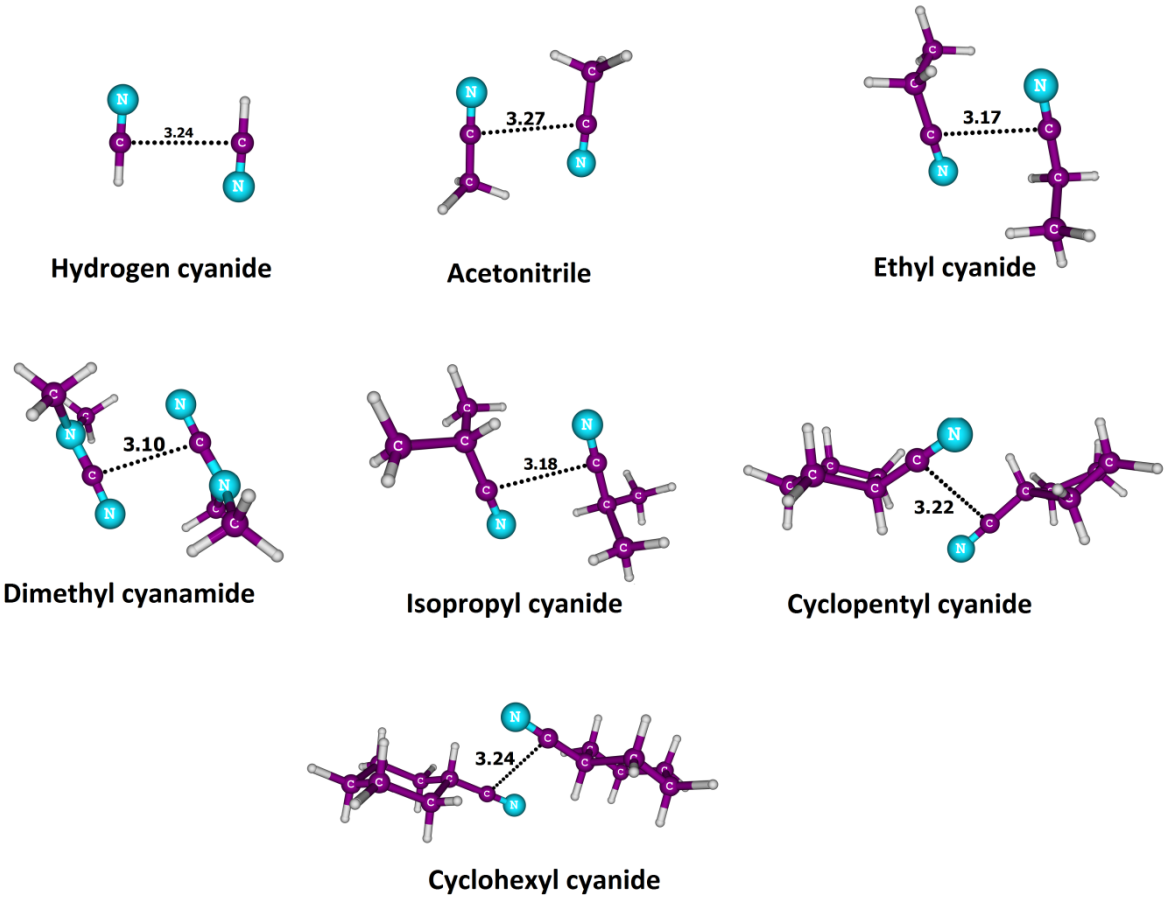

Figure 3.15 Dimers of different types of cyanides and methyl cyanamide showing C···C interactions (dotted lines) between carbon atoms in similar chemical environment. Distances are given in Å. Interactions other than C···C type are not shown in the figure for simplicity [Remya and Suresh 2015a].

The carbon atoms participating in the C···C interaction are from similar chemical environment and the distance between the interacting carbon-atoms are in the range 3.10 – 3.62 Å. Though this range of distance does not indicate a significant bonding interaction, the bonding MO analysis, the QTAIM electron density analysis and the NBO analysis suggest a stabilizing bonding interaction.

These C···C interactions are not of donor – acceptor type (the 'dicarbon bond' described by Varadwaj *et al* [Varadwaj *et al.* 2014]) since the interacting carbon-atoms are from similar chemical environments and hence neither of them can be portrayed as donor or acceptor. All the dimers showing this type of C···C interactions possess unsaturations either in the functional group or in the main chain. Any saturated compounds such as alkanes, alcohols, amines, alkyl halides and thiols could not be located to have C···C interactions between chemically similar carbon atoms.

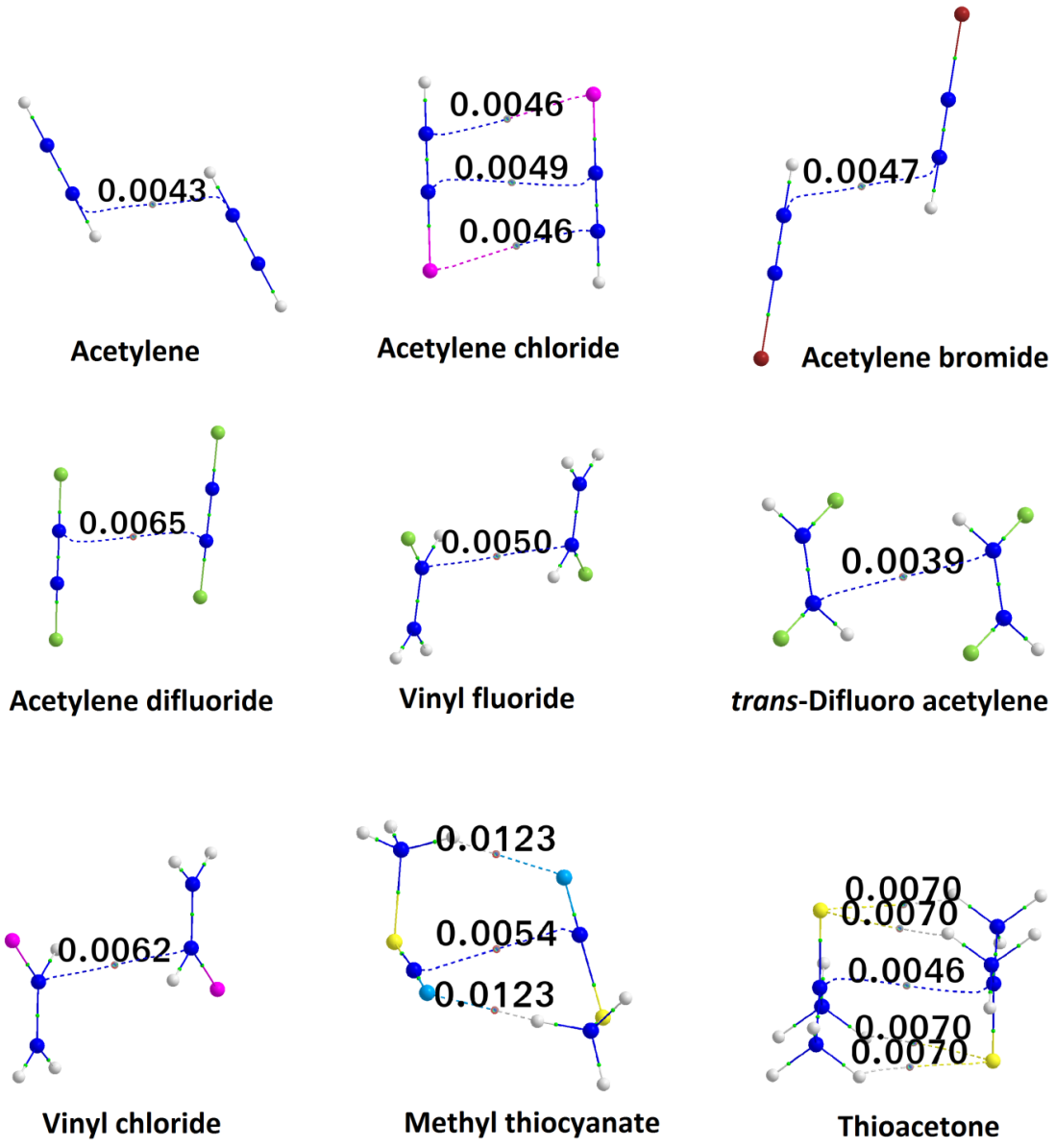

Figure 3.16 QTAIM plots of the dimers of acetylene, its halogenated derivatives, halides of ethylene, methyl thiocyanate and thioacetone showing C···C interaction between similar carbon atoms. The ρ values at the bond critical point are given in au. Color code for atoms: dark blue, carbon; light blue, nitrogen; light green, fluorine; yellow, sulfur; pink, chlorine; brown, bromine; ash, hydrogen [Remya and Suresh 2015a].

The QTAIM plots of the dimers given in Figure 3.16 - 3.17 show a bond critical point corresponding to every C···C interaction depicted in Figure 3.14 and Figure 3.15. The electron density at intermolecular BCPs is generally used as a measure of the strength of intermolecular interactions [Grabowski 2001; Knop *et al.* 2002; Parthasarathi *et al.* 2006; Popelier 1998; Remya and Suresh 2014]. The ρ values (0.0039 to 0.0086 au) given in Figure 3.16 – 3.17 for the C···C interactions are well within the typical range of values

observed for weak non-covalent interactions such as weak hydrogen bonds [Koch and Popelier 1995; Parthasarathi *et al.* 2006] and 'carbon bonds' [Mani and Arunan 2013]. Among all the cases, the weakest C···C interaction is observed in *trans*–difluoro ethylene (ρ = 0.0039 au) dimer and the strongest C···C interaction is observed in dimethyl cyanamide (ρ = 0.0086 au) dimer. The values of E_{int}, sum of ρ at intermolecular BCPs (∑ρ), and monomer dipole moments (μ) of all the dimers are given in Table 3.7.

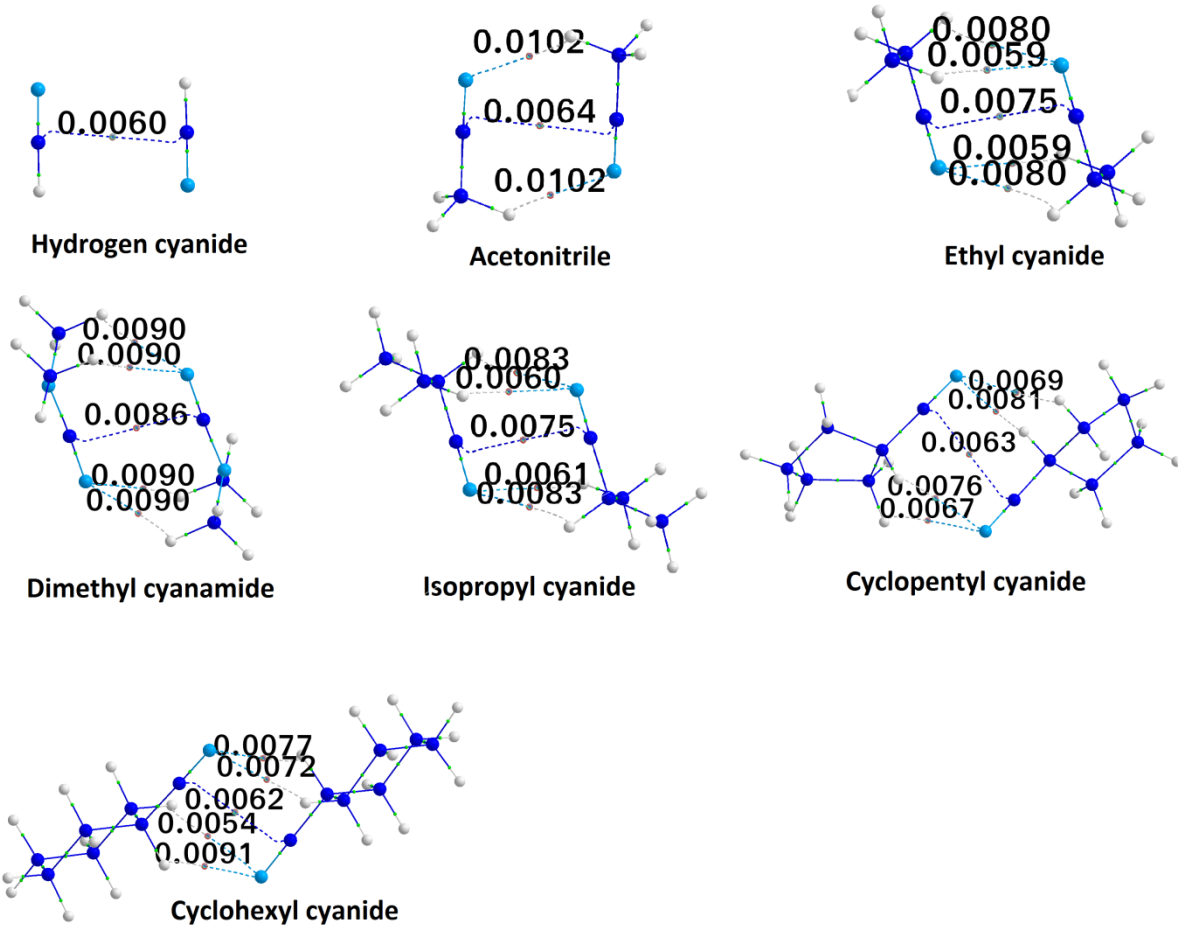

Figure 3.17 QTAIM plots of the dimers of different types of and methyl cyanamide showing C···C interaction between similar carbon atoms. The cyanides ρ values at the bond critical point are given in au. Color code for atoms: dark blue, carbon; light blue, nitrogen; light green, fluorine; yellow, sulfur; pink, chlorine; brown, bromine; ash, hydrogen [Remya and Suresh 2015a].

The bonding MOs (Figure 3.18) of every dimer clearly show interaction between the p orbitals of the carbon atoms involved in the C···C interactions. Compared to those of other systems, the orbital overlap is found to be stronger in cases such as the dimers of hydrogen cyanide, dimethyl cyanamide and acetylene difluoride.

Table 3.7 The interaction energies (E_{int}), the sum of ρ at inter molecular BCPs ((∑ρ), and monomer dipole moments (μ) of all the dimer complexes having intermolecular C···C interaction between similar carbon atoms. The predicted values of E_{int} using regression equation along with contributions from ∑ρ and μ terms are also given.

Dimer	E_{int} (kcal/mol)	∑ρ (a u)	μ (Debye)	Predicted E_{int} (kcal/mol)	Contribution From ∑ρ (kcal/mol)	Contribution from μ (kcal/mol)
acetylene	-1.07	0.0043	0.00	-0.51	-0.51	0.00
hydrogen cyanide	-2.59	0.0060	2.98	-2.81	-0.72	-2.09
acetonitrile	-5.93	0.0268	4.01	-6.01	-3.19	-2.81
ethyl cyanide	-6.91	0.0353	4.11	-7.09	-4.21	-2.88
isopropyl cyanide	-6.70	0.0361	4.13	-7.20	-4.31	-2.90
cyclopentyl cyanide	-6.79	0.0356	4.48	-7.38	-4.24	-3.14
cyclohexyl cyanide	-7.27	0.0356	4.52	-7.41	-4.24	-3.17
dimethyl cyanamide	-10.19	0.0445	4.94	-8.77	-5.30	-3.47
vinyl flouride	-1.29	0.0050	1.42	-1.59	-0.60	-0.99
vinyl chloride	-2.27	0.0062	1.39	-1.71	-0.74	-0.97
trans- difluoro ethylene	-1.09	0.0039	0.01	-0.47	-0.46	-0.01
actylene chloride	-0.87	0.0141	0.16	-1.79	-1.68	-0.11
acetylene bromide	-1.03	0.0047	0.03	-0.59	-0.56	-0.02
acetylene difluoride	-1.12	0.0065	0.00	-0.77	-0.77	0.00
methyl thiocyanate	-6.88	0.0299	4.32	-6.59	-3.56	-3.03
thioacetone	-5.45	0.0326	2.92	-5.94	-3.89	-2.05

The value of ∑ρ is usually taken as a measure of the total strength of the non-covalent interaction in intermolecular complexes [Mahadevi *et al.* 2011; Remya and Suresh 2014; Shahi and Arunan 2014]. Here, E_{int} values of the dimers shows an increasing trend with increase in the ∑ρ values (Figure 3.19 (a)). Recently, Mohan and Suresh [Mohan and Suresh 2014] showed that a linear correlation between ρ and interaction energy is applicable only for homogenous groups of complexes. The E_{int} is also found to increases with raise in the dipole moment μ of the interacting monomers (Figure 3.19 (b)). Since E_{int} values show dependency to both ∑ρ and μ, a double linear regression approach using the two quantities is tried to obtain a relationship to predict E_{int} values. The

regression equation is given in Eq. 3.3. The statistical parameters such as multiple R and R^2 are 0.9937 and 0.9875 respectively. The P values for ∑ρ and μ are 7.9781 ⨯ 10^{-5} and 0.0013 respectively, showing that Eq. 3.3 is reliable. The predicted values show only slight deviation from actual values (≤ 0.92 kcal/mol) except for dimethyl cyanamide where the deviation is 1.4 kcal/mol (Figure 3.19 (c)).

E_{int} (kcal/mol) = -119.179∑ρ (au) - 0.702 μ (Debye) (Eq. 3.3)

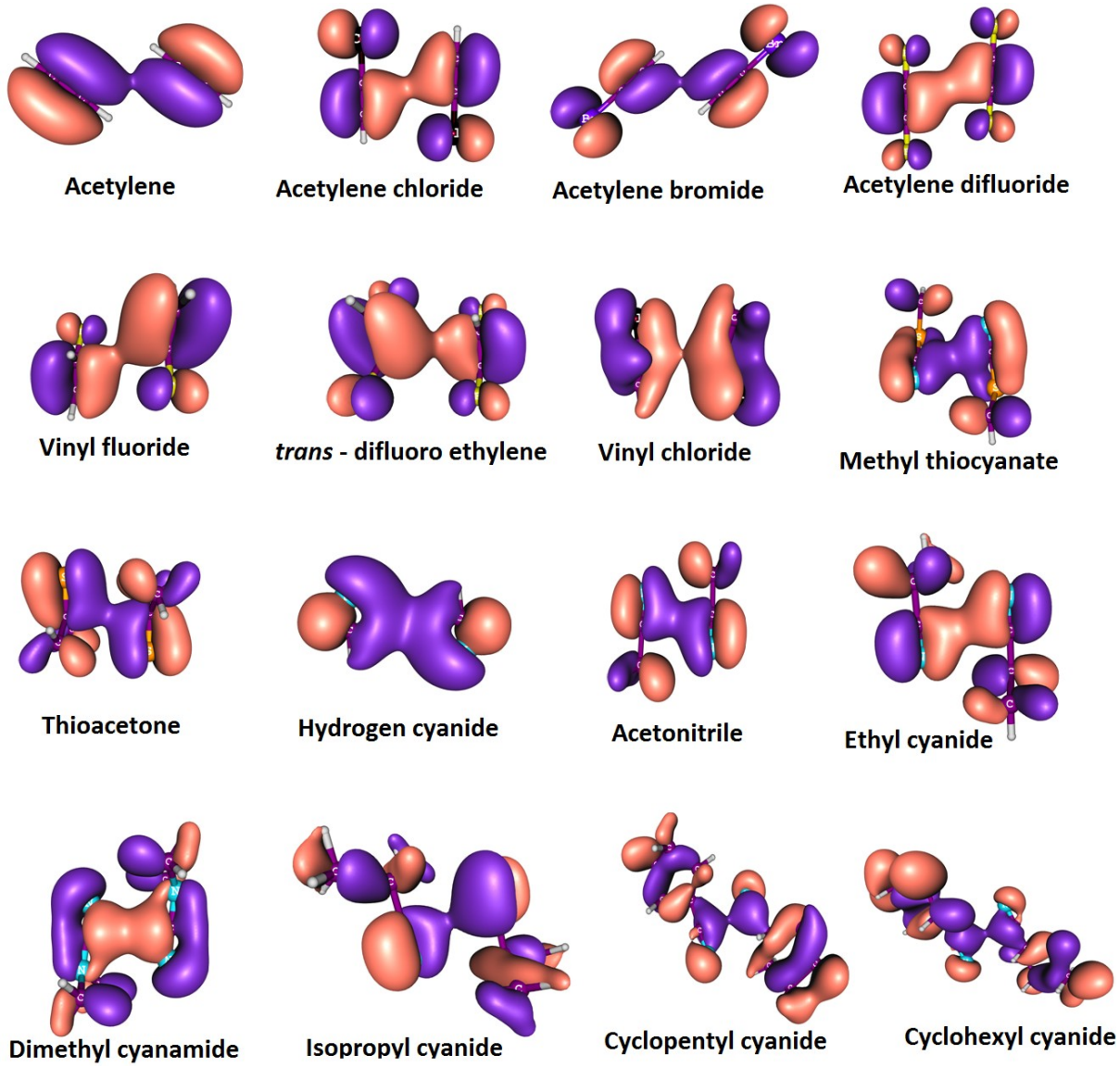

Figure 3.18 Occupied MOs corresponding to intermolecular C···C interactions. The isosurface value is 0.018 a.u. in all the cases.

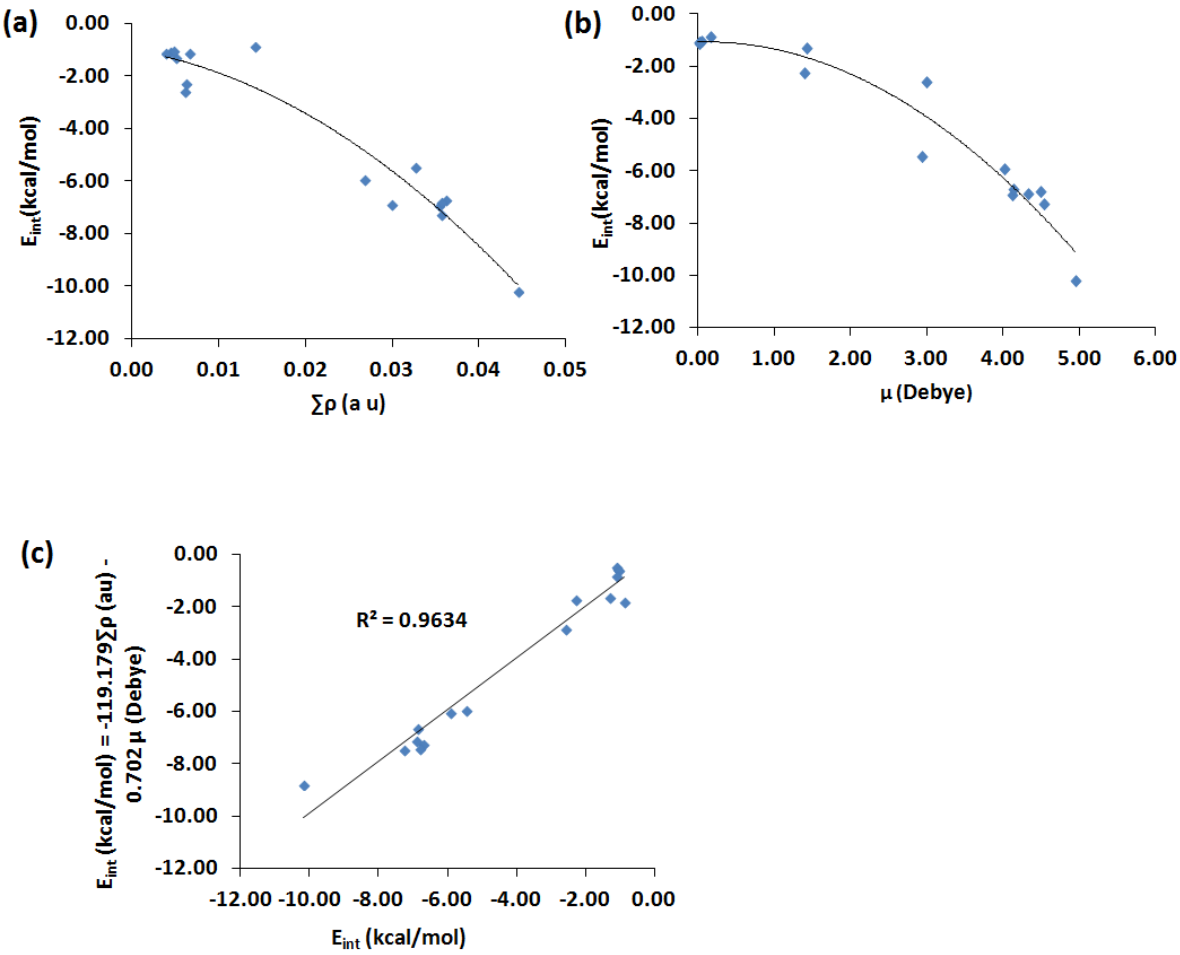

Figure 3.19 Variation of interaction energy (E_{int}) with (a) sum of electron density at in intermolecular BCPs (∑ρ), (b) monomer dipole moments (μ) and (c) predicted values of E_{int} using regression equation [Remya and Suresh 2015a].

Eq. 3.3 allows us to divide the total value of E_{int} into contributions from ∑ρ and μ which are also depicted in Table 3.7. In the cases of hydrogen cyanide, vinyl fluoride and vinyl chloride dimers, where a C···C interaction is the only intermolecular interaction between the monomers, 57 - 75% of the E_{int} is contributed from the dipole moment term. In the case of dimers with intermolecular hydrogen bonding interactions along with C···C interactions (cyanides, dimethyl cyanamide, methyl cyanate, and thioacetone), the contribution from the dipole moment term is 35 – 47%. For compounds with very low or even zero dipole moment, the role of the dipole moment term is very low (0 – 6%).

The MESP maps of the dimers are given in Figure 3.20. MESP features clearly show a partitioning of their monomers into relatively electron deficient (red) and electron rich (blue) regions and this immediately suggests that electron rich region of one of the monomers is close to electron deficient region of the other. This can be clearly shown in

all the cases, most visibly, in cases of cyanides and cyanamide. The approach of the electron rich region in one monomer to the electron deficient region in the second results in C···C bonding between carbon atoms in similar chemical environments. In acetylene and its derivatives, though the dipole moment is zero (or almost zero), for the monomer state, local variations in MESP in the interacting monomers (clearly visible from the MESP maps given in Figure 3.20) cause the C···C interactions in them.

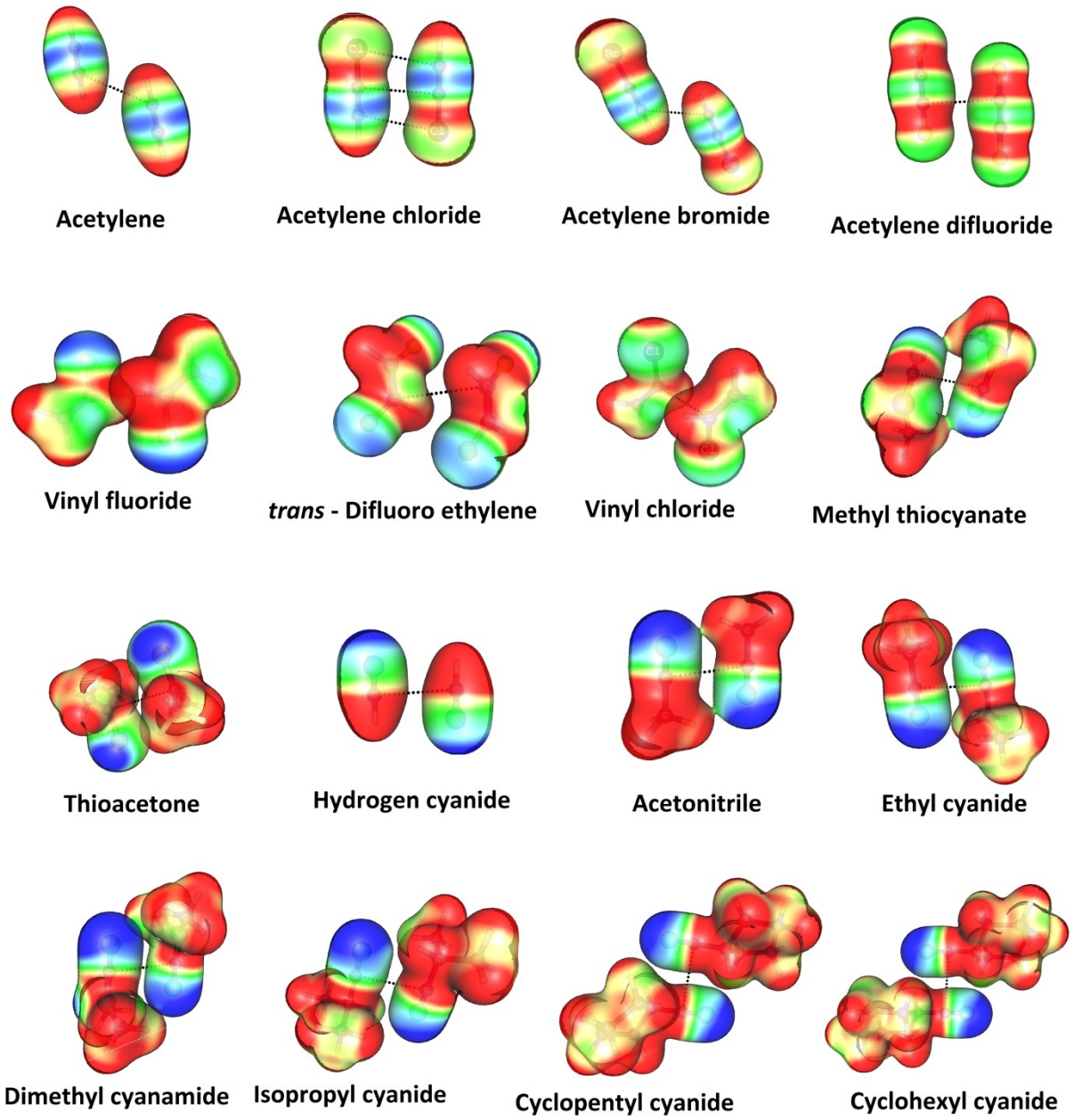

Figure 3.20 MESP plotted on isodensity surface of 0.01 au of dimers showing C···C interaction between similar carbon atoms. Range: from -0.03 (blue) to 0.05 (red) [Remya and Suresh 2015a].

Table 3.8 Percentage orbital and electrostatic contributions towards the total interaction energy of the dimers with intermolecular C···C interactions.

Dimer	% Electrostatic Interaction	% Orbital Interaction
Acetylene	92.74	7.26
Hydrogen cyanide	95.86	4.14
Acetonitrile	85.13	14.87
Ethyl cyanide	82.13	17.87
Isopropyl cyanide	80.83	19.17
Cyclopentyl cyanide	80.94	19.06
Cyclohexyl cyanide	76.96	23.04
Dimethyl cyanamide	78.11	21.89
Vinyl fluoride	67.81	32.19
Vinyl chloride	75.25	24.75
trans-difluoro ethylene	65.79	34.21
Acetylene chloride	33.33	66.67
Acetylene bromide	72.31	27.69
Acetylene difluoride	83.33	16.67
Methyl thiocyanate	78.44	21.56
Thioacetone	60.37	39.63

Results of energy decomposition analysis (EDA) show the interaction energies of these dimers to be mainly electrostatic in nature (Table 3.8). The highest (95.86%) value for electrostatic contribution towards E_{int} is found in the case of hydrogen cyanide dimer, where a C···C interaction is the only intermolecular interaction and has a high monomer dipole moment. Though μ value is zero, higher electrostatic contribution towards E_{int} in acetylene (92.74%) and difluoro acetylene (83.33%) show that electrostatic effects due to local polarization leads to these C···C interactions.

The Coulombic interactions incorporate polarization (and accordingly include dispersion) as a consequence of Hellmann-Feynman theorem [Politzer *et al.* 2015]. For the dimers such as acetonitrile and its derivatives, dimethyl cyanamide and thioacetone, where hydrogen bonds also contribute towards E_{int}, 60 - 85% of it is from electrostatic contribution.

3.7.2 Evidence for C···C interaction between Carbon Atoms in Similar Chemical Environments from Crystal Structures

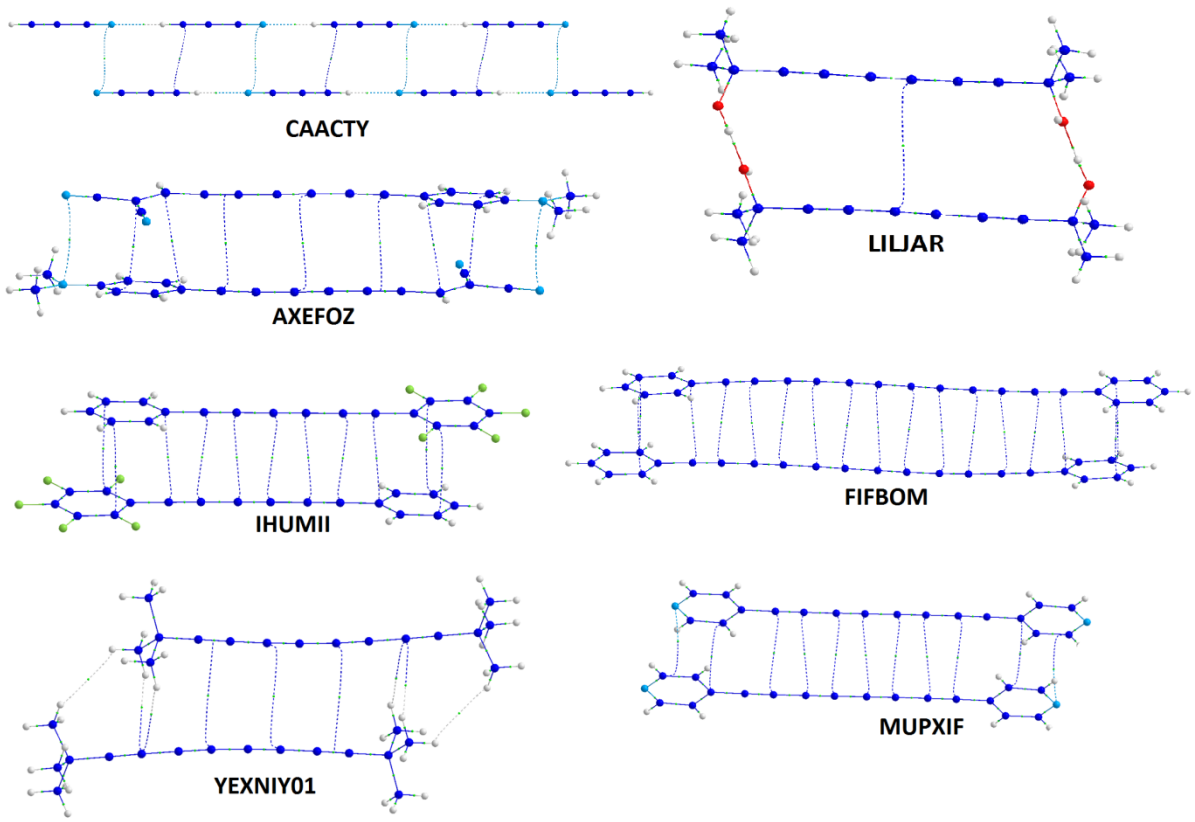

Figure 3.21 QTAIM plot of dimers obtained from crystal structures reported in the literature. The CSD ID is used for labeling. Color code for atoms: dark blue, carbon; light blue, nitrogen; red, oxygen; light green, fluorine; ash, hydrogen [Remya and Suresh 2015a].

Some molecules in the literature are located to have intermolecular C···C interaction between carbon atoms in similar chemical environment with the help of Cambridge structural database (CSD). Different types of intermolecular interactions present in these crystal structures can be seen in the QTAIM plots (labelled with their CSD ID) given in Figure 3.21. CAACTY, [Sutor 1958], the crystal structure of acetylene cyanide, and the crystals of polyynes with different end groups show intermolecular C···C interactions between chemically identical carbon atoms, as can be seen from Figure 3.21. The intermolecular C···C interaction in LILJAR [Enkelmann 1994] and the central C···C interactions in the case of AXEFOZ [Frank *et al.* 2011], FIFBOM [Luu *et al.* 2004], IHUMII [Tykwinski *et al.* 2009], MUPXIF, [Wang *et al.* 2009a] and YEXNIY01 [Chalifoux *et al.* 2009] are also between carbon atoms from identical

environments. In the remaining C···C interactions of these polyyne systems, though the carbon atoms involved are not of the identical types, many of them can be considered as of similar types. The crystal structure CAACTY shows BCPs corresponding to N···N interaction between nitrogen atoms of similar chemical environment apart from those for C···C interactions and hydrogen bonds. This fact directs us to the probability of extending the concept of interaction between atoms in similar chemical environments to atoms other than carbon.

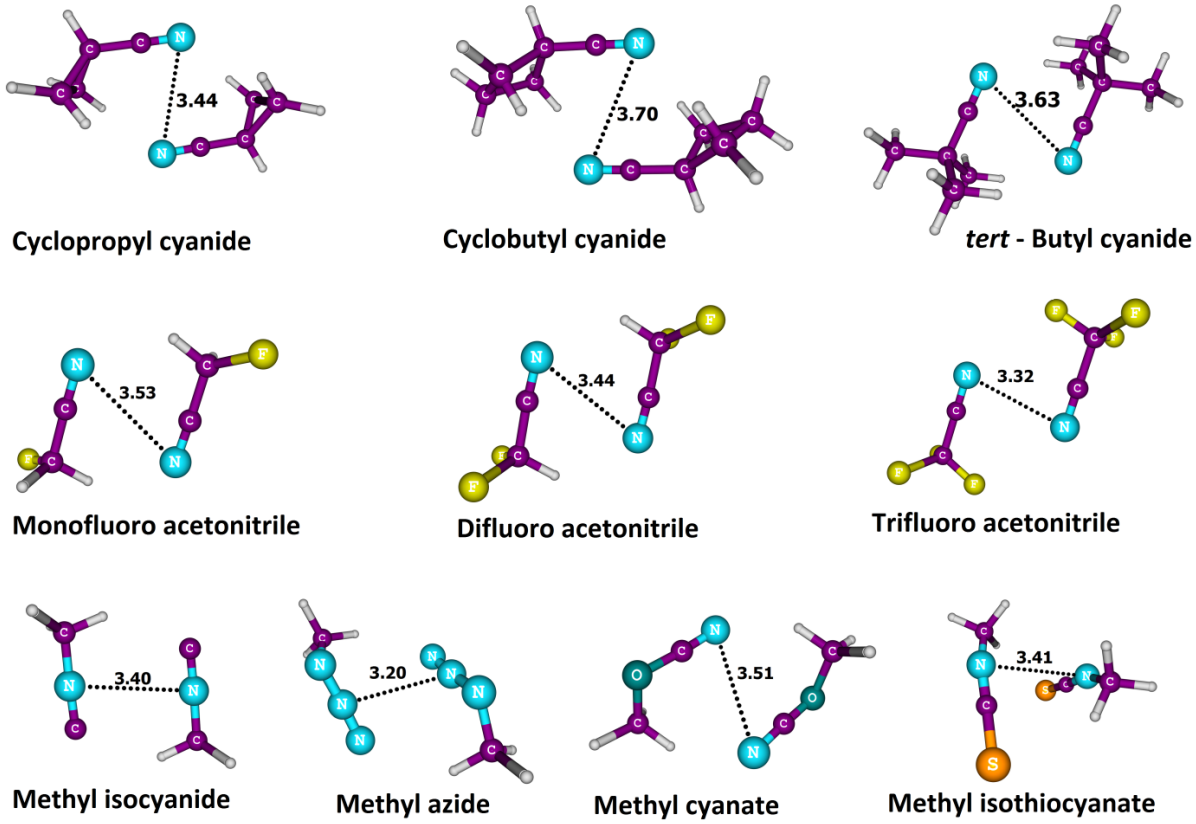

Figure 3.22 Dimers showing N···N interaction between chemically similar nitrogen atoms. Distances are in Å [Remya and Suresh 2015a].

3.7.3 Intermolecular N···N and O···O Interactions

Dimers of organic molecules located to possess N···N and O···O interaction in similar chemical environment are given in Figure 3.22 and Figure 3.23 respectively. N···N and O···O bonds in these dimers are marked with dotted lines in the figures. Dimers of molecules with functional groups such as cyanides, (acetonitrile derivatives and cycloalkanes with cyanide functional group), isocyanide, azide, cyanate and isothiocyante show intermolecular N···N interactions. Compounds with intermolecular O···O interactions include a cyclic ketone, an ester, a sulfoxide and a sulfone dimer. The bond

lengths vary from 3.20 to 3.70 Å for N···N interactions and 3.08 to 3.48 Å for O···O interactions. The QTAIM plots of these dimers show BCPs corresponding to N···N and O···O interaction (Figure 3.24 - 3.25).

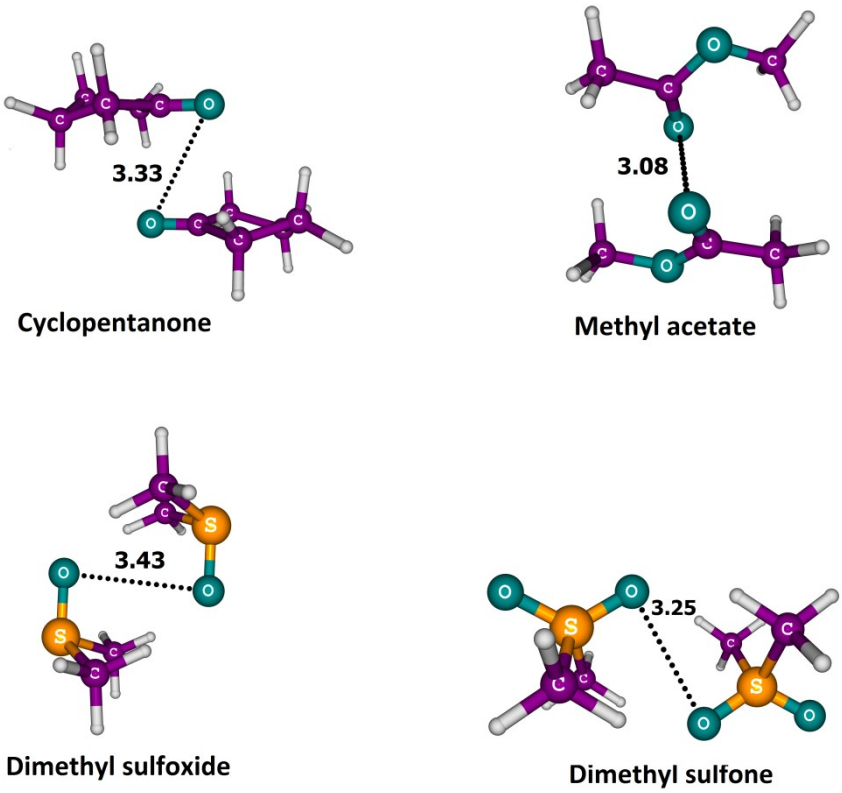

Figure 3.23 Dimers showing O···O interaction between chemically similar oxygen atoms. Distances are in Å [Remya and Suresh 2015a].

The values of E_{int}, ∑ρ and μ of all the dimers with N···N and O···O interactions are given in Table 3.9. For N···N and O···O BCPs, the ρ values range between 0.0047 - 0.0078 au and 0.0043 - 0.0082 au respectively. From Table 3.9, it is clear that E_{int} values of dimers having N···N as well as O···O interactions show increasing trend with increase in the values of ∑ρ and μ. In order to check the validity of the supposition that the concept of intermolecular interaction between atoms in chemically similar environments is atom independent, Eq. 3.3 (for dimers with C···C interactions) is used for predicting the values of E_{int} of the complexes with N···N and O···O interactions. The values of E_{int} thus predicted (Table 3.9) show good agreement with the actual E_{int} values (Figure 3.26) (the deviation is < 1 kcal/mol for all the dimers except those of methyl cyanate and dimethyl sulfoxide, where the deviation is 1.38 and 1.01 kcal/mol respectively).

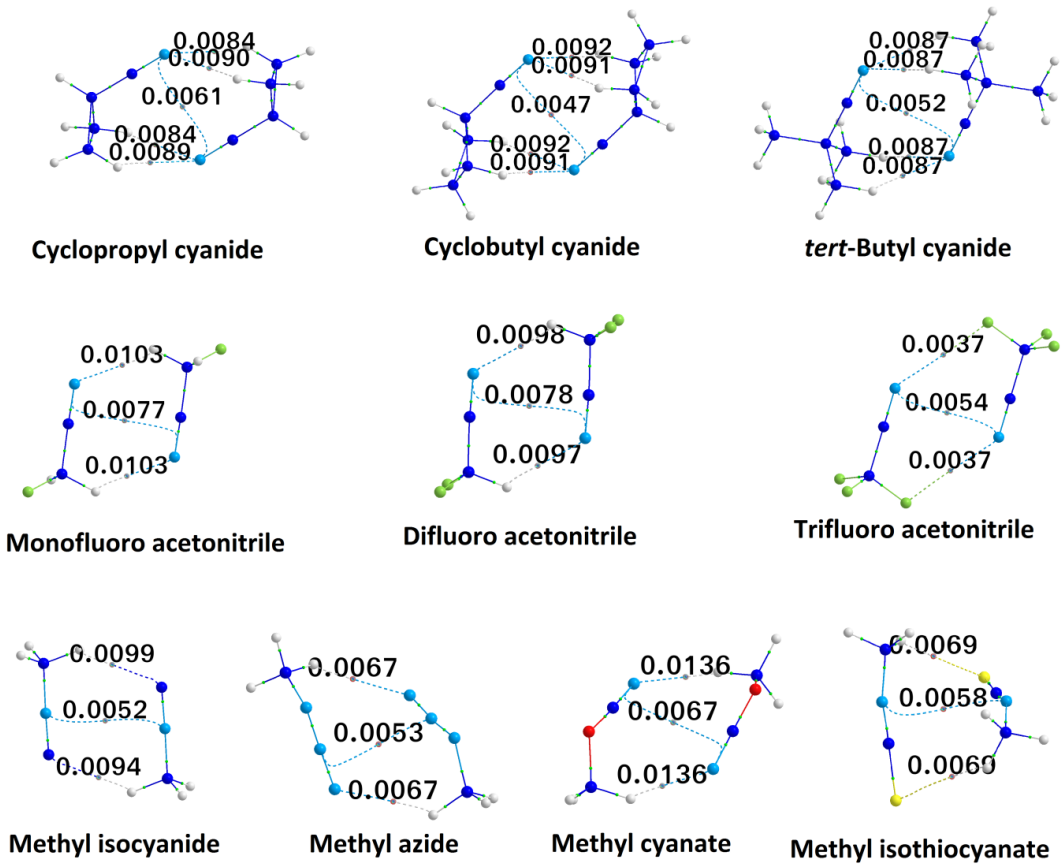

Figure 3.24 QTAIM plots of the dimers showing N···N interaction between chemically similar nitrogen atoms. The ρ values at intermolecular BCPs are given in au. Color code for atoms: dark blue, carbon; light blue, nitrogen; red, oxygen; light green, fluorine; yellow, sulfur; ash color, hydrogen [Remya and Suresh 2015a].

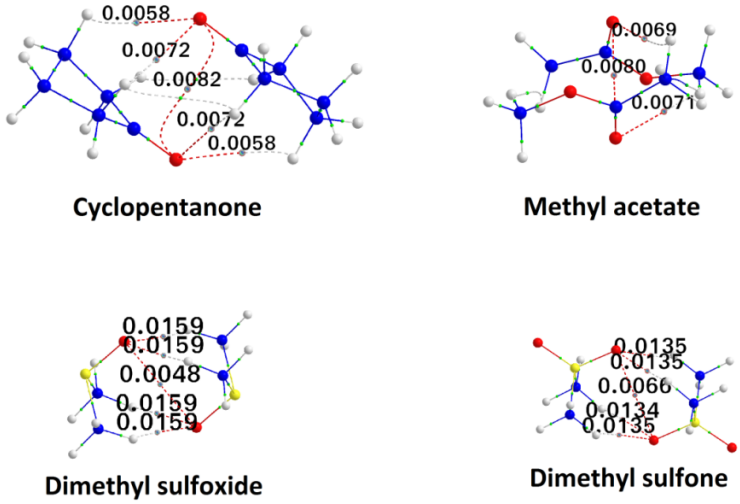

Figure 3.25 QTAIM plots of the dimers showing O···O interaction between chemically similar oxygen atoms. The ρ values at intermolecular BCPs are given in au. Color code for atoms: dark blue, carbon; light blue, nitrogen; red, oxygen; light green, fluorine; yellow, sulfur; ash color, hydrogen [Remya and Suresh 2015a].

Table 3.9 The interaction energy (E_{int}), sum of ρ at inter molecular BCPs (∑ρ), and monomer dipole moment (μ) of dimers with N···N and O···O interactions.

Dimer	E_{int} (kcal/mol)	∑ρ (a u)	μ (Debye)	Predicted E_{int} (kcal/mol)
cyclopropyl cyanide	-7.60	0.0407	4.39	-7.93
cyclobutyl cyanide	-7.74	0.0413	4.35	-7.97
tert - Butyl cyanide	-6.73	0.0399	4.11	-7.64
Monofluoro acetonitrile	-6.06	0.0284	3.21	-5.64
Difluoro acetonitrile	-5.48	0.0273	2.38	-4.92
Trifluoro acetonitrile	-1.53	0.0128	1.24	-2.40
methyl isocyanide	-4.84	0.0246	3.88	-5.65
methyl azide	-3.41	0.0188	2.47	-3.97
methyl cyanate	-8.69	0.0339	4.66	-7.31
Methyl isothiocyanate	-4.45	0.0196	3.12	-4.52
Cyclopentanone	-7.68	0.0408	3.14	-7.07
Methyl acetate	-5.14	0.0292	1.83	-4.76
Dimethyl sulfoxide	-12.03	0.0682	4.12	-11.02
Dimethylsulfone	-11.26	0.0605	4.57	-10.42

Similar to the case of dimers with C···C interactions, the geometry of the complexes with N···N and O···O interactions are also driven by the dipole moments of the interacting monomers which can be clearly visualized from their MESP plots given in Figure 3.27. as can be seen from Figure 3.27, the monomers in these complexes are partitioned into relatively electron rich and electron deficient regions and inter-molecular complimentary electrostatic interactions cause the N···N and O···O interactions between atoms in similar chemical environments in them similar to the case of molecules with C···C interactions. Occupied MOs corresponding to N···N and O···O non-covalent bonds are also located for all the dimer systems and are given in Figure 3.28.

The EDA data for complexes with N···N and O···O interaction between chemically similar atoms is given in Table 3.10. The electrostatic contribution to the values of E_{int} in these dimers is also found to be very high (62.52 – 88.73%), similar to the case of dimers with C···C interactions.

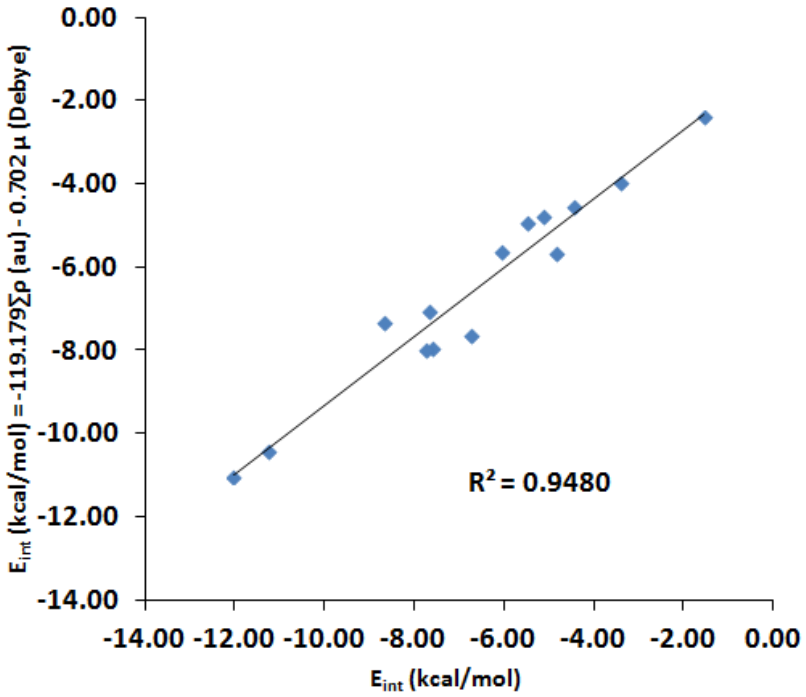

Figure 3.26 Correlation of E_{int} with E_{int} values predicted using Eq. 3.3 for complexes showing N···N and O···O interactions [Remya and Suresh 2015a].

3.7.4 Natural Bond Orbital Analysis

Examining each of the X1···X2 interaction (X = C, N and O) using NBO analysis shows a charge transfers from orbitals on X1 atom to those on X2 atom and similar charge transfers from orbitals on X2 to orbitals on X1 (the E_2 values for both the charge transfers being equal). Thus, both the X atoms involved in an X···X interaction can be considered both as donor and as acceptor. For instance, the interaction between C2 (molecule 1) and C6 (molecule 2) in acetylene dimer corresponds to charge transfers from the bonding orbitals on C2 to antibonding and RY* orbitals on C6 with E_2 values indicating a stabilizing interaction (sum of E_2 values = 0.84 kcal/mol). Similar charge transfers from the bonding orbitals on C6 to antibonding and RY* orbitals on C2 with same values of E_2 are also observed.

Except in the cases of trifluoroacetonitrile, methyl azide and dimethyl sulfoxide dimers, NBO analysis shows charge transfers from lone pairs or bonding orbitals to antibonding (BD*) orbitals corresponding to the X···X interactions. In the above mentioned exceptional cases, the acceptor orbitals are mainly RY* orbitals. Charge transfers corresponding to the X···X bonds (indicated by a BCP in QTAIM analysis) are

located in almost all the cases using NBO analysis. The orbitals involved in these charge

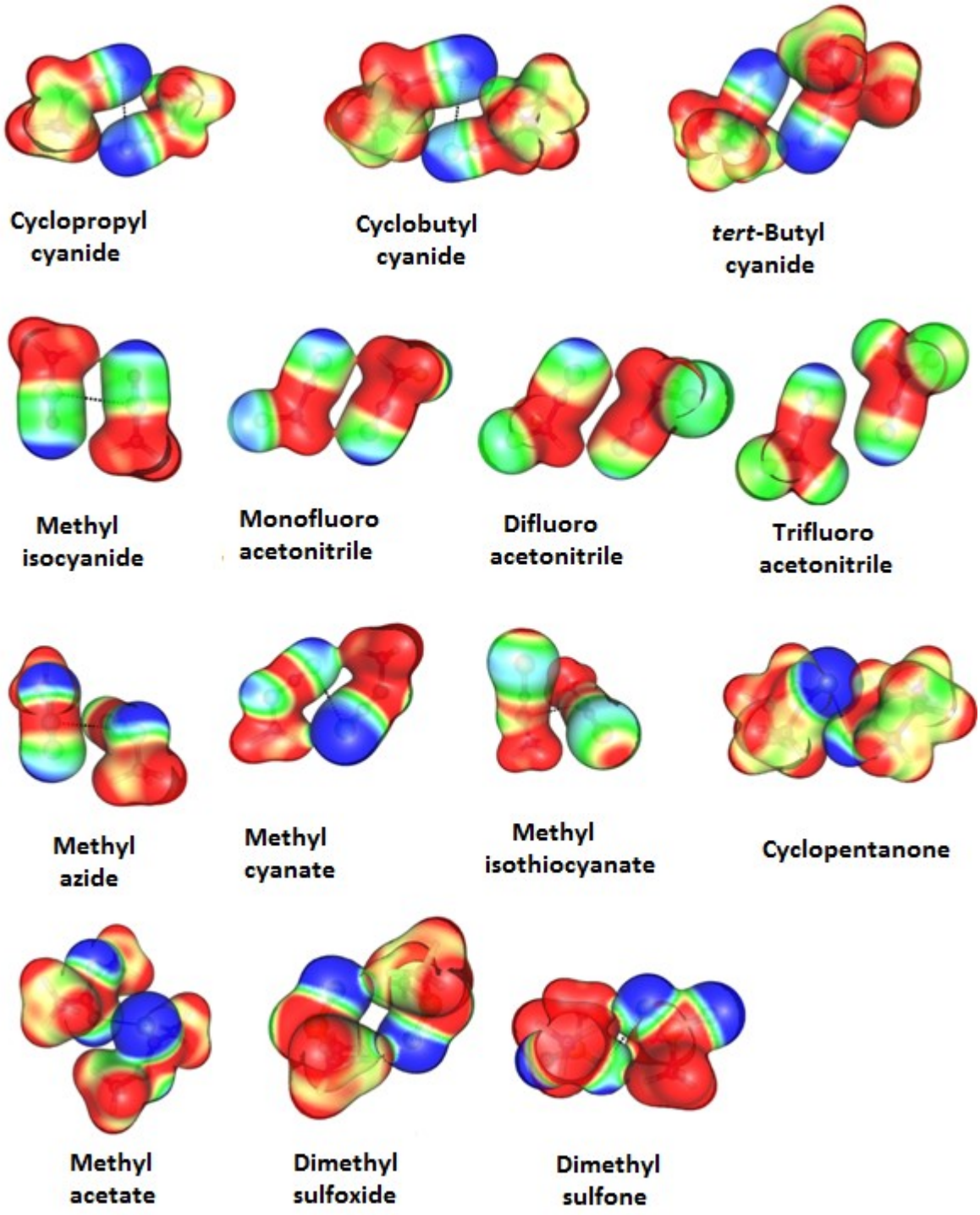

Figure 3.27 MESP plotted on isodensity surface of 0.01 au of dimers showing N···N and O···O interaction between similar atoms. Range: from -0.03 to 0.05 from blue to red [Remya and Suresh 2015a].

transfer interactions are shared by the X atoms in all cases except in trifluoroacetonitrile and dimethylsulfone dimers. In the case of trifluoroacetonitrile, where QTAIM analysis indicates N···N interaction, a charge transfer occurs from bonding orbitals on one N atom

to the RY* orbital on C near to the N atom. Similarly, in dimethyl sulfone, (where QTAIM analysis shows O2···O12 interaction) there is a charge transfer from the lone pair on O2 to antibonding orbital on the S atom next to O12. A similar charge transfer occurs from the lone pair on O12 to the antibonding orbital on the S atom next to O2 with an equal value of E_2.

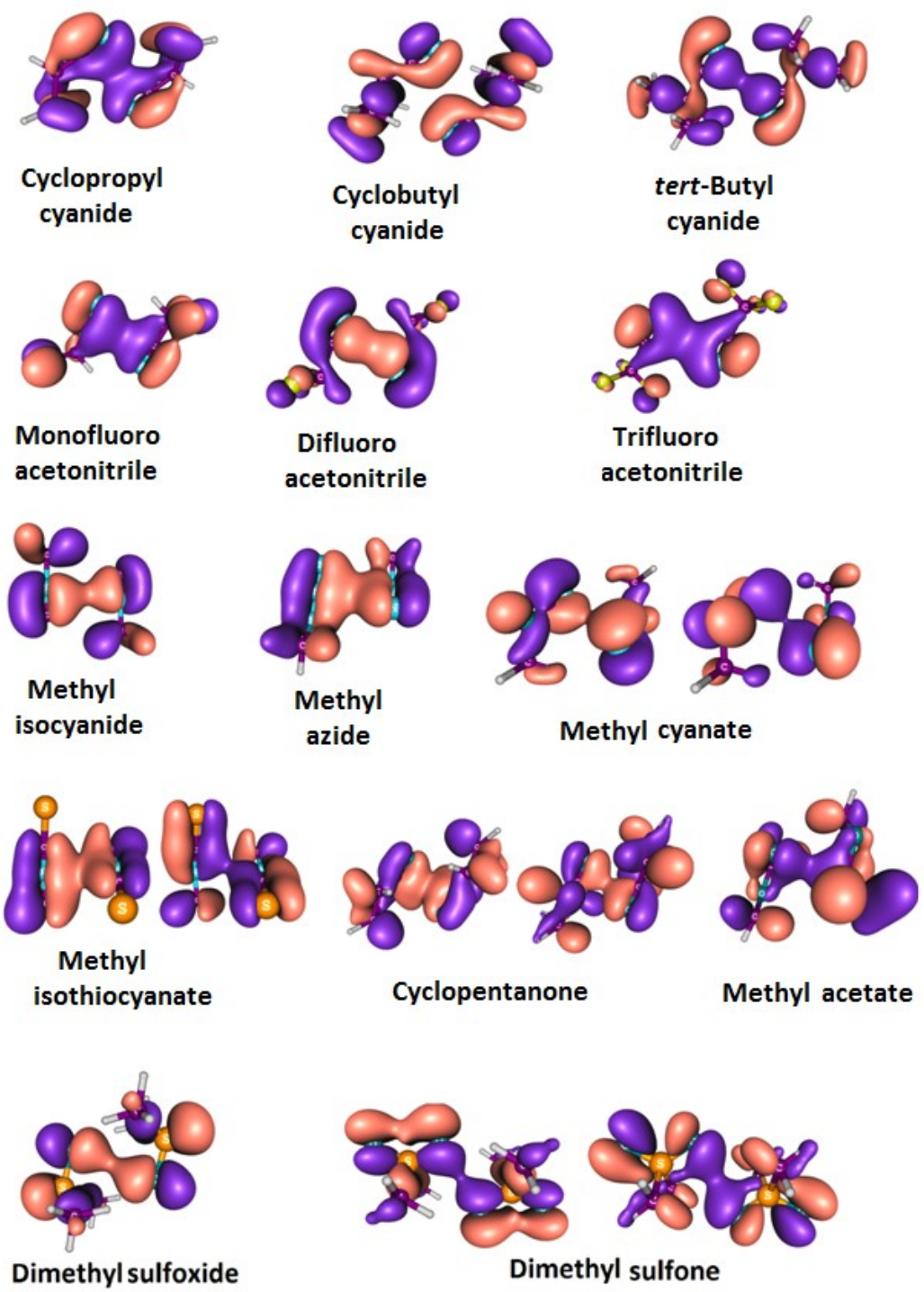

Figure 3.28 Occupied molecular orbitals corresponding to intermolecular N···N and O···O interactions in the dimers studied.

Table 3.10 Percentage orbital and electrostatic contributions towards the total interaction energy of the dimers with N···N and O···O interactions between similar atoms.

Dimer	% Electrostatic Interaction	% Orbital Interaction
cyclopropyl cyanide	79.64	20.36
cyclobutyl cyanide	73.95	26.05
tert - Butyl cyanide	75.77	24.23
Monofluoro acetonitrile	82.17	17.83
Difluoro acetonitrile	84.22	15.78
Trifluoro acetonitrile	88.73	11.27
methyl isocyanide	83.90	16.10
methyl azide	87.90	12.10
methyl cyanate	80.03	19.97
Methyl isothiocyanate	69.05	30.95
cyclopentanone	69.00	31.00
methyl acetate	70.79	29.21
Dimethyl sulfoxide	70.14	29.86
Dimethylsulfone	74.05	25.95

The total of E_2 values for charge transfers associated with each type of inter-molecular interactions (including X···X and hydrogen bonding interactions) in the dimers studied are given in Table 3.11. In many dimer systems (such as ethyl cyanide, isopropyl cyanide and dimethyl cyanamide etc.) the total E_2 value corresponding to C···C interaction is larger than those for the individual hydrogen bonds (HB). But in cases such as dimethyl sulfoxide and dimethyl sulfone, the E_2 value corresponding to O···O interaction is very small compared to that for the individual hydrogen bonds. However, the total stabilization obtained via hydrogen bonds is much larger compared to that by X···X interactions in all the cases. Thus, the geometry of these complexes must be determined by stronger interactions such as hydrogen bonds and the X···X interactions serve as a further stabilizing factor for such geometries. This can be illustrated in the study of growth patterns of acetonitrile clusters described in Part A of this chapter [Remya and Suresh 2014] where, the stacked clusters, with the highest possible number of C-H···N hydrogen

Table 3.11 Total E_2 values in kcal/mol corresponding to each interactions in the dimers.

Dimer	X···X	HB1[#]	HB2	HB3	HB4
Acetylene	0.84	-	-	-	-
HCN	1.39	-	-	-	-
Acetonitrile	1.04	1.76	1.76		
Ethyl cyanide	1.25	0.28	0.12	0.28	0.12
Isopropyl cyanide	1.12	0.33	0.13	0.38	0.08
Cyclopentyl cyanide	0.69	0.29	0.41	0.15	0.21
Cyclohexyl cyanide	0.61	0.08	0.70	0.37	0.27
Dimethyl cyanamide	1.88	0.76	0.76	0.76	0.76
Vinyl fluoride	0.52	-	-	-	-
Vinyl Chloride	1.00	-	-	-	-
trans - Difluoro ethylene	0.14	-	-	-	-
Acetylene chloride	0.58	0.41	0.41	-	-
Acetylene bromide	0.88	-	-	-	-
Acetylene difluoride	0.75	-	-	-	-
Methyl thiocyanate	0.32	3.04	3.04	-	-
Thioacetone	0.74	0.90	0.90	0.90	0.90
Cyclopropyl cyanide	0.15	0.57	0.71	0.74	0.58
Cyclobutyl cyanide	0.18	0.99	1.02	0.99	1.02
tert - Butyl cyanide	0.22	1.20	1.20	1.21	1.20
Monofluoroacetonitrile	0.50	1.42	1.43	-	-
Difluoroacetonitrile	0.56	1.38	1.40	-	-
Trifluoroacetonitrile	0.24	0.13	0.13	-	-
Methyl isocyanide	0.16	1.80	1.99	-	-
Methyl azide	0.61	0.54	0.62	-	-
Methyl cyanate	0.22	3.60	3.56	-	-
Methyl isothiocyanate	0.14	1.91	1.92	-	-
Cyclopentanone	1.47	0.19	0.18	0.20	0.18
Methyl acetate	0.64	0.23	0.25	0.07	-
Dimethyl sulfoxide	0.14	3.67	3.67	3.67	3.67
Dimethyl sufone	0.20	3.07	3.02	3.01	3.04

[#]HB indicates C···Cl interaction in acetylene chloride N···F interaction in trifluoroacetonitrile and hydrogen bonds in all other cases.

bonding interactions, is further stabilized by C···C interactions between the nitrile carbon atoms of antiparallelly arranged monomers. In cases such as trifluoroacetonitrile and dimethylsulfone, where QTAIM analysis shows N···N and O···O BCPs respectively, the NBO analysis shows charge transfers from the orbitals shared by one N/O atom (monomer 1) to the orbitals on the atoms next to second N/O atom (monomer 2) instead of the second N/O atom. This shows that the bond paths and BCPs shown in the QTAIM analysis should not be taken too literally [Foroutan-Nejad *et al.* 2014; Lane *et al.* 2013] and that the entire regions in the two molecules may be actually interacting.

3.7.5 Using Statistical Methods for the Validation of the Results

It is notable that the equation designed for dimers with C···C interactions (Eq. 3.3) is useful to predict the E_{int} values of those with N···N and O···O interactions with a good level of accuracy. This implies that the dipole enforced interaction could be a general phenomenon independent of the atoms involved. Considering the entire data for C···C, N···N and O···O interactions, a more general equation to predict E_{int} can be obtained using a double linear regression on $\sum\rho$ and μ (Eq. 3.4).

$$E_{int}\ (\text{kcal/mol}) = -138.395\sum\rho\ (\text{au}) - 0.551\mu\ (\text{Debye}) \qquad \text{(Eq. 3.4)}$$

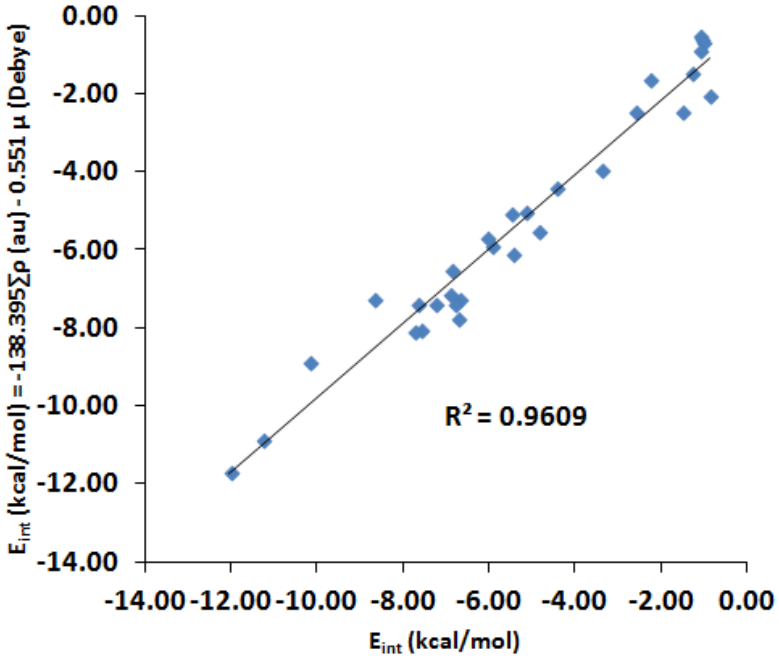

Figure 3.29 Correlation of E_{int} with predicted values of E_{int} using Eq. 3.4 for all the complexes with C···C, N···N and O···O interaction between atoms in similar chemical environments [Remya and Suresh 2015a].

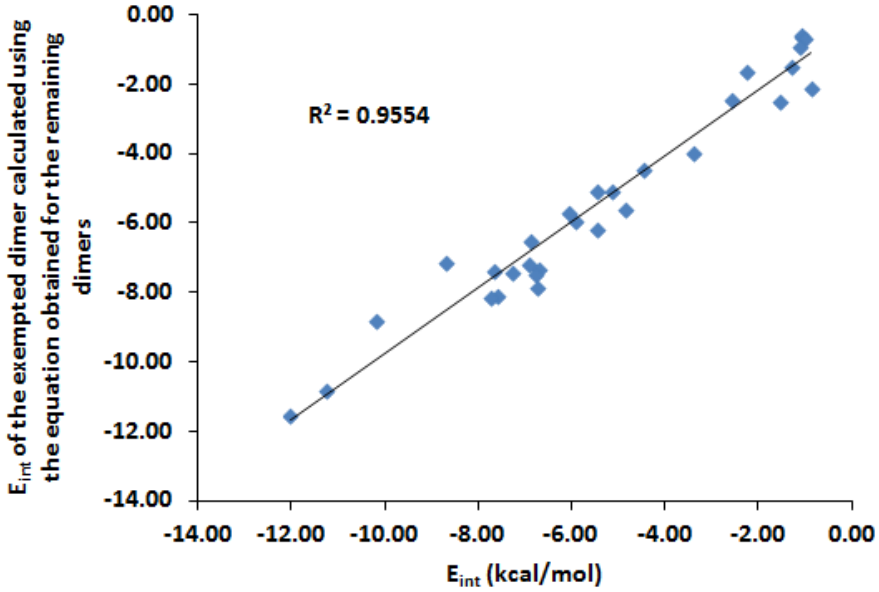

Figure 3.30 Correlation of E_{int} of each exempted dimer with its E_{int} value calculated from the equation obtained for the remaining dimers.

Figure 3.29 shows a good correlation between E_{int} values obtained using Eq. 3.4 and the actual E_{int} values of the dimers. The values of statistical parameters *viz.* multiple R and R^2 are 0.9950 and 0.9900 respectively. The P values for $\sum\rho$ and μ are 1.8×10^{-12} and 3.03×10^{-5} respectively, suggesting that Eq. 3.4 is trustworthy.

For further validation of the results, a method of statistical analysis known as 'leave one out' method is used. In this method, the E_{int} values of all except one dimer (the entire set of dimers showing C···C, N···N and O···O interactions are used) is predicted from their $\sum\rho$ and μ values using double linear regression analysis. The E_{int} value of the exempted dimer is calculated from the equation for the remaining dimers thus obtained. The process is repeated for all the dimers and E_{int} value of each of them is predicted from the equation obtained for the remaining ones. The values thus predicted show very good agreement with the actual E_{int} values (R^2 = 0.9554, Figure 3.30). Further, this method provides a set of regression equations. It is observed that there is only small variations among the coefficients of $\sum\rho$ (range between -133.170 and -143.577) and μ (range between -0.490 and -0.592) in these equations. The values of coefficients of $\sum\rho$ lie in between -137 and 139 in most of the cases. Only five out of thirty values show values out of this range. As a result, the E_{int} values predicted by these equations are also similar. Thus, the E_{int} values predicted using these equations agree well with each other as well as with the actual values of E_{int} of the dimers. The thirty equations for predicting E_{int} from 'leave one out' method are given in Table 3.12.

Table 3.12 Equations obtained by exempting each dimer in the 'leave one out' validation test for the multiple linear regression analysis method used for predicting the values of E_{int} (in kcal/mol) of the dimers from their ∑ρ (au) and μ (Debye) values.

Dimer exempted	Equation for E_{int}
acetylene	E_{int} = -137.713∑ρ -0.557μ
hydrogen cyanide	E_{int} = -139.383∑ρ - 0.541μ
acetonitrile	E_{int} = -138.436∑ρ -0.550μ
ethyl cyanide	E_{int} = -138.238∑ρ - 0.555μ
isopropyl cyanide	E_{int} = -138.152∑ρ - 0.561μ
cyclopentyl cyanide	E_{int} = -137.336∑ρ - 0.569μ
cyclohexyl cyanide	E_{int} = -138.123∑ρ - 0.556μ
dimethyl cyanamide	E_{int} = -138.514∑ρ - 0.529μ
vinyl flouride	E_{int} = -137.907∑ρ - 0.556μ
vinyl chloride	E_{int} = -139.787∑ρ - 0.536μ
trans - difluoro ethylene	E_{int} = -137.692∑ρ - 0.557μ
actylene chloride	E_{int} = -143.577∑ρ - 0.505μ
acetylene bromide	E_{int} = -137.862∑ρ - 0.556μ
acetylene difluoride	E_{int} = -137.912∑ρ - 0.555μ
methyl thiocyanate	E_{int} = -139.602∑ρ - 0.535μ
thioacetone	E_{int} = -139.819∑ρ - 0.544μ
cyclopropyl cyanide	E_{int} = -138.550∑ρ - 0.556μ
cyclobutyl cyanide	E_{int} = -138.649∑ρ - 0.554μ
tert - Butyl cyanide	E_{int} = -139.398∑ρ - 0.556μ
Monofluoro acetonitrile	E_{int} = -138.474∑ρ - 0.547μ
Difluoro acetonitrile	E_{int} = -137.626∑ρ- 0.555μ
Trifluoro acetonitrile	E_{int} = -138.882∑ρ - 0.550μ
methyl isocyanide	E_{int} = -135.728∑ρ - 0.584μ
methyl azide	E_{int} = -137.729∑ρ - 0.561μ
methyl cyanate	E_{int} = -142.698∑ρ - 0.490μ
Methyl isothiocyanate	E_{int} = -138.451∑ρ - 0.550μ
Cyclopentanone	E_{int} = -137.037∑ρ - 0.560μ
Methyl acetate	E_{int} = -137.989∑ρ - 0.554μ
Dimethyl sulfoxide	E_{int} = -133.170∑ρ - 0.592μ
Dimethylsulfone	E_{int} = -135.516∑ρ - 0.571μ

3.7.6 Using More Density Functionals and G3MP2 Method for the Validation of the Results

The E_{int} values obtained using the DFT methods *viz.* M06L, CAM-B3LYP, B971, B3LYP, and B3LYPD3 and also G3MP2 method are given in Table 3.13. The most reliable values of E_{int} must be given by the G3MP2 method. However, the geometry

obtained from G3MP2 is not trustworthy as it uses Hartree-Fock level optimized geometry for a subsequent MP2 level optimization. For some of the dimers, the geometries

Table 3.13 Values of E_{int} obtained at different levels of DFT and with G3MP2 method of all the dimers with X···X interactions

Dimer	M06L	CAM-B3LYP	B971	B3LYP	B3LYPD3	G3MP2
Acetylene	-1.07	-0.37	-0.89	-0.73#	-1.62#	-0.89#
HCN	-2.59	-1.39	-2.29	-4.22#	-4.95#	-4.15#
Acetonitrile	-5.93	-5.01	-5.20	-4.02	-6.46	-4.38
Ethyl cyanide	-6.91	-4.80	-5.10	-3.80	-7.06	-5.34
Isopropyl cyanide	-6.7	-4.55	-4.85	-3.61	-6.95	-5.38
Cyclopentyl cyanide	-6.79	-4.64	-5.03	-3.60	-7.42	-5.93
Cyclohexyl cyanide	-7.27	-4.56	-4.97	-3.40	-7.54	-6.19
Dimethyl cyanamide	-10.19	-6.97	-6.94	-5.40	-9.98	-8.17
Vinyl fluoride	-1.29	-1.15#	-0.73	-0.31	-1.96#	-0.46#
Vinyl Chloride	-2.27	-0.36	-0.93	-0.29	-2.57#	-0.83#
trans - Difluoro ethylene	-1.09	-0.67#	-1.65#	-1.40#	-2.65#	-0.63#
Acetylene chloride	-0.87	0.11	-0.35	-0.54#	-1.53#	-0.52
Acetylene bromide	-1.03	-0.73	-1.04	-0.58#	-1.94#	-0.34
Acetylene difluoride	-1.12	-0.24	-0.38	0.13	-1.28	-0.22
Methyl thiocyanate	-6.88	-5.50	-5.13	-4.63	-7.74	-5.63
Thioacetone	-5.45	-2.06	-2.98	-1.22	-5.83	-4.24
Cyclopropyl cyanide	-7.6	-5.17	-5.57	-3.94	-7.46	-5.55
Cyclobutyl cyanide	-7.74	-4.85	-5.32	-3.57	-7.77	-5.86
tert - Butyl cyanide	-6.73	-4.30	-4.80	-3.14	-6.85	-5.14
Monofluoroacetonitrile	-6.06	-5.19	-5.30	-4.12	-6.67	-5.06
Difluoroacetonitrile	-5.48	-4.75	-4.85	-3.68	-6.21	-4.62
Trifluoroacetonitrile	-1.53	-0.53	-1.20	-0.64#	-2.10	-2.24
Methyl isocyanide	-4.84	-3.74	-4.15	-3.01	-5.46	-3.41
Methyl azide	-3.41	-1.95	-0.66	-1.39	-3.50	-1.96
Methyl cyanate	-8.69	-7.27	-7.46	-6.29	-8.91	-6.29
Methyl isothiocyanate	-4.45	-2.35	-2.82	-2.27	-5.74	-4.22
Cyclopentanone	-7.68	-4.27	-4.70	-2.88	-7.38	-6.69
Methyl acetate	-5.14	-3.27	-3.07	-2.36#	-4.72	-3.63
Dimethyl sulfoxide	-12.03	-17.27	-15.54	-8.47	-13.82	-9.19
Dimethyl sufone	-11.26	-17.75	-15.76	-7.83	-13.36	-9.94

A considerable change in geometry compared to M06L, not showing X···X interaction.

calculated using the above mentioned methods deviate from the M06L geometry, which is indicated in the table with a # mark. However, according to the our benchmark study described in Chapter2 [Remya and Suresh 2013], M06L geometries are found to be the

most reliable.

The mean absolute deviation (MAD) of the deviation of the values of E_{int} from G3MP2 results for M06L, B3LYPD3, B3LYP, B971 and CAM-B3LYP are 0.52, 0.57, 0.86, 1.21 and 1.44 respectively, again indicating the highest reliability of M06L energies, which further support our benchmark study. M06L and B3LYP-D3 results show close agreement to overall trend and magnitude of the G3MP2 results, according to Table 3.13. Values of E_{int} calculated using B3LYPD3 are always larger compared to those given by B3LYP, indicating that dispersion effects play a significant role in the stability of the dimers. The difference between these two values (which range from -0.73 kcal/mol for hydrogen cyanide to -5.53 kcal/mol for dimethyl sulfone) gives an estimate of the effect of dispersion in each dimer. However, comparing G3MP2 and B3LYPD3 values indicate that the latter method slightly overestimate the E_{int} values.

3.8 Conclusions

In Part A of this chapter, the relative stability of different types of acetonitrile clusters with different growth patterns is explained based on the number of intermolecular interactions (including both C-H**...**N and dipolar interactions) and pair-wise interaction energies. Except for tetramers, stacked arrangement was the most stable followed by cross-stacked ones. A slightly higher stability of the cross-stacked form of tetramer compared to the stacked form is attributed to the lack of destabilizing monomer pairs in the former. The magnitudes of E_{int} as well as E_m were the highest in the case of stacked, followed by cross-stacked clusters, showing the highest stability and cooperativity in them. This is explained by the presence of the largest number of C-H**...**N interactions and favourable antiparallel orientation of the dipolar molecules in those clusters. Simple axial (vertical) extension of stacked and cross-stacked clusters to octamers and dodecamers gave further increase in the magnitudes of E_{int} and E_m, with the stacked clusters having the highest values. Lateral extension of the stacked hexamers to dodecamers with more end-on interactions and lateral interactions provided further increase in E_{int} and E_m values. Such patterns obtained for hexadecamer showed higher stability than α and β crystal patterns, thus, predicting a third form for acetonitrile crystal, which is more ordered and more stable than α and β forms. Maximum stability in the hexadecamer clusters is explained as resulting from the largest number of intermolecular interactions. The **27mer**, where the central molecule experiences interactions from all sides, showed the highest E_m and hence the largest cooperativity.

A correlation between E_{int} and the sum of electron densities at intermolecular BCP's ($\Sigma\rho$) in QTAIM analysis showed that the stability of clusters is directly related to the number and strength of C-H**...**N and dipolar interactions. Stacked, followed by cross-stacked clusters show the highest number of such interactions, explaining their stability. Analysis of MESP isodensity surface showed that the stacked clusters exhibits the least amount of area with negative potential followed by the cross-stacked ones, indicating the maximum contribution of lone pair electron density in intermolecular bonding of such clusters. The free energy data showed the dimer structures to be the most stable at room temperature. The stability of larger cluster increases with decrease in temperature and **27mer** had the least value for $\Delta G/n$ at 215 K. The ladder-type clusters came next in the stability order after the stacked and cross-ones. The cyclic structures are shown to have the least stability except for the cyclic trimer. The cyclic trimer had slightly higher stability compared to ladder type, which is attributed to the absence of any destabilizing monomer pairs. The stability of a mixed cluster increased with increase in number of monomers in the antiparallel (ladder-type) part and decrease in number of monomers in the cyclic part. Thus, it is concluded that an antiparallel orientation of monomers is always preferred in an acetonitrile dimer. For higher clusters, the preferred orientation is so as to get maximum cooperativity, which can be attained with stacked clusters containing the highest number of C-H**...**N interactions and favourable dipolar interactions. A 2.6 fold increase in the value of E_m with increase in cluster size from dimer to **27mer** is the most remarkable finding of this study which explains that strong cooperativity is essential for overcoming the large amount of entropy loss during cluster formation. The cooperativity explains the significantly high melting point of acetonitrile compared to its higher alkyl derivatives. Further, it explains why acetonitrile exists in liquid state at room temperature despite the weak intermolecular bonds.

In Part B of this chapter, clear evidence for intermolecular X···X interaction (where X = C, N and O) between atoms of similar chemical environment in homogeneous dimers of organic molecules are obtained from MO, NBO and electron density analyses. The X···X bonding is explained as resulting from complimentary electrostatic interaction between electron rich region of one monomer with electron deficient region of n another monomer and also satisfying the condition that both X are from similar chemical environment. NBO analysis shows stabilizing charge transfers between the two X atoms corresponding to each of the X···X interactions supporting the assumption that both X

atoms act as both donor and acceptor. Magnitude of binding energy of the dimers increases with increase in the dipole moment of the constituent monomers. Even in compounds such as acetylene and acetylene difluoride where the monomer dipole moment is zero, local variations in MESP create bonding interaction. The EDA analysis has shown that the binding energy (E_{int}), in most of the cases, is mainly electrostatic in nature. Further, the value of E_{int} is divided into contribution from the monomer dipole moment and contribution from the total gain in electron density at the non-covalently interacting intermolecular bonds using double linear regression analysis method. The dipole moment term contributes considerably to dimers of dipolar molecules where X···X interactions between atoms in similar chemical environment exist. The X···X interactions are characterized by BCPs in QTAIM analysis. The results are further validated by comparing the E_{int} values with those calculated using different density functionals and G3MP2 methods. Intermolecular C···C inetraction between chemically similar carbon atoms are located in the crystal structures of several organic compounds in the literature. This suggests that these interactions can play an important role in the crystal growth patterns as well as self assembly process of unsaturated organic molecules.

CHAPTER 4

Intermolecular C···C Interactions in Polyynes and Carbon Rings

Part A – Non-Covalent Intermolecular C···C Interactions in Polyynes

&

Part B - Geometry, Aromaticity and Intermolecular C···C Interactions in C_{4N+2} and C_{4N} Carbon Rings

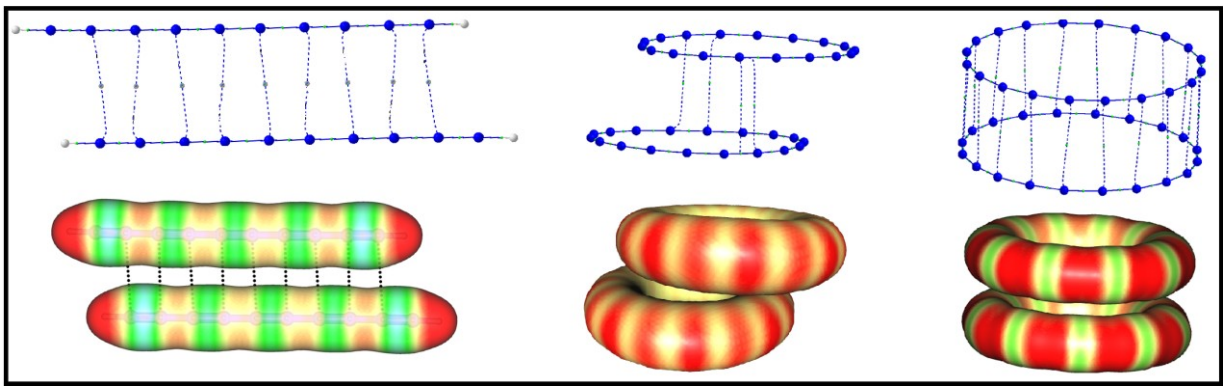

4.1 Abstract

In Part A, the nature and strength of intermolecular C···C interactions in dimer and tetramer complexes of polyynes have been analyzed. Polyynes are the small molecular weight analogues of the one dimensional infinite chain carbon allotrope of carbon, viz. carbyne. The effect of the chain length and end group functionalities of the interacting polyyne monomers on the binding energy of the dimers is also analyzed. All the polyyne complexes showed a multitude of non-covalent C···C interactions. As is evident from the molecular electrostatic potential analysis, these interactions resulted from complimentary electrostatic interaction between relatively electron rich formal triple bond region of one monomer and the electron deficient formal single bond region of the other monomer. These paired (C≡C)···(C-C) bonding interactions, also identified in the quantum theory of atoms-in-molecules analysis, increases in number with increase in the chain length of the monomers leading to significant increase in interaction energy (E_{int}); -1.07 kcal/mol for acetylene dimer to -45.83 kcal/mol for 50yne dimer. Substitution of one of the hydrogen atoms at the end position of polyynes with different functional groups increases the magnitude of E_{int} and this effect of end group on E_{int} persists even up to 50 triple bonds, the largest chain length analyzed in this study. Multiple minima with reduced number of C···C interactions and lower values of E_{int} are located in a dimer by sliding one monomer over the other, which illustrates the role of C···C interactions in stabilizing the polyyne dimers. Further, the tetramers complexes showed significantly higher values for interaction energy per monomer (E_m) (2.5 – 2.8 times higher) compared to the dimers, indicating strong cooperativity in C···C interactions. This huge gain in energy seen in large dimer and tetramer complexes of polyyenes predicts the formation of their molecular bundles which may find use in the design of new functional molecular materials.

In Part B of this chapter, intermolecular bonding features of planar monocyclic carbon rings with 4N and 4N+2 carbon atoms have been studied for N = 1- 8. The C_{4N+2} molecules show cumulenic structures with equal bond lengths and C_{4N} molecules form structures with clear bond length alternation. Two cyclic delocalized π-molecular orbitals and highly negative nucleus independent chemical shift (NICS) values show the doubly Hückel aromatic nature of C_{4N+2} systems while two localized π-molecular orbitals and highly positive NICS values show the doubly Hückel antiaromatic nature of C_{4N} systems. Further, analysis of the molecular electrostatic potential (MESP) features revealed the

uniform electron distribution over the delocalized CC bonds in C_{4N+2} and the alternate electron rich and electron deficient regions in C_{4N} systems. These contrasting geometric, electronic and magnetic features of C_{4N+2} systems compared to C_{4N} systems resulted in drastic difference in their intermolecular bonding and dimerization (formation of molecular dimers) features. The C_{4N} showed much higher tendency than C_{4N+2} for dimer formation. This is because, dimers of C_{4N} systems, in general show 4N number of intermolecular C···C interactions arising from complimentary electrostatic interactions between electron rich shorter CC bonds and electron deficient longer CC bonds. In C_{4N} dimers, a perfect sandwich configuration, which maximizes the attractive complementary electrostatic interactions, is observed while in C_{4N+2} dimers, a shifted-parallel stacked arrangement indicating the non-complementary character of interactions arising from smooth aromatic distribution of electrons is observed.

Part A: Non-Covalent Intermolecular C···C Interactions in Polyynes

4.2 Introduction

Two well known allotropes of carbon are the sp3 hybridized diamond and the sp2 hybridized graphite. The hypothetical one-dimensional sp hybridized allotrope of carbon, *viz*. carbyne ($(-C\equiv C-)_\infty$) consists of single atom thin infinite chains of carbon atoms [Heimann *et al.* 1983]. Polyynes with general formula $R(-C\equiv C)_n-R$ are the smaller oligomers of carbyne and are treated by synthetic chemists as the starting step towards the synthesis of carbynes. Polyynes are found to exist in meteorites [Hayatsu *et al.* 1980; Whittaker *et al.* 1980], biological systems [Shi Shun and Tykwinski 2006], carbon nanostructures [Ravagnan *et al.* 2002] and mixed sp-sp^2 carbon structures [Casari *et al.* 2008; Ravagnan *et al.* 2007]. Different types of polyynes with end group substituents containing metals and non-metals have been characterized crystallographically [Szafert and Gladysz 2003]. Longer polyynes require bulky substituents as their end groups to get stabilized [Gibtner *et al.* 2002; Zheng *et al.* 2006]. Polyynes with several end groups have been synthesized and characterized [Cataldo *et al.* 2010; Chalifoux and Tykwinski 2009; Eisler *et al.* 2005; Slepkov *et al.* 2004; Wang *et al.* 2008]. Polyynes containing up to 22 triple bonds that are stable at normal laboratory conditions have been synthesized and characterized recently by Chalifoux and Tykwinski [Chalifoux and Tykwinski 2010]. Polyyne systems synthesized by them include those with bulky end groups containing Pt and Si which stabilized the long-chain backbones. The physical properties of the hypothetical allotrope, carbyne are expected to be predicted by extrapolating the properties of polyynes [Chalifoux and Tykwinski 2009; Chalifoux and Tykwinski 2010]. Tuning the conjugated π electron circuit in polyynes can result in low HOMO-LUMO gap suitable for the development of molecular conductors. Unlike many other conducting organic compounds, the conjugation features of the π electrons in polyynes is not limited by rotation around single bonds [Chen and Reed 2002; Taylor *et al.* 2003], which is an additional advantage of these molecules. Hence, polyynes are expected to form an important class of molecules capable of forming one dimensional nano-wires [Ballmann *et al.* 2010; Börrnert *et al.* 2010; Crljen and Baranović 2007; Khoo *et al.* 2008; Lang and

Avouris 1998; Lang and Avouris 2000; Liu *et al.* 2013; Nair *et al.* 2011; Wang *et al.* 2009a] in atomic scale circuits. Other possible applications include forming spintronic devices [Zanolli *et al.* 2010] due to their high mobility of electrons, hydrogen storage materials [Sorokin *et al.* 2011] and as a structural component in atomic scale devices due to their favourable mechanical properties [Ashley *et al.* 2014; Kocsis *et al.* 2014; Liu *et al.* 2013; Mirzaeifar *et al.* 2014; Nair *et al.* 2011].

However, a thorough study on the nature of intermolecular interactions in polyynes is lacking in the literature. Many of the physical properties of polyynes are influenced by the nature of their end groups [Liu *et al.* 2013; Ravagnan *et al.* 2009]. In a similar way, the nature and strength of intermolecular interactions in polyynes can also be vulnerable to change with change in substitutions as well as length of the molecule. Tuning the strengths of such interactions can help in making materials with desirable mechanical properties. Stronger intermolecular forces can result in harder polyyne based materials. Thus, studying the nature and strength of intermolecular interactions in polyynes with different substitutions can help in predicting their performance as structural and functional components.

Intermolecular interactions involving carbon group elements have attained increased attention in recent years [Azofra *et al.* 2014; Bauzá *et al.* 2013; Bauzá *et al.* 2014; Bundhun *et al.* 2013; Grabowski 2014; Li *et al.* 2014; Mani and Arunan 2013; Mani and Arunan 2014; McDowell 2014; McDowell and Joseph 2014; Thomas *et al.* 2014; Varadwaj *et al.* 2014]. The interaction between an electron deficient 'σ-hole' [Clark *et al.* 2007; Murray *et al.* 2009] on a carbon group element and an electron rich centre such as a lone pair has been studied in detail [Bundhun *et al.* 2013] and is said to be analogous to other-σ hole interactions such as halogen, chalcogen and pnicogen bonds [Politzer *et al.* 2013]. The terms 'carbon bond' introduced by Mani and Arunan denotes a σ-hole interaction of a covalently bonded carbon atom with a donor species [Mani and Arunan 2013]. Similarly, the term 'tetrel bonding' [Bauzá *et al.* 2013] denotes the σ-hole interaction of heavier carbon group elements with electron rich donor cites.

In Part B of the third chapter, intermolecular C···C, N···N and O···O interactions between atoms in similar chemical environments [Remya and Suresh 2015a] resulting from the complimentary electrostatic interaction between electron rich and electron deficient regions on the interacting monomers have been

described. The Coulombic interactions in non-covalently interacting systems are described well by Politzer *et al* [Politzer et al. 2015]. Using natural bond order (NBO) analysis, it was shown that both the interacting X atoms act both as donor and as acceptor. Existence of such C···C interactions in the crystal structures of several known organic compounds was also proved. In polyynes, the presence of alternating triple bonds and formal single bonds can give rise to alternating electron rich and electron deficient regions. This can result in intermolecular complementary electrostatic interactions in their dimers and higher order clusters.

In this part of the chapter, an analysis of the type of intermolecular interactions in various polyyne molecules has been described. The intermolecular C···C interactions described here cannot be classified as σ-hole interactions, which, by definition, is observed along the extension of a σ-bond. Instead, as shall be seen, the interactions are perpendicular to the polyyne molecules, between the chains. The effect of length of the polyyne chains and nature of end groups on the intermolecular C···C interactions in polyyne dimers is also studied. The systems studied include dimers of polyyne molecules with H at one end and H, CN, NO_2, F, CF_3, and NMe_2 at the other end. Polyyne molecules with the aforesaid substitutions and with 1, 2, 3, 4, 5, 10, 15, 20, 30, 40 and 50 triple bonds are chosen for the study. A set of dimers with a donor group (NMe_2) at one end and an acceptor group (CN) at the other is also studied. Cooperativity of the C···C interactions is examined by studying a few tetramers.

Polyynes mentioned here are named by their end groups other than hydrogen and the number of triple bonds in the backbone. For example, a polyynes molecule with CN group at one end and H at the other and having five triple bonds is named as pentayne_CN. A polyyne molecule CN and NMe_2 as end groups and with four triple bonds is named as tetrayne_CN/NMe_2. Higher members are named by combining the number of triple bonds, the functional keyword –yne and the end group. For example, the name 50yne_CN denotes the polyyne with 50 triple bonds and CN group at one end.

4.3 Computational Methods

The calculations are done at the M06L level of DFT [Zhao and Truhlar 2006b], the best performer in the benchmark study described in Chapter 2 [Remya

and Suresh 2013]. For optimization of polyynes containing one to five triple bonds, the basis set used is 6-311++g(d,p). For larger systems, a smaller basis set *viz*. 6-31g(d,p) is used with the same DFT method for optimization and single point energy calculation is done at M06L/6-311++g(d,p) level. The geometries of polyynes containing up to 40 triple bonds have been confirmed to be minima by frequency calculation. For 50ynes, frequency calculations have not been conducted due to high computational coast. However, since the trends in their geometries are similar to the lower analogues, we assume that the dimers of 50ynes are also minima. The calculations are done using *Gaussian09* [Frisch *et al.* 2010] suit of programs.

For further validation of the results, the dimers of polyynes having one (monoynes) and five (pentaynes) triple bonds and different end groups are studied using B97D [Grimme 2006a] and the popular B3LYP [Becke 1993; Lee *et al.* 1988; Miehlich *et al.* 1989] method together with the D2 version of Grimme's dispersion [Grimme 2006b]. The interaction energies calculated using these methods are compared with the corresponding M06L values.

The total interaction energy (E_{int}) of a cluster consisting of 'n' monomer molecules is calculated as,

$$E_{int} = E_{cluster} - (n)E_{monomer} + E_{BSSE} \quad \text{Eq. (4.1)}$$

In Eq. (4.1), $E_{cluster}$ is the energy of the cluster, $E_{monomer}$ is the energy of an isolated monomer and E_{BSSE} is the counterpoise correction term by Boys and Bernardy method [Boys and Bernardi 1970] as implemented in *Gaussian09*. For studying cooperativity of the intermolecular interactions, the tetramers are optimized and the values of their interaction energy per monomer (E_m) are compared with those of the corresponding dimers. The intermolecular interactions are identified and their strength is compared with the help of quantum theory of atoms-in-molecule (QTAIM) [Bader 1990] analysis as implemented in AIMAll [Keith 2014] program. In this method, bonding interactions are identified as (3, -1) critical points, referred to as bond critical points (BCPs) in the electron density topology of a system. The value of electron density, ρ at intermolecular BCPs is generally taken as a measure of the strength of such an interaction [Grabowski 2001; Knop *et al.* 2002; Parthasarathi *et al.* 2006; Popelier 1998; Remya and Suresh 2014]. MESP [Gadre and Shirsat 2000; Murray and Sen 1996; Politzer and Truhlar 1981] mapped at 0.01 au isodensity surface of the

complexes are used for illustrating the Columbic nature of intermolecular interactions.

4.4 Results and Discussion

4.4.1 Geometry and Interaction Energy of Polyyne Dimers

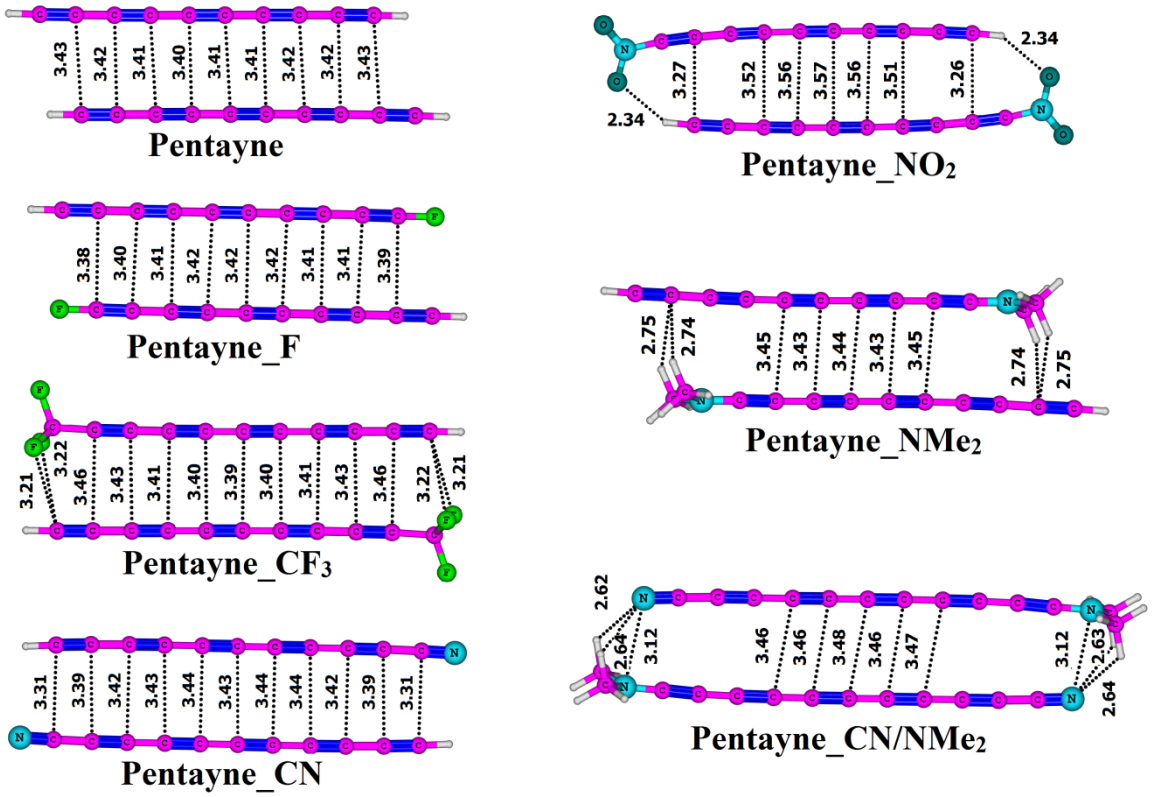

Figure 4.1 Optimized geometries of polyyne dimers with five triple bonds (pentaynes) and different end groups. Formal triple bonded regions are shown in blue colour. Distances are in Å [Remya and Suresh 2015b].

Optimized geometry of the dimers of polyynes with five triple bonds (pentaynes) and different end groups are given in Figure 4.1. All the intermolecular interactions (including C···C interactions and interactions between the end groups) are shown using dotted lines in the figure along with their distances. All these interactions are identified by the presence of a bond critical point (BCP) in the QTAIM analysis, which will be revealed in the next section. Most of these C···C interactions, except those towards the edges, are interactions between carbon atoms in similar chemical environments, similar to those described in Part B of Chapter 3 [Remya and Suresh 2015a]. From the C···C interaction lines shown in Figure 4.1, it can be seen that a formal CC triple bond towards the interior

region of the dimer (the shorter CC bond in the distance range 1.21 – 1.24 Å shown in blue colour) shows two C···C interaction to a formal CC single bond (the longer CC bond in the distance range 1.32 – 1.34 Å). In some of the polyyne dimers, (those with H, F and CN at one end and H at the other), C···C interaction is the only type of intermolecular interaction observed. In the dimers of polyynes with CF_3, NO_2 and NMe_2, as end groups, interactions between the end groups are also observed along with C···C interactions. However, while the number of end group interactions remains the same in all the analogues in a series of polyynes, the C···C interactions increases in number with increase in length of the interacting monomers. The range of C···C interaction distances in these dimes is between 3.26 – 3.56 Å with most of them being around 3.40 Å, which is the typical range of values observed for the C···C interaction between carbon atoms in similar chemical environments described in Chapter3, Part B [Remya and Suresh 2015a].

Table 4.1 Counterpoise corrected interaction energy (E_{int}, in kcal/mol) of the dimers of oligoynes with different chain lengths and end groups.

# C≡C	H/H	H/F	H/CF_3	H/CN	H/NO_2	H/NMe_2	CN/NMe_2
1	-1.1	-1.1	-2.6	-3.2	-4.0	-4.8	-11.7
2	-1.0	-2.1	-3.4	-4.0	-4.8	-7.7	-12.7
3	-1.9	-3.1	-4.1	-4.9	-5.8	-8.5	-13.6
4	-2.7	-3.9	-5.2	-5.8	-6.8	-8.2	-14.5
5	-3.6	-4.8	-6.0	-6.7	-7.7	-8.9	-15.0

In pentayne_CN and petayne_NO_2, the C···C distances are the shortest at the edges and show a clear increase towards the central part. In the case of pentayne_F, though a clear variation is not visible, C···C distances are shortest at the edges. On the other hand, the intermolecular C···C distances are the largest at the edges and tend to decrease towards the central part in pentayne_CF_3 dimer.

The counterpoise corrected interaction energy (E_{int}) of all the dimers with different end groups and having up to 5 triple bonds are given in Table 4.1. An increase in the magnitude of E_{int} with increase in number of triple bonds is clearly observed in all the cases. Since the interactions between the end groups in all the analogues are nearly the same, an increase in the magnitude of E_{int} with increase in polyyne chain length can only be attributed to the increased number of C···C interactions. Hence it is clear that the C···C

interactions play an significant role in the intermolecular interactions in longer polyyne derivatives. The highest magnitude of E_{int} among dimers with only C···C interactions as intermolecular interactions is shown by pentayne_CN as can be seen from Table 4.1. Dimers of oligoyynes with NMe_2 at one end and CN at the other end possess considerably higher value for E_{int} compared to those with NMe_2 or CN at one end and H at the other.

Table 4.2 Counterpoise corrected Interaction energy (E_{int}, in kcal/mol) of acetylene and pentayne derivatives obtained using B97D and B3LYPD2 density functionals.

	Acetylene derivatives		Pentayne derivatives	
End groups	B97D	B3LYPD2	B97D	B3LYPD2
H/H	-1.2	-1.4	-3.3	-3.3
H/F	-1.1	-1.4	-4.4	-4.9
H/CF_3	-2.4	-2.8	-5.7	-6.1
H/CN	-3.1	-3.3	-6.5	-6.7
H/NO_2	-4.0	-4.9	-7.8	-8.4
H/NMe_2	-4.5	-4.6	-10.7	-8.9
CN/NMe_2	-11.0	-11.9	-14.8	-15.0

The interaction energies of polyyne dimers with one and five triple bonds and different end groups calculated using B97D and B3LYPD2 methods are compared in Table 4.2. Comparing Table 4.1 and Table 4.2, it is clear that the trends in interaction energies given by these two density functionals are similar to those given by the M06L functional. All the three DFT methods show an increase in the value of E_{int} with increase in chain length from 2 to 10 carbon atoms. The effect of end groups on E_{int} values is also found to be similar in all the three cases. That is, the dimers of un-substituted polyynes (acetylene and pentayne) show the lowest values of interaction energy and the dimers of polyynes with CN at one end and NMe_2 at the other end show the highest values.

4.4.2 QTAIM Analysis of Intermolecular Bond Critical Points

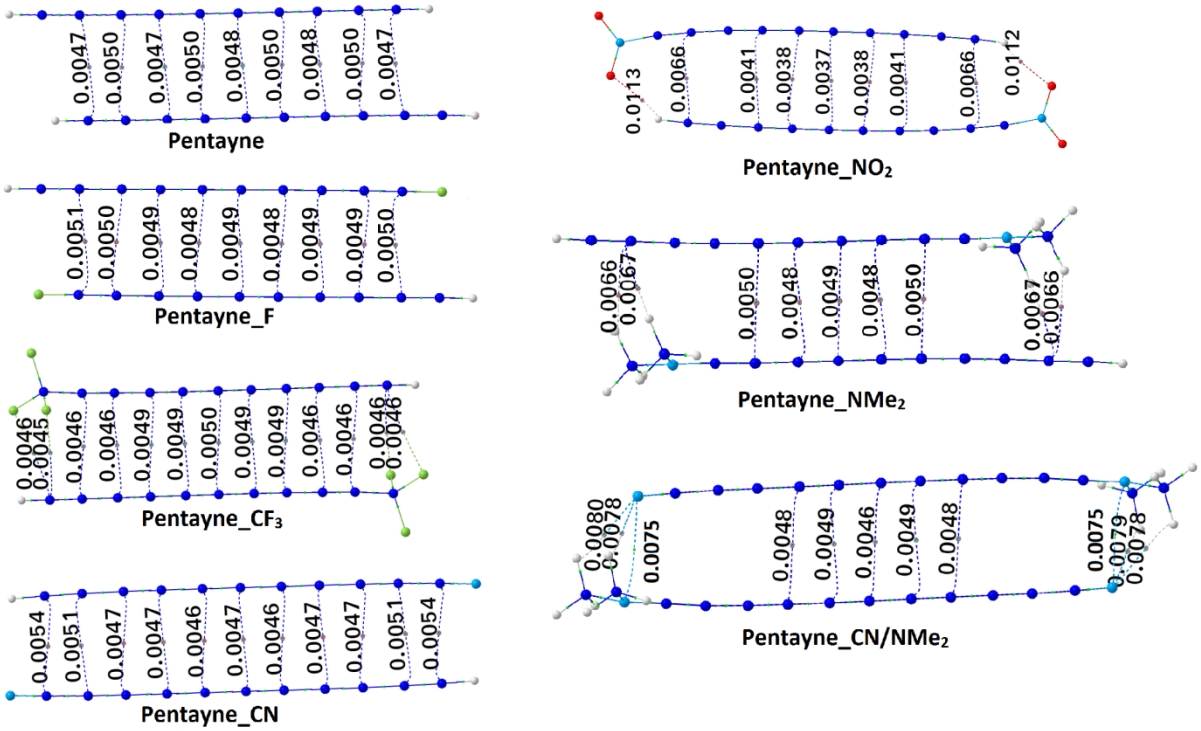

Figure 4.2 QTAIM plot of pentayne dimers with different end groups. Values of electron density (ρ) at intermolecular BCP's are given in the figures in au [Remya and Suresh 2015b].

The C···C interactions in all the polyyne dimers are marked by bond critical points (BCPs) in QTAIM analysis. Figure 4.2 portrays the QTAIM molecular graphs of pentaynes with different end groups. The values in au of electron density (ρ) at intermolecular BCPs are also given in Figure 4.2. The values of ρ at BCPs corresponding to intermolecular C···C interactions in these dimers (0.0037 – 0.0066 au) are within the range of values observed for C···C interaction between similar carbon atoms [Remya and Suresh 2015a] and other interactions such as 'carbon bonds' [Mani and Arunan 2013] and weak hydrogen bonds [Parthasarathi *et al.* 2006]. The values of ρ at intermolecular BCPs give an idea about the trend in intermolecular bond strengths in each dimer. In pentayne_CN, pentayne_NO_2 and pentayne_F, the strongest interactions towards the edges is indicated by the highest values of ρ at those points. In dimers with CN and NO_2 end groups, due to the stronger end group interactions, the interacting monomers are a little bent inwards at the edges. Moreover, there will be a larger difference in the electron density

between the interacting carbon atoms towards the edges due to the presence of electron withdrawing end groups and hence the C···C interactions here become more of 'donor-acceptor' type than interaction between carbon atoms in similar chemical environments, and hence become stronger. This is the reason for the curved geometry of these dimers where the C···C interactions are the shortest towards the edge of the dimers. At the same time, in pentayne_CF_3, the ρ values are the highest towards the interior, where the shortest C···C bonds are observed.

4.4.3 Analysis of Molecular Electrostatic Potential

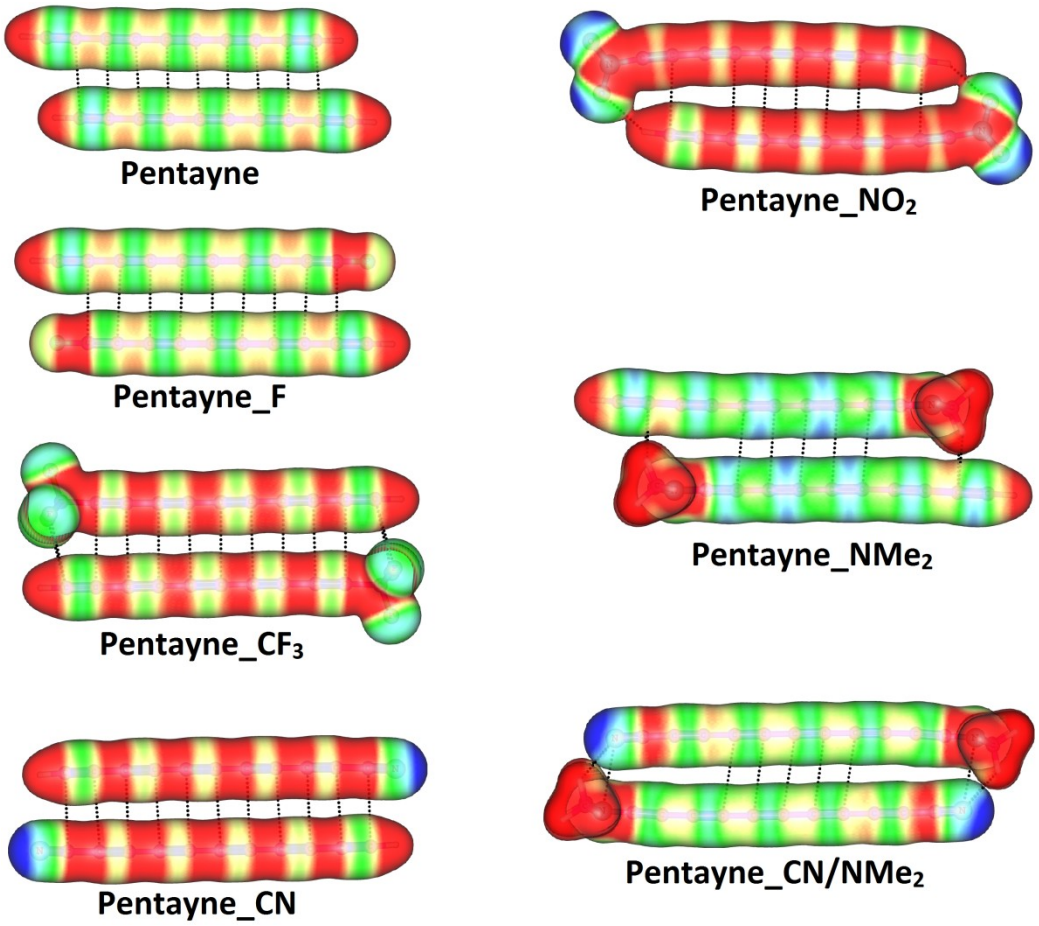

Figure 4.3 Map of molecular electrostatic potential at 0.01 au isodensity surface of pentayne dimers with different end groups. Potential range: -0.03 to +0.05 au from blue to red [Remya and Suresh 2015b].

The formation of X···X interactions (X = C, N and O) between atoms in similar chemical environments in Chapter 3, Part B is explained as resulting from complementary electrostatic interaction between electron rich and electron deficient regions of two interacting monomers [Remya and Suresh 2015a]. In polyynes, the

monomers are partitioned into relatively electron rich and electron deficient regions due to the presence of alternate single and triple bonds. The consequence of this partitioning is intermolecular complementary electrostatic interactions between electron rich regions on one monomer with relatively electron deficient regions on the second resulting in C···C interactions. Figure 4.3 gives an illustration of the complementary electrostatic interactions in the dimers of pentaynes with different end groups using the MESP maps (mapped at 0.01 au isodensity surface). As is clear from the MESP features, the interacting carbon atoms in these dimers are of similar chemical nature. These maps show that the constituent monomers in each dimer are partitioned into alternating rich, poor electron density regions throughout the length of the molecules to varying degrees in molecules with different end groups. Thus end groups have a clear effect on the distribution of electron density throughout the length of a polyyne molecule.

The optimized geometries of the dimers given in Figure 4.1 show that the triple bond of one monomer is arranged close to the single bond of the second, resulting in slightly shifted orientation of the oligoyne part of one monomer with respect to the other. It is also obvious from the MESP maps that the entire complementary electrostatic regions in the dimers are contributing to the strength of the C···C interactions. It may be noted that the bond paths in QTAIM analysis show only the atoms giving major contribution towards the non-covalent bonding interactions whereas it cannot portray the whole interacting region [Foroutan-Nejad *et al.* 2014]. In pentayne_CN and pentayne_NO_2, higher strength of C···C interactions towards the edges can be attributed to larger difference in electrostatic potential between the interacting carbon atoms due to the presence of electron withdrawing groups.

4.4.4 Multiple Minima with Lesser C···C Interactions and Lower Interaction Energy

Due to the presence of a large number of alternating electron rich and electron deficient regions in polyyne molecules, any of the electron rich regions on a molecule can form complimentary electrostatic interaction with any of the electron deficient regions on a second one. This puts forward the possibility of multiple minima on the potential energy surface of a dimer with varying number of

C···C interactions. Among these structures, the global minimum could be the one with the largest number of C···C interactions. Tetrayne, pentayne_F and tetrayne_CN are selected for this study. These dimers possess only C···C interactions as inter-molecular interactions and hence are suitable for studying the effect of change in number of C···C interactions on total binding energy. Figure 4.4 shows the QTAIM plots and MESP maps (plotted at 0.01 au isosurface) of the five minima located for tetrayne_CN dimer. The figure also gives the E_{int} values and the values of ρ at intermolecular C···C BCPs of these configurations.

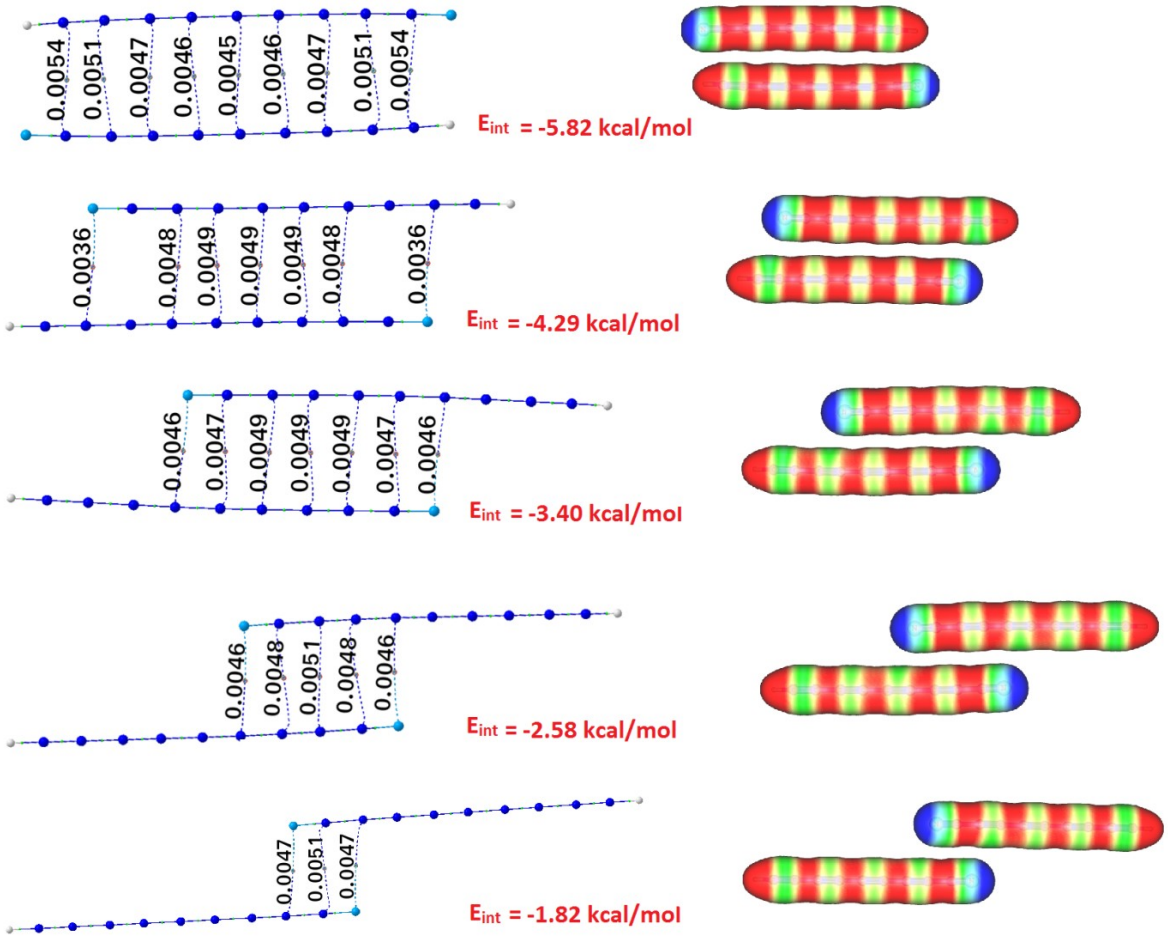

Figure 4.4 QTAIM plots of five different minima located by sliding one of the monomers in the tetrayne_CN dimer over the other. The values of electron density (ρ) at intermolecular BCPs are given in au. Molecular electrostatic potential mapped at the 0.01 au isosurface of each minimum is also given. Potential range: -0.03 to +0.05 au from blue to red [Remya and Suresh 2015b].

Figure 4.5 displays the QTAIM molecular graphs of the three minima located for tetrayne dimer and the five minima located for pentayne_F dimer. The

interaction energies and the values of ρ at C···C BCPs for all the structures are also shown in the figure. This analysis shows that several minima with difference in number of C···C interactions can be located by sliding one of the monomers over the other. The interaction energy of the structures thus obtained decreases with decrease in the number of C···C interactions. Clearly, the one with the largest number of C···C interactions is the most stable, as indicated by the E_{int} values. It is clear from Figure 4.4 - 4.5 that in all the three cases studied, decrease in number of C···C interactions results in a clear decrease in the value of E_{int}. This also shows that the C···C interactions play an important role in the stabilization of polyynes clusters. Alternating electron rich and electron deficient regions create attractive Columbic interactions throughout the length of the polyyne molecules resulting in a large number of stabilizing C···C interactions in the cluster.

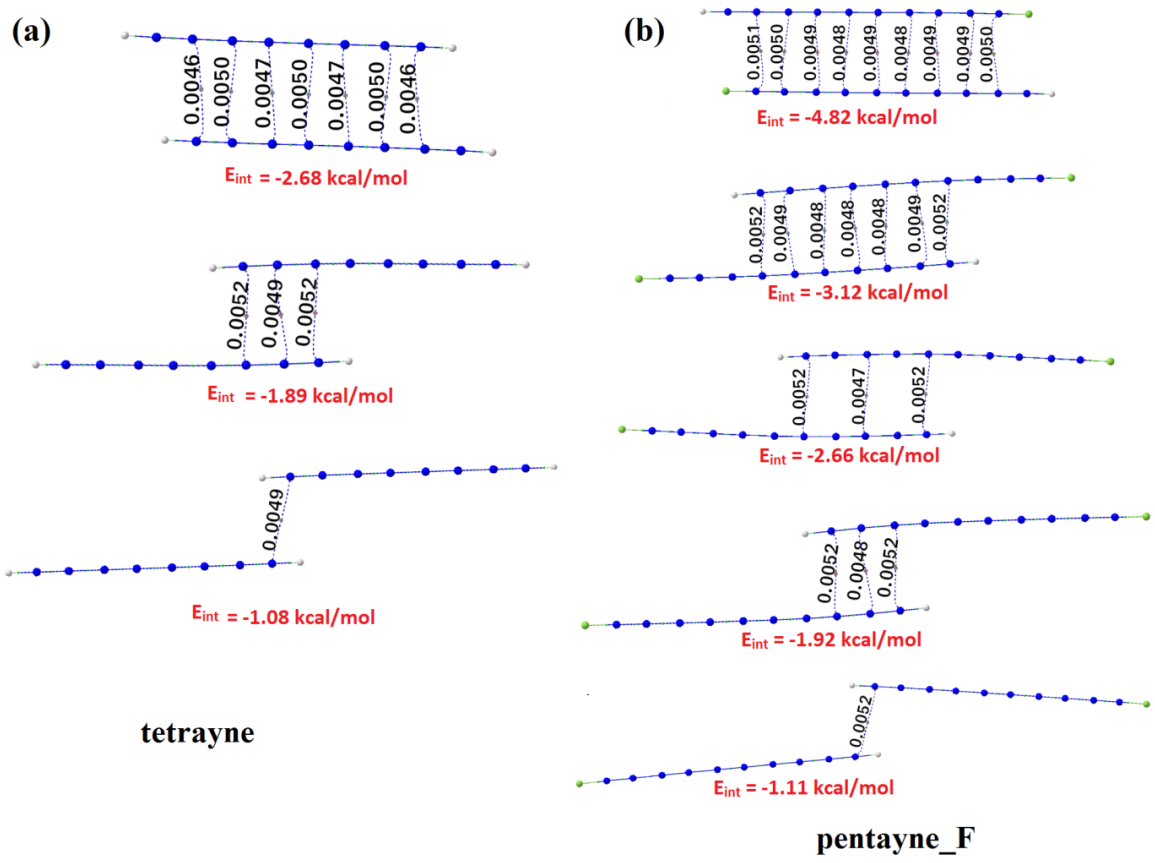

Figure 4.5 QTAIM plots of (a) the three minima of tetrayne dimer and (b) the five minima of pentayne_F dimer located by sliding one of the monomers over the other. The values in au of electron density (ρ) at intermolecular BCPs are also given.

4.4.5 Study of Longer Polyynes Containing up to 100 Carbon Atoms

The possibility of extrapolating the intermolecular bonding features to larger polyynes and finally to the allotrope carbyne is tested by systematically increasing the chain length of the polyynes up to 100 carbon atoms (50 triple bonds). The E_{int} values of the dimers of these larger polyynes with different end groups are given in Table 4.3. The values of E_{int} show a clear increase with increase in chain length in all the series of dimers possessing different end groups. The E_{int} value increases from -1.07 kcal/mol to -45.83 kcal/mol with increases in the number of carbon atoms from 2 to 100 (acetylene dimer to 50yne dimer). The effect of end groups on the values of E_{int} also persists up to 100 carbon atoms. E_{int} values of dimers with substitutions other than hydrogen are higher than those with hydrogen at both ends. The series of polyyne dimers with CN as one end group and NMe_2 as the second possess the highest value for E_{int}.

Table 4.3 Counterpoise corrected interaction energy (E_{int}, in kcal/mol) of the dimers of polyynes with different chain lengths and end groups.

# C≡C	H/H	H/F	H/CF_3	H/CN	H/NO_2	H/NMe_2	CN/NMe_2
10	-8.3	-9.4	-10.4	-11.4	-12.4	-13.5	-20.2
15	-13.0	-14.0	-15.3	-16.1	-17.0	-18.2	-25.2
20	-17.7	-18.7	-20.0	-20.9	-21.8	-23.0	-30.1
30	-22.5	-27.7	-29.5	-30.3	-31.2	-32.4	-39.9
40	-37.2	-37.5	-38.6	-39.5	-40.6	-41.4	-49.2
50	-45.8	-45.7	-48.2	-49.0	-49.9	-51.1	-58.6

Figure 4.6 displays the MESP maps of 50ynes with different end groups plotted at 0.01 au isodensity surface. In all the dimers, the electron rich region in one monomer is arranged near to the electron deficient region of the second facilitating intermolecular complimentary electrostatic interactions. The effect of end groups on relative electron density of electron rich and electron deficient regions on polyyne molecules (and hence on the strength of C···C interactions) can persists up to large chain lengths, which is evident from the E_{int} values of dimers with various end group substitutions. This can be clearly visualized from the MESP maps given in Figure 4.6 where a stronger electron withdrawing end group causes a

larger difference in electron density between the alternating electron rich and electron deficient regions on a polyyne molecule.

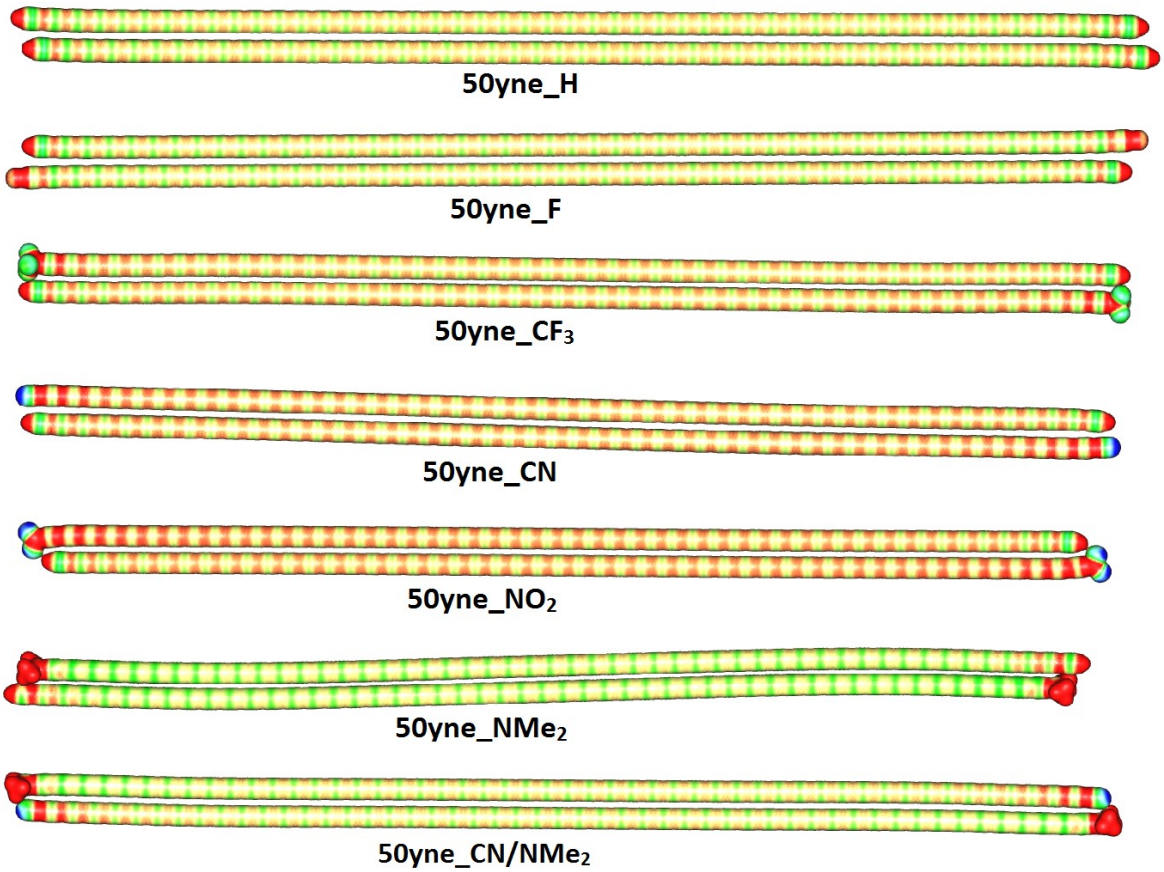

Figure 4.6 Map of molecular electrostatic potential at 0.01 au isodensity surface of 50yne dimers with different end groups. Potential range: -0.03 to +0.05 au from blue to red [Remya and Suresh 2015b].

4.4.6 Effect of Monomer Dipole Moment on the Interaction Energy of Dimers

It is already seen that the E_{int} values of the polyyne dimers increase with increase in the monomer chain length. The E_{int} values are also influenced by the nature of end groups. A physical property that increases with increase in the length and is affected by the nature of the substituents in a molecule is the dipole moment. The variation of E_{int} values of polyyne dimers with monomers dipole moments (μ) is shown in Figure 4.7. The figure shows a clear increase in E_{int} with increase in the value of μ. This trend is followed by all the series of polyynes except the un-substituted ones with H atoms at both ends, where the monomer dipole moment is zero. This observation is in accordance with the supposition that the intermolecular C···C interactions are caused by complimentary electrostatic

interactions between the electron rich and electron deficient portions of the interacting molecules since an increase in overall dipole moment can enhance the local dipoles throughout the length of a monomer and hence the strength of the C···C interactions. Thus, the series of polyyne analogues with highest values of monomer dipole moment shows the largest E_{int} values. Thus, the highest E_{int} values of dimers of oligoyynes substituted with CN at one end and NMe_2 at the other has been explained.

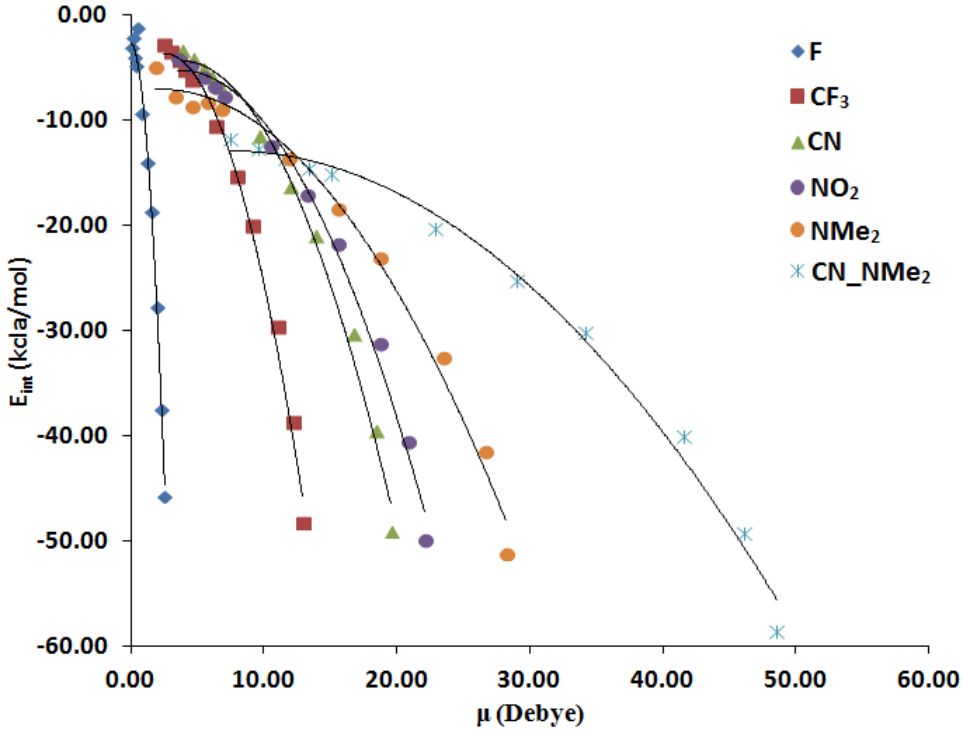

Figure 4.7 Variation of E_{int} of the dimers of polyynes having different end groups with the dipole moment of the interacting monomers (μ) [Remya and Suresh 2015b].

4.4.7 Study of Polyyne Tetramers

The presence of a large number of electron rich and electron deficient regions on the polyyne molecules as well as their cylindrical symmetry imply that more than one molecule can be self-assembled around a monomer forming molecular complexes provided that the intermolecular C···C interactions retain their strength in larger complexes. This hypothesis is tested by studying the tetramer clusters of pentayne, pentayne_F, 10yne and 10yne_F. Optimized geometries of these clusters are given in Figure 4.8. Table 4.4 lists the values of E_{int} and interaction energy per monomer (E_m) of the tetramers and the E_m values of the corresponding dimers. E_{int} values of all these tetramers showed a severe increase

(more than 5 times in all the cases) compared to the corresponding dimers. For instance, the E_{int} value of dimer of pentayne is 3.6 kcal/mol while that of its tetramer is 20.0 kcal/mol. This clearly implies a strong cooperativity in C···C interactions in higher order clusters, which may drive the system to form self-assembled molecular wire like materials.

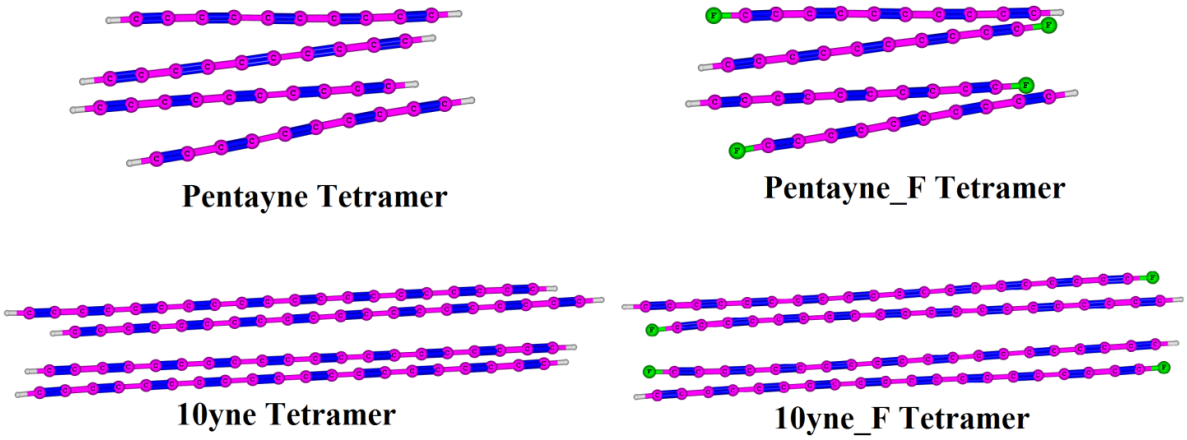

Figure 4.8 Optimized geometries of the tetramers of pentayne, pentayne_F, 10yne and 10yne_F [Remya and Suresh 2015b].

Table 4.4 E_{int} and E_m values of the tetramers and E_m values of the corresponding dimers (all values in kcal/mol).

Tetramer of	E_{int}	E_m	E_m of Dimer
5yne	-20.0	-5.0	-1.8
5yne_F	-24.4	-6.1	-2.4
10yne	-47.0	-11.8	-4.2
10yne_F	-52.1	-13.0	-4.7

Figure 4.9 - 4.10 give the QTAIM molecular graphs of the tetramers. These figures show a large number of intermolecular C···C interactions in the tetramers, which could be the reason for the large increase in E_{int} values on going from dimer to tetramer. Since each of the molecules in a tetramer can form interactions with two adjacent molecules, one would expect four sets of C···C interactions. However, including the interactions between the monomers in diagonal positions, five sets of interactions are shown in the QTAIM analysis. A notable fact is that even in the presence of multiple C···C interactions from the same carbon atom, the strength of individual C···C interactions is not diminished, which can be attributed to the large cooperativity in intermolecular interactions.

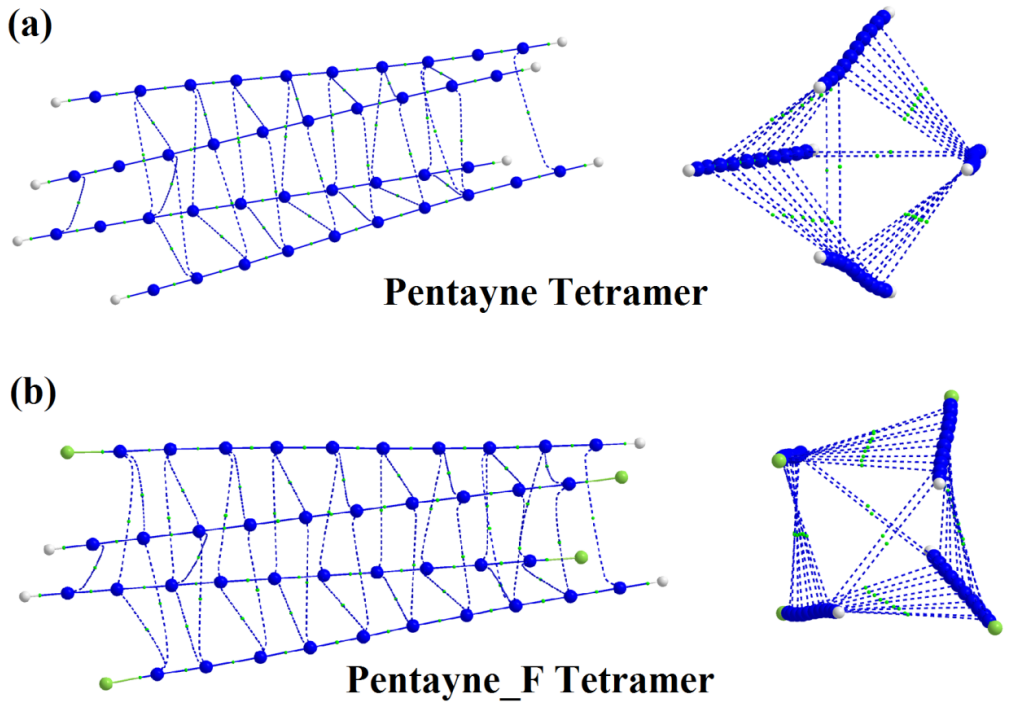

Figure 4.9 Two different views of the QTAIM plots of the tetramers of (a) Pentayne and (b) Pentayne _F [Remya and Suresh 2015b].

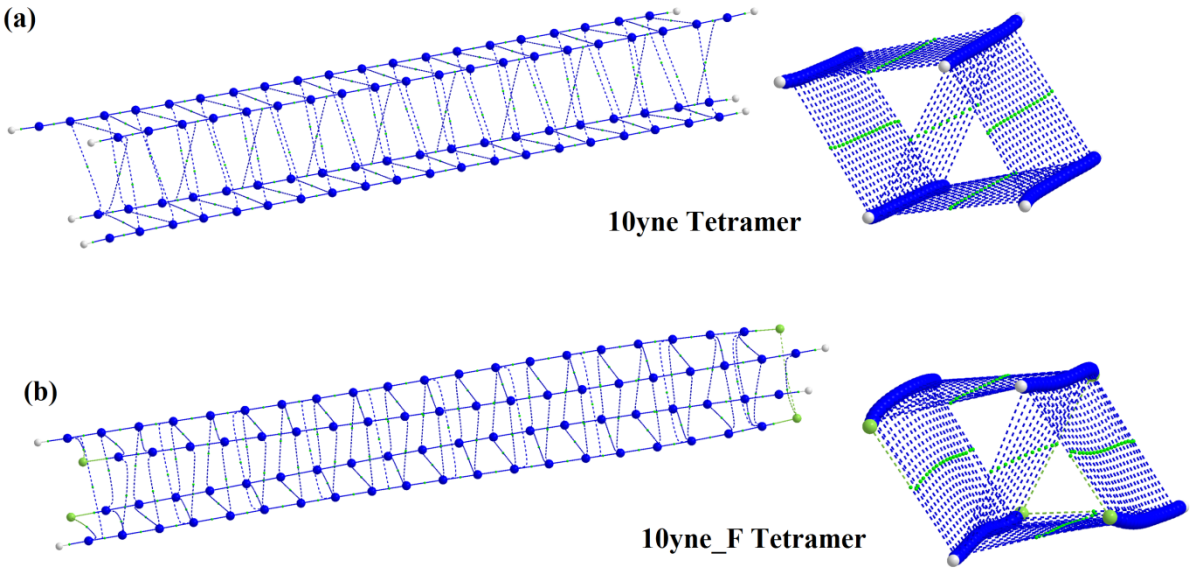

Figure 4.10 Two different views of the QTAIM plots of (a) 10yne tetramer and (b) 10yne_F tetramer [Remya and Suresh 2015b].

Part B: Geometry, Aromaticity and Intermolecular C···C Interactions in C_{4N+2} and C_{4N} Carbon Rings

4.5 Introduction

Different types of carbon clusters are formed as a result of laser vaporization of graphite [Hunter *et al.* 1993a]. The carbon clusters exist as linear chains, rings, bowls, plates and cages depending on their size [Hutter *et al.* 1994; Jones 1999; Tongay *et al.* 2005; Van Orden and Saykally 1998; von Helden *et al.* 1993]. Linear chains are formed at very small sizes such as C_2 and C_3. At slightly larger sizes, rings are formed. These carbon rings exist in the size range of approximately C_6 – C_{30}, which show slight variation with the experimental conditions as well as the theoretical methods used for the study. At even higher sizes, the rings tend to be converted into plates and cages, where the high energy sp hybridized form of carbon atoms start converting into sp2 hybridized forms. Finally, these structures rearrange to form fullerenes, the mechanism of which has been studied extensively [Goroff 1996; Hunter *et al.* 1994; Irle *et al.* 2006; Lin *et al.* 2005; Rama *et al.* 2001; Schwarz 1993; von Helden *et al.* 1991]. Among the non-spheroidal forms, relatively stable are the ring structures. Compared to other configurations, the monocyclic rings are relatively more stable Among the ring structures [Jones and Seifert 1997].

The properties of planar monocyclic carbon rings have been comprehensively studied theoretically as well as experimentally. [Bylaska *et al.* 1998; Fernandéz-Lima *et al.* 2007; Giesen *et al.* 1994; Gotts *et al.* 1995; Hunter *et al.* 1993b; Hutter *et al.* 1994; Jones 1999; Jones and Seifert 1997; Raghavachari and Binkley 1987; Saito and Okamoto 1999; Schweigert *et al.* 1995; Shelimov *et al.* 1994; Tongay *et al.* 2004; Torelli and Mitas 2000; von Helden *et al.* 1994; von Helden *et al.* 1993; Wakabayashi *et al.* 1997] The carbon rings show different properties depending on whether the number of carbon atoms, n is odd, n = 4N or n = 4N+2 where N is an integer. Different mechanisms such as of aromaticity, second order Jahn-Teller distortions and Peierls instability effects explain the stabilization of the molecules of different structural types of carbon rings [Torelli and Mitas 2000]. Torelli and Mitas reported three different types of structures for the molecules with 4N+2 carbon atoms using quantum Monte Carlo methods *viz*. (i) rings with all bond lengths and bond angles equal (D_{nh} symmetry), (ii) rings with

alternating bond angles ($D_{n/2}h$ symmetry) or (iii) rings with alternating bond lengths ($D_{n/2}h$ symmetry) [Torelli and Mitas 2000]. Schleyer and co-workers in 1979 first introduced the concept of double aromaticity [Chandrasekhar *et al.* 1979]. There are two sets of conjugated π electron systems in carbon rings with 4N+2 carbon atoms *viz*. one in the plane of the molecule and one perpendicular to it. This suggests double aromaticity in cyclic C_{4N+2} molecules. Different theoretical studies have revealed that, at smaller sizes, carbon rings with 4N+2 and 4N carbon atoms show double aromaticity and double antiaromaticity respectively [Bylaska *et al.* 2000; Wodrich *et al.* 2007; Xu *et al.* 2006]. Fowler *et al* have very well illustrated the diatropic and paratropic ring currents in both the delocalized π electron systems of C_{4N+2} and C_{4N} molecules respectively [Fowler et al. 2009] using the maps of current density. At very large sizes, both C_{4N+2} and C_{4N} rings are expected to show non aromatic behaviour [Bylaska *et al.* 2000]. A C_{4N+2} ring is predicted to possess type (ii) structure (cumulenic with bond angle alternation) while a C_{4N} ring is expected to possess type (iii) structure (acetylenic with bond length alternation) [Bylaska *et al.* 2000; Bylaska *et al.* 1998; Fowler *et al.* 2009; Saito and Okamoto 1999; Sen *et al.* 2006; Torelli and Mitas 2000]. Both these types of structures possess a $D_{n/2h}$ symmetry.

In this study, the main focus is on the intermolecular interactions in planar monocyclic carbon rings. Inter-molecular C···C interactions between carbon atoms in similar chemical environments in dipolar organic molecules resulting from complimentary electrostatic interaction of electron rich region of one molecule with electron deficient region of another has been described in Part B of Chater 3 [Remya and Suresh 2015a]. This type of C···C interactions in polyyne molecules formed as a result of interactions of the electron rich formal triple bonds of one molecule with electron deficient formal single bond of another is described in Part A of this chapter [Remya and Suresh 2015b]. A multitude of such interactions between long chain polyyne molecules lead to significant stabilization of their dimers, approximately 1.00 kcal/mol for each C···C interactions. Intermolecular C···C interactions in polyyne dimers is schematically represented in Scheme 4.1. Both the interacting carbon atoms in a C···C interaction are shown to have both the donor and acceptor character using natural bond orbital (NBO) analysis (i.e., a $C_1 \cdots C_2$ interaction corresponds to a charge transfer from C_1 to C_2 and a similar

charge transfer from C_2 to C_1, where C_1 and C_2 are chemically almost identical). [Remya and Suresh 2015a]

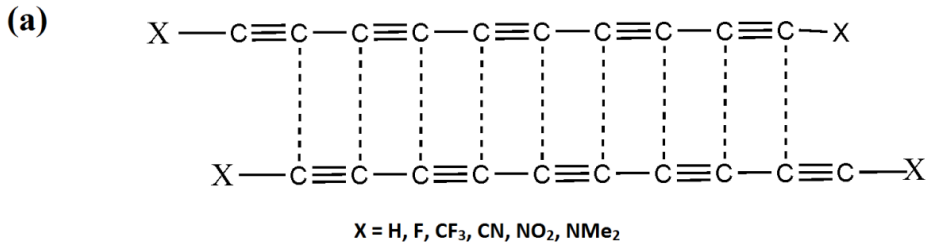

Scheme 4.1 Schematic representation of (a) Polyyne dimers showing intermolecular C···C interactions and examples for (b) a C_{4N} system (C_{16}) with acetylenic structure and (c) a C_{4N+2} systems (C_{18}) with cumulenic structure [Remya and Suresh 2016].

In polyynes, local differences in electron density result in C···C interactions between carbon atoms in to similar chemical environments. The end groups, which affected the electron distribution throughout the length of the polyyne molecules, had a strong influence on the strength of the C···C interactions [Remya and Suresh 2015b]. In the case of C_n rings, varying the intermolecular interaction strengths by changing the substitutions cannot be done since such manipulations are not possible for them. The only choice is to vary the electronic configuration of the ring structure. Similar to the polyyne systems, the C_{4N} rings possess alternate electron rich and electron deficient regions as illustrated in Scheme 4.1, which would lead to intermolecular C···C interactions. On the other hand, all the CC bonds are alike due to aromatic π-electron delocalization in C_{4N+2} molecules and hence the chance of seeing several C···C interactions is fewer. For testing this hypothesis, dimers of C_n molecules are studied for n = 4N+2 and n = 4N, where N is a

natural number. First, the double aromatic/antiaromatic nature C_{4N+2}/ C_{4N} molecules is illustrated using their geometric, molecular electrostatic potential (MESP) and magnetic features for C_6 to C_{32} systems followed by a study of the intermolecular C···C interactions in them. Use of MESP features for the illustration of aromatic and antiaromatic character of planar carbon and intermolecular bonding behaviour in such molecules has not been reported in the literature.

4.6 Computational Methods

Planar monocyclic carbon rings (C_n) with n = 4N+2 and n = 4N are optimized for n varying from 6 to 32. Dimers of C_n molecules up to C_{28} are also optimized. The meta-GGA density functional M06L [Zhao and Truhlar 2006b] with the basis set 6-311++g(d,p) is used for optimizing all these systems. The results for non-covalently interacting systems produced by this model chemistry, revealed to be the best performer in the benchmark study described in Chapter 2, [Remya and Suresh 2013] are further confirmed using several other reliable DFT as well as *ab initio* methods [Mohan and Suresh 2014; Remya and Suresh 2014; Remya and Suresh 2015a; Remya and Suresh 2015b]. The optimized geometries of the rings and their dimers are confirmed to be minima by frequency calculation. All the calculations are performed using *Gaussian09* [Frisch *et al.* 2010] suit of programs. The interaction energy (E_{int}) of a dimer is calculated by subtracting twice the energy of an isolated monomer from the energy of the dimer. The interaction energies are corrected for basis set superposition error (BSSE) using Boys and Bernardi method [Boys and Bernardi 1970] as implemented in the *Gaussian09* software. The delocalized and localized nature of electrons in C_{4N+2} and C_{4N} are illustrated using the maps of MESP [Gadre and Shirsat 2000]. Also, the MESP features of the dimers are used for explaining the intermolecular interactions. MESP features have been used for understanding several phenomena in chemistry [Murray *et al.* 1994; Sjoberg and Politzer 1990] including different types of intermolecular interactions, which also includes our studies described in Part B of Chapter 3 and Part A of this chapter [Clark *et al.* 2007; Murray *et al.* ; Politzer *et al.* 2013; Remya and Suresh 2015a; Remya and Suresh 2015b]. The most negative value of MESP in a molecule is denoted as V_{min}. Information on the position and strength of electron rich regions such as lone pairs of molecules and their interactions with nucleophiles can be

obtained from the position and magnitude of V_{min} [Gadre *et al.* 1996; Gadre and Pundlik 1997; Kumar *et al.* 2014; Tomasi *et al.* 1996]. In this study the position and magnitude of V_{min} is considered as indicators of localization/delocalization nature of π electrons in the carbon rings. The intermolecular interactions are identified as bond critical points in QTAIM analysis as implemented in AIMAll software package [Keith 2014]. The value of electron density, ρ at a BCP is usually taken as a measure of the strength of such bonding interactions. The aromatic/antiaromatic nature of the C_n systems are analyzed with the help of nucleus-independent chemical shift (NICS) [Schleyer *et al.* 1996], which is the absolute magnetic shielding of the induced ring currents at the centre of the rings. Negative value for NICS indicates aromaticity and positive value indicates antiaromaticity. The chemical shift values calculated at the centre of a ring is given the notation NICS(0). Since NICS(0) can be contaminated by shielding contributions from the core as well as σ electrons, NICS(1) [Schleyer *et al.* 1997], which is calculated 1 Å above the plane of the ring, are also considered. At 1 Å above the plane of the ring, the effect of σ electrons is reduced and the π system is maximized [Foroutan-Nejad *et al.* 2010].

4.7 Results and Discussion

4.7.1 Geometry of the Carbon Rings

All C_{4N+2} molecules show a cumulenic structure in which all the bond lengths are equal. On the other hand, the C_{4N} molecules show acetylenic structure with clear bond length alternation which shows alternate shorter (formal triple) and longer (formal single) bonds. The cumulenic structure of C_{4N+2} systems indicates delocalized π-electron distribution and aromatic stabilization in them. The variation of average of all the CC bond lengths in C_{4N+2} and C_{4N} (both shorter and longer bond lengths) molecules with n varying from 6 to 30 is represented in Figure 4.11.

All the CC bonds in C_{4N+2} rings and the single and triple bonds in C_{4N} rings first decrease with size and them becomes almost constant. The largest CC bond length among C_{4N+2} rings (1.33 Å) is observed in the smallest ring, viz. C_6, which is decreased to 1.29 Å in C_{10} and is almost constant (around 1.28 Å) in all the larger rings. The bond length alternation with localized triple bonds shown by C_{4N} molecules is a characteristic feature

of antiaromatic molecules [Schleyer *et al.* 1996]. In C_8 to C_{32}, the shorter (triple) bonds vary from 1.27 to 1.24 Å and the longer (single) bond lengths vary in the range 1.39 to 1.32 Å as given in Figure 4.11.

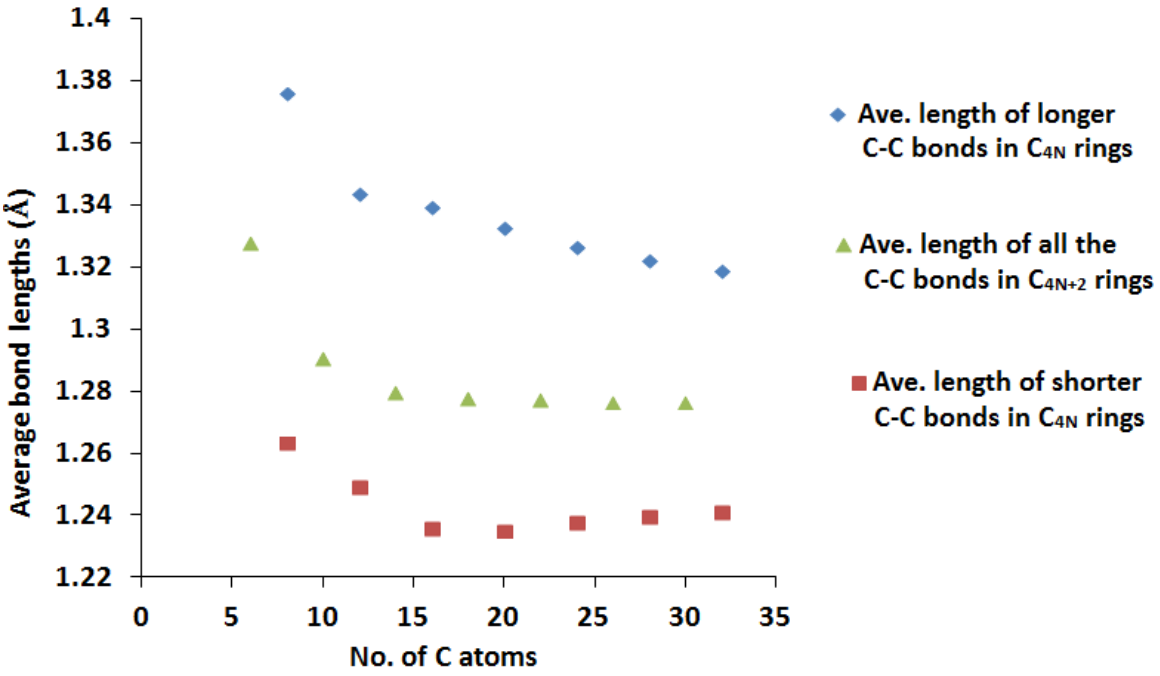

Figure 4.11 Average bond lengths of the planar carbon rings (C_n). C_{4N+2} molecules show equal lengths for all the C-C bonds indicating delocalization. At the same time, C_{4N} molecules show alternating long and short bonds [Remya and Suresh 2016].

The bond angles are found to depend only on the size of the C_n rings and not on their aromatic/antiaromatic nature. All the C_n molecules show bond angle alternation to some extent. With increase in ring size, the difference between two adjacent bond angels decreases. The adjacent bond angles in the rings possess almost the similar value in larger rings. Thus, the two bond angles seen in the smallest ring (C_6) are 154° and 86° while in the largest ring (C_{32}), the adjacent bond angles show only a small variation between 168° and 170°. In every C_{4N+2} and C_{4N} systems, two symmetrically unequal sets of carbon atoms can be identified, which will be referred to as C_α and C_β in this study. Compared to C_β, the C_α atoms possess larger CCC angles centred on them and at larger sizes, the symmetrical inequality to distinguish C_α and C_β decreases. Thus, there is a tendency for bond angle equalization in both C_{4N+2} and C_{4N} rings. Hence at very large sizes, C_{4N+2} molecules will have all the carbon-atoms, angles and bonds identical while in C_{4N} rings, the

carbon-atoms and the bond angles tend to be equal while the bonds remain as alternate longer and shorter bonds.

4.7.2 Analysis of Molecular Electrostatic Potential

Figure 4.12 displays the MESP mapped on to 0.01 au electron density surface and MESP isosurface of -0.00075 au for the C_{4N+2} molecules. The V_{min} values of all the C_n rings are given in Table 4.5. From the MESP features given in Figure 4.12, it is clear that the C_β atoms in C_6 are more electron rich compared to the C_α atoms. The C_6 molecule possesses the highest magnitude for MESP minimum (V_{min} = -12.14 kcal/mol) and is located on the C_β atoms. This shows some amount of divalent carbene type character to these atoms due to underutilization of its electrons for π-conjugation. The inter-atomic distance between C_α carbon atoms (1.809 Å) in C_6 is indicative of weak interactions between them. The electron deficient nature of these carbon atoms could be attributed to the utilization of their electrons for those interactions.

In C_{10}, the V_{min} value of the electron rich C_β atoms is -3.53 kcal/mol, which is 8.63 kcal/mol less negative than C_6, showing increased delocalization of the π-electrons in this molecule. In C_{14}, a near perfect π-electron delocalization, which is a characteristic feature of aromatic systems, is suggested by the smaller bond angle alternation at C_α and C_β atoms (about 10^0) compared to C_6 (about 68^0) and C_{10} (about 38^0). Unlike C_6 and C_{10}, the MESP isosurface map does not show significant electron localization in the molecular plane of C_{14}. Instead, negative-valued MESP appears above and below the ring plane in C_{14}, which is a characteristic identified as typical of a π-electron cloud well-known in the case of benzene. Also, C_{14} shows the lowest magnitude for V_{min} among all the molecules, indicating highly delocalized nature of π electrons. Beyond C_{14}, all larger molecules of C_{4N+2} series show the π-electron cloud. However, unlike C_{14}, the higher members show the influence of the π-electron in the interior central regions of the rigs.

In the case of C_{4N} series, MESP features of C_8 and C_{12} show electron rich character of C_β compared to C_α (Figure 4.13). The V_{min} values of C_8 and C_{12} are -11.81 and -5.11 kcal/mol, respectively. In the case of C_{16} and other higher systems, the MESP map and isosurface show electron localization at the shorter CC bonds. The red-coloured regions in the maps of MESP indicate electron deficient longer

CC bonds. With increase in the ring size, the colour difference indicating relatively electron rich and electron deficient region decreases. Such an effect is more evident in C_{4N+2} systems than C_{4N} indicating more delocalized distribution of electrons in the former than the latter.

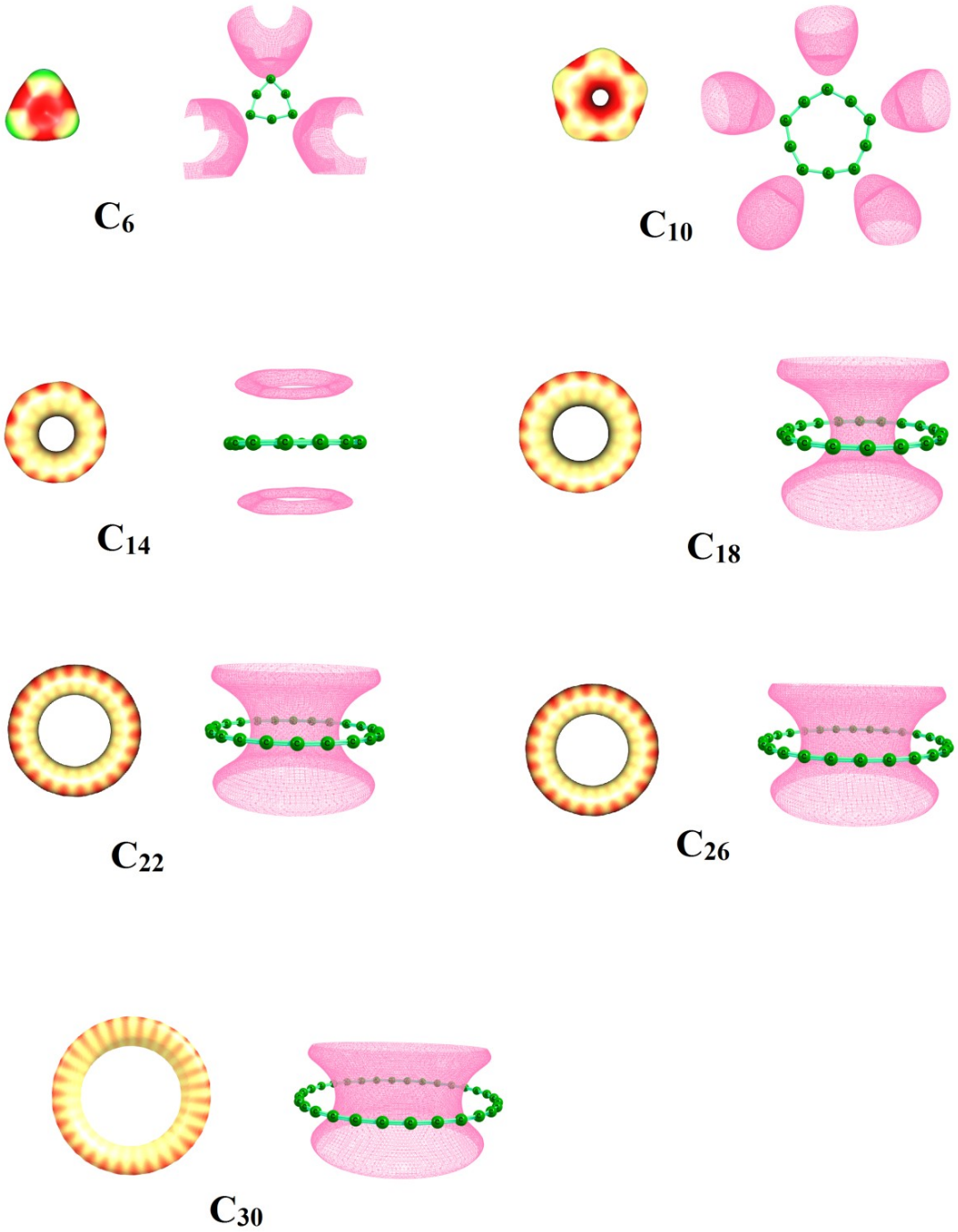

Figure 4.12 MESP mapped on to 0.01 au electron density isosurface (left) and MESP isosurface (pink-coloured) at -0.00075 au of C_{4N+2} molecules. Colour coding from blue to red indicates MESP values in the range -0.03 to 0.05 au [Remya and Suresh 2016].

Table 4.5 The values of lowest negative electrostatic potential (V_{min}, in kcal/mol) of C_{4N+2} and C_{4N} rings.

C_{4N+2}	V_{min}	C_{4N}	V_{min}
C_6	-12.14	C_8	-11.81
C_{10}	-3.53	C_{12}	-5.11
C_{14}	-0.54	C_{16}	-2.35
C_{18}	-1.29	C_{20}	-1.16
C_{22}	-1.39	C_{24}	-1.24
C_{26}	-1.30	C_{28}	-1.22
C_{30}	-1.17	C_{32}	-1.27

The MESP map also suggests that C_{4N} rings possess acetylenic carbyne structure while C_{4N+2} rings possess a cumulenic carbyne structure. The acetylenic character of the C_{4N} rigs can be related to the cylindrical distribution of π-electrons characterized by the MESP isosurface shaped like a 'ring' around the shorter CC bonds as seen in $C_{20} – C_{32}$.

4.7.3 Nucleus-Independent Chemical Shift (NICS)

Table 4.6 lists the NICS(0) and NICS(1) values of all the C_n rings. The aromatic behaviour of the C_{4N+2} rings are evident from their negative NICS values. The high magnitudes of NICS in these rings support double aromaticity, *viz*. one due to the conjugation of the π-electron that lie in the σ-plane and the other due to the conjugation of π-electrons orthogonal to this plane. To illustrate this point, the two delocalized π-molecular orbitals of a representative C_{4N+2} system *viz.* C_{18} is shown in Figure 4.14. The anti-aromatic character of C_{4N} rings is evident from their positive NICS(0) and NICS(1) values. The high positive values of NICS may indicate the possibility of double antiaromaticity in C_{4N} rings due to the two sets of conjugated 4N π-electrons *viz.* in the σ-plane and in the plane perpendicular to the σ-plane. The assumption of double antiaromatic nature of C_{4N} systems is supported by the localized nature of the two π-molecular orbitals of C_{16} given in Figure 4.14.

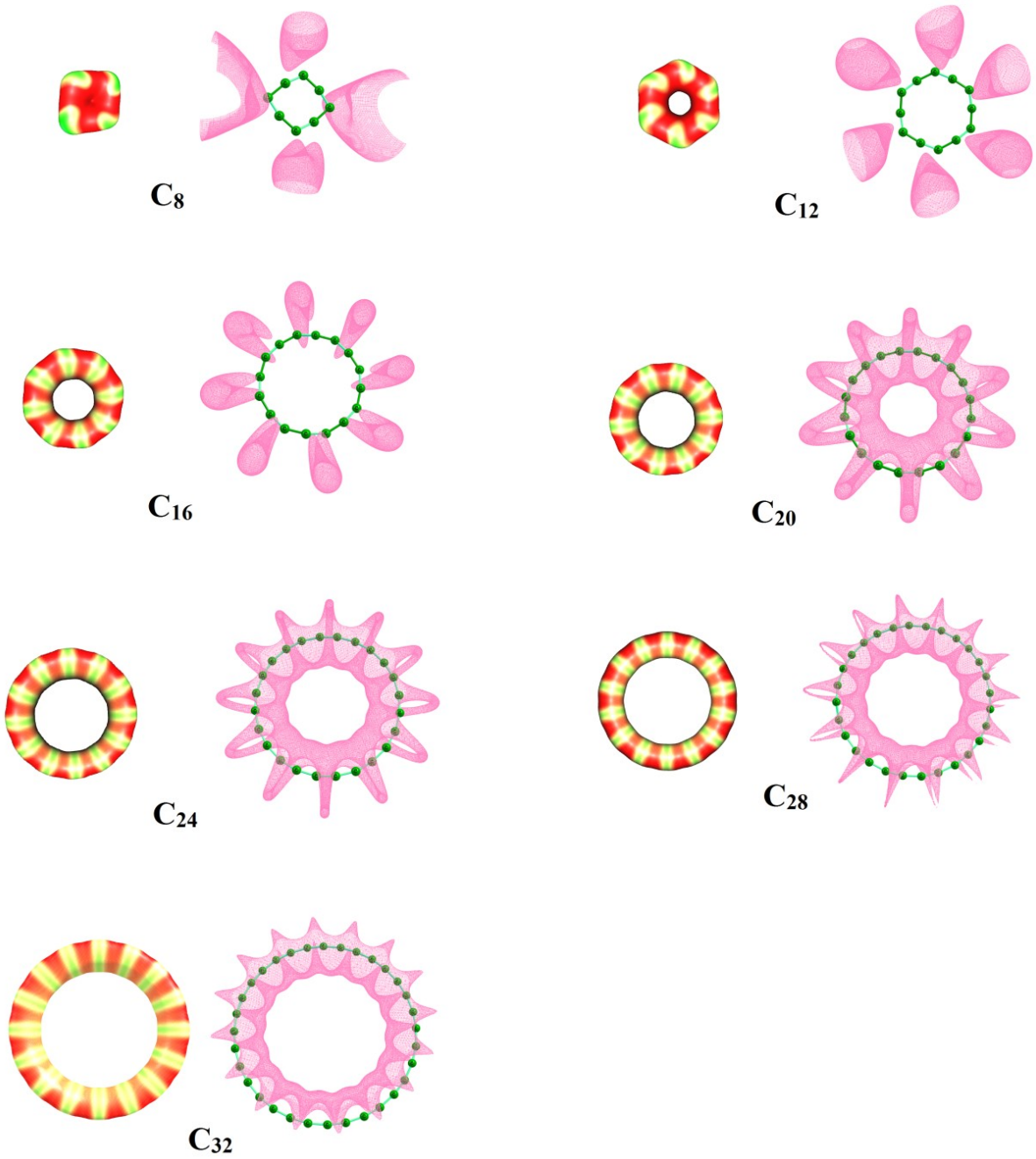

Figure 4.13 MESP mapped on to 0.01 au electron density isosurface (left) and MESP isosurface (pink-coloured) at -0.00075 au of C_{4N} molecules. Colour coding from blue to red indicates MESP values in the range -0.03 to 0.05 au [Remya and Suresh 2016].

The magnitude of NICS(0) of C_{4N+2} rings show a steady increases with the ring size from C_6 – C_{18} and then remains almost constant up to C_{30}. NICS(1) values also follow roughly the same trends. This data may suggest an enhancement in aromaticity of the C_{4N+2} rings with increase in its size up to C_{18} and not much variation afterwards. However, a confirmation of this feature is difficult as NICS is dependent on the ring size. Therefore,

we compare the NICS(0) value of C_6 (-22.64) with that of benzene (-9.7 [Schleyer *et al.* 1996]), which certainly suggests double aromatic character to the former. Both the NICS(0) and NICS(1) values are higher for C_{12} than for C_8 in the case of C_{4N} systems. After C_{12}, both the NICS values show a steady decrease with further increase in size. Although this may suggest increasing stabilization of larger rings, the size dependency of NICS should be taken into account to get the true effect. Hence, we compare the NICS(0) of C_8 (44.21) with that of similar sized ring system cyclooctatetraene (NICS(0) (30.1 [Schleyer *et al.* 1996]) and propose that the former has significant double antiaromatic character.

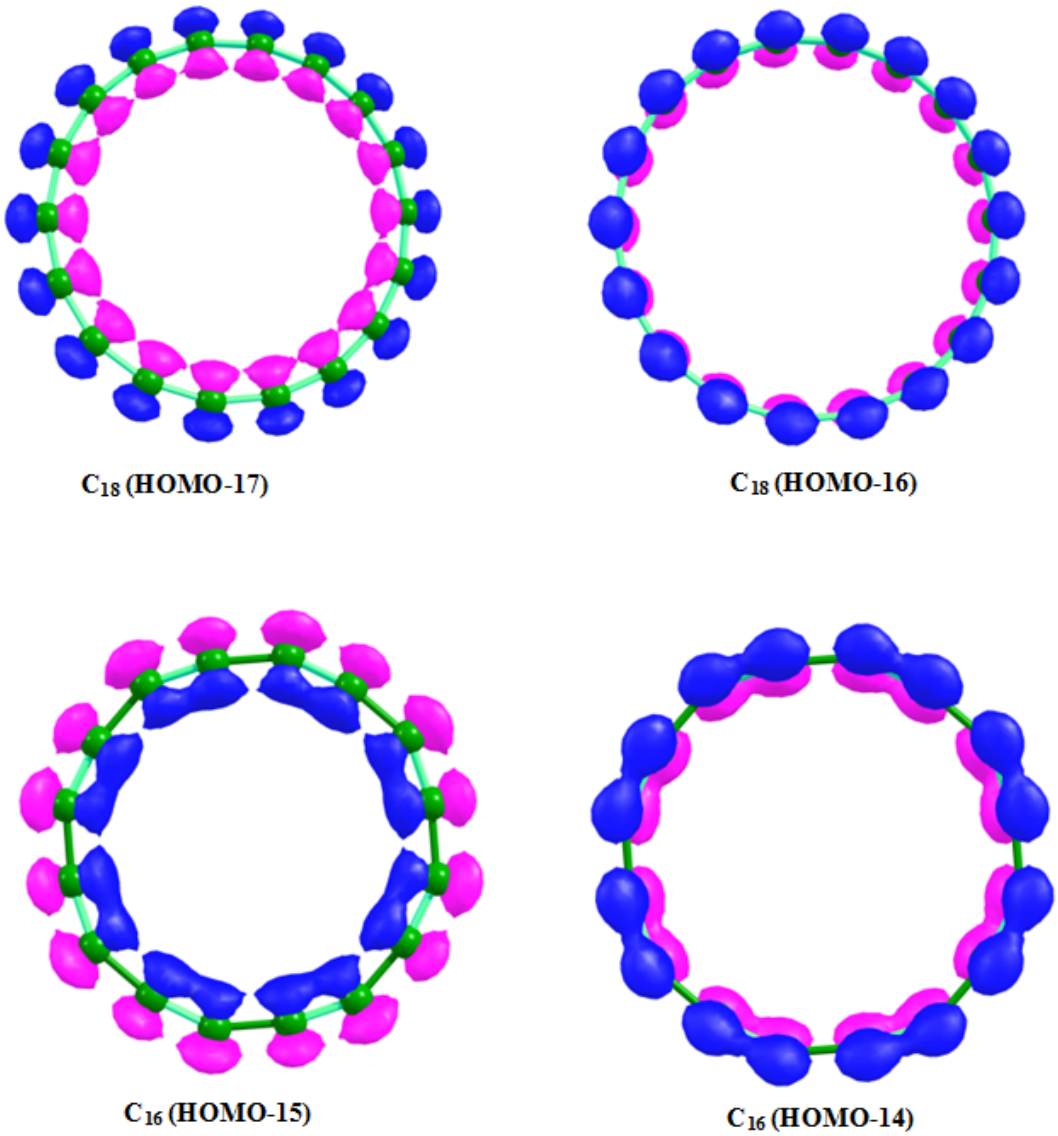

Figure 4.14 The delocalized π-molecular orbitals of a C_{4N+2} system (C_{18}) (HOMO-17 and HOMO-16) and the localized π-molecular orbitals of a C_{4N} system (C_{16}) (HOMO-15 and HOMO-14) [Remya and Suresh 2016].

Table 4.6 NICS values in ppm of the C_{4N+2} and C_{4N} rings.

C_{4N+2}	NICS(0)	NICS(1)	C_{4N}	NICS(0)	NICS(1)
C_6	-22.64	-9.30	C_8	44.21	36.39
C_{10}	-30.89	-22.82	C_{12}	54.69	45.42
C_{14}	-40.53	-34.10	C_{16}	50.31	44.10
C_{18}	-42.30	-37.94	C_{20}	43.47	39.83
C_{22}	-42.54	-39.52	C_{24}	37.49	35.25
C_{26}	-42.73	-40.51	C_{28}	32.14	30.71
C_{30}	-42.87	-41.18	C_{32}	28.26	27.29

4.7.4 Study of Intermolecular Interactions: Formation of Dimers

Dimers of C_{4N+2} and C_{4N} rings are studied for understanding the nature of intermolecular interactions in these molecules. The optimized geometries of C_n dimers containing 6 to 28 carbon atoms are given in Figure 4.15 along with their centre-to-centre distances and the nearest C···C distances. While a shifted-parallel stacked orientation of the monomers is observed in the case of C_{4N+2} dimers, C_{4N} dimers show a perfect stacking arrangement of the monomers. The dimers of C_{4N} systems can be described as a sandwich type configuration wherein the shorter CC bonds orient on top of the longer CC bonds.

Whereas the centre-to-centre distances and the nearest C···C distances are almost constant in C_{4N+2} dimers, the centre-to-centre distances show a slight decrease of 0.57 Å with increase in ring size from C_8 (2.77 Å) to C_{28} (3.34 Å) in the case of C_{4N} dimers. The centre-to-centre distances and nearest C···C distances possess similar values in the case of C_{4N} systems. The QTAIM plots of dimers of C_{4N+2} and C_{4N} molecules are shown in Figure 4.16. From the QTAIM plots, it is clear that in C_{4N} dimers, the monomers are connected together by a larger number of C···C interactions compared to C_{4N+2} dimers. Bond paths are shown by dotted lines in Figure 4.16 and each of these bond paths are characterized by a bond critical point at the midpoint region. Except for C_8, the number of C···C interactions in a C_{4N} dimer is equals to the number of carbon atoms in (4N) a monomer.

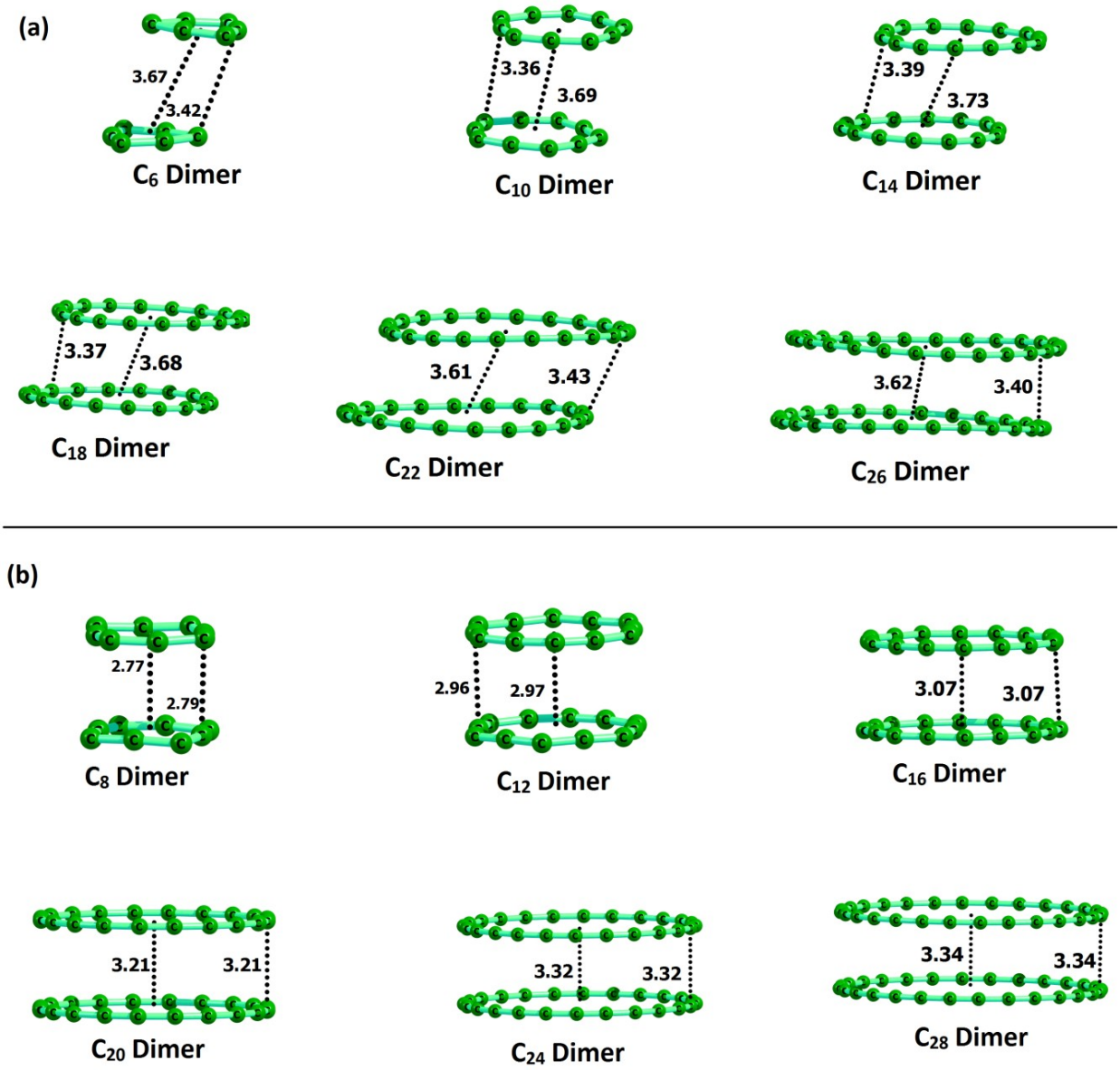

Figure 4.15 Optimized geometry of (a) C_{4N+2} dimers and (b) C_{4N} dimers. The centre-to-centre distances and the nearest C···C distances in the dimers are given in Å [Remya and Suresh 2016].

The difference in intermolecular bonding behaviour in the dimers of C_{4N} and C_{4N+2} rings can be explained with the help of their MESP maps given in Figure 4.17. As we have already shown, partitioning of the monomers into alternate electron rich and electron deficient regions is clearly observed in C_{4N} rings. When these molecules form dimers, the electron rich regions on one monomer align near to the electron deficient regions of the second. This type of an arrangement facilitates maximum complimentary electrostatic interactions leading to large number of intermolecular C···C interactions. On the other hand, partitioning of the

monomers into electron rich and electron deficient regions is not clearly distinguishable in the case of C_{4N+2} rings due to double aromaticity. This leads to fewer number of C···C interactions, lower interaction energy and lower tendency towards dimerization in them compared to the C_{4N} systems.

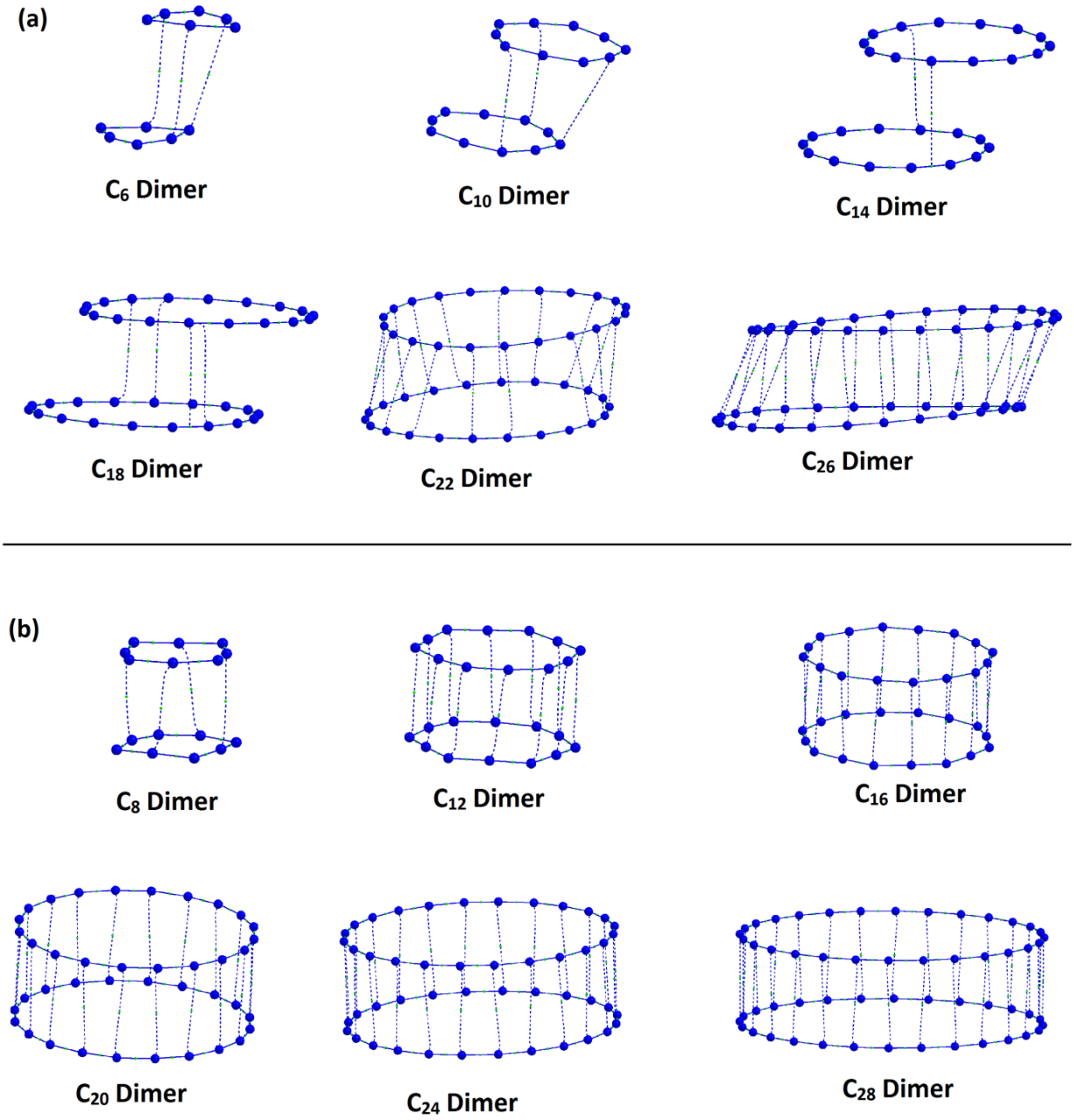

Figure 4.16 QTAIM plots of (a) C_{4N+2} dimers and (b) C_{4N} dimers. Dotted lines indicate bond paths for the C···C interactions [Remya and Suresh 2016].

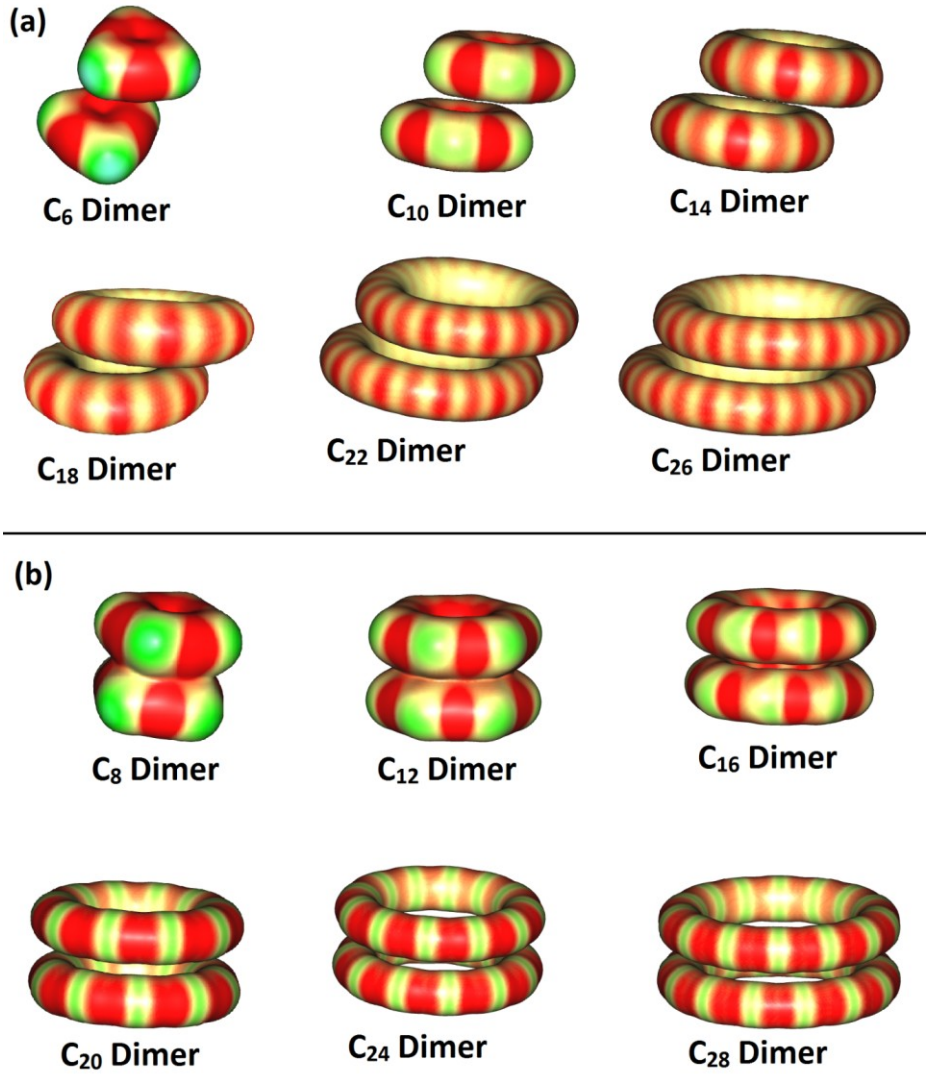

Figure 4.17 MESP mapped on to 0.01 au isosurface of dimers of (a) C_{4N+2} and (b) C_{4N}. Colour coding from blue to red indicates MESP values in the range -0.03 to 0.05 au [Remya and Suresh 2016].

The interaction energies (E_{int}) and average electron density at intermolecular bond critical points (ρ_{ave}) of each of the C_n dimers are given in Table 4.7. In the case of C_{4N+2} dimers, a steady increase in the magnitudes of E_{int} is observed from C_6 (-2.23 kcal/mol) to C_{26} (-11.77 kcal/mol). The ρ_{ave} values are almost similar in all the C_{4N+2} dimers (a small variation between 0.0049-0.0057 au) showing similar strength of intermolecular C···C interactions in all of them. On the other hand, in C_{4N} dimers, the highest magnitudes for E_{int} are shown by dimers of the smallest rings, *viz*. C_8 (-23.31 kcal/mol) and C_{12} (-21.80 kcal/mol). The magnitude of E_{int} shows a steady decrease from C_8 to C_{20} and then increases for C_{24} and C_{28}. This trend in the values of E_{int} is the outcome of a balance between the number of C···C interactions and the strength of individual C···C interactions.

The ρ_{ave} values indicate the strongest C···C interactions in C_8 (ρ_{ave} = 0.0179 au) and C_{12} (ρ_{ave} = 0.0113 au) dimers that can be attributed to the highest amount of charge separation in them, which is clear from their MESP features. In C_{4N} dimers, the ρ_{ave} values gradually decreases with increase in ring size from 0.0179 au in C_8 to 0.0056 au in C_{28}. The ρ_{ave} value of C_{24}, 0.0058 au is close to that of C_{28} and suggests that with further increase in ring size, the ρ_{ave} value may not undergo considerable changes. Since the number of C···C interactions is equal to 4N in C_{4N} dimers, an increase in the ring size beyond C_{28} is bound to increase the total interaction energy. The presence of a large number of intermolecular C···C interactions in C_{4N} molecules also supports the studies described in Part B of Chapter 3 and Part A of this chapter [Remya and Suresh 2015a; Remya and Suresh 2015b] where we have shown that that a clear separation of electron rich and electron deficient regions in molecules can result in intermolecular complimentary electrostatic interactions between chemically similar atoms.

Table 4.7 Interaction energy (E_{int}) and average of electron density (ρ_{ave}) at intermolecular BCPs corresponding to C···C interactions of C_{4N+2} and C_{4N} dimers

C_{4N+2}	E_{int} (kcal/mol)	ρ_{ave} (au)	C_{4N}	E_{int} (kcal/mol)	ρ_{ave} (au)
C_6	-2.23	0.0053	C_8	-23.31	0.0179
C_{10}	-5.20	0.0049	C_{12}	-21.80	0.0113
C_{14}	-6.92	0.0057	C_{16}	-15.83	0.0092
C_{18}	-8.32	0.0055	C_{20}	-15.39	0.0061
C_{22}	-9.98	0.0049	C_{24}	-16.88	0.0058
C_{26}	-11.77	0.0049	C_{28}	-18.27	0.0056

Though the presence of a BCP in QTIM analysis may not always be suggestive of a bonding situation [Poater *et al.* 2006a; Poater *et al.* 2006b], analysis of molecular orbitals (MOs) suggests strong orbital overlap between the two monomers in C_{4N} dimers. Occupied MOs corresponding to the C···C interactions in C_{16} are given in Figure 4.18 as a typical example for the C_{4N} systems. On the other hand, C_{4N+2} systems show very few such MOs corresponding to C···C interactions. For e.g., C_{18} shows only one such MO as can be seen in Figure 4.18.

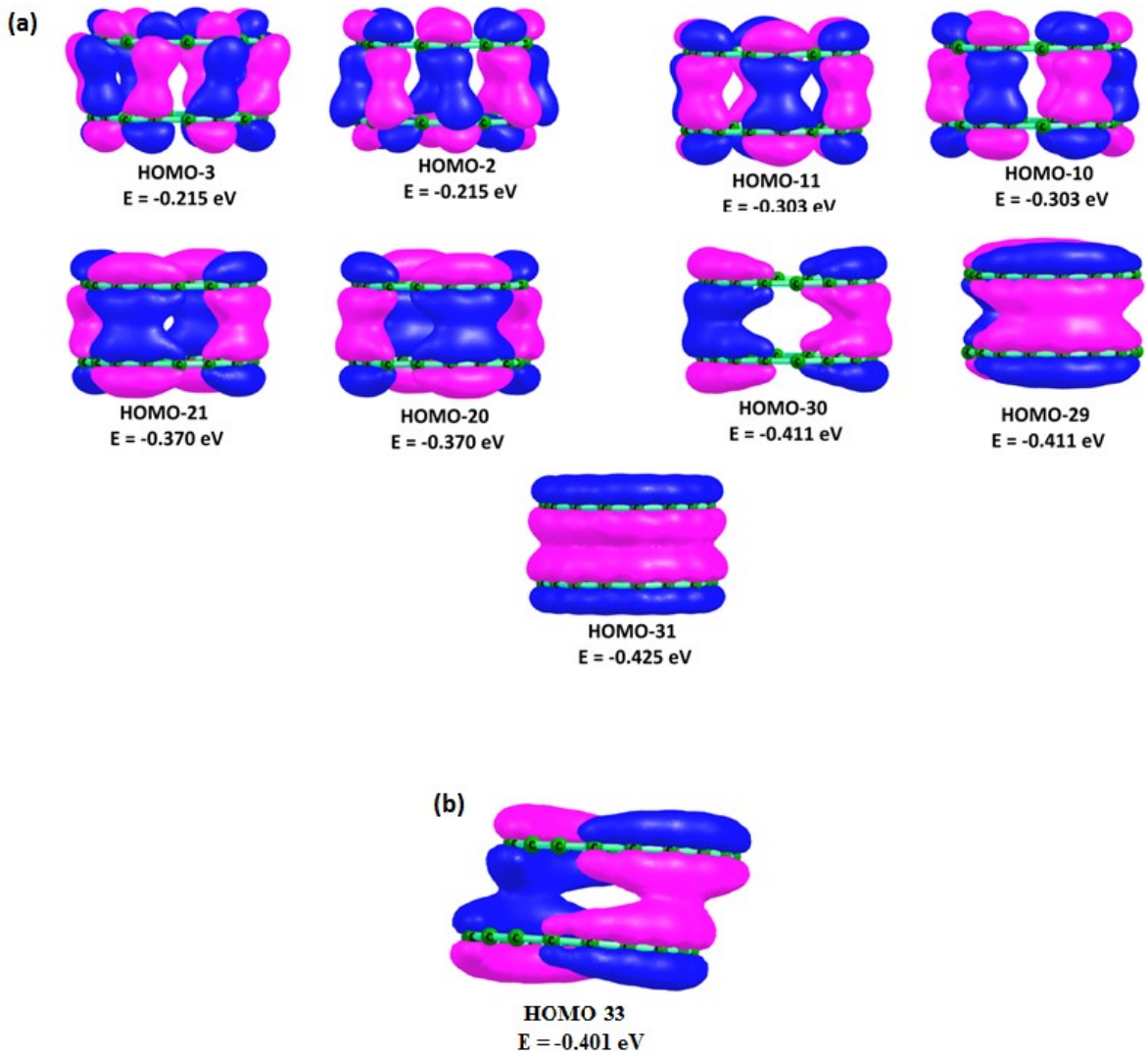

Figure 4.18 Occupied MOs corresponding to the inter-molecular C···C interactions in (a) C_{16} and (b) in C_{18} plotted at 0.02 au isosurface [Remya and Suresh 2016].

4.8 Conclusions

Studies on intermolecular C···C interactions between carbon-atoms in similar chemical environments in two classes of compounds *viz*. polyynes and carbon rings are described in this chapter. In Part A, non-covalent interactions in molecular dimers of seven series of polyynes with different substitutions at their end positions and having 1, 2, 3, 4, 5, 10, 15, 20, 30, 40 and 50 CC triple bonds have been studied. The most important type of intermolecular interaction in these molecular complexes is C···C interaction between chemically similar carbon atoms. The number of such interactions increases with increase in the monomer chain length resulting in substantial stabilization of the dimers. Since the number of interactions between the end groups remains the same for the dimers all the

analogues in a series with same substitutions and different chain lengths, the increase in interaction energy is fully attributed to increase in the number of C···C interactions. These C···C interactions result from intermolecular complimentary electrostatic interactions between relatively electron rich formal triple bond regions and electron deficient formal single bond regions in the interacting monomers. These complementary electrostatic interactions are clearly visualized with the help of MESP maps of the dimers. The nature of end group possesses a strong influence on the strength of the C···C interactions and it persists even up to 100 carbon atom chain length, the size of the largest systems analyzed in this study. This implies that tuning the interaction energies of these dimers can be brought about by selecting appropriate end groups. The E_{int} values are also influenced by the dipole moment of the interacting monomers, which increases with increase in chain length. It is shown that a dimer can have several minima with varying number of C···C interactions on its potential energy surface. Among these, the one having the highest number of C···C interactions is always found to be the global minimum. This clearly shows that the C···C interactions play a key role in stabilizing the supramolecular complexes of polyynes. Due to the cylindrical nature of the electron distribution and the presence of large number of interacting surfaces in polyyne molecules, higher order clusters showing multiple complementary electrostatic interactions from same CC region in different lateral directions is possible, resulting in further stabilization of the cluster. Due to this effect, the tetramers showed more than five-fold increase in the total interaction energy compared to the dimers and this brings out the strong cooperativity in cluster formation of the polyynes molecules. These results clearly indicate that long chain polyynes are promising materials for the development of molecular wire-like materials for structural and functional applications.

Part B of this chapter describes a detailed study of the aromatic features and intermolecular interactions of planar monocyclic C_n rings (from n = 6 - 32) with even number of carbon atoms. The geometric, electrostatic, magnetic and energetic features showed strong aromatic stabilization in C_{4N+2} rings and strong antiaromatic character in C_{4N} rings. Whereas the C_{4N+2} systems had cumulenic structures with all the bond lengths being equal, the C_{4N} rings showed acetylenic structures with clear bond length alternation. The MESP features clearly indicated delocalization of π-electrons and aromaticity in C_{4N+2} rings. On the other hand, in C_{4N} rings MESP features clearly showed electron localization around the shorter CC bonds (formal

triple bonds) proposing their antiaromaticity. The NICS analysis showed high negative values for NICS(0) and NICS(1) in C_{4N+2} and high positive values in C_{4N} rings. The magnitude of these values was much higher than aromatic/antiaromatic hydrocarbon rings of similar sizes and indicated double aromatic/antiaromatic features of the corresponding C_n rings. With increase in the ring size, the magnitude of NICS in a C_{4N+2} ring increased while those of C_{4N} ring decreased, both indicating stabilization, which is attributed mainly to the decrease in ring strain effects. In fact, the aromatic C_{4N+2} systems such as C_{14}, C_{18}, C_{22}, C_{26} and C_{30} possessing a smooth MESP distribution should be targeted for synthesis.

The dimerization behaviour of C_{4N+2} and C_{4N} rings are clearly influenced by the difference in their geometric features. The dimer of a C_{4N+2} ring always possessed significantly lower magnitude of E_{int} compared to the dimer of a C_{4N} ring. C_{4N+2} systems with equal bond lengths and a well delocalized system of π electrons have very low tendency for dimerization compared to the C_{4N} systems. The number and strength of intermolecular C···C interactions are also very less in C_{4N+2} dimers due to the lack of intermolecular complimentary electrostatic interactions. On the other hand, the very high magnitudes of E_{int} observed for C_{4N} could be attributed to the large number (equal to the number of carbon atoms in the C_{4N} monomer, except for C_8) of inter-molecular C···C interactions as observed in the QTAIM analysis. These interactions are formed as a result of complimentary electrostatic interactions between electron rich formal triple bond regions of one monomer with the relatively electron deficient region of the second. These complimentary interactions give rise to perfect stacking sandwich type arrangement of the monomers in a C_{4N} dimer. The fact that the C_{4N} dimers possess large number of C···C interactions supports studies described Chapter 3 and the first part of this chapter [Remya and Suresh 2015a; Remya and Suresh 2015b] that a clear partitioning of electron rich and electron deficient regions in a molecule can result in the formation of intermolecular complimentary electrostatic interactions between atoms in similar chemical environments.

List of Publications

A) Articles in Journals

- **Remya, K.**; Suresh, C. H. "Which density functional is close to CCSD accuracy to describe geometry and interaction energy of small non-covalent dimers? A benchmark study using Gaussian09," *J. Comput. Chem.* 34 (15), 1341-1353 (2013).
- **Remya, K.**; Suresh, C. H. "Cooperativity and cluster growth patterns in acetonitrile: A DFT study," *J. Comput. Chem.* 35 (12), 910-922 (2014).
- **Remya, K.**; Suresh, C. H. "Intermolecular carbon-carbon, nitrogen-nitrogen and oxygen-oxygen non-covalent bonding in dipolar molecules," *Phys. Chem. Chem. Phys.* 17 (28), 18380-18392 (2015).
- **Remya, K.**; Suresh, C. H. "Non-covalent intermolecular carbon-carbon interactions in polyynes," *Phys. Chem. Chem. Phys.*17 (40), 27035-27044 (2015).
- **Remya, K.**; Suresh, C. H. "Carbon Rings: A DFT Study on Geometry, Aromaticity and Intermolecular Carbon-Carbon Interactions," *RSC Adv.* 6 (50), 44261-44271(2016).

B) Published Contributions to Academic Conferences

- Presented a poster entitled "Which density functional is close to CCSD accuracy to describe geometry and interaction energy of small non-covalent dimers? a benchmark study using *Gaussian09*", in the 3rd Indo-German Conference on "Modeling Chemical & Biological (Re)activity (MCBR 2013) " held at NIPER and IISER, Mohali, Punjab, India, during 26th February – 1st March, 2013.
- Presented a poster entitled "Non-covalent carbon···carbon interactions: 'Dicarbon bonds' and 'dipole bonds' in homogeneous dimers of dipolar molecules" in "Theoretical Chemistry Symposium" held at CSIR-NCL, Pune, India, during December 18-21, 2014.
- Presented a paper entitled "Non-covalent intermolecular carbon···carbon interactions in polyynes" in "National Seminar & Training on Machine Learning Approaches: a new Trend in Quantum Mechanics" held at SN College, Chengannur, Kerala, India, during August 4-6, 2015.

References

Adamo, C.; Barone, V. "Toward reliable adiabatic connection models free from adjustable parameters" *Chem. Phys. Lett.* 274, **1997,** 242.

Adamo, C.; Barone, V. "Exchange functionals with improved long-range behavior and adiabatic connection methods without adjustable parameters: The mPW and mPW1PW models" *J. Chem. Phys* 108, **1998,** 664.

Adamo, C.; Barone, V. "Toward reliable density functional methods without adjustable parameters: The PBE0 model" *J. Chem. Phys* 110, **1999,** 6158.

Aiga, F.; Tada, T.; Yoshimura, R. "Frequency-dependent polarizabilities, hyperpolarizabilities, and excitation energies from time-dependent density-functional theory based on the quasienergy derivative method" *J. Chem. Phys.* 111, **1999,** 2878.

Al-Mubarak, A. S.; Mistro, G. D.; Lethbridge, P. G.; Abdul-Sattar, N. Y.; Stace, A. J. "Infrared absorption profiles for small acetonitrile clusters. Theory and experiment" *Faraday Discuss. Chem. Soc.* 86, **1988,** 209.

Albrecht, L.; Boyd, R. J.; Mo, O.; Yanez, M. "Cooperativity between hydrogen bonds and beryllium bonds in $(H_2O)_nBeX_2$ (n = 1-3, X = H, F) complexes. A new perspective" *Phys. Chem. Chem. Phys.* 14, **2012,** 14540.

Allen, F. "The cambridge structural database: a quarter of a million crystal structures and rising" *Acta Crystallogr., Sect. B* 58, **2002,** 380.

Alston Steiner, P.; Gordy, W. "Precision measurement of dipole moments and other spectral constants of normal and deuterated methyl fluoride and methyl cyanide" *J. Mol. Spectrosc.* 21, **1966,** 291.

An, X.; Zhuo, H.; Wang, Y.; Li, Q. "Competition between hydrogen bonds and halogen bonds in complexes of formamidine and hypohalous acids" *J. Mol. Model.* 19, **2013,** 4529.

Antony, J.; Bruske, B.; Grimme, S. "Cooperativity in noncovalent interactions of biologically relevant molecules" *Phys. Chem. Chem. Phys.* 11, **2009,** 8440.

Arunan, E.; Desiraju Gautam, R.; Klein Roger, A.; Sadlej, J.; Scheiner, S.; Alkorta, I.; Clary David, C.; Crabtree Robert, H.; Dannenberg Joseph, J.; Hobza, P.; Kjaergaard Henrik, G.; Legon Anthony, C.; Mennucci, B.; Nesbitt David, J. Defining the hydrogen bond: An account (IUPAC Technical Report). In *Pure Appl. Chem.*, 83, **2011**, 1619.

Ashley, J. K.; Neta Aditya Reddy, Y.; Steven, W. C. "Confinement and controlling the effective compressive stiffness of carbyne" *Nanotechnology* 25, **2014,** 335709.

Azofra, L. M.; Quesada-Moreno, M. M.; Alkorta, I.; Aviles-Moreno, J. R.; Lopez-Gonzalez, J. J.; Elguero, J. "Carbohydrates in the gas phase: conformational preference of d-ribose and 2-deoxy-d-ribose" *New J. Chem.* 38, **2014,** 529.

Azofra, L. M.; Scheiner, S. "Substituent effects in the noncovalent bonding of SO_2 to molecules containing a carbonyl group. the dominating role of the chalcogen bond" *J. Phys. Chem. A* 118, **2014,** 3835.

Bacelo, D. E. "Theoretical study of microscopic solvation of ammonia in water clusters: $NH_3(H_2O)_n$, n = 3, 4" *J. Phys. Chem. A* 106, **2002,** 11190.

Bader, R. F. W. *Atoms in molecules: a quantum theory*. Clarendon Press: Oxford, **1990**.

Bai, M.; Thomas, S. P.; Kottokkaran, R.; Nayak, S. K.; Ramamurthy, P. C.; Guru Row, T. N. "A donor–acceptor–donor structured organic conductor with S···S chalcogen bonding" *Cryst. Growth Des.* 14, **2013,** 459.

Ballmann, S.; Hieringer, W.; Secker, D.; Zheng, Q.; Gladysz, J. A.; Görling, A.; Weber, H. B. "Molecular wires in single-molecule junctions: charge transport and vibrational excitations" *ChemPhysChem* 11, **2010,** 2256.

Barrow, M. "α-Acetonitrile at 215 K" *Acta Crystallogr., Sect. B* 37, **1981,** 2239.

Bauzá, A.; Mooibroek, T. J.; Frontera, A. "Tetrel-bonding interaction: rediscovered supramolecular force?" *Angew. Chem. Int. Ed.* 52, **2013,** 12317.

Bauzá, A.; Mooibroek, T. J.; Frontera, A. "Small cycloalkane $(CN)_2C$-$C(CN)_2$ structures are highly directional non-covalent carbon-bond donors" *Chem. Eur. J.* 20, **2014a,** 10245.

Bauzá, A.; Ramis, R.; Frontera, A. "Computational study of anion recognition based on tetrel and hydrogen bonding interaction by calix[4]pyrrole derivatives" *Comput. Theor. Chem.* 1038, **2014b,** 67.

Becke, A. D. "Density-functional exchange-energy approximation with correct asymptotic-behavior" *Phys. Rev. A* 38, **1988,** 3098.

Becke, A. D. "Density-functional thermochemistry. III. The role of exact exchange" *J. Chem. Phys* 98, **1993,** 5648.

Becke, A. D. "Density-functional thermochemistry. IV. A new dynamical correlation functional and implications for exact-exchange mixing" *J. Chem. Phys* 104, **1996,** 1040.

Becke, A. D. "Density-functional thermochemistry. V. Systematic optimization of exchange-correlation functionals" *J. Chem. Phys* 107, **1997,** 8554.

Becke, A. D.; Roussel, M. R. "Exchange holes in inhomogeneous systems: A coordinate-space model" *Phys. Rev. A* 39, **1989,** 3761.

Benighaus, T.; DiStasio, R. A.; Lochan, R. C.; Chai, J.-D.; Head-Gordon, M. "Semiempirical double-hybrid density functional with improved description of long-range correlation" *J. Phys. Chem. A* 112, **2008,** 2702.

Berg, J. M.; Tymoczko, J. L.; Stryer, L. *Biochemistry, 6th ed.* Freeman: New York, **2007**.

Bertagnolli, H.; Chieux, P.; Zeidler, M. D. "A neutron-diffraction study of liquid acetonitrile" *Mol. Phys.* 32, **1976,** 759.

Bertagnolli, H.; Zeidler, M. D. "Molecular pair-correlation function of liquid acetonitrile from X-ray and neutron-diffraction studies" *Mol. Phys.* 35, **1978,** 177.

Bickelhaupt, F. M.; Baerends, E. J. Kohn-Sham density functional theory: predicting and understanding chemistry. In *Rev. Comput. Chem.*, K.B. Lipkowitz, E. D. B. Boyd, Eds. Wiley-VCH: New York, 15, **2000**, 1.

Biegler-König, F.; Schönbohm, J. "Update of the AIM2000-Program for atoms in molecules" *J. Comput. Chem.* 23, **2002,** 1489.

Biegler-König, F.; Schönbohm, J.; Bayles, D. "AIM2000" *J. Comput. Chem.* 22, **2001,** 545.

Biegler-König, F.; Schönbohm, J.; Derdau, R.; Bayles, D.; Bader, R. F. W. *AIM2000 Version 1*, Germany, 2000.

Blanco, S.; López, J. C.; Lesarri, A.; Alonso, J. L. "Microsolvation of formamide: A rotational study" *J. Am. Chem. Soc.* 128, **2006,** 12111.

Bleiholder, C.; Werz, D. B.; Köppel, H.; Gleiter, R. "Theoretical investigations on chalcogen−chalcogen interactions: what makes these nonbonded interactions bonding?" *J. Am. Chem. Soc.* 128, **2006,** 2666.

Boese, A. D.; Doltsinis, N. L.; Handy, N. C.; Sprik, M. "New generalized gradient approximation functionals" *J. Chem. Phys* 112, **2000,** 1670.

Boese, A. D.; Handy, N. C. "A new parametrization of exchange-correlation generalized gradient approximation functionals" *J. Chem. Phys* 114, **2001,** 5497.

Boese, A. D.; Handy, N. C. "New exchange-correlation density functionals: The role of the kinetic-energy density" *J. Chem. Phys* 116, **2002,** 9559.

Boese, A. D.; Martin, J. M. L. "Development of density functionals for thermochemical kinetics" *J. Chem. Phys* 121, **2004,** 3405.

Böhm, H. J.; Ahlrichs, R.; Scharf, P.; Schiffer, H. "Intermolecular potentials for CH_4, CH_3F, CHF_3, CH_3Cl, CH_2Cl_2, CH_3CN and CO_2" *J. Chem. Phys.* 81, **1984,** 1389.

Börrnert, F.; Börrnert, C.; Gorantla, S.; Liu, X.; Bachmatiuk, A.; Joswig, J.-O.; Wagner, F. R.; Schäffel, F.; Warner, J. H.; Schönfelder, R.; Rellinghaus, B.; Gemming, T.;

Thomas, J.; Knupfer, M.; Büchner, B.; Rümmeli, M. H. "Single-wall-carbon-nanotube/single-carbon-chain molecular junctions" *Phys. Rev. B* 81, **2010,** 085439.

Boys, S. F.; Bernardi, F. "The calculation of small molecular interactions by the differences of separate total energies. Some procedures with reduced errors" *Mol. Phys.* 19, **1970,** 553.

Bundhun, A.; Ramasami, P.; Murray, J.; Politzer, P. "Trends in σ-hole strengths and interactions of F_3MX molecules (M = C, Si, Ge and X = F, Cl, Br, I)" *J. Mol. Model.* 19, **2013,** 2739.

Burke, K.; Perdew, J. P.; Wang, Y. *Electronic Density Functional Theory: Recent Progress and New Directions*. Plenum: **1998**.

Burling, F. T.; Goldstein, B. M. "Computational studies of nonbonded sulfur-oxygen and selenium-oxygen interactions in the thiazole and selenazole nucleosides" *J. Am. Chem. Soc.* 114, **1992,** 2313.

Burns, L. A.; Mayagoitia, Á. V.-; Sumpter, B. G.; Sherrill, C. D. "Density-functional approaches to noncovalent interactions: A comparison of dispersion corrections (DFT-D), exchange-hole dipole moment (XDM) theory, and specialized functionals" *J. Chem. Phys.* 134, **2011a,** 084107.

Burns, L. A.; Vazquez-Mayagoitia, A.; Sumpter, B. G.; Sherrill, C. D. "Density-functional approaches to noncovalent interactionas: A comparison of dispersion corrections (DFT-D), exchangge-hole dipole moment (XDM) theory, and specialized functionals" *J. Chem. Phys* 134, **2011b,** 084107: 1.

Bylaska, E. J.; Kawai, R.; Weare, J. H. "From small to large behavior: The transition from the aromatic to the Peierls regime in carbon rings" *J. Chem. Phys.* 113, **2000,** 6096.

Bylaska, E. J.; Weare, J. H.; Kawai, R. "Development of bond-length alternation in very large carbon rings: LDA pseudopotential results" *Phys. Rev. B* 58, **1998,** R7488.

C. P. Schullz, I. V. H. *Clusters of atoms and molecules II*. Springer: Berlin, **1994**.

Cabaleiro-Lago, E. M.; Hermida-Ramón, J. M.; Peña-Gallego, A.; Martínez-Núñez, E.; Fernández-Ramos, A. "Intermolecular interactions and cooperative effects in acetonitrile clusters. An ab initio molecular orbital study" *J. Mol. Struct. THEOCHEM* 498, **2000,** 21.

Cabaleiro-Lago, E. M.; Ríos, M. A. "A potential function for intermolecular interaction in the acetonitrile dimer constructed from ab initio data" *J. Phys. Chem. A* 101, **1997,** 8327.

Cabaleiro-Lago, E. M.; Ríos, M. A. "Ab initio study of interactions in hydrazine clusters of one to four molecules: cooperativity in the interaction" *J. Phys. Chem. A* 103, **1999a,** 6468.

Cabaleiro-Lago, E. M.; Ríos, M. A. "Intermolecular potential for acetonitrile based on ab initio calculations" *Mol. Phys.* 96, **1999b,** 309.

Casari, C. S.; Li Bassi, A.; Baserga, A.; Ravagnan, L.; Piseri, P.; Lenardi, C.; Tommasini, M.; Milani, A.; Fazzi, D.; Bottani, C. E.; Milani, P. "Low-frequency modes in the Raman spectrum of *sp*-sp^2 nanostructured carbon" *Phys. Rev. B* 77, **2008,** 195444.

Castleman, A. W.; Bowen, K. H. "Clusters: structure, energetics, and dynamics of intermediate states of matter" *J. Phys. Chem.* 100, **1996,** 12911.

Cataldo, F.; Ravagnan, L.; Cinquanta, E.; Castelli, I. E.; Manini, N.; Onida, G.; Milani, P. "Synthesis, characterization, and modeling of naphthyl-terminated *sp* carbon chains: dinaphthylpolyynes" *J. Phys. Chem. B* 114, **2010,** 14834.

Černý, J.; Pitoňák, M.; Riley, K. E.; Hobza, P. "Complete basis set extrapolation and hybrid schemes for geometry gradients of noncovalent complexes" *J. Chem. Theory Comput.* 7, **2011,** 3924.

Chai, J.-D.; Head-Gordon, M. "Long-range corrected hybrid density functionals with damped atom-atom dispersion corrections" *Phys. Chem. Chem. Phys.* 10, **2008a,** 6615.

Chai, J.-D.; Head-Gordon, M. "Systematic optimization of long-range corrected hybrid density functionals" *J. Chem. Phys* 128, **2008b,** 084106.

Chalifoux, W. A.; McDonald, R.; Ferguson, M. J.; Tykwinski, R. R. "tert-Butyl-end-capped polyynes: crystallographic evidence of reduced bond-length alternation" *Angew. Chem. Int. Ed.* 48, **2009,** 7915.

Chalifoux, W. A.; Tykwinski, R. R. "Synthesis of extended polyynes: Toward carbyne" *C.R. Chim* 12, **2009,** 341.

Chalifoux, W. A.; Tykwinski, R. R. "Synthesis of polyynes to model the *sp*-carbon allotrope carbyne" *Nat Chem* 2, **2010,** 967.

Chandrasekhar, J.; Jemmis, E. D.; von Ragué Schleyer, P. "Double aromaticity: aromaticity in orthogonal planes. The 3,5-dehydrophenyl cation" *Tetrahedron Lett.* 20, **1979,** 3707.

Chen, J.; Reed, M. A. "Electronic transport of molecular systems" *Chem. Phys.* 281, **2002,** 127.

Clark, T.; Hennemann, M.; Murray, J.; Politzer, P. "Halogen bonding: the σ-hole" *J. Mol. Model.* 13, **2007,** 291.

Clementi, E.; kołos, W.; Lie, G. C.; Ranghino, G. "Nonadditivity of interaction in water trimers" *Int. J. Quantum Chem.* 17, **1980,** 377.

Cohen, A. J.; Handy, N. C. "Dynamic correlation" *Mol. Phys.* 99, **2001,** 607.

Cramer, C. J. *Essentials of Computational Chemistry: Theories and Models*. John Wiley & Sons: West Sussex, England, **2004**.

Crittenden, D. L. "A systematic CCSD(T) study of long-range and noncovalent interactions between benzene and a series of first- and second-row hydrides and rare gas atoms" *J. Phys. Chem. A* 113, **2009,** 1663.

Crljen, Ž.; Baranović, G. "Unusual conductance of polyyne-based molecular wires" *Phys. Rev. Lett.* 98, **2007,** 116801.

Cruzan, J. D.; Braly, L. B.; Liu, K.; Brown, M. G.; Loeser, J. G.; Saykally, R. J. "Quantifying hydrogen bond cooperativity in water: VRT spectroscopy of the water tetramer" *Science* 271, **1996,** 59.

Curtiss, L. A.; Redfern, P. C.; Raghavachari, K.; Rassolov, V.; Pople, J. A. "Gaussian-3 theory using reduced Møller-Plesset order" *J. Chem. Phys.* 110 **1999,** 4703.

Dąbkowska, I.; Gonzalez, H. V.; Jurečka, P.; Hobza, P. "Stabilization energies of the hydrogen-bonded and stacked structures of nucleic acid base pairs in the crystal geometries of CG, AT, and AC DNA steps and in the NMR geometry of the 5'-d(GCGAAGC)-3' hairpin: complete basis set calculations at the MP2 and CCSD(T) levels" *J. Phys. Chem. A* 109, **2005,** 1131.

De Meyts, P.; Roth, J.; Neville, D. M.; Gavin, J. R.; Lesniak, M. A. "Insulin interactions with its receptors: Experimental evidence for negative cooperativity" *Biochem. Biophys. Res. Commun.* 55, **1973,** 154.

Defranceschi, M.; Peeters, D.; Mathieu, D.; Delhalle, J.; Lécayon, G. "Study of intermolecular associations in liquid acetonitrile from *ab initio* calculations of IR frequencies and intensities" *J. Mol. Struct. THEOCHEM* 287, **1993,** 153.

Del Bene, J.; Pople, J. A. "Intermolecular energies of small water polymers" *Chem. Phys. Lett.* 4, **1969,** 426.

Del Bene, J. E.; Alkorta, I.; Sanchez-Sanz, G.; Elguero, J. "Structures, energies, bonding, and NMR properties of pnicogen complexes $H_2XP{:}NXH_2$ (X = H, CH_3, NH_2, OH, F, Cl)" *J. Phys. Chem. A* 115, **2011,** 13724.

Del Bene, J. E.; Alkorta, I.; Sánchez-Sanz, G.; Elguero, J. "Interplay of F–H...F hydrogen bonds and P...N pnicogen bonds" *J. Phys. Chem. A* 116, **2012,** 9205.

Deshmukh, M. M.; Bartolotti, L. J.; Gadre, S. R. "Intramolecular hydrogen bonding and cooperative interactions in carbohydrates via the molecular tailoring approach" *J. Phys. Chem. A* 112, **2008,** 312.

Desiraju, G. R.; Parthasarathy, R. "The nature of halogen...halogen interactions: are short halogen contacts due to specific attractive forces or due to close packing of nonspherical atoms?" *J. Am. Chem. Soc.* 111, **1989,** 8725.

Desiraju, G. R.; Steiner, T. *The Weak Hydrogen Bond*. Oxford University Press: Oxford **1999**.

DiLabio, G.; Koleini, M.; Torres, E. "Extension of the B3LYP–dispersion-correcting potential approach to the accurate treatment of both inter- and intra-molecular interactions" *Theor. Chem. Acc.* 132, **2013,** 1.

Dion, M.; Rydberg, H.; Schröder, E.; Langreth, D. C.; Lundqvist, B. I. "Van der Waals density functional for general geometries" *Phys. Rev. Lett.* 92, **2004,** 246401.

E.J. Baerends, T. Z., J. Autschbach, D. Bashford, A. Bérces, F.M. Bickelhaupt, C. Bo, P.M. Boerrigter, L. Cavallo, D.P. Chong, L. Deng, R.M. Dickson, D.E. Ellis, M. van Faassen, L. Fan, T.H. Fischer, C. Fonseca Guerra, A. Ghysels, A. Giammona, S.J.A. van Gisbergen, A.W. Götz, J.A. Groeneveld, O.V. Gritsenko, M. Grüning, S. Gusarov, F.E. Harris, P. van den Hoek, C.R. Jacob, H. Jacobsen, L. Jensen, J.W. Kaminski, G. van Kessel, F. Kootstra, A. Kovalenko, M.V. Krykunov, E. van Lenthe, D.A. McCormack, A. Michalak, M. Mitoraj, J. Neugebauer, V.P. Nicu, L. Noodleman, V.P. Osinga, S. Patchkovskii, P.H.T. Philipsen, D. Post, C.C. Pye, W. Ravenek, J.I. Rodríguez, P. Ros, P.R.T. Schipper, G. Schreckenbach, J.S. Seldenthuis, M. Seth, J.G. Snijders, M. Solà, M. Swart, D. Swerhone, G. te Velde, P. Vernooijs, L. Versluis, L. Visscher, O. Visser, F. Wang, T.A. Wesolowski, E.M. van Wezenbeek, G. Wiesenekker, S.K. Wolff, T.K. Woo, A.L. Yakovlev. *ADF2010, SCM*, Theoretical Chemistry, Vrije Universiteit: Amsterdam, The Netherlands, 2010.

Edwards, D. M. F.; Madden, P. A. "A computer simulation study of the dielectric properties of a model of methyl cyanide" *Mol. Phys.* 51, **1984,** 1163.

Eisler, S.; Slepkov, A. D.; Elliott, E.; Luu, T.; McDonald, R.; Hegmann, F. A.; Tykwinski, R. R. "Polyynes as a model for carbyne: synthesis, physical properties, and nonlinear optical response" *J. Am. Chem. Soc.* 127, **2005,** 2666.

Enjalbert, R.; Galy, J. "CH_3CN: X-ray structural investigation of a unique single crystal. β --> α phase transition and crystal structure" *Acta Crystallogr., Sect. B* 58, **2002,** 1005.

Enkelmann, V. "Solid-state reactivity of triacetylenes" *Chem. Mater.* 6, **1994,** 1337.

Ernzerhof, M.; Perdew, J. P. “Generalized gradient approximation to the angle- and system-averaged exchange hole” *J. Chem. Phys* 109, **1998,** 3313.

Eshuis, H.; Furche, F. “A parameter-free density functional that works for noncovalent interactions” *J. Phys. Chem. Lett.* 2, **2011,** 983.

Eskandari, K.; Mahmoodabadi, N. “Pnicogen bonds: a theoretical study based on the laplacian of electron density” *J. Phys. Chem. A* 117, **2013,** 13018.

Esrafili, M. “Investigation of H-bonding and halogen-bonding effects in dichloroacetic acid: DFT calculations of NQR parameters and QTAIM analysis” *J. Mol. Model.* 18, **2012,** 5005.

Esrafili, M.; Behzadi, H.; Hadipour, N. “Theoretical study of N–H· · ·O hydrogen bonding properties and cooperativity effects in linear acetamide clusters” *Theor. Chem. Acc.* 121, **2008,** 135.

Esrafili, M. D.; Beheshtian, J.; Hadipour, N. L. “Computational study on the characteristics of the interaction in linear urea clusters” *Int. J. Quantum Chem.* 111, **2011,** 3184.

Esrafili, M. D.; Fatehi, P.; Solimannejad, M. “Cooperative effects in cyclic LiCN and HCN clusters: A comparative study” *Comput. Theor. Chem.* 1022, **2013,** 115.

Fernandéz-Lima, F. A.; Ponciano, C. R.; da Silveira, E. F.; Nascimento, M. A. C. “Experimental and theoretical characterization of the clusters produced by 337 nm UV laser” *Chem. Phys. Lett.* 445, **2007,** 147.

Fonseca Guerra, C.; Snijders, J. G.; te Velde, G.; Baerends, E. J. “Towards an order-N DFT method” *Theor. Chem. Acc.* 99, **1998,** 391.

Ford, T. A.; Glasser, L. “Ab initio calculations of the structural, energetic, and vibrational properties of some hydrogen bonded and van der Waals dimers. Part 4. The acetonitrile dimer” *Int. J. Quantum Chem.* 84, **2001,** 226.

Foroutan-Nejad, C.; Shahbazian, S.; Marek, R. “Toward a consistent interpretation of the QTAIM: tortuous link between chemical bonds, interactions, and bond/line paths” *Chem. Eur. J.* 20, **2014,** 10140.

Foroutan-Nejad, C.; Shahbazian, S.; Rashidi-Ranjbar, P. “The electron density vs. NICS scan: a new approach to assess aromaticity in molecules with different ring sizes” *Phys. Chem. Chem. Phys.* 12, **2010,** 12630.

Fowler, P. W.; Mizoguchi, N.; Bean, D. E.; Havenith, R. W. A. “Double aromaticity and ring currents in all-carbon rings” *Chem. Eur. J.* 15, **2009,** 6964.

Frank, B. B.; Laporta, P. R.; Breiten, B.; Kuzyk, M. C.; Jarowski, P. D.; Schweizer, W. B.; Seiler, P.; Biaggio, I.; Boudon, C.; Gisselbrecht, J.-P.; Diederich, F. “Comparison of

CC triple and double bonds as spacers in push–pull chromophores" *Eur. J. Org. Chem.* 2011, **2011,** 4307.

Frisch, M. J.; Trucks, G. W.; Schlegel, H. B.; Scuseria, G. E.; Robb, M. A.; Cheeseman, J. R.; Scalmani, G.; Barone, V.; Mennucci, B.; Petersson, G. A.; Nakatsuji, H.; Caricato, M.; Li, X.; Hratchian, H. P.; Izmaylov, A. F.; Bloino, J.; Zheng, G.; Sonnenberg, J. L.; Hada, M.; Ehara, M.; Toyota, K.; Fukuda, R.; Hasegawa, J.; Ishida, M.; Nakajima, T.; Honda, Y.; Kitao, O.; Nakai, H.; Vreven, T.; J. A. Montgomery, J.; Peralta, J. E.; Ogliaro, F.; Bearpark, M.; Heyd, J. J.; Brothers, E.; Kudin, K. N.; Staroverov, V. N.; Keith, T.; Kobayashi, R.; Normand, J.; Raghavachari, K.; Rendell, A.; Burant, J. C.; Iyengar, S. S.; Tomasi, J.; Cossi, M.; Rega, N.; Millam, J. M.; Klene, M.; Knox, J. E.; Cross, J. B.; Bakken, V.; Adamo, C.; Jaramillo, J.; Gomperts, R.; Stratmann, R. E.; Yazyev, O.; Austin, A. J.; Cammi, R.; Pomelli, C.; Ochterski, J. W.; Martin, R. L.; Morokuma, K.; Zakrzewski, V. G.; Voth, G. A.; Salvador, P.; Dannenberg, J. J.; Dapprich, S.; Daniels, A. D.; Farkas, O.; Foresman, J. B.; Ortiz, J. V.; Cioslowski, J.; Fox, D. J. *Gaussian 09, Revision C.01*, Gaussian, Inc.: Wallingford CT, 2010.

Gadre, S. R.; Bhadane, P.; Pundlik, S. S.; Pingale, S. S. *Molecular Electrostatic Potentials: Concepts and Applications. In Molecular Electrostatic Potentials: Concepts and Applications*. Elsevier: Amsterdam, **1996**; Vol. 3.

Gadre, S. R.; Pundlik, S. S. "Complementary electrostatics for the study of DNA base-pair interactions" *J. Phys. Chem. B* 101, **1997,** 3298.

Gadre, S. R.; Shirsat, R. N. *Elelectrostatics of Atoms and Molecules*. Universities Press: Hyderabad, India, **2000**.

Gibtner, T.; Hampel, F.; Gisselbrecht, J.-P.; Hirsch, A. "End-cap stabilized oligoynes: model compounds for the linear sp carbon allotrope carbyne" *Chem. Eur. J.* 8, **2002,** 408.

Giesen, T.; Van Orden, A.; Hwang, H.; Fellers, R.; Provencal, R.; Saykally, R. "Infrared laser spectroscopy of the linear C13 carbon cluster" *Science* 265, **1994,** 756.

Gill, P. M. W. "A new gradient-corrected exchange functional" *Mol. Phys.* 89, **1996,** 433.

Gkionis, K.; Hill, J. G.; Oldfield, S.; Platts, J. "Performance of Becke's half-and-half functional for non-covalent interactions: energetics, geometries and electron densities" *J. Mol. Model.* 15, **2009,** 1051.

Gleiter, R.; Werz, D. B.; Rausch, B. J. "A world beyond hydrogen bonds?—chalcogen–chalcogen interactions yielding tubular structures" *Chem. Eur. J.* 9, **2003,** 2676.

Goerigk, L.; Grimme, S. “A general database for main group thermochemistry, kinetics, and noncovalent interactions − assessment of common and reparameterized (meta-)GGA density functionals” *J. Chem. Theory Comput.* 6, **2010,** 107.

Goerigk, L.; Grimme, S. “Efficient and accurate double-hybrid-meta-GGA density functionals—evaluation with the extended GMTKN30 database for general main group thermochemistry, kinetics, and noncovalent interactions” *J. Chem. Theory Comput.* 7, **2011a,** 291.

Goerigk, L.; Grimme, S. “A thorough benchmark of density functional methods for general main group thermochemistry, kinetics, and noncovalent interactions” *Phys. Chem. Chem. Phys.* 13, **2011b,** 6670.

Görling, A.; Heinze, H. H.; Ruzankin, S. P.; Staufer, M.; Rösch, N. “Density- and density-matrix-based coupled Kohn–Sham methods for dynamic polarizabilities and excitation energies of molecules” *J. Chem. Phys.* 110, **1999,** 2785.

Goroff, N. S. “Mechanism of fullerene formation” *Acc. Chem. Res.* 29, **1996,** 77.

Gotts, N. G.; von Helden, G.; Bowers, M. T. “Carbon cluster anions: structure and growth from C_5^- to C_{62}^-” *Int. J. Mass Spectrom. Ion Processes* 149–150, **1995,** 217.

Grabowski, S. J. “Ab initio calculations on conventional and unconventional hydrogen bondsstudy of the hydrogen bond strength” *J. Phys. Chem. A* 105, **2001,** 10739.

Grabowski, S. J. “Tetrel bond-σ-hole bond as a preliminary stage of the S_N2 reaction” *Phys. Chem. Chem. Phys.* 16, **2014,** 1824.

Gráfová, L.; Pitoňák, M.; Řezáč, J.; Hobza, P. “Comparative study of selected wave function and density functional methods for noncovalent interaction energy calculations using the extended S22 data set” *J. Chem. Theory Comput.* 6, **2010,** 2365.

Granatier, J.; Pitoňák, M.; Hobza, P. “Accuracy of several wave function and density functional theory methods for description of noncovalent interaction of saturated and unsaturated hydrocarbon dimers” *J. Chem. Theory Comput.* 8, **2012,** 2282.

Grimme, S. “Accurate description of van der Waals complexes by density functional theory including empirical corrections” *J. Comput. Chem.* 25, **2004,** 1463.

Grimme, S. “Semiempirical GGA-type density functional constructed with a long-range dispersion correction” *J. Comp. Chem.* 27, **2006a,** 1787.

Grimme, S. “Semiempirical hybrid density functional with perturbative second-order correlation” *J. Chem. Phys* 124, **2006b**.

Grimme, S.; Ehrlich, S.; Goerigk, L. “Effect of the damping function in dispersion corrected density functional theory” *J. Comp. Chem.* 32 **2011,** 1456.

Guan, L.; Mo, Y. “Electron transfer in pnicogen bonds” *J. Phys. Chem. A* 118, **2014,** 8911.

Hamprecht, F. A.; Cohen, A.; Tozer, D. J.; Handy, N. C. “Development and assessment of new exchange-correlation functionals” *J. Chem. Phys* 109, **1998,** 6264.

Handy, N. C.; Cohen, A. J. “Left-right correlation energy” *Mol. Phys.* 99, **2001,** 403.

Hayatsu, R.; Scott, R. G.; Studier, M. H.; Lewis, R. S.; Anders, E. “Carbynes in meteorites: detection, low-temperature origin, and implications for interstellar molecules” *Science* 209, **1980,** 1515.

Heimann, R. B.; Kleiman, J.; Salansky, N. M. “A unified structural approach to linear carbon polytypes” *Nature* 306, **1983,** 164.

Henderson, T. M.; Izmaylov, A. F.; Scalmani, G.; Scuseria, G. E. “Can short-range hybrids describe long-range-dependent properties?” *J. Chem. Phys.* 131, **2009,** 044108: 1.

Heyd, J.; Peralta, J. E.; Scuseria, G. E.; Martin, R. L. “Energy band gaps and lattice parameters evaluated with the Heyd-Scuseria-Ernzerhof screened hybrid functional” *J. Chem. Phys* 123, **2005,** 8.

Heyd, J.; Scuseria, G. “Efficient hybrid density functional calculations in solids: The HS-Ernzerhof screened Coulomb hybrid functional” *J. Chem. Phys* 121, **2004a,** 1187.

Heyd, J.; Scuseria, G.; Ernzerhof, M. “Hybrid functionals based on a screened Coulomb potential” *J. Chem. Phys* 118, **2003,** 9.

Heyd, J.; Scuseria, G. E. “Assessment and validation of a screened Coulomb hybrid density functional” *J. Chem. Phys* 120, **2004b**.

Heyd, J.; Scuseria, G. E.; Ernzerhof, M. “Erratum: "Hybrid functionals based on a screened Coulomb potential” *J. Chem. Phys* 124, **2006**.

Hobza, P. “Calculations on noncovalent interactions and databases of benchmark interaction energies” *Acc. Chem. Res.* 45, **2012,** 663.

Hobza, P.; Šponer, J. “Toward true DNA base-stacking energies: MP2, CCSD(T), and complete basis set calculations” *J. Am. Chem. Soc.* 124, **2002,** 11802.

Hobzaa, P.; Zahradníkb, R.; Müller-Dethlefsc, K. “The world of non-covalent interactions: 2006” *Collect. Czech. Chem. Commun.* 71, **2006,** 443.

Hoe, W.-M.; Cohen, A.; Handy, N. C. “Assessment of a new local exchange functional OPTX” *Chem. Phys. Lett.* 341, **2001,** 319.

Hohenberg, P.; Kohn, W. “Inhomogeneous electron gas” *Phys. Rev.* 136, **1964,** B864.

Hohenstein, E. G.; Chill, S. T.; Sherrill, C. D. “Assessment of the performance of the M05−2X and M06−2X exchange-correlation functionals for noncovalent interactions in biomolecules” *J. Chem. Theory Comput.* 4, **2008,** 1996.

Huelsekopf, M.; Ludwig, R. "Temperature dependence of hydrogen bonding in alcohols" *J. Mol. Liq.* 85, **2000,** 105.

Hujo, W.; Grimme, S. "Performance of the van der Waals density functional VV10 and (hybrid)GGA variants for thermochemistry and noncovalent interactions" *J. Chem. Theory Comput.* 7, **2011,** 3866.

Hunter, C. A.; Anderson, H. L. "What is cooperativity?" *Angew. Chem. Int. Ed.* 48, **2009,** 7488.

Hunter, J.; Fye, J.; Jarrold, M. F. "Annealing C_{60}^{+}: synthesis of fullerenes and large carbon rings" *Science* 260, **1993a,** 784.

Hunter, J. M.; Fye, J. L.; Jarrold, M. F. "Annealing and dissociation of carbon rings" *J. Chem. Phys.* 99, **1993b,** 1785.

Hunter, J. M.; Fye, J. L.; Roskamp, E. J.; Jarrold, M. F. "Annealing carbon cluster ions: a mechanism for fullerene synthesis" *J. Phys. Chem.* 98, **1994,** 1810.

Hutter, J.; Luethi, H. P.; Diederich, F. "Structures and vibrational frequencies of the carbon molecules C_2-C_{18} calculated by density functional theory" *J. Am. Chem. Soc.* 116, **1994,** 750.

Iikura, H.; Tsuneda, T.; Yanai, T.; Hirao, K. "Long-range correction scheme for generalized-gradient-approximation exchange functionals" *J. Chem. Phys.* 115, **2001,** 3540.

Ireta, J.; Neugebauer, J.; Scheffler, M.; Rojo, A.; Galván, M. "Density functional theory study of the cooperativity of hydrogen bonds in finite and infinite α-helices" *J. Phys. Chem. B* 107, **2003,** 1432.

Irle, S.; Zheng, G.; Wang, Z.; Morokuma, K. "The C_{60} formation puzzle "solved": QM/MD simulations reveal the shrinking hot giant road of the dynamic fullerene self-assembly mechanism" *J. Phys. Chem. B* 110, **2006,** 14531.

Iwaoka, M.; Takemoto, S.; Tomoda, S. "Statistical and Theoretical investigations on the directionality of nonbonded S···O interactions. implications for molecular design and protein engineering" *J. Am. Chem. Soc.* 124, **2002,** 10613.

Izmaylov, A. F.; Scuseria, G.; Frisch, M. J. "Efficient evaluation of short-range Hartree-Fock exchange in large molecules and periodic systems" *J. Chem. Phys* 125, **2006,** 104103.

Janesko, B. G. "Rung 3.5 density functionals: Another step on Jacob's ladder" *Int. J. Quant. Chem.* 113, **2013,** 83.

Jiang, X.-N.; Wang, C.-S. "Rapid prediction of the hydrogen bond cooperativity in N-methylacetamide chains" *ChemPhysChem* 10, **2009,** 3330.

Johnson, E. R.; DiLabio, G. A. "Structure and binding energies in van der Waals dimers: Comparison between density functional theory and correlated ab initio methods" *Chem. Phys. Lett.* 419, **2006,** 333.

Johnson, E. R.; Otero-de-la-Roza, A.; Dale, S. G.; DiLabio, G. A. "Efficient basis sets for non-covalent interactions in XDM-corrected density-functional theory" *J. Chem. Phys.* 139, **2013,** 214109.

Jones, R. O. "Density functional study of carbon clusters C_{2n}($2 \leqslant n \leqslant 16$). I. Structure and bonding in the neutral clusters" *J. Chem. Phys.* 110, **1999,** 5189.

Jones, R. O.; Seifert, G. "Structure and bonding in carbon clusters C_{14} to C_{24}: chains, rings, bowls, plates, and cages" *Phys. Rev. Lett.* 79, **1997,** 443.

Jorgensen, W. L.; Briggs, J. M. "Monte Carlo simulations of liquid acetonitrile with a three-site model" *Mol. Phys.* 63, **1988,** 547.

Jurečka, P.; Hobza, P. "True stabilization energies for the optimal planar hydrogen-bonded and stacked structures of Guanine···Cytosine, Adenine···Thymine, and their 9- and 1-Methyl derivatives: complete basis set calculations at the MP2 and CCSD(T) levels and comparison with experiment" *J. Am. Chem. Soc.* 125, **2003,** 15608.

Jurečka, P.; Šponer, J.; Cerny, J.; Hobza, P. "Benchmark database of accurate (MP2 and CCSD(T) complete basis set limit) interaction energies of small model complexes, DNA base pairs, and amino acid pairs" *Phys. Chem. Chem. Phys.* 8, **2006,** 1985.

Jurečka, P.; Šponer, J.; Hobza, P. "Potential energy surface of the cytosine dimer: MP2 complete basis set limit interaction energies, CCSD(T) correction term, and comparison with the AMBER force field" *J. Phys. Chem. B* 108, **2004,** 5466.

Keith, T. A. *AIMAll (Version 14.04.17)*, TK Gristmill Software: Overland Park KS, USA, 2014.

Kharat, B.; Deshmukh, V.; Chaudhari, A. "Computational study of $(CH_3C{\equiv}N)_n$ (n = 1-5) oligomers using density functional theory method" *J. Mol. Liq.* 177, **2013,** 172.

Khoo, K. H.; Neaton, J. B.; Son, Y. W.; Cohen, M. L.; Louie, S. G. "Negative differential resistance in carbon atomic wire-carbon nanotube junctions" *Nano Lett.* 8, **2008,** 2900.

King, B. F.; Weinhold, F. "Structure and spectroscopy of $(HCN)_n$ clusters: Cooperative and electronic delocalization effects in C–H···N hydrogen bonding" *J. Chem. Phys.* 103, **1995,** 333.

Kitaura, K.; Morokuma, K. "A new energy decomposition scheme for molecular interactions within the Hartree-Fock approximation" *Int. J. Quantum Chem.* 10, **1976,** 325.

Knop, O.; Rankin, K. N.; Boyd, R. J. "Coming to grips with N−H···N bonds. 2. homocorrelations between parameters deriving from the electron density at the bond critical point1" *J. Phys. Chem. A* 107, **2002,** 272.

Kobko, N.; Dannenberg, J. J. "Cooperativity in amide hydrogen bonding chains. a comparison between vibrational coupling through hydrogen bonds and covalent bonds. implications for peptide vibrational spectra" *J. Phys. Chem. A* 107, **2003a,** 6688.

Kobko, N.; Dannenberg, J. J. "Cooperativity in amide hydrogen bonding chains. relation between energy, position, and H-bond chain length in peptide and protein folding models" *J. Phys. Chem. A* 107, **2003b,** 10389.

Kobko, N.; Paraskevas, L.; del Rio, E.; Dannenberg, J. J. "Cooperativity in amide hydrogen bonding chains: implications for protein-folding models" *J. Am. Chem. Soc.* 123, **2001,** 4348.

Koch, U.; Popelier, P. L. A. "Characterization of C-H-O hydrogen bonds on the basis of the charge density" *J. Phys. Chem.* 99, **1995,** 9747.

Kocsis, A. J.; Yedama, N. A. R.; Cranford, S. W. "Confinement and controlling the effective compressive stiffness of carbyne" *Nanotechnology* 25, **2014,** 335709.

Kohn, W.; Sham, L. J. "Self-consistent equations including exchange and correlation effects" *Phys. Rev.* 140, **1965,** A1133.

Kollman, P. A.; Allen., L. C. *Chem. Rev.* 72, **1972,** 283

Krieger, J. B.; Chen, J. Q.; Iafrate, G. J.; Savin, A. *Electron correlations and materials properties*. Kluwer Academic: New York, **1999**.

Krieger, J. B.; Chen, J. Q.; Kurth, S. *Density functional theory and its application to materials*. A.I.P: New York, **2001**; Vol. 577.

Krukau, A. V.; Vydrov, O. A.; Izmaylov, A. F.; Scuseria, G. E. "Influence of the exchange screening parameter on the performance of screened hybrid functionals" *J. Chem. Phys* 125, **2006,** 224106: 1.

Kumar, A.; Gadre, S. R.; Mohan, N.; Suresh, C. H. "Lone pairs: an electrostatic viewpoint" *J. Phys. Chem. A* 118, **2014,** 526.

Kumler, W. D. "The effect of the hydrogen bond on the dielectric constants and boiling points of organic liquids" *J. Am. Chem. Soc.* 57, **1935,** 600.

La Manna, C. "Intermolecular potential of the acetonitrile dimer obtained from ab initio calculations" *Chem. Phys. Lett.* 103, **1983,** 55.

Lane, J. R.; Contreras-García, J.; Piquemal, J.-P.; Miller, B. J.; Kjaergaard, H. G. "Are bond critical points really critical for hydrogen bonding?" *J. Chem. Theory Comput.* 9, **2013,** 3263.

Lang, N. D.; Avouris, P. "Oscillatory conductance of carbon-atom wires" *Phys. Rev. Lett.* 81, **1998,** 3515.

Lang, N. D.; Avouris, P. "Carbon-atom wires: charge-transfer doping, voltage drop, and the effect of distortions" *Phys. Rev. Lett.* 84, **2000,** 358.

Lee, C.; Yang, W.; Parr, R. G. "Development of the Colle-Salvetti correlation-energy formula into a functional of the electron density" *Phys. Rev. B* 37, **1988,** 785.

Legon, A. C. "The halogen bond: an interim perspective" *Phys. Chem. Chem. Phys.* 12, **2010,** 7736.

Lehn, J.-M. "Towards self-organizationa and complex matter" *Science* 295, **2002,** 2400.

Li, Q.; Guo, X.; Yang, X.; Li, W.; Cheng, J.; Li, H.-B. "A σ-hole interaction with radical species as electron donors: does single-electron tetrel bonding exist?" *Phys. Chem. Chem. Phys.* 16, **2014,** 11617.

Li, Q.; Jiang, L.; Wang, X.; Li, W.; Cheng, J.; Sun, J. "Ab initio study of the structure, cooperativity, and vibrational properties in the mixed hydrogen-bonded trimers of hydrogen isocyanide and water" *Int. J. Quantum Chem.* 111, **2011,** 1072.

Li, Q.; Lin, Q.; Li, W.; Cheng, J.; Gong, B.; Sun, J. "Cooperativity between the Halogen Bond and the Hydrogen Bond in $H_3N\cdots XY\cdots HF$ Complexes (X, Y=F, Cl, Br)" *ChemPhysChem* 9, **2008,** 2265.

Lin, W.-H.; Tu, C.-C.; Lee, S.-L. "Theoretical studies of growth mechanism of small fullerene cage C_{24} $(D_{6d})^{+}$" *Int. J. Quantum Chem.* 103, **2005,** 355.

Liu, K.; Cruzan, J. D.; Saykally, R. J. "Water clusters" *Science* 271, **1996,** 929.

Liu, M.; Artyukhov, V. I.; Lee, H.; Xu, F.; Yakobson, B. I. "Carbyne from first principles: Chain of C atoms, a nanorod or a nanorope" *ACS Nano* 7, **2013,** 10075.

Lommerse, J. P. M.; Stone, A. J.; Taylor, R.; Allen, F. H. "The nature and geometry of intermolecular interactions between halogens and oxygen or nitrogen" *J. Am. Chem. Soc.* 118, **1996,** 3108.

Ludwig, R. "Cooperative hydrogen bonding in amides and peptides" *J. Mol. Liq.* 84, **2000,** 65.

Ludwig, R.; Appelhagen, A. "Calculation of clathrate-like water clusters including H_2O-Buckminsterfullerene" *Angew. Chem. Int. Ed.* 44, **2005,** 811.

Ludwig, R.; Weinhold, F.; Farrar, T. C. "Experimental and theoretical determination of the temperature dependence of deuteron and oxygen quadrupole coupling constants of liquid water" *J. Chem. Phys.* 103, **1995,** 6941.

Ludwig, R.; Weinhold, F.; Farrar, T. C. "Structure of liquid N-methylacetamide: temperature dependence of NMR chemical shifts and quadrupole coupling constants" *J. Phys. Chem. A* 101, **1997a,** 8861.

Ludwig, R.; Weinhold, F.; Farrar, T. C. "Theoretical study of hydrogen bonding in liquid and gaseous N-methylformamide" *J. Chem. Phys.* 107, **1997b,** 499.

Ludwig, R.; Weinhold, F.; Farrar, T. C. "Quantum cluster equilibrium theory of liquids part I: Molecular clusters and thermodynamics of liquid ammonia" *Berichte der Bunsengesellschaft für physikalische Chemie* 102, **1998,** 197.

Luu, T.; Elliott, E.; Slepkov, A. D.; Eisler, S.; McDonald, R.; Hegmann, F. A.; Tykwinski, R. R. "Synthesis, structure, and nonlinear optical properties of diarylpolyynes" *Org. Lett.* 7, **2004,** 51.

Mackie, I. D.; DiLabio, G. A. "Approximations to complete basis set-extrapolated, highly correlated non-covalent interaction energies" *J. Chem. Phys.* 135, **2011a,** 134318:1.

Mahadevi, A. S.; Neela, Y. I.; Sastry, G. N. "A theoretical study on structural, spectroscopic and energetic properties of acetamide clusters [CH_3CONH_2] (n = 1-15)" *Phys. Chem. Chem. Phys.* 13, **2011,** 15211.

Mahadevi, A. S.; Sastry, G. N. "Cooperativity in Noncovalent Interactions" *Chem. Rev.* 116, **2016,** 2775.

Maheshwary, S.; Patel, N.; Sathyamurthy, N.; Kulkarni, A. D.; Gadre, S. R. "Structure and stability of water clusters $(H_2O)_n$, n = 8−20: An *ab initio* investigation" *J. Phys. Chem. A* 105, **2001,** 10525.

Mani, D.; Arunan, E. "The X-CY (X = O/F, Y = O/S/F/Cl/Br/N/P) 'carbon bond' and hydrophobic interactions" *Phys. Chem. Chem. Phys.* 15, **2013,** 14377.

Mani, D.; Arunan, E. "The X–C$\cdots\pi$ (X = F, Cl, Br, CN) carbon bond" *J. Phys. Chem. A* 118, **2014,** 10081.

Manna, D.; Mugesh, G. "Regioselective deiodination of thyroxine by iodothyronine deiodinase mimics: An unusual mechanistic pathway involving cooperative chalcogen and halogen bonding" *J. Am. Chem. Soc.* 134, **2012,** 4269.

Marom, N.; Tkatchenko, A.; Rossi, M.; Gobre, V. V.; Hod, O.; Scheffler, M.; Kronik, L. "Dispersion interactions with density-functional theory: benchmarking semiempirical

and interatomic pairwise corrected density functionals" *J. Chem. Theory Comput.* 7, **2011,** 3944.

Masunov, A.; Dannenberg, J. J. "Theoretical study of urea and thiourea. 2. Chains and ribbons" *J. Phys. Chem. B* 104, **2000,** 806.

Mata, R. A.; Costa Cabral, B. J. "Structural, energetic, and electronic properties of $(CH_3CN)_{2-8}$ clusters by density functional theory" *J. Mol. Struct. THEOCHEM* 673, **2004,** 155.

Mathieu, D.; Defranceschi, M.; Delhalle, J. "Ab initio study of the influence of aggregation on the infrared spectrum of acetonitrile" *Int. J. Quantum Chem.* 45, **1993,** 735.

McDowell, S. A. C. "σ-hole cooperativity in anionic $[FX\cdots CH_3\cdots YF]^-$ (X, Y = Cl, Br) complexes" *Chem. Phys. Lett.* 598, **2014,** 1.

McDowell, S. A. C.; Buckingham, A. D. "Cooperative and diminutive hydrogen bonding in Y···HCN···HCN and NCH···Y···HCN trimers (Y=BF,CO,N_2)" *J. Chem. Phys.* 132, **2010,** 064303.

McDowell, S. A. C.; Joseph, J. A. "The effect of atomic ions on model σ-hole bonded complexes of AH_3Y (A = C, Si, Ge; Y = F, Cl, Br)" *Phys. Chem. Chem. Phys.* 16, **2014,** 10854.

Metrangolo, P.; Resnati, G. "Halogen bonding: A paradigm in supramolecular chemistry" *Chem. Eur. J.* 7, **2001,** 2511.

Metrangolo, P.; Resnati, G. "Halogen versus hydrogen" *Science* 321, **2008,** 918.

Metrangolo, P.; Resnati, G.; Pilati, T.; Biella, S. Halogen bonding in crystal engineering. In *Halogen bonding*, P. Metrangolo, G. Resnati, Eds. Springer Berlin Heidelberg: 2008; Vol. 126, pp 105.

Miehlich, B.; Savin, A.; Stoll, H.; Preuss, H. "Results obtained with the correlation-energy density functionals of Becke and Lee, Yang and Parr" *Chem. Phys. Lett.* 157 **1989,** 200.

Mirzaeifar, R.; Qin, Z.; Buehler, M. J. "Tensile strength of carbyne chains in varied chemical environments and structural lengths" *Nanotechnology* 25, **2014,** 371001.

Mohan, N.; Suresh, C. H. "Accurate binding energies of hydrogen, halogen, and dihydrogen bonded complexes and cation enhanced binding strengths" *Int. J. Quantum Chem.* 114, **2014a,** 885.

Mohan, N.; Suresh, C. H. "A molecular electrostatic potential analysis of hydrogen, halogen, and dihydrogen bonds" *J. Phys. Chem. A* 118, **2014b,** 1697.

Mohan, N.; Suresh, C. H.; Kumar, A.; Gadre, S. R. "Molecular electrostatics for probing lone pair-π interactions" *Phys. Chem. Chem. Phys.* 15, **2013,** 18401.

Murray, J.; Lane, P.; Clark, T.; Politzer, P. "σ-hole bonding: molecules containing group VI atoms" *J. Mol. Model.* 13, **2007a,** 1033.

Murray, J.; Lane, P.; Politzer, P. "Expansion of the σ-hole concept" *J. Mol. Model.* 15, **2009,** 723.

Murray, J. S.; Lane, P.; Politzer, P. "A predicted new type of directional noncovalent interaction" *Int. J. Quantum Chem.* 107, **2007b,** 2286.

Murray, J. S.; Macaveiu, L.; Politzer, P. "Factors affecting the strengths of σ-hole electrostatic potentials" *J. Comput. Sci.* 5, **2014,** 590

Murray, J. S.; Paulsen, K.; Politzer, P. "Molecular surface electrostatic potentials in the analysis of non-hydrogen-bonding noncovalent interactions." *Proc. Ind. Acad. Sci. (Chem. Sci.)* 106, **1994,** 267.

Murray, J. S.; Sen, K. *Molecular electrostatic potentials: concepts and applications*. Elsevier Science: Amsterdam, The Netherlands, **1996**.

Nagao, Y.; Hirata, T.; Goto, S.; Sano, S.; Kakehi, A.; Iizuka, K.; Shiro, M. "Intramolecular nonbonded S···O interaction recognized in (acylimino)thiadiazoline derivatives as angiotensin ii receptor antagonists and related compounds" *J. Am. Chem. Soc.* 120, **1998,** 3104.

Nair, A. K.; Cranford, S. W.; Buehler, M. J. "The minimal nanowire: Mechanical properties of carbyne" *Europhys. Lett.* 95, **2011,** 16002.

Neela, Y. I.; Mahadevi, A. S.; Sastry, G. N. "Hydrogen bonding in water clusters and their ionized counterparts" *J. Phys. Chem. B* 114, **2010,** 17162.

Nigam, S.; Majumder, C. "Growth pattern and electronic properties of acetonitrile clusters: A density functional study" *J. Chem. Phys.* 128, **2008**.

Orabi, E. A.; Lamoureux, G. "Molecular dynamics investigation of alkali metal ions in liquid and aqueous ammonia" *J. Chem. Theory Comput.* 9, **2013,** 2324.

Parra, R. D.; Bulusu, S.; Zeng, X. C. "Cooperative effects in two-dimensional ring-like networks of three-center hydrogen bonding interactions" *J. Chem. Phys.* 122, **2005,** 184325.

Parra, R. D.; Furukawa, M.; Gong, B.; Zeng, X. C. "Energetics and cooperativity in three-center hydrogen bonding interactions. I. Diacetamide-X dimers (X=HCN,CH_3OH)" *J. Chem. Phys.* 115, **2001,** 6030.

Parra, R. D.; Ohlssen, J. "Cooperativity in intramolecular bifurcated hydrogen bonds: an ab initio study" *J. Phys. Chem. A* 112, **2008,** 3492.

Parra, R. D.; Streu, K. "Cooperative effects in regular and bifurcated intramolecular OH···OC interactions: A computational study" *Comput. Theor. Chem.* 977, **2011,** 181.

Parthasarathi, R.; Subramanian, V.; Sathyamurthy, N. "Hydrogen bonding without borders: an atoms-in-molecules perspective" *J. Phys. Chem. A* 110, **2006,** 3349.

Pauling, L. *The nature of the chemical bond*. Cornell University Press, Ithaca: New York, **1960**.

Pedireddi, V. R.; Reddy, D. S.; Goud, B. S.; Craig, D. C.; Rae, A. D.; Desiraju, G. R. "The nature of halogen…halogen interactions and the crystal structure of 1,3,5,7-tetraiodoadamantane" *J. Chem. Soc., Perkin Trans. 2* **1994,** 2353.

Perdew, J. P. "Density-functional approximation for the correlation energy of the inhomogeneous electron gas" *Phys. Rev. B* 33, **1986,** 8822.

Perdew, J. P. *Electronic structure of solids '91* Akademie Verlag: Berlin, **1991**; Vol. 11.

Perdew, J. P.; Burke, K.; Ernzerhof, M. "Generalized gradient approximation made simple" *Phys. Rev. Lett.* 77, **1996a,** 3865.

Perdew, J. P.; Burke, K.; Ernzerhof, M. "Errata: Generalized gradient approximation made simple" *Phys. Rev. Lett.* 78, **1997,** 1396.

Perdew, J. P.; Burke, K.; Wang, Y. "Generalized gradient approximation for the exchange-correlation hole of a many-electron system" *Phys. Rev. B* 54, **1996b,** 16533.

Perdew, J. P.; Chevary, J. A.; Vosko, S. H.; Jackson, K. A.; Pederson, M. R.; Singh, D. J.; Fiolhais, C. "Atoms, molecules, solids, and surfaces: Applications of the generalized gradient approximation for exchange and correlation" *Phys. Rev. B* 46, **1992,** 6671.

Perdew, J. P.; Chevary, J. A.; Vosko, S. H.; Jackson, K. A.; Pederson, M. R.; Singh, D. J.; Fiolhais, C. "Erratum: Atoms, molecules, solids, and surfaces - Applications of the generalized gradient approximation for exchange and correlation" *Phys. Rev. B* 48, **1993,** 4978.

Perdew, J. P.; Kurth, S.; Zupan, A.; Blaha, P. "Accurate density functional with correct formal properties: A step beyond the generalized gradient approximation" *Phys. Rev. Lett.* 82, **1999,** 2544.

Perdew, J. P.; Ruzsinszky, A.; Constantin, L. A.; Sun, J.; Csonka, G. I. "Some fundamental issues in ground-state density functional theory: A guide for the perplexed" *J. Chem. Theory Comput.* 5, **2009,** 902.

Perdew, J. P.; Ruzsinszky, A.; Tao, J.; Staroverov, V. N.; Scuseria, G. E.; Csonka, G. I. "Prescription for the design and selection of density functional approximations: More constraint satisfaction with fewer fits" *J. Chem. Phys* 123, **2005,** 062201: 1.

Perdew, J. P.; Schmidt, K. "Jacob's ladder of density functional approximations for the exchange-correlation energy" *AIP Conference Proceedings* 577, **2001,** 1.

Perdew, J. P.; Zunger, A. ""Self-interaction correction to density-functional approximations for many-electron systems," *Phys. Rev. B* 23, **1981,** 5048.

Pérez, A.; Sponer, J.; Jurecka, P.; Hobza, P.; Luque, F. J.; Orozco, M. "Are the hydrogen bonds of RNA (A·U) stronger than those of DNA (A·T)? a quantum mechanics study" *Chem. Eur. J.* 11, **2005,** 5062.

Perutz, M. F. "Mechanisms of cooperativity and allosteric regulation in proteins" *Q. Rev. Biophys.* 22, **1989,** 139

Poater, J.; Solà, M.; Bickelhaupt, F. M. "Hydrogen–hydrogen bonding in planar biphenyl, predicted by atoms-in-molecules theory, does not exist" *Chem. Eur. J.* 12, **2006a,** 2889.

Poater, J.; Solà, M.; Bickelhaupt, F. M. "A model of the chemical bond must be rooted in quantum mechanics, provide insight, and possess predictive power" *Chem. Eur. J.* 12, **2006b,** 2902.

Politzer, P.; Murray, J. "Some molecular/crystalline factors that affect the sensitivities of energetic materials: molecular surface electrostatic potentials, lattice free space and maximum heat of detonation per unit volume" *J. Mol. Model.* 21, **2015,** 1.

Politzer, P.; Murray, J.; Clark, T. "Mathematical modeling and physical reality in noncovalent interactions" *J. Mol. Model.* 21, **2015,** 1.

Politzer, P.; Murray, J. S. "Halogen bonding: An interim discussion" *ChemPhysChem* 14, **2013,** 278.

Politzer, P.; Murray, J. S.; Clark, T. "Halogen bonding and other σ-hole interactions: a perspective" *Phys. Chem. Chem. Phys.* 15, **2013,** 11178.

Politzer, P.; Truhlar, D. G. *Chemical applications of atomic and molecular electrostatic potentials: reactivity, structure, scattering: Energetics of organic, inorganic, and biological systems*. Springer: New York, **1981**.

Popelier, P. L. A. "Characterization of a dihydrogen bond on the basis of the electron density" *J. Phys. Chem. A* 102, **1998,** 1873.

Raghavachari, K.; Binkley, J. S. "Structure, stability, and fragmentation of small carbon clusters" *J. Chem. Phys.* 87, **1987,** 2191.

Rama, K. M.; Lin, Y.-T.; Lee, S.-L. "C_{28} (D_2): Fullerene growth mechanism" *Int. J. Quantum Chem.* 84, **2001,** 642.

Ravagnan, L.; Manini, N.; Cinquanta, E.; Onida, G.; Sangalli, D.; Motta, C.; Devetta, M.; Bordoni, A.; Piseri, P.; Milani, P. "Effect of axial torsion on *sp* carbon atomic wires" *Phys. Rev. Lett.* 102, **2009,** 245502.

Ravagnan, L.; Piseri, P.; Bruzzi, M.; Miglio, S.; Bongiorno, G.; Baserga, A.; Casari, C. S.; Li Bassi, A.; Lenardi, C.; Yamaguchi, Y.; Wakabayashi, T.; Bottani, C. E.; Milani, P. "Influence of cumulenic chains on the vibrational and electronic properties of *sp-sp*^{2} amorphous carbon" *Phys. Rev. Lett.* 98, **2007,** 216103.

Ravagnan, L.; Siviero, F.; Lenardi, C.; Piseri, P.; Barborini, E.; Milani, P.; Casari, C. S.; Li Bassi, A.; Bottani, C. E. "Cluster-beam deposition and *in situ* characterization of carbyne-rich carbon films" *Phys. Rev. Lett.* 89, **2002,** 285506.

Remya, K.; Suresh, C. H. "Which density functional is close to CCSD accuracy to describe geometry and interaction energy of small non-covalent dimers? A benchmark study using gaussian09" *J. Comput. Chem.* 34, **2013,** 1341.

Remya, K.; Suresh, C. H. "Cooperativity and cluster growth patterns in acetonitrile: A DFT study" *J. Comput. Chem.* 35, **2014,** 910.

Remya, K.; Suresh, C. H. "Intermolecular carbon-carbon, nitrogen-nitrogen and oxygen-oxygen non-covalent bonding in dipolar molecules" *Phys. Chem. Chem. Phys.* 17, **2015a,** 18380.

Remya, K.; Suresh, C. H. "Non-covalent intermolecular carbon-carbon interactions in polyynes" *Phys. Chem. Chem. Phys.* 17, **2015b,** 27035.

Remya, K.; Suresh, C. H. "Carbon rings: a DFT study on geometry, aromaticity, intermolecular carbon-carbon interactions and stability" *RSC Adv.* 6, **2016,** 44261.

Rey, J.; Savin, A. "Virtual space level shifting and correlation energies" *Int. J. Quantum Chem.* 69, **1998,** 581.

Řezáč, J.; Riley, K. E.; Hobza, P. "S66: A well-balanced database of benchmark interaction energies relevant to biomolecular structures" *J. Chem. Theory Comput.* 7, **2011,** 2427.

Řezáč, J.; Riley, K. E.; Hobza, P. "Benchmark calculations of noncovalent interactions of halogenated molecules" *J. Chem. Theory Comput.* 8, **2012a,** 4285.

Řezáč, J.; Riley, K. E.; Hobza, P. "Evaluation of the performance of post-Hartree-Fock methods in terms of intermolecular distance in noncovalent complexes" *J. Comput. Chem.* 33, **2012b,** 691.

Richardi, J.; Fries, P. H.; Krienke, H. "The solvation of ions in acetonitrile and acetone: A molecular Ornstein--Zernike study" *J. Chem. Phys.* 108, **1998,** 4079.

Riley, K. E.; Pitoňák, M.; Jurečka, P.; Hobza, P. "Stabilization and Structure calculations for noncovalent interactions in extended molecular systems based on wave function and density functional theories" *Chem. Rev.* 110, **2010,** 5023.

Rincón, L.; Almeida, R.; García-Aldea, D.; Diez y Riega, H. "Hydrogen bond cooperativity and electron delocalization in hydrogen fluoride clusters" *J. Chem. Phys.* 114, **2001,** 5552.

Robertson, W. H.; Karapetian, K.; Ayotte, P.; Jordan, K. D.; Johnson, M. A. "Infrared predissociation spectroscopy of $I^-\cdot(CH_3OH)_n$, n=1,2: Cooperativity in asymmetric solvation" *J. Chem. Phys.* 116, **2002,** 4853.

Rosenfield, R. E.; Parthasarathy, R.; Dunitz, J. D. "Directional preferences of nonbonded atomic contacts with divalent sulfur. 1. Electrophiles and nucleophiles" *J. Am. Chem. Soc.* 99, **1977,** 4860.

Row, T. N. G.; Parthasarathy, R. "Directional preferences of nonbonded atomic contacts with divalent sulfur in terms of its orbital orientations. 2. S...S interactions and nonspherical shape of sulfur in crystals" *J. Am. Chem. Soc.* 103, **1981,** 477.

Saito, M.; Okamoto, Y. "Second-order Jahn-Teller effect on carbon 4N+2 member ring clusters" *Phys. Rev. B* 60, **1999,** 8939.

Sanchez-Sanz, G.; Trujillo, C.; Solimannejad, M.; Alkorta, I.; Elguero, J. "Orthogonal interactions between nitryl derivatives and electron donors: pnictogen bonds" *Phys. Chem. Chem. Phys.* 15, **2013,** 14310.

Scheiner, S. *Hydrogen bonding : A theoretical perspective*. Oxford University Press: New York, **1997**.

Scheiner, S. "Effects of multiple substitution upon the P···N noncovalent interaction" *Chem. Phys.* 387, **2011a,** 79.

Scheiner, S. "A new noncovalent force: Comparison of P···N interaction with hydrogen and halogen bonds" *J. Chem. Phys.* 134, **2011b,** 094315.

Scheiner, S. "On the properties of X···N noncovalent interactions for first-, second-, and third-row X atoms" *J. Chem. Phys.* 134, **2011c,** 164313.

Scheiner, S. "Detailed comparison of the pnicogen bond with chalcogen, halogen, and hydrogen bonds" *Int. J. Quantum Chem.* 113, **2013,** 1609.

Schleyer, P. v. R.; Jiao, H.; Hommes, N. J. R. v. E.; Malkin, V. G.; Malkina, O. L. "An evaluation of the aromaticity of inorganic rings: refined evidence from magnetic properties" *J. Am. Chem. Soc.* 119, **1997,** 12669.

Schleyer, P. v. R.; Maerker, C.; Dransfeld, A.; Jiao, H.; Hommes, N. J. R. v. E. "Nucleus-independent chemical shifts: a simple and efficient aromaticity probe" *J. Am. Chem. Soc.* 118, **1996,** 6317.

Schmider, H. L.; Becke, A. D. "Optimized density functionals from the extended G2 test set" *J. Chem. Phys* 108, **1998,** 9624.

Schwabe, T.; Grimme, S. "Towards chemical accuracy for the thermodynamics of large molecules: new hybrid density functionals including non-local correlation effects" *Phys. Chem. Chem. Phys.* 8, **2006,** 4398.

Schwabe, T.; Grimme, S. "Double-hybrid density functionals with long-range dispersion corrections: higher accuracy and extended applicability" *Phys. Chem. Chem. Phys.* 9, **2007,** 3397.

Schwarz, H. "The mechanism of fullerence formation" *Angew. Chem. Int. Ed.* 32, **1993,** 1412.

Schweigert, V. A.; Alexandrov, A. L.; Morokov, Y. N.; Bedanov, V. M. "MINDO/3 study of the interaction of small carbon clusters" *Chem. Phys. Lett.* 238, **1995,** 110.

Sen, S.; Seal, P.; Chakrabarti, S. "Explicit role of dynamical and nondynamical electron correlations on broken symmetry in C_{4N+2} clusters" *Phys. Rev. B* 73, **2006,** 245401.

Shahi, A.; Arunan, E. "Hydrogen bonding, halogen bonding and lithium bonding: an atoms in molecules and natural bond orbital perspective towards conservation of total bond order, inter- and intra-molecular bonding" *Phys. Chem. Chem. Phys.* 16, **2014,** 22935.

Shelimov, K. B.; Hunter, J. M.; Jarrold, M. F. "Small carbon rings: dissociation, isomerization, and a simple model based on strain" *Int. J. Mass Spectrom. Ion Processes* 138, **1994,** 17.

Sherrill, C. D.; Takatani, T.; Hohenstein, E. G. *J. Phys. Chem. A* 113, **2009,** 10146.

Shi Shun, A. L. K.; Tykwinski, R. R. "Synthesis of naturally occurring polyynes" *Angew. Chem. Int. Ed.* 45, **2006,** 1034.

Siebers, J. G.; Buck, U.; Beu, T. A. "Calculation of structures and vibrational spectra of acetonitrile clusters" *Chem. Phys.* 239, **1998,** 549.

Sjoberg, P.; Politzer, P. "Use of the electrostatic potential at the molecular surface to interpret and predict nucleophilic processes" *J.Phys. Chem.* 94, **1990,** 3959.

Slater, J. C. *The self-consistent field for molecular and solids, quantum theory of molecular and solids*. McGraw-Hill: New York, **1974**; Vol. 4.

Slepkov, A. D.; Hegmann, F. A.; Eisler, S.; Elliott, E.; Tykwinski, R. R. "The surprising nonlinear optical properties of conjugated polyyne oligomers" *J. Chem. Phys.* 120, **2004,** 6807.

Solimannejad, M.; Gharabaghi, M.; Scheiner, S. "SH···N and SH···P blue-shifting H-bonds and N···P interactions in complexes pairing HSN with amines and phosphines" *J. Chem. Phys.* 134, **2011,** 024312.

Song, Y.; Akin-Ojo, O.; Wang, F. "Correcting for dispersion interaction and beyond in density functional theory through force matching" *J. Chem. Phys.* 133, **2010,** 174115.

Sorokin, P. B.; Lee, H.; Antipina, L. Y.; Singh, A. K.; Yakobson, B. I. "Calcium-decorated carbyne networks as hydrogen storage media" *Nano Lett.* 11, **2011,** 2660.

Šponer, J.; Jurečka, P.; Hobza, P. "Accurate interaction energies of hydrogen-bonded nucleic acid base pairs" *J. Am. Chem. Soc.* 126, **2004,** 10142.

Steinmann, S. N.; Corminboeuf, C. "A system-dependent density-based dispersion correction" *J. Chem. Theory Comput.* 6, **2010,** 1990.

Suhai, S. "Cooperative effects in hydrogen bonding: Fourth-order many-body perturbation theory studies of water oligomers and of an infinite water chain as a model for ice" *J. Chem. Phys.* 101, **1994a,** 9766.

Suhai, S. "Cooperativity and electron correlation effects on hydrogen bonding in infinite systems" *Int. J. Quantum Chem.* 52, **1994b,** 395.

Suhai, S. "Density functional theory of molecular solids: local versus periodic effects in the two-dimensional infinite hydrogen-bonded sheet of formamide" *J. Chem. Phys.* 100, **1996,** 3950.

Sum, A. K.; Sandler, S. I. "Ab initio calculations of cooperativity effects on clusters of methanol, ethanol, 1-propanol, and methanethiol" *J. Phys. Chem. A* 104, **2000,** 1121.

Sun, Y. Y.; Lee, K.; Wang, L.; Kim, Y.-H.; Chen, W.; Chen, Z.; Zhang, S. B. "Accuracy of density functional theory methods for weakly bonded systems: The case of dihydrogen binding on metal centers" *Phys. Rev. B* 82, **2010,** 073401.

Sutor, D. "The structures of the pyrimidines and purines. VII. The crystal structure of caffeine" *Acta Crystallogr.* 11, **1958,** 453.

Szabo, A.; Ostlund, N. S. *Modern quantum chemistry: Introduction to advanced electronic structure theory*. Dover Publications, INC.: Mineola, New York, **1989**.

Szafert, S.; Gladysz, J. A. "Carbon in one dimension: Structural analysis of the higher conjugated polyynes" *Chem. Rev.* 103, **2003,** 4175.

Takatani, T.; Hohenstein, E. G.; Malagoli, M.; Marshall, M. S.; Sherrill, C. D. "Basis set consistent revision of the S22 test set of noncovalent interaction energies" *J. Chem. Phys.* 132, **2010,** 144104.

Tan, H.; Qu, W.; Chen, G.; Liu, R. "The Role of charge transfer in the hydrogen bond cooperative effect of *cis*-N-methylformamide oligomers" *J. Phys. Chem. A* 109, **2005,** 6303.

Tao, J.; Perdew, J. P. "Climbing the density functional ladder: nonempirical meta-generalized gradient approximation designed for molecules and solids" *Phys. Rev. Lett.* 91, **2003,** 146401: 1.

Tawada, Y.; Tsuneda, T.; Yanagisawa, S.; Yanai, T.; Hirao, K. "A long-range-corrected time-dependent density functional theory" *J. Chem. Phys* 120, **2004,** 8425.

Taylor, J.; Brandbyge, M.; Stokbro, K. "Conductance switching in a molecular device: The role of side groups and intermolecular interactions" *Phys. Rev. B* 68, **2003,** 121101.

te Velde, G.; Bickelhaupt, F. M.; Baerends, E. J.; Fonseca Guerra, C.; van Gisbergen, S. J. A.; Snijders, J. G.; Ziegler, T. "Chemistry with ADF" *J. Comput. Chem.* 22, **2001,** 931.

Thomas, S. P.; Pavan, M. S.; Guru Row, T. N. "Experimental evidence for 'carbon bonding' in the solid state from charge density analysis" *Chem. Commun.* 50, **2014,** 49.

Tomasi, J.; Mennucci, B.; Cammi, R. *A tool for interpretation and prediction. From Molecular structure to solvation effects. In molecular electrostatic potentials: concepts and applications*. Elsevier: Amsterdam, **1996**.

Tongay, S.; Dag, S.; Durgun, E.; Senger, R. T.; Ciraci, S. "Atomic and electronic structure of carbon strings" *J. Phys.: Condens. Matter* 17, **2005,** 3823.

Tongay, S.; Senger, R. T.; Dag, S.; Ciraci, S. "*Ab-initio* electron transport calculations of carbon based string structures" *Phys. Rev. Lett.* 93, **2004,** 136404.

Torelli, T.; Mitas, L. "Electron correlation in C_{4N+2} carbon rings: Aromatic versus Dimerized structures" *Phys. Rev. Lett.* 85, **2000,** 1702.

Torres, E.; DiLabio, G. A. "A (Nearly) universally applicable method for modeling noncovalent interactions using B3LYP" *J. Phys. Chem. Lett.* 3, **2012,** 1738.

Torrie, B. H.; Powell, B. M. "Phase transition in solid acetonitrile" *Mol. Phys.* 75, **1992,** 613.

Toulouse, J.; Savin, A.; Adamo, C. "Validation and assessment of an accurate approach to the correlation problem in density functional theory: The Krieger-Chen-Iafrate-Savin model" *J. Chem. Phys* 117, **2002,** 10465.

Turi, L.; Dannenberg, J. J. "Molecular orbital studies of crystalline nitroanilines" *J. Phys. Chem.* 100, **1996,** 9638.

Tykwinski, R. R.; Kendall, J.; McDonald, R. "Thieme chemistry journal awardees - where are they now? pentafluorophenyl end-capped polyynes as supramolecular building blocks" *Synlett* 2009, **2009,** 2068.

van Gisbergen, S. J. A.; Snijders, J. G.; Baerends, E. J. "Accurate density functional calculations on frequency-dependent hyperpolarizabilities of small molecules" *J. Chem. Phys.* 109, **1998,** 10657.

Van Orden, A.; Saykally, R. J. "Small carbon clusters: spectroscopy, structure, and energetics" *Chem. Rev.* 98, **1998,** 2313.

Varadwaj, P. R.; Varadwaj, A.; Jin, B.-Y. "Significant evidence of CO and CC long-range contacts in several heterodimeric complexes of CO with CH_3-X, should one refer to them as carbon and dicarbon bonds!" *Phys. Chem. Chem. Phys.* 16, **2014,** 17238.

Vijay, D.; Zipse, H.; Sastry, G. N. "On the cooperativity of cation−π and hydrogen bonding interactions" *J. Phys. Chem. B* 112, **2008,** 8863.

Viswanathan, R.; Dannenberg, J. J. "A density functional theory study of vibrational coupling in the amide I band of β-sheet models" *J. Phys. Chem. B* 112, **2008,** 5199.

von Helden, G.; Gotts, N. G.; Maitre, P.; Bowers, M. T. "The structures of small iron-carbon cluster anions. Linear to planar to three-dimensional" *Chem. Phys. Lett.* 227, **1994,** 601.

von Helden, G.; Hsu, M. T.; Gotts, N.; Bowers, M. T. "Carbon cluster cations with up to 84 atoms: structures, formation mechanism, and reactivity" *J. Phys. Chem.* 97, **1993,** 8182.

von Helden, G.; Hsu, M. T.; Kemper, P. R.; Bowers, M. T. "Structures of carbon cluster ions from 3 to 60 atoms: Linears to rings to fullerenes" *J. Chem. Phys.* 95, **1991,** 3835.

Vondrášek, J.; Bendová, L.; Klusák, V.; Hobza, P. "Unexpectedly Strong energy stabilization inside the hydrophobic core of small protein rubredoxin mediated by aromatic residues: correlated ab initio quantum chemical calculations" *J. Am. Chem. Soc.* 127, **2005,** 2615.

Voorhis, T. V.; Scuseria, G. E. "A novel form for the exchange-correlation energy functional" *J. Chem. Phys* 109, **1998,** 400.

Vosko, S. H.; Wilk, L.; Nusair, M. "Accurate spin-dependent electron liquid correlation energies for local spin density calculations: A critical analysis" *Can. J. Phys.* 58, **1980,** 1200.

Vydrov, O. A.; Scuseria, G. E. "Assessment of a long range corrected hybrid functional" *J. Chem. Phys* 125, **2006,** 234109: 1.

Vydrov, O. A.; Scuseria, G. E.; Perdew, J. P. "Tests of functionals for systems with fractional electron number" *J. Chem. Phys* 126, **2007,** 154109: 1.

Vydrov, O. A.; Van Voorhis, T. "Nonlocal van der Waals density functional: The simpler the better" *J. Chem. Phys.* 133, **2010,** 244103.

Vydrov, O. A.; Wu, Q.; Van Voorhis, T. "Self-consistent implementation of a nonlocal van der Waals density functional with a Gaussian basis set" *J. Chem. Phys.* 129, **2008,** 014106.

Wakabayashi, T.; Kohno, M.; Achiba, Y.; Shiromaru, H.; Momose, T.; Shida, T.; Naemura, K.; Tobe, Y. "Photoelectron spectroscopy of C_n^- produced from laser ablated dehydroannulene derivatives having carbon ring size of n=12, 16, 18, 20, and 24" *J. Chem. Phys.* 107, **1997,** 4783.

Wang, C.; Batsanov, A. S.; Bryce, M. R.; Martín, S.; Nichols, R. J.; Higgins, S. J.; García-Suárez, V. M.; Lambert, C. J. "Oligoyne Single molecule wires" *J. Am. Chem. Soc.* 131, **2009a,** 15647.

Wang, C.; Batsanov, A. S.; West, K.; Bryce, M. R. "Synthesis and crystal structures of isolable terminal aryl hexatriyne and octatetrayne derivatives: Ar−$(C{\equiv}C)_n$H (n = 3, 4)" *Org. Lett.* 10, **2008,** 3069.

Wang, C.; Danovich, D.; Mo, Y.; Shaik, S. "On The nature of the halogen bond" *J. Chem. Theory Comput.* 10, **2014,** 3726.

Wang, W.; Ji, B.; Zhang, Y. "Chalcogen bond: a sister noncovalent bond to halogen bond" *J. Phys. Chem. A* 113, **2009b,** 8132.

Weinhold, F.; Landis, C. R. *Valency and bonding: A natural bond orbital donor-acceptor perspective*. Cambridge University Press: UK, **2005**.

Werz, D. B.; Gleiter, R.; Rominger, F. "Nanotube formation favored by chalcogen−chalcogen interactions" *J. Am. Chem. Soc.* 124, **2002,** 10638.

Whittaker, A. G.; Watts, E. J.; Lewis, R. S.; Anders, E. "Carbynes: Carriers of primordial noble gases in meteorites" *Science* 209, **1980,** 1512.

Wieczorek, R.; Dannenberg, J. J. "H-bonding cooperativity and energetics of α-helix formation of five 17-amino acid peptides" *J. Am. Chem. Soc.* 125, **2003a,** 8124.

Wieczorek, R.; Dannenberg, J. J. "Hydrogen-bond cooperativity, vibrational coupling, and dependence of helix stability on changes in amino acid sequence in small 3_{10}-helical peptides. a density functional theory study" *J. Am. Chem. Soc.* 125, **2003b,** 14065.

Wilson, P. J.; Bradley, T. J.; Tozer, D. J. "Hybrid exchange-correlation functional determined from thermochemical data and ab initio potentials" *J. Chem. Phys* 115, **2001,** 9233.

Wodrich, M. D.; Corminboeuf, C.; Park, S. S.; Schleyer, P. v. R. "Double aromaticity in monocyclic carbon, boron, and borocarbon rings based on magnetic criteria" *Chem. Eur. J.* 13, **2007,** 4582.

Wu, X.; Vargas, M. C.; Nayak, S.; Lotrich, V.; Scoles, G. "Towards extending the applicability of density functional theory to weakly bound systems" *J. Chem. Phys* 115, **2001,** 8748.

Wu, Y.-D.; Zhao, Y.-L. "A theoretical study on the origin of cooperativity in the formation of 3_{10}- and α-helices" *J. Am. Chem. Soc.* 123, **2001,** 5313.

Wulf, O. R.; Liddel, U.; Henricks, S. B." The effect of ortho substitution on the absorption of the OH group of phenol in the infrared1" *J. Am. Chem. Soc.* 58, **1936,** 2287

Xantheas, S. S. "Cooperativity and hydrogen bonding network in water clusters" *Chem. Phys.* 258, **2000,** 225.

Xia, Q. Y.; Xiao, H. M.; Ju, X. H.; Gong, X. D. "DFT study on cooperativity in the interactions of hydrazoic acid clusters" *Int. J. Quantum Chem.* 94, **2003,** 279.

Xu, S.-h.; Zhang, M.-y.; Zhao, Y.-y.; Chen, B.-g.; Zhang, J.; Sun, C.-C. "Stability and properties of planar carbon clusters" *Chem. Phys. Lett.* 421, **2006a,** 444.

Xu, W.; Li, X.-C.; Tan, H.; Chen, G.-J. "Theoretical study on stabilities of multiple hydrogen bonded dimers" *Phys. Chem. Chem. Phys.* 8, **2006b,** 4427.

Xu, X.; III, W. A. G. "The X3LYP extended density functional for accurate descriptions of nonbond interactions, spin states, and thermochemical properties" *PNAS* 101, **2004,** 2673.

Yanai, T.; Tew, D.; Handy, N. "A new hybrid exchange-correlation functional using the Coulomb-attenuating method (CAM-B3LYP)" *Chem. Phys. Lett.* 393, **2004,** 51.

Ylva, A.; Henrik, R. "Dispersion coefficients for van der Waals complexes, including C_{60} – C_{60}" *Phys. Scr.* 60, **1999,** 211.

Young, D. C. *Computational chemistry: A practical guide for applying techniques to real-world problems*. Wiley-Interscience: New York, **2001**.

Zahn, S.; Frank, R.; Hey-Hawkins, E.; Kirchner, B. "Pnicogen bonds: A new molecular linker?" *Chem. Eur. J.* 17, **2011,** 6034.

Zanolli, Z.; Onida, G.; Charlier, J. C. "Quantum spin transport in carbon chains" *ACS Nano* 4, **2010,** 5174.

Zhang, I. Y.; Wu, J.; Xu, X. "Extending the reliability and applicability of B3LYP" *Chem. Commun.* 46, **2010,** 3057.

Zhao, Y.-L.; Wu, Y.-D. "A theoretical study of β-sheet models: Is the formation of hydrogen-bond networks cooperative?" *J. Am. Chem. Soc.* 124, **2002,** 1570.

Zhao, Y.; Schultz, N. E.; Truhlar, D. G. "Exchange-correlation functional with broad accuracy for metallic and nonmetallic compounds, kinetics, and noncovalent interactions" *J. Chem. Phys.* 123, **2005,** 161103.

Zhao, Y.; Schultz, N. E.; Truhlar, D. G. "Design of density functionals by combining the method of constraint satisfaction with parametrization for thermochemistry, thermochemical kinetics, and noncovalent interactions" *J. Chem. Theory and Comput.* 2, **2006,** 364.

Zhao, Y.; Truhlar, D. G. "Benchmark databases for nonbonded interactions and their use to test density functional theory" *J. Chem. Theory Comput.* 1, **2005a,** 415.

Zhao, Y.; Truhlar, D. G. "Design of density functionals that are broadly accurate for thermochemistry, thermochemical kinetics, and nonbonded interactions" *J. Phys. Chem. A* 109, **2005b,** 5656.

Zhao, Y.; Truhlar, D. G. "Comparative DFT study of van der Waals complexes: Rare-gas dimers, alkaline-earth dimers, zinc dimer, and zinc-rare-gas dimers" *J. Phys. Chem.* **2006a,** 5121.

Zhao, Y.; Truhlar, D. G. "A new local density functional for main-group thermochemistry, transition metal bonding, thermochemical kinetics, and noncovalent interactions" *J. Chem. Phys* 125, **2006b,** 194101: 1.

Zhao, Y.; Truhlar, D. G. "Density functionals with broad applicability in chemistry" *Acc. Chem. Res.* 41, **2008a,** 157.

Zhao, Y.; Truhlar, D. G. "Exploring the limit of accuracy of the global hybrid meta density functional for main-group thermochemistry, kinetics, and noncovalent interactions" *J. Chem. Theory Comput.* 4, **2008b,** 1849.

Zhao, Y.; Truhlar, D. G. "The M06 suite of density functionals for main group thermochemistry, thermochemical kinetics, noncovalent interactions, excited states, and transition elements: two new functionals and systematic testing of four M06-class functionals and 12 other functionals" *Theor. Chem. Acc.* 120, **2008c,** 215.

Zheng, Q.; Bohling, J. C.; Peters, T. B.; Frisch, A. C.; Hampel, F.; Gladysz, J. A. "A synthetic breakthrough into an unanticipated stability regime: a series of isolable complexes in which C_6, C_8, C_{10}, C_{12}, C_{16}, C_{20}, C_{24}, and C_{28} polyynediyl chains span two platinum atoms" *Chem. Eur. J.* 12, **2006,** 6486.

Ziegler, T.; Rauk, A. "Carbon monoxide, carbon monosulfide, molecular nitrogen, phosphorus trifluoride, and methyl isocyanide as σ donors and π acceptors. A theoretical study by the Hartree-Fock-Slater transition-state method" *Inorg. Chem.* 18, **1979a,** 1755.

Ziegler, T.; Rauk, A. "A theoretical study of the ethylene-metal bond in complexes between copper(1+), silver(1+), gold(1+), platinum(0) or platinum(2+) and ethylene, based on the Hartree-Fock-Slater transition-state method" *Inorg. Chem.* 18, **1979b,** 1558.